

# INFLUENCE OF MOISTURE AND RELATIVE HUMIDITY IN THE ENERGY CONSUMPTION OF RETROFITTED WALLS

**OLÍVIA MAFALDA AFONSO AMORIM ROCHA**

Doctoral Thesis submitted to obtain the Doctor Degree in Civil Engineering

---

Supervisor: Professor Vasco Manuel Araújo Peixoto de Freitas

---

Co-Supervisor: Professor Maria Isabel Morais Torres

JANUARY 2022



DOCTORAL PROGRAM IN CIVIL ENGINEERING

Phone +351-22-508 1901

Fax +351-22-508 1446

✉ [prodec@fe.up.pt](mailto:prodec@fe.up.pt)

*Edited by*

FACULDADE DE ENGENHARIA DA UNIVERSIDADE DO PORTO

Rua Dr. Roberto Frias

4200-465 PORTO

Portugal

Phone +351-22-508 1400

Fax +351-22-508 1440

✉ [feup@fe.up.pt](mailto:feup@fe.up.pt)

🌐 <http://www.fe.up.pt>

Partial reproduction of this document is allowed provided that credit is given to the author and to *Programa Doutoral em Engenharia Civil - Departamento de Engenharia Civil, Faculdade de Engenharia da Universidade do Porto, Porto, Portugal.*

The opinions and information included herein represent the point of view of the author. The Editor cannot accept any legal liability or otherwise for errors or omissions that may exist.

This document was produced from an electronic version provided by the author.

To André and my Parents



## ACKNOWLEDGEMENTS

Having concluded this project, I would like to express my sincere gratitude to all those who contributed to it. In particular, I emphasize my thanks:

To Professor Dr. Vasco Peixoto de Freitas, supervisor of this thesis, for all the readiness and interest shown in the follow-up and scientific support of the project, for the constant encouragement and for the teachings transmitted.

To Professor Isabel Torres, co-supervisor of the thesis, also for her availability and interest, for her support in carrying out the project and for her willingness to travel to FEUP.

I would like to thank Secil for the collaboration in assembling the experimental prototype, essential for this study.

To the Building Physics Laboratory (LFC) for the opportunity to develop the experimental prototype and for providing the equipment for the experimental work. To Eng. Eduardo Costa for his helpful collaboration in preparing and carrying out the experimental tests.

To LFC colleagues Sara Freitas, Joana Maia and Pedro Pereira for the knowledge transmitted about the laboratory equipment and for the assistance provided.

To my peers and LFC colleagues, Cláudia Ferreira, Sílvia Magalhães, Francisca Cavaleiro Barbosa, Teresa Freitas, Magda Posani and Guilherme Coelho, for their enthusiasm in sharing experiences and knowledge, for their support and friendship.

I would like to thank the EcoCoRe Doctoral Program for the opportunity provided and the Foundation for Science and Technology (FCT) for supporting my work through the doctoral scholarship PD/BD/135165/2017.



## **ABSTRACT**

The rehabilitation of existing buildings façades should be based on the improvement in comfort and the decrease of energy consumption. For this purpose, it is necessary to select a retrofitted solution capable of minimizing the heat losses across the building envelope, thereby reducing the buildings heating energy demand. However, it is not only the retrofitted solution of the wall that influences the amount of heat transported across it, but also the outdoor climate, which influences the moisture content in the wall under in-service conditions.

Therefore, the main objective of this thesis is a further elaboration of the current knowledge related to the influence of moisture content on the energy performance of retrofitted walls. To that aim, this study is based on numerical as well as experimental research, and specific attention is paid to masonry walls with a traditional interior insulation system or an innovative external insulating render system.

An experimental prototype was developed in the Building Physics Laboratory – Faculty of Engineering University of Porto to experimentally assess the impact of wetting periods on the energy performance of wall test specimens and to collect data to experimentally validate the selected hygrothermal model. The experiment simulated the exposure of the specimens to rainy periods with a continuous record of the heat fluxes across both surfaces of the specimens. Additionally, the validation of the WUFI hygrothermal simulation model, based on the experimental measurements performed, was carried out.

The WUFI hygrothermal simulation model developed by Fraunhofer Institute for Building Physics IBP was used to carry out a sensitivity study on the influence of moisture content on the energy performance of retrofitted walls under in-service conditions. The results showed that uncoated brick masonry walls with a traditional interior insulation system have significantly higher heat losses than quantified without the influence of moisture. It was also shown that the hydric properties of wall finishing coatings can limit the influence of moisture on their energy performance.

**KEYWORDS:** Rehabilitation, Exterior walls, Moisture, Wind-driven rain, Energy performance, Energy efficiency, Experimental assessment, Numerical simulation





## **RESUMO**

A reabilitação das fachadas dos edifícios antigos deve basear-se numa estratégia de melhoria do conforto e diminuição dos consumos de energia. Para isso, é necessário selecionar soluções construtivas capazes de minimizar as perdas de calor através da envolvente, reduzindo assim as necessidades de energia para aquecimento dos edifícios. No entanto, não é apenas a configuração que influencia a quantidade de calor que atravessa um elemento, mas também as condições climáticas das ambiências, em particular o clima exterior, que condiciona o seu teor humidade em condições de serviço. Assim, o objetivo principal desta tese é aprofundar o conhecimento atual sobre a influência do teor de humidade no desempenho energético de paredes reabilitadas. Para esse efeito, o presente trabalho baseia-se num estudo experimental e numérico, focando-se nas paredes de alvenaria com isolamento térmico aplicado pelo interior associado a gesso cartonado ou com reboco térmico aplicado pelo exterior.

Foi desenvolvido um protótipo experimental no Laboratório de Física das Construções da Faculdade de Engenharia da Universidade do Porto para avaliar o impacto de períodos de humificação no desempenho energético de paredes reabilitadas e para recolher dados que permitissem validar o modelo numérico selecionado. O ensaio simulou a exposição dos provetes a vários períodos de precipitação, com medição em contínuo dos fluxos de calor que atravessaram perpendicularmente ambas as superfícies dos provetes. Adicionalmente, realizou-se a validação do modelo de simulação higrotérmica WUFI, com base nos resultados experimentais obtidos.

O modelo de simulação higrotérmica WUFI foi usado para efetuar um estudo de sensibilidade sobre o impacto do teor de humidade no desempenho energético de paredes reabilitadas em condições de serviço. Os resultados mostram que paredes de alvenaria com o tijolo à vista e com isolamento térmico pelo interior têm perdas de calor significativamente maiores do que o quantificado sem a influência da humidade. Também se mostrou que as propriedades hídricas dos revestimentos das paredes podem limitar a influência da humidade no seu desempenho energético.

**PALAVRAS-CHAVE:** Reabilitação, Paredes exteriores, Humidade, Chuva incidente, Eficiência energética, Avaliação experimental, Simulação numérica



**CONTENTS**

1. INTRODUCTION.....	1
1.1. Background and problem statement.....	1
1.1.1. Declared and design thermal properties .....	3
1.1.2. Energy performance requirements for exterior walls .....	4
1.2. Aim and methodology .....	6
1.3. Outline of the thesis .....	7
2. STATE OF THE ART .....	9
2.1. Methodology .....	9
2.2. Humidification of walls .....	9
2.2.1. Wind-driven rain .....	12
2.2.2. Capillary water absorption .....	16
2.3. Energy performance of wall assemblies .....	18
2.4. Hydric effects on heat transport across a wall .....	20
2.4.1. Thermal conductivities as a function of moisture content .....	21
2.4.2. Impact of moisture on the energy performance of exterior walls .....	28
2.5. Synthesis of the available knowledge .....	37
3. EXPERIMENTAL ASSESSMENT OF THE IMPACT OF WETTING PERIODS ON THE ENERGY PERFORMANCE OF RETROFITTED WALLS .....	41
3.1. Methodology .....	41
3.2. Experimental test setup .....	42
3.2.1. Wall assemblies .....	42
3.2.2. Rain chamber .....	44
3.2.3. Monitored parameters and equipment .....	47
3.3. Rain sequences and boundary conditions .....	51
3.4. Experimental results .....	59

3.4.1. Temperature profiles.....	59
3.4.2. Relative humidity between masonry and insulation.....	66
3.4.3. Heat fluxes.....	71
3.5. Final considerations .....	77
4. VALIDATION OF AN HYGROTHERMAL MODEL WITH EXPERIMENTAL MEASUREMENTS .....	79
4.1. Methodology.....	79
4.2. Hygrothermal model.....	80
4.3. Comparison between experimental and numerical results.....	90
4.3.1. Geometry, material properties and boundary conditions .....	90
4.3.1.1. Experimental characterization of brick and insulating render system....	93
4.3.2. Results .....	104
4.3.2.1. Temperature profiles.....	105
4.3.2.2. Relative humidity between masonry and insulation.....	107
4.3.2.3. Heat fluxes.....	108
4.3.3. Statistical analysis .....	110
4.4. Final considerations .....	112
5. SENSITIVITY ANALYSIS AND PERFORMANCE EVALUATION OF RETROFITTED WALLS UNDER IN-SERVICE CONDITIONS.....	115
5.1. Methodology.....	115
5.1.1. Wall configurations .....	116
5.1.2. Boundary conditions .....	118
5.1.3. Material properties .....	120
5.2. Influence of climate .....	122
5.3. Influence of insulation thickness .....	126
5.4. Influence of wall thickness .....	129

5.5. Influence of finishing coating .....	132
5.6. Influence of initial moisture in masonry .....	137
5.7. Final considerations .....	141
6. CONCLUSION .....	145
6.1. Final conclusions .....	145
6.2. Future developments.....	152
REFERENCES .....	153
APPENDICES .....	159
A. Determination of water vapour permeability .....	160
A.1. Solid brick .....	160
A.2. Insulating render system.....	163
B. Equipment verification.....	166
C. Temperature and relative humidity in Porto, Krakow and Brussel.....	167



## **ÍNDICE OF FIGURES**

Figure 1. Final energy consumption in the residential sector by use in the European Union in 2017 (Eurostat 2019a). .....	1
Figure 2. Existing buildings of the historic center of Porto classified as a World Heritage site in 2001 (credits: Lauren Maganete). .....	2
Figure 3. Winter climatic zones in mainland Portugal (Despacho (extrato) n.º 15793-F/2013). .....	5
Figure 4. Schematic diagrams showing the effect and distribution of moisture in an outside wall caused by irrigation, dew water on the inside, rising ground moisture and initial moisture from construction (Künzel 1995). .....	10
Figure 5. a) Open-porous material (permeable); b) Closed-porous material (impermeable) (De Freitas and Pinto 1998). .....	11
Figure 6. Typical sorption isotherm, giving the equilibrium moisture content as a function of relative humidity (ASHRAE 2017). .....	11
Figure 7. Wind-driven load on façades in Porto in December (De Freitas 2011). .....	13
Figure 8. Velocity pressure profile of a building whose height $h$ is less than length $b$ (EN 1991-1-4: 2005). .....	16
Figure 9. Schematic representation of the heat flux across a wall assembly. ....	18
Figure 10. Hygrothermal loads and driving forces acting on an external wall (ASHRAE 2017). .....	19
Figure 11. Thermal conductivity of a) brick and b) gypsum board as a function of moisture content (adapted from (Kumaran 1996)). .....	21
Figure 12. Thermal conductivities of gypsum board (W1) and plywood (W10) as a function of relative humidity at 10 °C mean temperature (Valovirta and Vinha 2004). .....	22
Figure 13. Thermal conductivity of three types of mineral wool (hard hydrophilic mineral wool MW-HLH, soft hydrophilic mineral wool MW-HLS and hydrophobic mineral wool MW-HB) as a function of moisture content. (Jerman and Černý 2012). .....	23
Figure 14. Thermal conductivity of a) mineral wool; b) and c) expanded polystyrene; and b) extruded polystyrene as a function of moisture content (Szodrai and Lakatos 2014). .....	24

Figure 15. Thermal conductivity of six different insulation materials (three types of polystyrene (EPS 200, XPS, graphite doped EPS), two types of wool samples (glass and mineral) and gypsum boards) as a function of relative humidity (Lakatos 2016)..... 25

Figure 16. Thermal conductivity of a) load bearing materials; b) plasters; c) MW; and d) EPS as a function of moisture content (Kočí et al. 2017)..... 26

Figure 17. Thermal conductivity of cement-based thermal mortars as a function of moisture content (Gomes et al. 2017)..... 27

Figure 18. Thermal conductivity of thermal renders as a function of moisture content (Maia, Ramos and Veiga 2018)..... 27

Figure 19. Variation of thermal resistance of an uncoated solid brick wall subjected to continuous humidification (De Freitas 1992)..... 28

Figure 20. a) Experimental test buildings; b) Heat flux density measurements; c) Measured U-values of external walls for all test buildings just after test buildings were built (in 2013) and after one year of operation (in 2014) (Jakovics et al. 2014)..... 29

Figure 21. (a) Calculated U-values in function of moisture content for 0.4 m thick concrete wall in combination with different EPS materials with 0.1 m thickness and (b) calculated U-values in function of moisture content for 0.4 m thick brick wall in combination with different EPS materials with 0.1 m thickness (Lakatos and Kalmár 2014)..... 29

Figure 22. Decrease in thermal resistance for the total wall assemblies (Vereecken and Roels 2015)..... 30

Figure 23. Map that indicates de CCF proposed values in Spain (percentage value) (Pérez-Bella et al. 2015)..... 31

Figure 24. Thermal transmittance calculated in steady-state conditions ( $U_{WUFI}$ ) and thermal transmittance in transient conditions for a year and for the adopted wetting and drying phases, and the relationship between the steady and transient thermal transmittances for the standard-case, and 340 mm and 450 mm solid brick layer cases in: a) Lisbon; b) San Francisco; and c) Montreal (Coelho and Henriques 2016)..... 32

Figure 25. Values of thermal transmittance in steady-state conditions  $U_{dry}$  and  $U_{80\%}$  relative humidity, and in transient conditions  $U_{monthly}$  for the open-joint ventilated façade facing north in A Coruña. Wufi Pro 5.3 results. (m-monthly; prom-average; seco-dry) (Alonso Alonso 2017)..... 33



Figure 26. Comparison of energy losses calculated from the different thermal transmittance values previously presented in Figure 25 (Alonso Alonso 2017)..... 33

Figure 27. a) Comparison of monthly thermal transmittances of the 1<sup>st</sup> and 5<sup>th</sup> year between Madrid (MAD) and A Coruña (COR); b) Variation in percentage between the values for the 5<sup>th</sup> year (Alonso Alonso 2017)..... 34

Figure 28. Cross-section of the specimen. Position identification of the thermocouples and heat flux sensors (Fino, Tadeu and Simões 2018). ..... 34

Figure 29. Experimental (solid lines) and analytical (dashed lines) temperatures along the thickness of the wall in winter conditions as boundary conditions: a) before, during and after wetting; b) during wetting; c) heat fluxes. The number 6.1 is the number of the panel on which the group of the thermocouples was placed. The numbering used in the analytical model r1, r2, r3, r4, r5, r6 and r7 relates to the thermocouple positions OSB, in, a, b, c, d and s, respectively. (Fino, Tadeu and Simões 2018). ..... 35

Figure 30. Monthly ratio between average and reference U-values in Porto, Nancy and Oslo, with north orientation, for solar absorption of: a) 0.27 and b) 0.8..... 36

Figure 31. Monthly ratio between average and reference U-values in Porto, Nancy and Oslo, with south orientation, for solar absorption of: a) 0.27 and b) 0.8 ..... 36

Figure 32. Overview of the thermal conductivity of building materials as a function of moisture content. .... 38

Figure 33. Schematic representation of the experimental prototype. .... 41

Figure 34. Cross-section of: a) wall test specimen A; b) wall test specimen B. .... 43

Figure 35. Construction of wall test specimens: a) construction of the solid brick masonry; b) application of the mineral wool on the interior surface of wall A; c) application of the insulating render on the exterior surface of wall B. .... 44

Figure 36. Rain chamber and its components: a) rain room; b) control room. .... 45

Figure 37. Close-up of rain chamber's components – rain room: a) sprinkler; b) temperature, relative humidity and pressure sensors; c) discharge pressure. .... 46

Figure 38. Close-up of rain chamber's components – control room: a) flow meters (hydraulic circuit); b) electrical panel; c) display setting of creating or modifying a program..... 47

Figure 39. Position identification of the thermocouples – T, relative humidity probes – H and heat flux sensors – F along the constructive solutions: a) cross section of specimen A; b) cross section of specimen B; c) elevation plan of both specimens. .... 48

Figure 40. Mikromec Data loggers..... 49

Figure 41. Different sensors inside the climatic chamber: a) thermocouples; b) relative humidity probes and air temperature and relative humidity sensors. .... 50

Figure 42. Cycle programmed in the climatic chamber. .... 51

Figure 43. Precipitation sequences applied against the specimens. .... 53

Figure 44. Temperature in the rain room and in the control room during: a) the preliminary test; b) the first test; c) the second test; d) the third test; e) the fourth test. 55

Figure 45. Temperature gradient between the rain room and the control room during the tests. .... 56

Figure 46. Relative humidity in the rain room and in the control room during: a) the preliminary test; b) the first test; c) the second test; d) the third test; e) the fourth test. 58

Figure 47. Temperatures at the surfaces and inside the specimen A during: a) the preliminary test; b) the first test; c) the second test; d) the third test; e) the fourth test. 60

Figure 48. Temperatures at the surfaces and inside the specimen B during: a) the preliminary test; b) the first test; c) the second test; d) the third test; e) the fourth test. 63

Figure 49. Temperature profiles of specimen A before and after each rain sequence for: a) the first test; b) the second test; c) the third test; d) the fourth test. .... 64

Figure 50. Temperature profiles of specimen B before and after each rain sequence for: a) the first test; b) the second test; c) the third test; d) the fourth test. .... 65

Figure 51. Relative humidity inside the wall test specimen A during: a) the preliminary test; b) the first test; c) the second test; d) the third test; e) the fourth test..... 67

Figure 52. Relative humidity profiles of specimen A before and after each rain sequence for: a) the first test; b) the second test; c) the third test; d) the fourth test..... 69

Figure 53. Vapor saturation pressure and partial water vapour pressure between the masonry and the insulation of specimen A throughout the fourth test..... 71

Figure 54. Heat fluxes across the specimen A during: a) the preliminary test; b) the first test; c) the second test; d) the third test; e) the fourth test. .... 73

Figure 55. Heat fluxes across the specimen B during: a) the preliminary test; b) the first test; c) the second test; d) the third test; e) the fourth test. .... 75

Figure 56. Temperature in the rain room and in the control room during the third experiment .....	92
Figure 57. Relative humidity in the rain room and in the control room during the third experiment. ....	92
Figure 58. Capillary absorption as a function of the square root of time for: a) solid brick; b) insulating render system.....	96
Figure 59. Specimens of brick and insulating render system for the water vapour permeability test. ....	97
Figure 60. Scheme of the assembly for the wet-cup measurements (Ramos 2007).....	98
Figure 61. Test cups with the specimens inside the climatic chamber.....	99
Figure 62. a) CT-Metre equipment measuring the thermal conductivity of insulating render test specimens; b) Brick test specimens with the “anneau” probe placed between them. ....	101
Figure 63. Thermal conductivity of brick and insulating render as a function of moisture content. ....	102
Figure 64. Measured and simulated temperatures at the surfaces and inside the: a) configuration A; b) configuration B. ....	105
Figure 65. Measured and simulated temperature profiles before and after the rainy period, for: a) configuration A; b) configuration B. ....	106
Figure 66. Measured and simulated relative humidity inside the wall configuration A. ....	107
Figure 67. Measured and simulated relative humidity profiles before and after the rainy period for wall configuration A.....	108
Figure 68. Measured and simulated heat fluxes across: a) configuration A; b) configuration B.....	109
Figure 69. Indoor conditions: a) indoor temperature; b) indoor relative humidity. ....	120
Figure 70. Thermal conductivities as a function of moisture content. ....	121
Figure 71. Accumulated moisture content: a) in the masonry and b) in the insulation (if the walls are exposed to WDR loads).....	122
Figure 72. Annual maximum and average moisture content for the walls exposed to WDR loads and annual average moisture content for the walls not exposed to WDR loads. ....	123

Figure 73. Heat fluxes across the interior surface of the walls: a) throughout the year; b) comparison between the heat fluxes through the walls exposed to WDR loads (solid lines) and through the walls not exposed to WDR loads (dashed lines) during January. .... 124

Figure 74. Accumulated moisture content: a) in the masonry and b) in the insulation (if the walls are exposed to WDR loads)..... 126

Figure 75. Maximum and average moisture content for the walls exposed to WDR loads and average moisture content for the walls not exposed to WDR loads. .... 127

Figure 76. Heat fluxes across the interior surface of the walls: a) throughout the year; b) comparison between the heat fluxes through the walls exposed to WDR loads (solid lines) and through the walls not exposed to WDR loads (dashed lines) during January. .... 128

Figure 77. Accumulated moisture content: a) in the masonry and b) in the insulation (if the walls are exposed to WDR loads)..... 130

Figure 78. Maximum and average moisture content for the walls exposed to WDR loads and average moisture content for the walls not exposed to WDR loads. .... 131

Figure 79. Heat fluxes across the interior surface of the walls: a) throughout the year; b) comparison between the heat fluxes through the walls exposed to WDR loads (solid lines) and through the walls not exposed to WDR loads (dashed lines) during January. .... 131

Figure 80. Accumulated moisture content: a) in the brick or stone masonry and b) in the insulation (if the walls are exposed to WDR loads). .... 133

Figure 81. Maximum and average moisture content for the walls exposed to WDR loads and average moisture content for the walls not exposed to WDR loads. .... 134

Figure 82. Heat fluxes across the interior surface of the walls: a) throughout the year; b) comparison between the heat fluxes through the walls exposed to WDR loads (solid lines) and through the walls not exposed to WDR loads (dashed lines) during January. .... 135

Figure 83. Accumulated moisture content in brick masonry of wall configuration 3 (C3) and wall configuration 7 (C7) over time. .... 137

Figure 84. Annual maximum and average moisture content in the walls: a) configuration 3 (masonry wall with interior insulation system); b) configuration 7 (masonry wall with external insulating render system)..... 138

Figure 85. Heat fluxes across the interior surface of the walls over time. .... 139

## **INDEX OF TABLES**

Table 1. Reference conditions for determining declared thermal values (EN ISO 10456:2007).....	4
Table 2. Energy requirements - Maximum admissible thermal transmittances of exterior walls, $U_{max}$ ( $W/(m^2 \cdot K)$ ) (Portaria n.º 297/2019 , Portaria n.º 379-A/2015) .....	5
Table 3. List of moisture transport mechanisms occurring in practice and driving forces (adapted from (Hens 2017)). .....	12
Table 4. Classification of precipitation intensity according to IPMA (IPMA 2019). ....	14
Table 5. Precipitation sequences (De Freitas 1992). .....	14
Table 6. Typical values of wind pressure acting on the walls of old buildings calculated according to Eurocode EN 1991-1-4. ....	16
Table 7. Classification of materials in function of the capillary water absorption coefficient.....	17
Table 8. Building material capillary water absorption coefficients (Sousa 1996, Maia, Ramos and Veiga 2018) .....	17
Table 9. Overview of the thermal conductivity of building materials as a function of moisture content. ....	37
Table 10. Overview of the results considering the influence of moisture on the energy performance of exterior walls.....	39
Table 11. Accuracy and range of the installed sensors.....	48
Table 12. Rain sequence used in each test.....	52
Table 13. WUFI Pro inputs to define the component (Wufi-wiki 2019d, Wufi-wiki 2019e) .....	83
Table 14. WUFI Pro inputs: climate conditions .....	85
Table 15. $R_2$ values.....	86
Table 16. FE values .....	87
Table 17. FD values .....	87
Table 18. Wufi Pro results .....	88
Table 19. Material properties.....	91
Table 20. Thermal conductivities as a function of moisture content.....	91
Table 21. Capillary water absorption coefficient results.....	96

Table 22. Results of the water vapour transmission properties of solid brick and insulating render system.....	99
Table 23. Thermal conductivity of brick and insulating render as a function of moisture content. ....	101
Table 24. Summary of the hygrothermal properties of brick and insulating render system. ....	103
Table 25. Thermal conductivity of brick and insulating render as a function of moisture content. ....	104
Table 26. Temperature (T), relative humidity (RH) and heat flux (HF) statistical parameters.....	112
Table 27. Temperature, relative humidity, solar radiation, and rain load on the west orientated facades located in Porto, Krakow and Brussels.....	119
Table 28. Material properties.....	121
Table 29. Energy losses for the walls exposed to WDR loads as well as for the walls not exposed to WDR loads. ....	125
Table 30. Energy losses for the walls exposed to WDR loads as well as for the walls not exposed to WDR loads. ....	129
Table 31. Energy losses for the walls exposed to WDR as well as for the walls not exposed to WDR.....	132
Table 32. Energy losses for the walls exposed to WDR as well as for the walls not exposed to WDR.....	136
Table 33. Energy losses through the walls per year. ....	140
Table 34. Overview of results of energy losses through the walls exposed and not exposed to wind-driven rain (WDR). ....	142

## NOMENCLATURE

### ROMAN-LETTER NOTATIONS

A	[kg/m <sup>2</sup> s <sup>1/2</sup> ]	Water absorption coefficient
c	[J/(kg K)]	Specific heat capacity
c <sub>e</sub>	-	Exposure factor
c <sub>pe</sub>	-	Pressure coefficient for the external pressure
d	[m]	Thickness
D <sub>ws</sub>	[m <sup>2</sup> /s]	Liquid transport coefficient, suction
F <sub>m</sub>	-	Moisture conversion factor
f <sub>ψ</sub>	[m <sup>3</sup> /m <sup>3</sup> ]	Moisture conversion coefficient volume by volume
f <sub>u</sub>	[kg/kg]	Moisture conversion coefficient mass by mass
g <sub>w</sub>	[kg/(m <sup>2</sup> s)]	Liquid transport flux density
m	[kg]	Mass
L <sub>v</sub>	[kJ/kg]	Latent heat of vaporization
q	W/m <sup>2</sup>	Density of heat flow rate or Heat flux
q <sub>b</sub>	-	Basic velocity pressure
q <sub>in</sub>	W/m <sup>2</sup>	Heat flux across the interior surface of the element
q <sub>out</sub>	W/m <sup>2</sup>	Heat flux across the exterior surface of the element
q <sub>p</sub>	[Pa]	Peak velocity pressure
Q	[J]	Energy in the form of heat
rh	[%]	Relative humidity
R	[m <sup>2</sup> ·K/W]	Thermal resistance
R <sub>air</sub>	[m <sup>2</sup> ·K/W]	Thermal resistance of unventilated air layer

$R_h$	[mm/h]	Normal rain or rain intensity on a horizontal surface in open field
$R_{se}$	[m <sup>2</sup> ·K/W]	Interior surface resistance
$R_{si}$	[m <sup>2</sup> ·K/W]	Exterior surface resistance
$R_{WDR}$	[l/(m <sup>2</sup> h)]	Wind-driven rain load or wind-driven rain intensity
Sd-Value	[m]	Vapor diffusion thickness
T	[K]	Temperature
u	[kg/kg]	Moisture content mass by mass
U	[W/(m <sup>2</sup> ·K)]	Thermal transmittance of an assembly
$U_{design}$	[W/(m <sup>2</sup> ·K)]	Thermal transmittance of an assembly under typical conditions of use
$U_{dry}$	[W/(m <sup>2</sup> ·K)]	Thermal transmittance of a dry assembly
$U_{transient}$	[W/(m <sup>2</sup> ·K)]	Thermal transmittance of an assembly under typical conditions of use
$U_{wet}$	[W/(m <sup>2</sup> ·K)]	Thermal transmittance of a moist assembly
$V_{10}$	[m/s]	Mean wind velocity measured at a height of 10 m in open area
w	[kg/m <sup>3</sup> ]	Moisture content mass by volume
$w_{cr}$ or $w_{95}$	[kg/m <sup>3</sup> ]	Equilibrium moisture content at 95 % relative humidity
WDR	-	Wind-driven rain
wf	[kg/m <sup>3</sup> ]	Moisture content at free saturation
$w_{max}$		Maximum moisture content
z	[m]	Height
$z_e$	[m]	Reference height for the external pressure



GREEK-LETTER NOTATIONS

$\alpha_s$	-	Solar Radiation Absorptivity
$\Delta T$	[°C]	Temperature gradient
$\varepsilon$	-	Porosity
$\theta$	[°C]	Temperature
$\theta$	[°]	Angle between the wind direction and the orthogonal to the façade
$\lambda$	[W/(m·K)]	Thermal conductivity of a material
$\lambda_0$	[W/(m·K)]	Thermal conductivity of a dry material
$\lambda_w$	[W/(m·K)]	Thermal conductivity of a moist material
$\mu$	-	Water vapour diffusion resistance factor
$\rho$	[kg/m <sup>3</sup> ]	Bulk density
$\varphi$	-	Relative humidity
$\Psi$	[m <sup>3</sup> /m <sup>3</sup> ]	Moisture content volume by volume



# 1

## INTRODUCTION

### 1.1. BACKGROUND AND PROBLEM STATEMENT

Reduction of energy consumption in the building sector constitutes an important measure needed to reduce the European Union’s energy dependency and greenhouse gas emissions. In particular, reduction of energy needs for heating has significant potential for energy savings in the building sector, since heating represents the main use of energy in the residential sector (it represents 64.1% of the final energy consumption, see Figure 1) (Eurostat 2019a). In the case of Portugal in particular, the proportion of energy used for heating is lower (21.2%) (Eurostat 2019b).

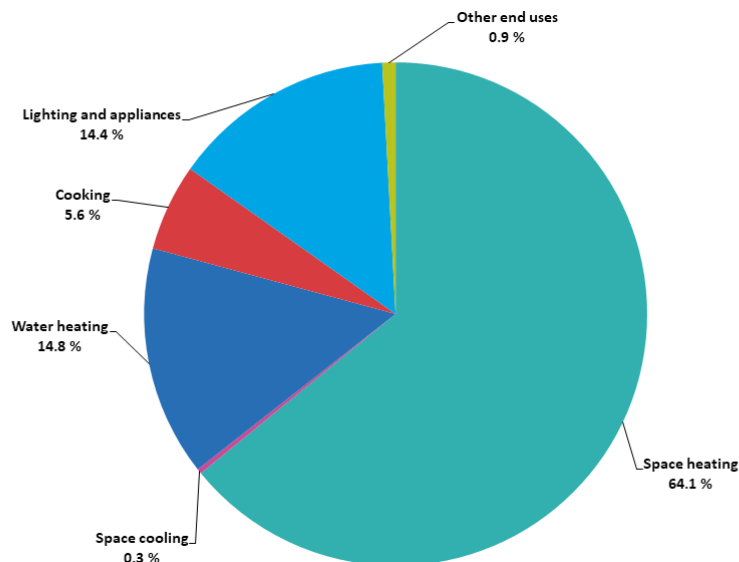


Figure 1. Final energy consumption in the residential sector by use in the European Union in 2017 (Eurostat 2019a).

One energy efficient measure to decrease the energy needs for heating is adding thermal insulation internally or externally to the outer walls during renovations of existing buildings (Verma et al. 2022). In this thesis, “existing buildings” term represents all types of protected and non-protected buildings built in Europe before 1945, composed of heavy walls of stone and brick. These buildings account for 24% to 35% expressed in percentage of total building stock area (Blumberga et al. 2015) and are quite common in historic centers of European cities, oftentimes classified as world heritage cultural sites by UNESCO for their outstanding universal value. One example is the historic center of Porto, see Figure 2.



Figure 2. Existing buildings of the historic center of Porto classified as a World Heritage site in 2001 (credits: Lauren Maganete).

Interior insulation may be a risky insulation technique due to potential interstitial condensation, frost damage, salt efflorescence, mould growth and other damage patterns, but nevertheless it remains the only post-insulation technique for buildings with a worth-preserving façade (Verecken et al. 2015).

In fact, adding thermal insulation on the exterior walls allows the reduction of heat transmission losses, decreasing the overall energy needs for heating while maintaining acceptable occupant comfort. That energy performance of walls is, however, worsened by the presence of moisture (Tejeda-Vázquez et al. 2021). For certain building materials,

the thermal conductivities are significantly affected by moisture and consequently the currently calculated thermal transmittance values from the dry conductivities may not be accurate if the walls are wet.

The influence of water content due to wind driven rain and fluctuation of relative humidity in the energy consumption of retrofitted walls is therefore an important research topic in order to better understand the real energy performance of retrofitted façades under in-service conditions.

#### 1.1.1. DECLARED AND DESIGN THERMAL PROPERTIES

Due to the influence of moisture on thermal properties, namely thermal conductivity  $\lambda$  and thermal transmittance  $U$  of a building material or element, there is a distinction between the declared and the design thermal properties. The declared thermal values correspond to the dry state of a material or element, whereas the design thermal values should consider the moisture content under in-service conditions.

The determination of declared values shall be given under the reference conditions given in EN ISO 10456:2007 - *Building materials and products - Hygrothermal properties - Tabulated design values and procedures for determining declared and design thermal values* (EN ISO 10456: 2007) and presented in Table 1. The reference moisture content of the material during the tests shall be a low moisture content reached by drying, or the moisture content when in equilibrium with air at a relative humidity of 50%. That is to say, the declared thermal value corresponds to the dry state of a material.

The methods that shall be used for determination of the declared thermal conductivity of a material are the guarded hot plate (according to ISO 8302:1991 - *Thermal insulation - Determination of steady-state thermal resistance and related properties - Guarded hot plate apparatus* (ISO 8302 1991)) and the heat flow meter apparatus (according to ISO 8301:1991 - *Thermal insulation - Determination of steady-state thermal resistance and related properties - Heat flow meter apparatus* (ISO 8301 1991)). The method that shall be used for determination of the declared thermal transmittance of a building component is the hot box (according to ISO 8990:1994 - *Thermal insulation - Determination of steady-state thermal transmission properties - Calibrated and guarded hot box* (ISO 8990 1994)).

Table 1. Reference conditions for determining declared thermal values (EN ISO 10456: 2007).

Property	Set of conditions			
	I (10 °C)		II (23 °C)	
	a	b	a	b
Reference temperature	10 °C	10 °C	23 °C	23 °C
Moisture	u <sub>dry</sub>	u <sub>23,50</sub>	u <sub>dry</sub>	u <sub>23,50</sub>
Ageing	aged	aged	aged	aged
u <sub>dry</sub> is a low moisture content reached by drying according to specifications or standards for the material concerned.  u <sub>23,50</sub> is the moisture content when in equilibrium with air at 23 °C and relative humidity of 50%.				

The determination of design/practical thermal conductivity of a building material or thermal transmittance of a building element is difficult because it is necessary to know the expected moisture content of the material or element under in-service conditions.

Nevertheless, there are tabulated design values for materials and elements commonly used in building constructions in order to support studies in the scope of the thermal performance of buildings. Those tabulated design values were obtained from declared values or measured values and can be found in the standard EN 12524:2000 - *Building materials and products. Hygrothermal properties. Tabulated design values* (EN 12524: 2000) or in the publication ITE 50 - *Coeficientes de Transmissão Térmica de Elementos da Envolvente dos Edifícios* (Dos Santos and Matias 2006).

#### 1.1.2. ENERGY PERFORMANCE REQUIREMENTS FOR EXTERIOR WALLS

The Directive 2010/31/EU of the European Parliament and of the Council of 19 May 2010 has promoted the improvement of the energy performance of buildings within the Union and one of the requirements that is laid down in his Directive is that Member States shall take the necessary measures to ensure that minimum energy performance requirements are set for building elements that form part of the building envelope (Directive 2010/31/EU). As a consequence, in Portugal and with effect from 31 December 2015, in order to limit the amount of energy used for heating, no exterior walls shall have a thermal transmittance higher than 0.50, 0.40 or 0.30 W/(m<sup>2</sup>·K) depending on the winter climate zone where the wall is located (see Table 2).

However, those requirements may not apply in some exceptional cases, namely the renovations of existing buildings classified as heritage due to their patrimonial value. For those exceptional cases (Portaria n.º 297/2019), with effect from 9 September 2019, no exterior wall shall have a thermal transmittance higher than 1.70, 1.50 or 1.40 W/(m<sup>2</sup>·K) depending also on the winter climate zone where the wall is located (see Table 2).

Table 2. Energy requirements - Maximum admissible thermal transmittances of exterior walls,  $U_{max}$  (W/(m<sup>2</sup>·K))

Building element	Climate zone		
	I1	I2	I3
Exterior walls	0.50	0.40	0.35
Exterior walls – exceptional cases	1.70	1.50	1.40

The winter climatic zones (I1, I2, and I3) are defined from the number of degree days (GD) at the base 18 ° C as it is shown in Figure 3.

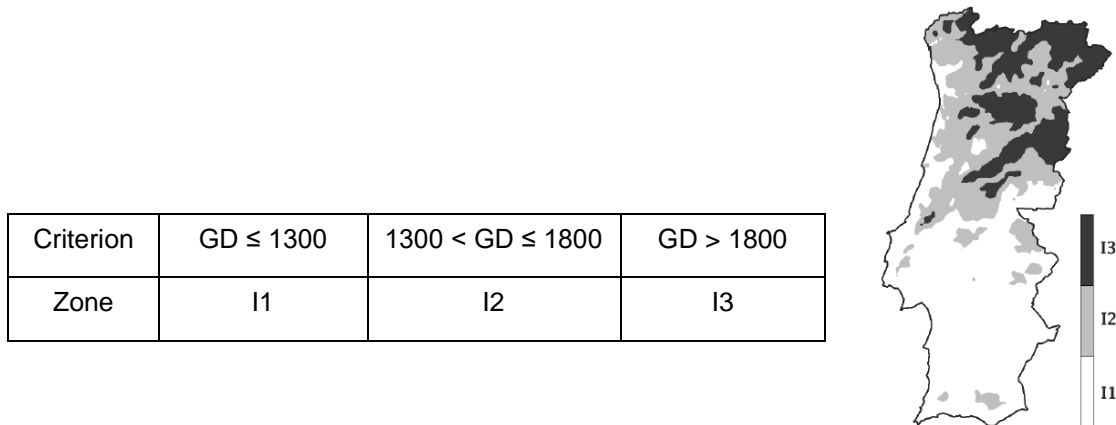


Figure 3. Winter climatic zones in mainland Portugal (Despacho (extrato) n.º 15793-F/2013).

It should be noted that the method presented in the Regulation and currently used in practice to determine the thermal transmittance of exterior walls is the simplified calculation based on the design thermal conductivities and the thicknesses of the materials involved and described in ISO 6946:2007 - *Building components and building elements - Thermal resistance and thermal transmittance - Calculation methods* (EN ISO 6946: 2007).

## **1.2. AIM AND METHODOLOGY**

The general objective of this thesis is a further elaboration of the knowledge on the influence of moisture on the energy performance of retrofitted walls. This is an important subject nowadays due to the need to improve the energy efficiency of exterior walls of existing buildings and to reduce the buildings' energy needs for heating and the energy consumption in the building sector.

For that purpose, the following main goals were defined:

- (1) Experimental measurement of the influence of moisture content on the energy performance of retrofitted walls;
- (2) Quantification of the impact of wind-driven rain (WDR) on the energy performance of different retrofitted walls exposed to real climatic conditions through a sensitivity analysis.

In order to address the previously proposed main goals, this thesis focuses on:

- Literature review highlighting the difference between the thermal properties (thermal conductivity and thermal transmittance) of dry and wet building materials and wall assemblies.
- Development of an experimental prototype to simulate the exposure of the wall test specimens to rainy periods, while a continuous measurement of heat fluxes through the walls and temperature and relative humidity profiles is recorded. The experimental laboratory work to assess the influence of wind-driven rain on the heat fluxes across the wall test specimens, restricted by the COVID-19 pandemic.
- Laboratory measurements of some hygrothermal properties to characterize the materials that constitute the wall test specimens.
- Validation of the one-dimensional WUFI advanced hygrothermal simulation model, based on the experimental measurements performed.
- Numerical simulations of the dynamic hygrothermal behaviour and energy performance of retrofitted walls under in-service conditions, using WUFI Pro software.



- Sensitivity studies to assess key factors for the influence of moisture on the energy performance of retrofitted walls, centred on energy efficiency and energy consumption.

Furthermore, the following main research questions were established: How does moisture influence the energy performance of retrofitted walls? What are the consequences for the energy consumption?

The following further questions will be dealt with: i) What are the heat losses through retrofitted walls, taking into account the moisture content in the walls under in-service conditions? ii) In a more humid climate is there an increase in heat losses through retrofitted walls compared to other climates due to the higher humidity? iii) What is the impact of wind-driven rain on the energy performance of retrofitted walls? iv) What are the key factors related to wall thickness, insulation option and finishing coating that most prevent the harmful moisture effects on the energy performance of retrofitted walls?

### **1.3. OUTLINE OF THE THESIS**

The thesis comprises the following six main chapters:

**Chapter 1** provides the introduction on the topic and defines the goals and the research questions of this study.

**Chapter 2** provides a background on humidification of walls and energy performance of walls. In addition, it presents the literature review concerning the influence of moisture and relative humidity in the energy consumption of exterior walls.

**Chapter 3** experimentally assesses the impact of wetting periods on the energy performance of the wall test specimens. The first part describes the experimental prototype that has been set up and the second part presents the results obtained that are divided into: air temperature and relative humidity of the surroundings of the specimens, temperatures and relative humidity inside the specimens and heat fluxes through the specimens' surfaces.

**Chapter 4** experimentally validates the one-dimensional WUFI hygrothermal model. The experimental hygrothermal properties characterization of brick and insulating render system used in the experimental prototype is presented.

**Chapter 5** refers to the numerical simulation of the hygrothermal and energy performance of retrofitted walls under in-service conditions. The impact of wind-driven rain on the energy losses through the walls is numerically studied.

Finally, in **Chapter 6** the main conclusions are drawn. Additionally, some recommendations for further research are enumerated.

# 2

## STATE OF THE ART

### 2.1. METHODOLOGY

In this chapter, a background on humidification of walls and energy performance of walls is given. Since wind-driven rain is a leading moisture source in wet climates, attention is paid to wind-driven rain and the capillary water absorption coefficient. Additionally, the relevant state of the art on hydric effects on heat transport across a wall assembly is provided. An overview of the measurements of thermal conductivities of the materials that compose the retrofitted walls of existing buildings as a function of moisture content is given. Finally, experimental and numerical studies that investigated the influence of moisture on thermal transmittance of wall assemblies are critically analysed.

### 2.2. HUMIDIFICATION OF WALLS

Moisture may enter a building component in liquid form as water leaks, wind-driven rain or rising damp. On the other hand, it can do so in the form of water vapour that activates sorption in the envelope materials or condenses on the surface or inside the component. In the case of components with several layers, condensation sometimes happens at the interface between layers. This is feared as it may remain unnoticed for a long time, only emerging when rot or corrosion becomes visible or moisture starts dripping out (Henriques 1994, ASHRAE 2017). The increased water content of a building component can also occur during its construction phase, for example caused by the mixing water for mortar, the production moisture of bricks or the lack of rain protection during that phase (Künzel 1995). Figure 4 schematically shows the effect and distribution of moisture in an exterior wall caused by some of the referred moisture sources, namely wind-driven rain, interstitial condensation, rising damp and initial construction moisture.

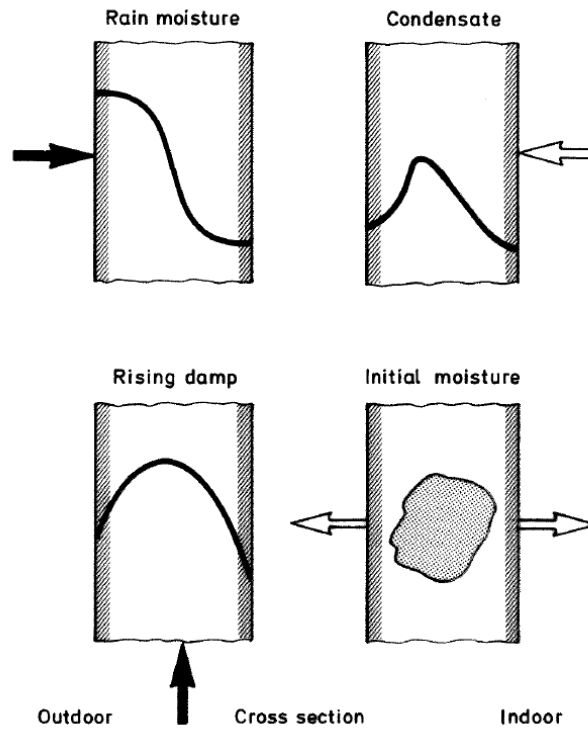


Figure 4. Schematic diagrams showing the effect and distribution of moisture in an outside wall caused by irrigation, dew water on the inside, rising ground moisture and initial moisture from construction (Künzel 1995).

Air and liquid water transfer across materials and building assemblies can only develop in materials that are open-porous (Figure 5a), that is, have accessible pores with an equivalent diameter larger than the diameter of the relevant molecules. In materials without pores, with smaller pores than the said diameter (Figure 5b), air and moisture transfer fails (Hens 2017). Most building materials are open-porous, allowing liquids or gases to go through it. The material can be more or less permeable, depending on pore size and geometry (De Freitas and Pinto 1998, ASHRAE 2017).

Looking to open-porous materials, moisture includes ice, liquid and vapour. In water vapour the molecules move separately, whereas in the liquid they form clusters of much larger diameter. Therefore pores that allow vapour to pass may be inaccessible for liquid water. Some materials are thus waterproof but not vapourproof. The solid state, ice, is crystalline with a 10% larger volume compared with liquid, which is the reason why frost can be so destructive (Hens 2017).

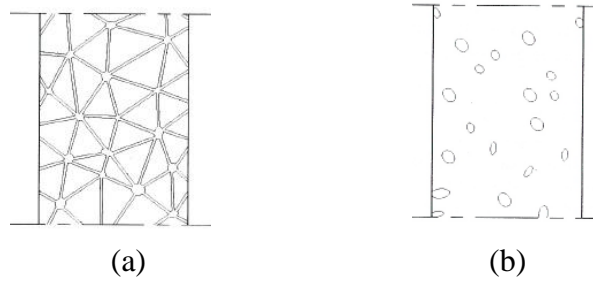


Figure 5. a) Open-porous material (permeable); b) Closed-porous material (impermeable) (De Freitas and Pinto 1998).

In some building materials, moisture may also be adsorbed in the cell wall of the pores itself. The amount of water in these hygroscopic (water-attracting) materials is related to the relative humidity of the surrounding air. When relative humidity rises, hygroscopic materials gain moisture (adsorption), and when the relative humidity drops, they lose moisture (desorption). The relationship between relative humidity and moisture content at a particular temperature can be represented by the sorption isotherm (see Figure 6). Isotherms obtained by adsorption are not identical to those obtained by desorption and this difference is called hysteresis (ASHRAE 2017).

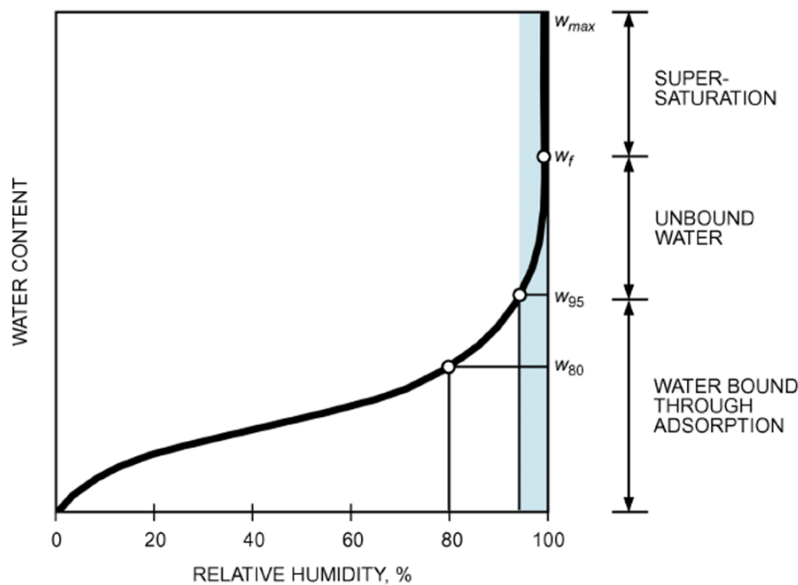


Figure 6. Typical sorption isotherm, giving the equilibrium moisture content as a function of relative humidity (ASHRAE 2017).

The equilibrium moisture content increases with relative humidity, especially above 80% rh. Moisture contents above  $w_{95}$  or  $w_{cr}$  (the equilibrium water content at 95% rh) cannot be achieved solely by vapor adsorption, because this region is characterized by capillary unbound water. At very high relative humidity, small pores become entirely

filled with water by capillary condensation. The maximum moisture content  $w_{max}$  should be reached at 100% rh, when all pores are filled, but experimentally this can only be achieved in a vacuum. In practice, the maximum moisture content of a porous material is lower. That value is referred to as free water saturation  $w_f$  or  $w_{sat}$  (ASHRAE 2017).

Air and moisture transfer across porous materials can occur due to the mechanisms listed in Table 3. These moisture transfer mechanisms are very complex. For air transport, the drivers are external forces such as wind and differences in air temperature and air composition. Moisture transport combines vapour and liquid movement. Equivalent diffusion, air mitigation, capillary suction, gravity and external pressures all act as driving forces (Hens 2017).

Table 3. List of moisture transport mechanisms occurring in practice and driving forces (adapted from (Hens 2017)).

Transport mechanism		Driving force
Water vapour	Equivalent diffusion	Differentials in vapour pressure in the pore air and in the ambient air at both sides of an assembly.
	Air transport (convection)	Vapour migrates together with the air in and across assemblies.
Liquid water	Capillarity	Differentials in capillary suction connected to pore width. The larger the pore, the less it sucks but the more intense the flow. Capillary suction is caused by molecular attraction between the pore wall and the water molecules within small pores of an equivalent diameter less than 0.1 mm.
	Gravity	Differentials in weight between water heads. Gravity activates liquid flow in wider pores that hardly show capillary suction.
	Pressure	Differentials in external total pressure. Air, as well as water, are responsible.

### 2.2.1. WIND-DRIVEN RAIN

From all the moisture sources, this study pays specific attention to wind-driven rain. In fact, wind-driven rain is a leading moisture source for building façades in wet climates. In simple terms, the drag force that wind exerts inclines rain droplet trajectories generating wind-driven rain. Its quantification is highly complex, yet there are semi-empirical models to calculate the wind-driven rain load for vertical surfaces from wind

velocity, wind direction and precipitation data measured at weather stations. However, not only regional precipitation and wind are significant factors in determining local wind-driven rain. Also, local exposure conditions are of equal importance. In fact, the semi-empirical models consider also parameters which depends on the building geometry and surrounding environment (De Freitas, Barreira and De Freitas 2013, ASHRAE 2017).

The semi-empirical models used to calculate the wind-driven rain load were developed by Lacy, Henriques, Meteonorm, Straube and Burnett, WUFI, ASHRAE and standard EN ISO 15927-3:2009 - *Hygrothermal performance of buildings - Calculation and presentation of climatic data — Part 3: Calculation of a driving rain index for vertical surfaces from hourly wind and rain data*. However, it should be noted that the application of those semi-empirical models can lead to meaningfully different amounts of wind-driven rain load as demonstrated in (De Freitas 2011). That study compared the results of wind-driven rain load acting on a façade in Oporto calculated from different semi-empirical models and with those obtained from in situ measurements and the obtained results are shown in Figure 7. The ASHRAE model corresponds to the maximum amount of WDR to occur in that façade. In addition, it was observed that the measured values are lower than the calculated ones for all orientations except West (De Freitas 2011).

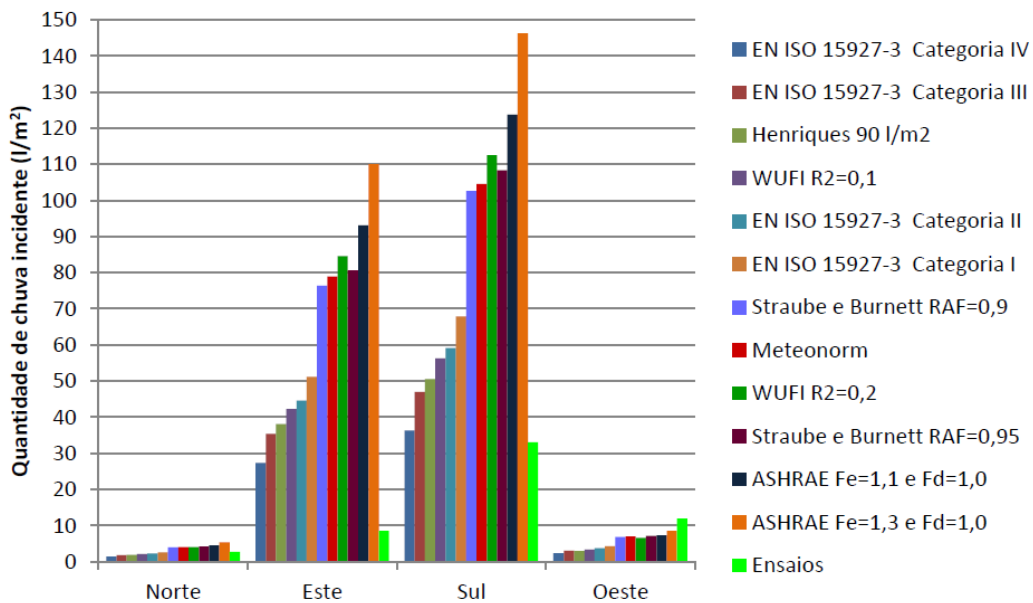


Figure 7. Wind-driven load on façades in Porto in December (De Freitas 2011).

In fact, precipitation is a climatic variable with large variability. This may occur with greater or lesser intensity and with different temporal distribution. Rain intensity is

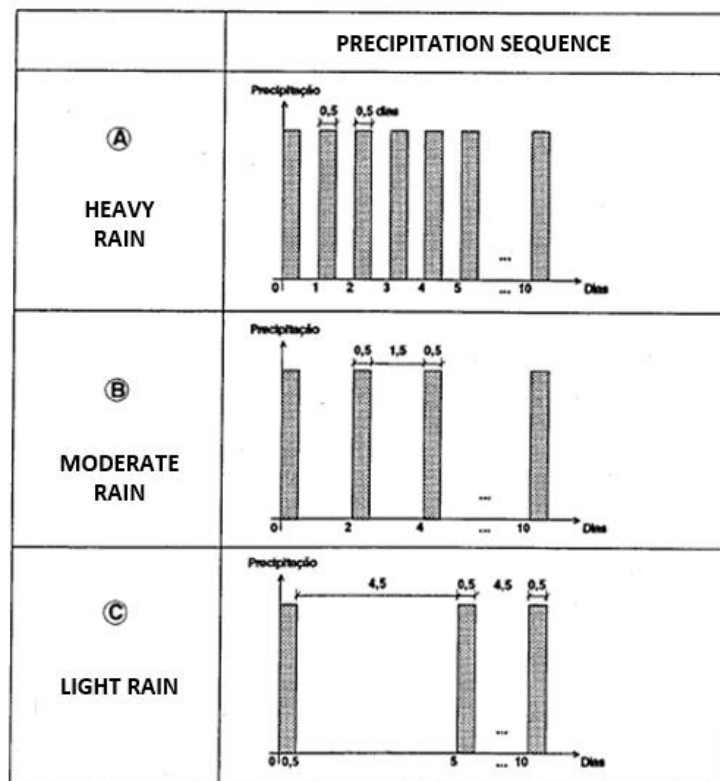
defined as the ratio of the total amount of rain (rainfall depth) falling during a given period to the duration of the period. It is expressed in depth units per unit time, usually as mm per hour (mm/h). Rain rate is generally described as light, moderate, heavy or very heavy depending on its intensity. Table 4 presents the categories that are used to classify rain intensity according to the Portuguese Institute of the Sea and the Atmosphere (IPMA).

Table 4. Classification of precipitation intensity according to IPMA (IPMA 2019).

Description	Rain intensity
Light rain	< 2 mm/h
Moderate rain	2 – 10 mm/h
Heavy rain	10 – 50 mm/h
Very heavy rain	> 50 mm/h

Table 5 presents the conventional precipitation sequences in time mentioned in (De Freitas 1992) which represent simulating scenarios of heavy, moderate and light rain.

Table 5. Precipitation sequences (De Freitas 1992).





Sequence A is characterized by 12 hours rain, followed by 12 hours without rain, then again 12 hours rain and so on. Sequence B is characterized by 12 hours rain, followed by 36 hours without rain, then again 12 hours rain, and so on. Finally, sequence C is characterized by 12 hours rain, followed by four days and a half without rain, then again 12 hours rain, and so on.

With respect to wind pressure, EN 1991-1-4 *Eurocode 1: Actions on structures – Part 1-4: General actions – Wind action* (EN 1991-1-4: 2005) was used to predict the wind pressure acting on the exterior walls of existing buildings  $w_e$ , in Pa, as a function of wind velocity  $v$ , in m/s. The following expression was used:

$$w_e = q_p(z_e) \cdot c_{pe} \quad (1)$$

where

$q_p(z_e)$	[Pa]	peak velocity pressure
$z_e$	[m]	reference height for the external pressure
$c_{pe}$	[-]	pressure coefficient for the external pressure

The peak velocity pressure at height  $z$  was determined by:

$$q_p(z) = [1 + 7 \cdot I_v(z)] \cdot \frac{1}{2} \cdot \rho \cdot v_m^2(z) = c_e(z) \cdot q_b \quad (2)$$

where

$\rho$	[kg/m <sup>3</sup> ]	air density
$c_e(z)$	[-]	exposure factor
$q_b$	[-]	basic velocity pressure, given in Equation 3

$$q_b = \frac{1}{2} \cdot \rho \cdot v^2 \quad (3)$$

In the calculations, it was considered terrain category IV (area in which at least 15% of the surface is covered with buildings and their average height exceeds 15 m), fundamental value of the basic wind velocity  $v_{b,0}$  of 27 m/s and height  $z$  above the terrain of 12 m. The roughness factor  $c_r(z)$  and the orography factor  $c_o(z)$ , were taken as 1.0. A rectangular plan building whose height  $h$  is less than length  $b$  as shown in Figure 8 was considered since that is the most common case of existing buildings (Teixeira 2014). For this case, it is considered that the peak velocity pressure  $q_p$  do not vary with the height.

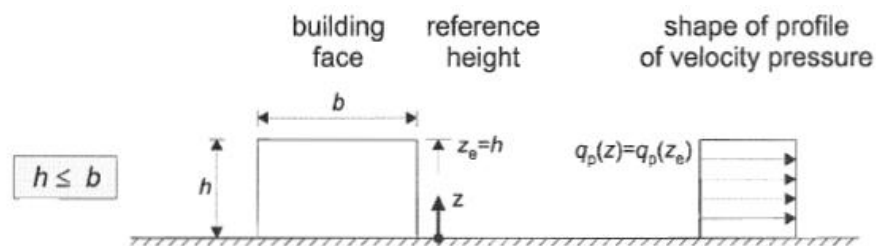


Figure 8. Velocity pressure profile of a building whose height  $h$  is less than length  $b$  (EN 1991-1-4: 2005).

Table 6 presents the obtained results of wind pressure in function of the wind velocity. Typically, the wind pressure acting on the façades of existing buildings can vary between 10 and 285 Pa, depending on the wind speed (IPMA 2019). The wind pressure acting on the façades was determined because there was the possibility of applying wind pressure against the wall test specimens during the experimental tests, but this was not done. Due to restrictions imposed by the COVID-19 pandemic, the experimental campaign was shorter than anticipated.

Table 6. Typical values of wind pressure acting on the walls of old buildings calculated according to Eurocode EN 1991-1-4.

Wind velocity	Description according to IPMA	Wind pressure acting on the exterior surfaces $w_e$
< 4 m/s	Weak wind	< 10 Pa
4 – 10 m/s	Moderate wind	10 – 70 Pa
10 – 15 m/s	Strong wind	70 – 160 Pa
15 – 20 m/s	Very strong wind	160 – 285 Pa
> 20 m/s	Exceptionally strong wind	> 285 Pa

### 2.2.2. CAPILLARY WATER ABSORPTION

During rainy and windy weather, the humidification of facades depends mainly on the finish's capillary water absorption coefficient  $A$ . That coefficient quantifies the amount of water entry into a porous material due to absorption when its surface is in direct contact with liquid water and is expressed in units of  $\text{kg}/(\text{m}^2 \text{ s}^{1/2})$  or  $\text{kg}/(\text{m}^2 \text{ h}^{1/2})$ .

Depending on the value of the water absorption coefficient the material can be classified into four groups (quick suction, prevents water, nearly waterproof and waterproof) according to German standard DIN 52 617 (DIN 1987), see Table 7.

Table 7. Classification of materials in function of the capillary water absorption coefficient

<b>Capillary water absorption coefficient</b>	<b>Classification</b>
$A > 2.0 \text{ kg}/(\text{m}^2 \text{ h}^{1/2})$	Quick suction
$A < 2.0 \text{ kg}/(\text{m}^2 \text{ h}^{1/2})$	Prevents water
$A < 0.5 \text{ kg}/(\text{m}^2 \text{ h}^{1/2})$	Nearly waterproof
$A < 0.001 \text{ kg}/(\text{m}^2 \text{ h}^{1/2})$	Waterproof

The capillary water absorption coefficient can be determined by the capillary water absorption test based on the European standard EN ISO 15148:2002 – *Hygrothermal performance of building materials and products – Determination of water absorption coefficient by partial immersion* (EN ISO 15148: 2002). The test consists in placing a surface of each test specimen in contact with water and afterwards register the mass variation due to capillary rise as a function of time.

Table 8 presents values of capillary water absorption coefficient for some building materials. Bricks are highly capillary active, whereas granite stones and exterior renders are moderately capillary active. Conversely, ceramic tiles and thermal render systems with different coatings are hardly capillary active. They mainly act as a drainage planes. Non-porous materials such as glass, plastics and metals give almost instant run-off.

Table 8. Building material capillary water absorption coefficients (Sousa 1996, Maia, Ramos and Veiga 2018)

<b>Material</b>	<b>A</b>		<b>Classification</b>
	$\text{kg}/(\text{m}^2 \text{ s}^{1/2})$	$\text{kg}/(\text{m}^2 \text{ h}^{1/2})$	
Brick	0.0505	3.03	Quick suction
Render	0.0110	0.70	Prevents water
Granite	0.0107	0.64	
Ceramic tiles	0.0030	0.18	
Thermal render system with an organic coating	0.00156	0.09	Nearly waterproof
Thermal render system with an aqueous painting	0.00219	0.13	

### **2.3. ENERGY PERFORMANCE OF WALL ASSEMBLIES**

Exterior walls provide physical separation between the indoor space and the outdoor environment. For the purpose of this study, energy performance of a wall assembly means the calculated or measured amount of heat flux across the wall (see Figure 9) associated with the typical use of the building. The higher the heat losses during the heating season, the higher will be the quantity of energy needed for heating.

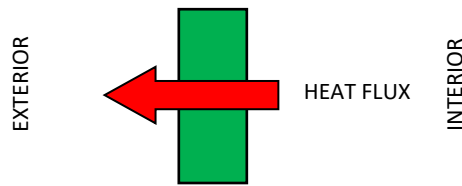


Figure 9. Schematic representation of the heat flux across a wall assembly.

The dynamic energy performance of a wall assembly depends on the hygrothermal loads acting on the wall shown in Figure 10. Generally, the hygrothermal loads show diurnal and seasonal variations at the exterior surface and mainly seasonal variations at the interior surface. The exterior wall surface heats by solar radiation, leading to evaporation of moisture from the surface layer. The exterior surface is also exposed to moisture from wind-driven rain. In terms of indoor humidity conditions, they are often influenced by the outdoor climate and by occupant behaviour. Moisture loads from the ground, from penetrating precipitation, or from construction moisture in the building materials may also increase the indoor humidity substantially. The excess of water vapor in a room must be removed by ventilation or air conditioning. In addition, humidity-buffering envelope materials, namely partition wall materials and furniture may help to dampen indoor humidity peaks (ASHRAE 2017).

Incident solar radiation is the major thermal load at the building exterior. For direct solar radiation, the resultant irradiation depends on the angle between the sun and the normal on the exposed surface and on its colour (short-wave absorptivity).

Adding exterior or interior insulation to the exterior walls can significantly improve their energy performance. That retrofit measure mainly plays an important role in reducing the heat transmission losses through the walls in the heating season and, as a consequence, contributes to reduce the buildings' energy needs for heating. Exterior insulation system is known as the most efficient insulation system, however, in case of buildings with a

worth-preserving façade, interior insulation system remains the only possible solution. If an interior insulation system is applied, the insulation layer is placed at the inner side of the existing wall. As a result, the wall temperature will strongly decrease which may induce a risk of interstitial condensation, frost damage, mould growth and other damage patterns (Vereecken et al. 2015).

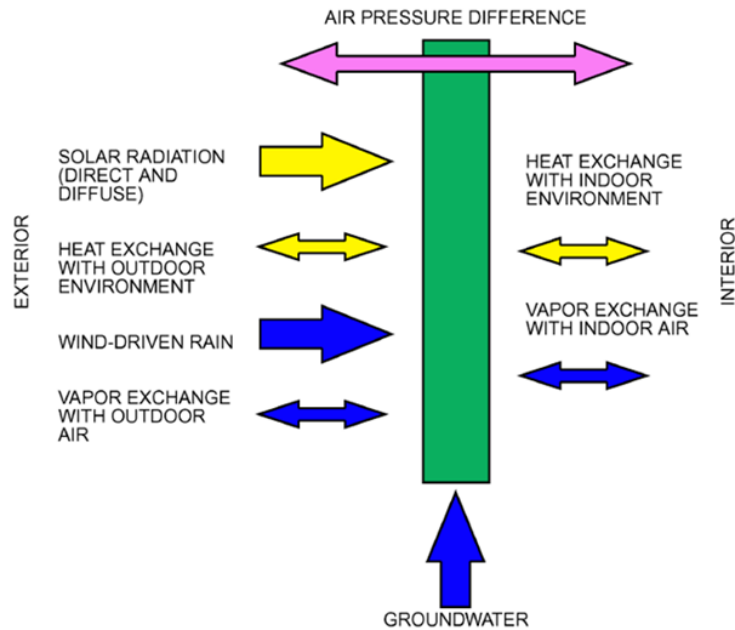


Figure 10. Hygrothermal loads and driving forces acting on an external wall (ASHRAE 2017).

The energy performance of a wall assembly is typically characterized by its thermal transmittance  $U$ . Thermal transmittance is the steady-state density of heat flow rate across a flat assembly at a temperature difference of 1 K between the surroundings of both surfaces and is expressed in units of  $W/(m^2 K)$ . The lower the thermal transmittance of a wall, the better it is the energy performance.

The most common method to determine the steady-state thermal transmittance of a wall assembly is the simplified calculation described in ISO 6946:2007 - *Building components and building elements - Thermal resistance and thermal transmittance - Calculation methods* (EN ISO 6946: 2007). This calculation method is based on the thermal conductivities and the dimensions of the materials involved and applies to elements consisting of thermally homogeneous layers (which can include air layers).

However, steady state conditions are never encountered on a site in practice and the thermal transmittance of a wall assembly depends on moisture content.

## **2.4. HYDRIC EFFECTS ON HEAT TRANSPORT ACROSS A WALL**

The hydric effects on heat transport across a wall assembly are so important that they have to be dealt with. These effects can be the following:

- Moisture-dependent thermal conductivity of building materials;
- Phase changes such as drying processes;
- Enthalpy flows as a result of liquid transport.

The dependence of thermal conductivity on the water content describes the effect of localized water on heat transport. When porous material pores are filled with water, its thermal conductivity increases (Svärd and Holstein 2015).

Evaporation (liquid to vapor) and condensation (vapor to liquid) of moisture also affects heat transport. Evaporation and condensation are examples of a change of state wherein temperature remains constant. While heat transfer whether by conduction, convection or radiation links to sensible heat, changes of state directly links to latent heat. In fact, it takes energy to remove molecules from a liquid to form a gas. To give an example, evaporation of penetrated rainwater or construction moisture in a building component absorbs a certain quantity of energy acting as a heat sink. In contrast, when the water vapor moves to a colder spot where it condenses, the heat of evaporation is released, forming a heat source. These heat sinks and heat sources not only impact the temperature in materials and assemblies but also impact the latent heat transferred (Hens 2017). If the phase change is from liquid to gas, the heat required  $Q_v$  is calculated from (Tipler and Mosca 2007):

$$Q_v = m \cdot L_v \quad (4)$$

where

m	[kg]	Mass
$L_v$	[kJ/kg]	Latent heat of vaporization (for water $L_v$ is 2257 kJ/kg)

The last effect is not very relevant. As vapor and liquid migrate, they carry their respective enthalpies, a condition which can lead to an increase of heat transfer. However, enthalpy flows as the result of vapor and liquid transport play a negligible role in comparison with the other two effects (Künzel 1995).

This study pays specific attention to the moisture-dependent thermal conductivity effect.

2.4.1. THERMAL CONDUCTIVITIES AS A FUNCTION OF MOISTURE CONTENT

This section presents a compilation of experimental results for thermal conductivities of materials as a function of moisture content or relative humidity. The materials analysed are the ones that can be part of retrofitted walls of existing buildings.

The International Energy Agency report “IEA ANNEX 24 Heat, Air and Moisture Transfer through New and Retrofitted Insulated Envelope Parts (Hamtie): Task 3 Material Properties” (Kumaran 1996) compiles lists of common building material properties from all the 14 countries that participated in the Annex, including data about the thermal conductivity of moist materials. Figure 11a and Figure 11b shows the experimental results for thermal conductivity of brick and gypsum board, respectively, as a function of moisture content. From the results it can be concluded that moisture content influences the thermal conductivity of both materials, especially that of brick. Thermal conductivity of brick increased from 1 to 2 W/(m K).

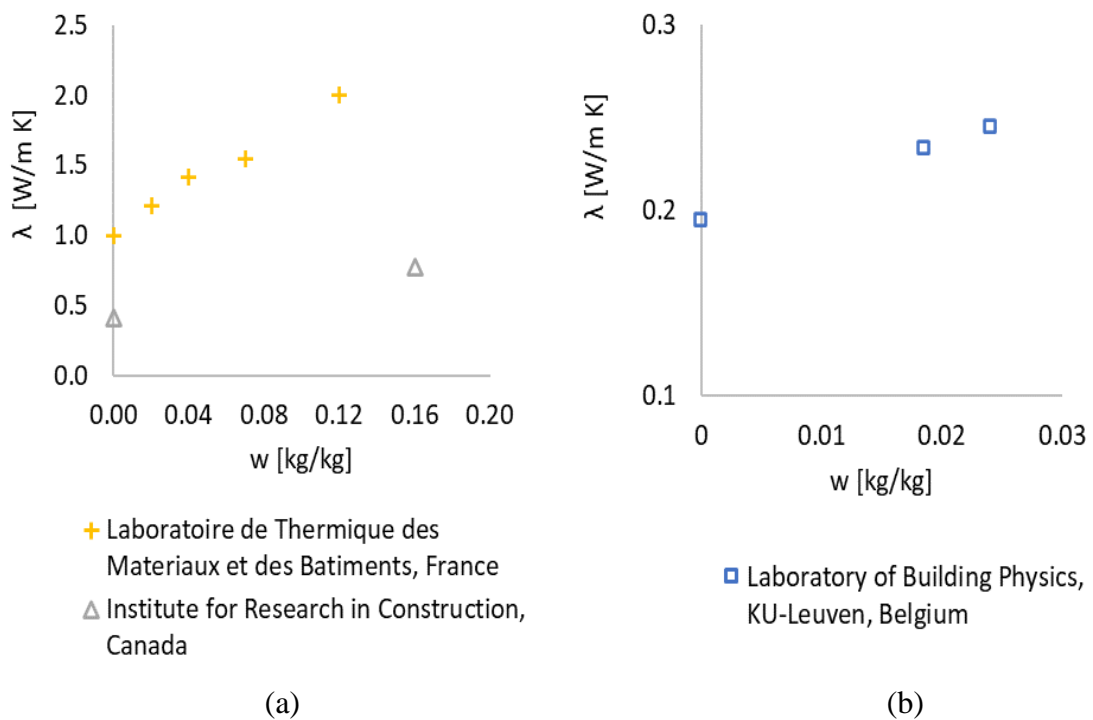


Figure 11. Thermal conductivity of a) brick and b) gypsum board as a function of moisture content (adapted from (Kumaran 1996)).

Valovirta and Vinha (2004) presented measured data of thermal conductivity not as a function of moisture content, but at various relative humidity, for building materials used in wall assemblies. Thermal conductivities of studied materials were measured with a heat flow meter. Before measurements, test specimens were positioned in certain relative

humidity conditions to achieve an equivalent moisture equilibrium. Relative humidity used were 33%, 65%, 86% and 97%. In Figure 12 obtained thermal conductivity of gypsum board and plywood are presented as a function of RH to demonstrate the effect of moisture on thermal conductivity. Thermal conductivities of mineral-wool-based products are not shown in the figure because the effect of moisture on thermal conductivity at hygroscopic range is negligible.

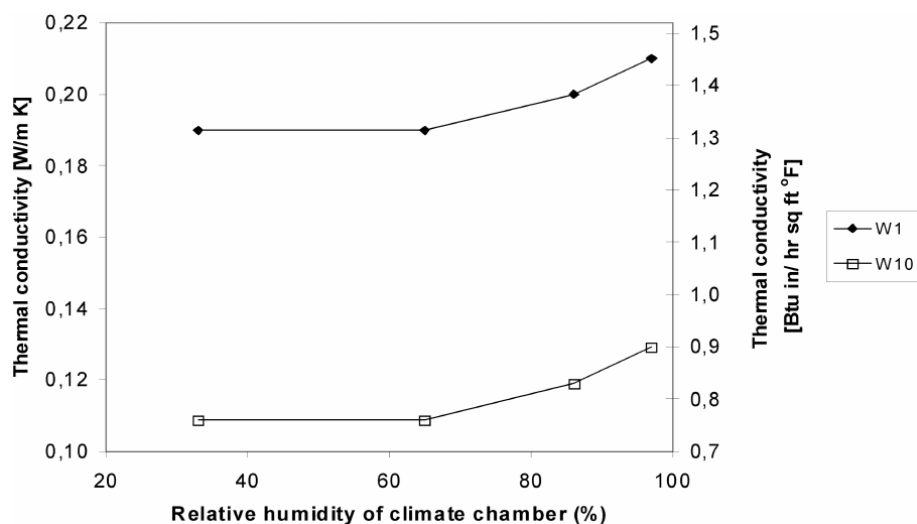


Figure 12. Thermal conductivities of gypsum board (W1) and plywood (W10) as a function of relative humidity at 10 °C mean temperature (Valovirta and Vinha 2004).

It was concluded that gypsum board and plywood had a slight rise in thermal conductivity when relative humidity increased. On the other hand, mineral wool products did not react to rise of relative humidity because they are non-hygroscopic.

Jerman and Černý (2012) presented measurements of heat and moisture transport and storage parameters including thermal conductivity in dependence of moisture content. The material analysed was a common thermal insulation material, namely mineral wool. Figure 13 presents the obtained results for the thermal conductivity of three types of mineral wools as a function of moisture content. It was concluded that the thermal conductivity of all mineral wools increased very fast with increasing moisture content. The thermal conductivity at saturation  $\lambda_{sat}$  was within a range of 0.7-0.9 W/m K. It is worth highlighting also that the reduction of the thermal insulation function was significant already for relatively low moisture contents of 5-20% by volume where  $\lambda$  was typically 0.10-0.14 W/m K.



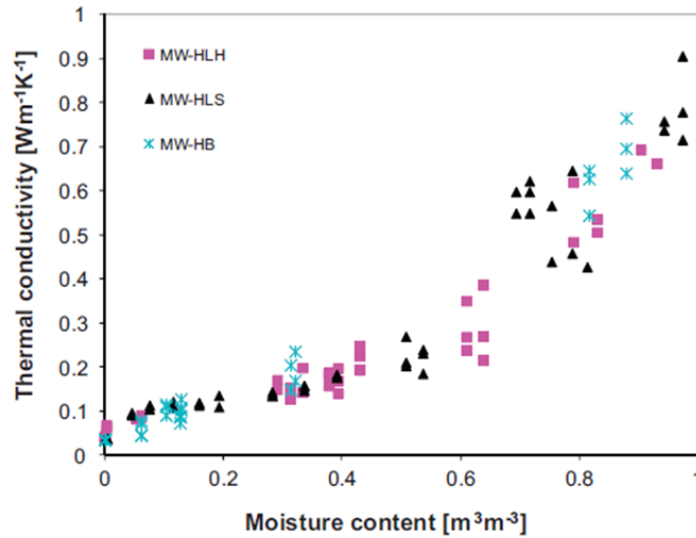


Figure 13. Thermal conductivity of three types of mineral wool (hard hydrophilic mineral wool MW-HLH, soft hydrophilic mineral wool MW-HLS and hydrophobic mineral wool MW-HB) as a function of moisture content. (Jerman and Černý 2012).

Szodrai and Lakatos (2014) investigated experimentally the effect of water on the thermal conductivity of a mineral wool and of extruded and expanded polystyrene insulating materials. Four types of insulations were measured: mineral wool, EPS30, graphite-doped EPS and a yellow Extruded Polystyrene. The samples were exposed to wetting treatment for 0 to 20 hours. The relationships between the thermal conductivities and water contents measured are presented in Figure 14.

For mineral wool, the value of thermal conductivity remains constant until the mineral wool reaches approximately 4% moisture content, above which an exponentially increasing thermal conductivity change is observed with increasing moisture content, see Figure 14a. After wetting for 20 hours, an approximately 200% change was found for the thermal conductivity change. For EPS30, a linear increase of the thermal conductivity of EPS30 as a function of moisture content is observed from measurements. After 20 hours of wetting 15% moisture content was measured, and the maximum change in the thermal conductivity was approximately 20%, see Figure 14b. For graphite-doped EPS, Figure 14c shows that the greatest amount of the water content is found to be approximately 16% but the thermal conductivity does not go significantly above 0.044 W/(m K). Finally, for the yellow extruded polystyrene, by increasing the moisture content, no significant change was observed in the thermal conductivity, see Figure 14d. This phenomena arises from the structure of the XPS materials which has small sized and closed cells so the

water cannot diffuse inside the XPS materials and can only gather on the outer surface of the material as condensed water.

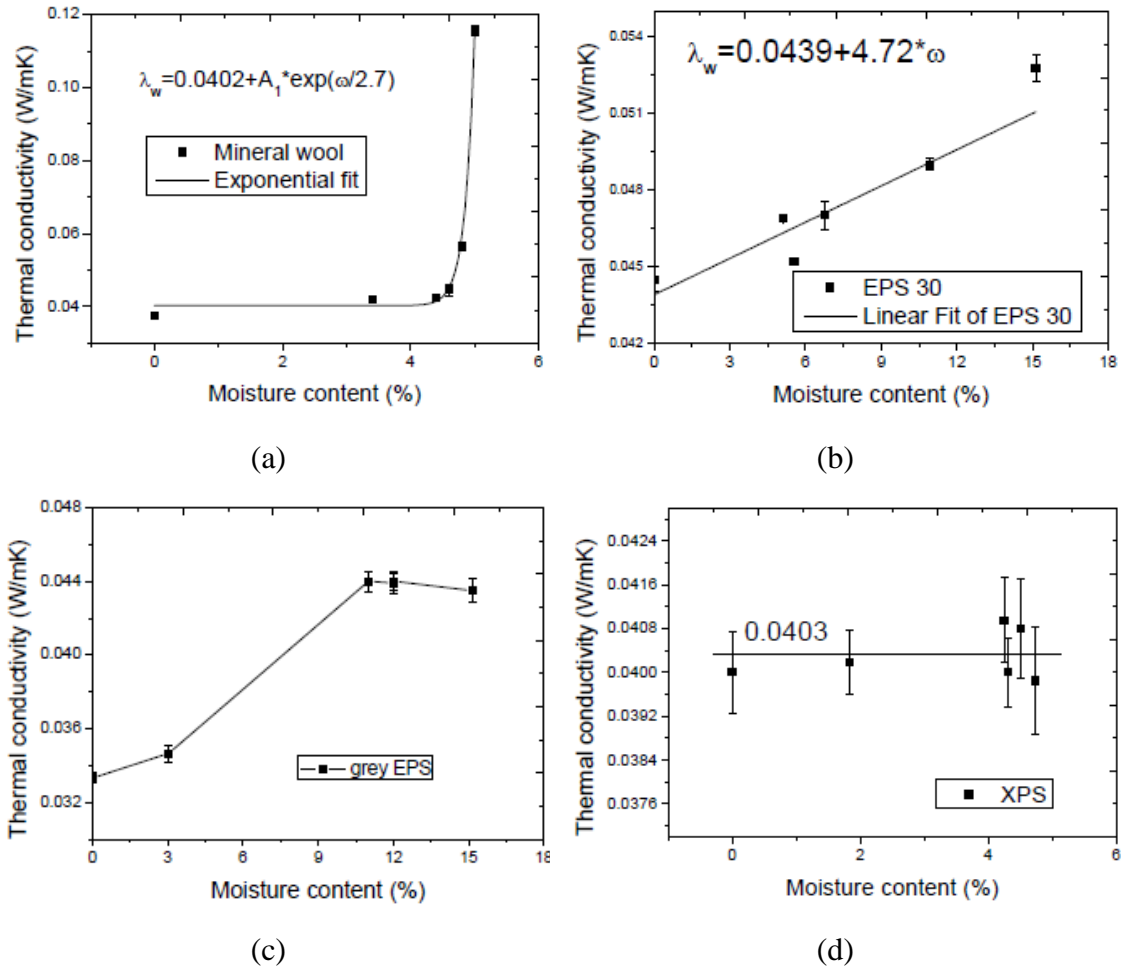


Figure 14. Thermal conductivity of a) mineral wool; b) and c) expanded polystyrene; and b) extruded polystyrene as a function of moisture content (Szodrai and Lakatos 2014).

Lakatos (2016) investigated the influence of relative humidity on the thermal conductivity of insulating materials. Three different types of polystyrene (expanded, graphite doped expanded, extruded), mineral and glass wool fibers, as well as gypsum boards were tested. The relative humidity varied from 25% to 90% at 293 K for 4 hours.

Figure 15 shows the measurements results of the thermal conductivities of the different insulation materials as a function of relative humidity. The changes in the thermal conductivities shows a slight increase for all materials. It can be seen that the greatest change belongs to gypsum boards and to graphite doped EPS.

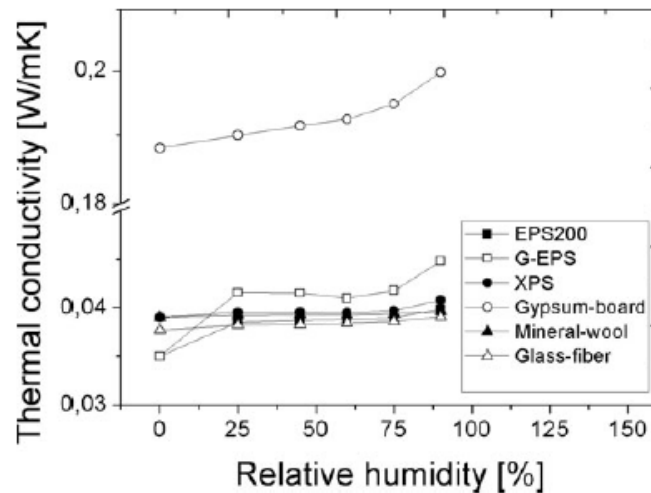


Figure 15. Thermal conductivity of six different insulation materials (three types of polystyrene (EPS 200, XPS, graphite doped EPS), two types of wool samples (glass and mineral) and gypsum boards) as a function of relative humidity (Lakatos 2016).

Koci et al. (2017) determined experimentally the thermal conductivity of characteristics types of porous building materials in the whole range of moisture content from dry to fully water-saturated state. The investigated specimens include autoclaved aerated concrete (further denoted as AAC), high performance concrete (HPC), solid clay brick (SCB), lime-cement plaster (LCP), thermal insulating plaster (TIP) containing perlite aggregates, hydrophobic mineral wool (MW) and expanded polystyrene (EPS). The results of the measurements of thermal conductivities of studied building materials as a function of moisture content are shown in Figure 16.

The effect of moisture differed case by case. Apparently, the most negative effect could be observed in the case of SCB as its thermal conductivity increased from 0.590 to 1.735 W/(m K). The thermal insulating plaster evidenced lower values of thermal conductivity than the lime-cement plaster in the whole range of moisture content. Expanded polystyrene, with its closed pore structure, was able to absorb only 3.3 % of moisture and therefore its thermal conductivity remained practically unaffected. Thermal conductivity of mineral wool increased from 0.037 to 0.772 W/(m K) which meant it was much more sensitive to moisture effects. In summary, the experimental results presented showed that the moisture effect can lead to a significant increase of thermal conductivity of porous building materials.

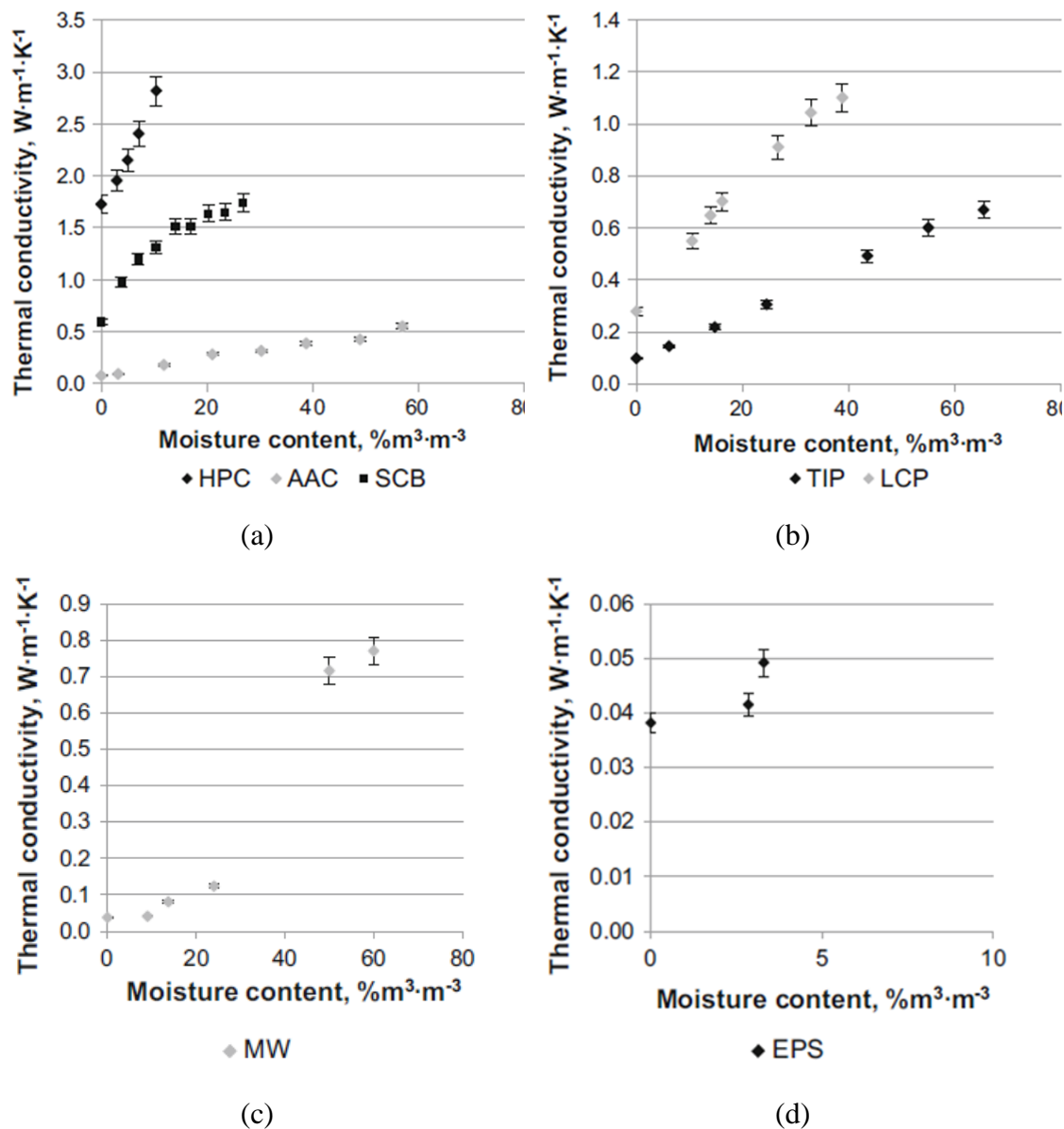


Figure 16. Thermal conductivity of a) load bearing materials; b) plasters; c) MW; and d) EPS as a function of moisture content (Kočí et al. 2017).

Gomes et al. (2017) carried out an experimental campaign to evaluate the influence of the moisture content on the thermal conductivity of 17 cement-based thermal mortars (N1 to N17). These mortars have different lightweight aggregates (expanded clay, expanded cork, silica aerogels), binders (cement, aerated lime, fly ash) and admixtures/addition. Also, they have low bulk density values (367-836 kg/m<sup>3</sup>) and low thermal conductivity values (below 0.2 W/m K). Figure 17 shows the different mortars' behaviour in the presence of moisture. The experiment results have demonstrated that the thermal

conductivity of cement-based thermal mortars is significantly dependent on moisture content.

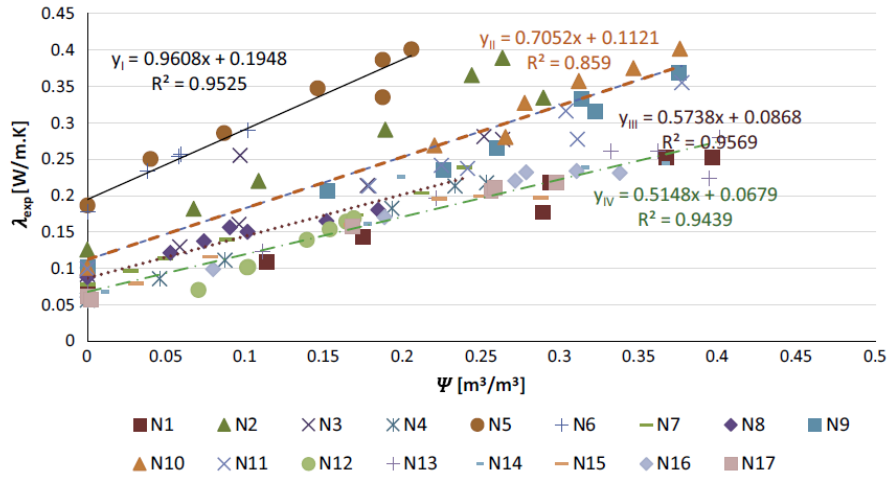


Figure 17. Thermal conductivity of cement-based thermal mortars as a function of moisture content (Gomes et al. 2017).

Maia, Ramos and Veiga (2018) performed an extensive laboratory characterization, measuring physical and hygrothermal material properties of three thermal render systems. Each system consists of a thermal render and a finishing render. Figure 18 analyses the relation between thermal conductivity and moisture content of the studied thermal renders, TR1, TR2 and TR3 which have different binders (lime, mixed binders and gypsum, respectively) and aggregates (EPS, EPS and cork, respectively). It was verified that thermal conductivity linearly increases with water content, so thermal performance can be directly compromised if hydric behaviour is unfavorable. Consequently, the application of finishing coatings with low capillary absorption is decisive for the successful use of external thermal render systems in building envelopes.

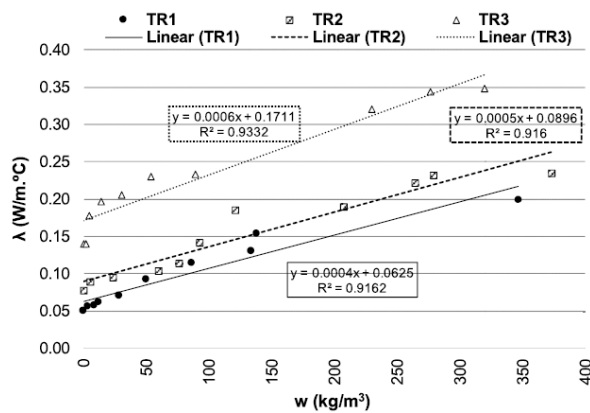


Figure 18. Thermal conductivity of thermal renders as a function of moisture content (Maia, Ramos and Veiga 2018).

#### 2.4.2. IMPACT OF MOISTURE ON THE ENERGY PERFORMANCE OF EXTERIOR WALLS

This section presents several studies, experimental and numerical, that investigated the effect of the climate and wind-driven-rain on the thermal transmittance or thermal resistance of different types of exterior walls.

De Freitas (1992) analysed the influence of moisture on thermal resistance of building elements by use of TRHUMIDADE, a program that he had developed. It was concluded that the humidification of building elements can significantly decrease their thermal insulation. In the case of an uncoated solid brick walls, the direct incidence of rainwater humidifies it and reduces its thermal resistance by 60% over a period of 70 hours of soaking (see Figure 19).

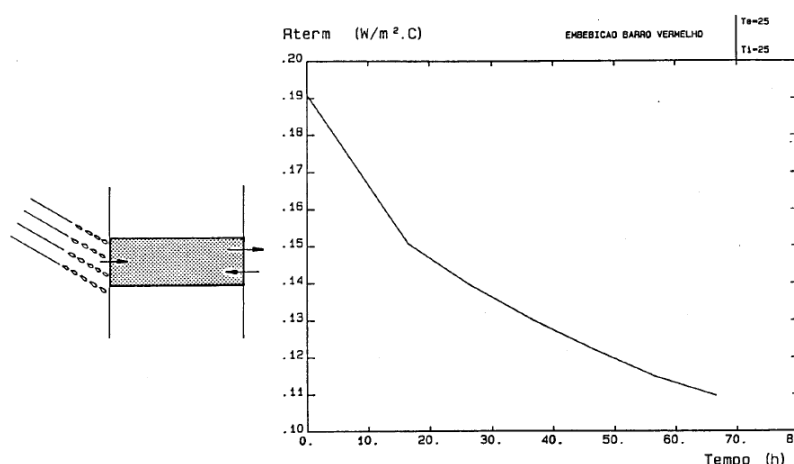


Figure 19. Variation of thermal resistance of an uncoated solid brick wall subjected to continuous humidification (De Freitas 1992).

Jakovics et al. (2014) carried out an experimental research in Riga, Latvia. Five experimental test buildings were built (see Figure 20a). They are identical except external walls for which different materials were used. For all types of external wall constructions, namely ceramic block with external insulation (type CER), aerated concrete with external insulation (type AER), plywood boards with mineral wool filling (type PLY), polystyrene filled ceramic blocks (type EXP) and log house with internal insulation (type LOG) the U-value, calculated according to the standard EN ISO 6946, equals 0.16 W/(m<sup>2</sup> K). Measurements were carried out using long-term monitoring of heat flux (see Figure 20b) and the obtained results for all test buildings are presented in Figure 20c.

The authors state that the variation in determined U-values shown above is mainly caused by different humidity conditions of the wall structures. They also concluded that after one

year of operation, wet constructions dry out and room's air humidity decreases which means decreasing in heating energy consumption for the next heating seasons.

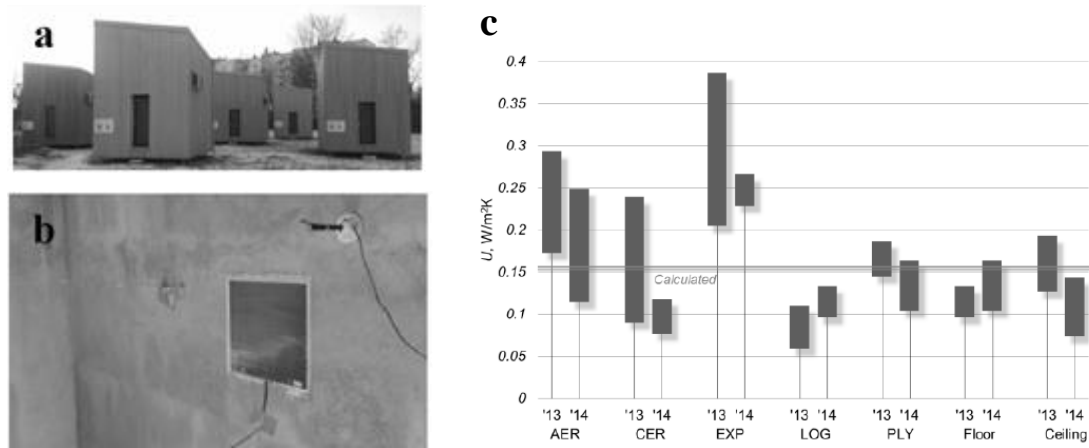


Figure 20. a) Experimental test buildings; b) Heat flux density measurements; c) Measured U-values of external walls for all test buildings just after test buildings were built (in 2013) and after one year of operation (in 2014) (Jakovics et al. 2014).

Lakatos and Kalmár (2014) gave predictions for the change of the thermal transmittance (U-value) of an insulated wall in function of moisture content. Five different EPS with 0.1 m thickness were tested (EPS 30, 100, 150, 200 and grey). These materials were combined with concrete and brick with 0.4 m thickness. The U-values were calculated based on the thermal conductivity measurements. Figure 21 shows the estimated U-values (Concrete + EPS and Brick +EPS) in function of the moisture content. The slight increasing U-values in function of moisture content can be observed. The authors verified also that water causes greater increase in the U-value of the brick than the concrete's.

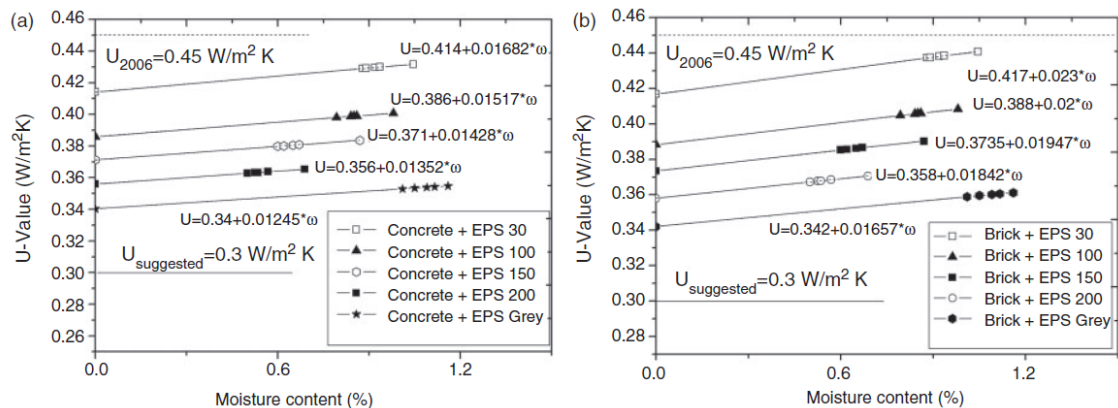


Figure 21. (a) Calculated U-values in function of moisture content for 0.4 m thick concrete wall in combination with different EPS materials with 0.1 m thickness and (b) calculated U-values in function of moisture content for 0.4 m thick brick wall in combination with different EPS materials with 0.1 m thickness (Lakatos and Kalmár 2014).

Vereecken and Roels (2015) compared the hygrothermal performance of a capillary active interior insulation system to this of a tradition vapour tight system. Both interior insulation systems were applied to the 29 cm thick masonry brick walls with north-west orientation and located in Essen, Germany. The insulation thicknesses were chosen in such a way that the dry thermal performance at 50% relative humidity is equal for both walls ( $R_{dry} = 1.56 \text{ m}^2 \text{ K/W}$ , which corresponds to a  $U_{dry} = 0.64 \text{ W}/(\text{m}^2 \text{ K})$ ). The impact that wind-driven rain has on the hygrothermal behaviour of the retrofitted walls have been analysed with HAMFEM, a program that solves the conservation equations of energy and mass by means of a finite element method. The influence of the accumulated moisture content on the thermal resistance is shown in Figure 22, where the absolute decrease in thermal resistance is defined by  $R_{dry} - R_{wet}$ .

The wind driven rain loads are found to influence the thermal resistance. The largest decrease in total thermal resistance (compared to the dry thermal performance) is found for the capillary active system at the beginning of June, due to the large wind driven rain peak. A decrease of more than 30% is found. However, this decrease is of minor importance given its appearance during the summer. During the heating season, a decrease up to  $0.2 \text{ m}^2 \text{ K/W}$  is found, which corresponds to a decrease of approximately 15%. For the vapor tight system, a smaller decrease in thermal resistance is found. It was also found that if no wind-driven rain is included, the accumulated moisture content in the brick layer is negligible.

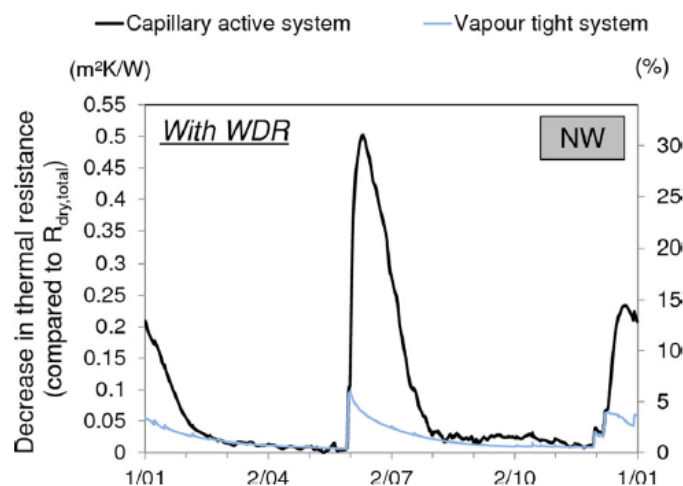


Figure 22. Decrease in thermal resistance for the total wall assemblies (Vereecken and Roels 2015).



Pérez-Bella et al. (2015) proposed a correction factor called CCF (conductivity correction factor) to calculate the design thermal conductivity of construction materials at different locations of Spain based on the normative/declared thermal conductivities, tabulated in building regulations and determined under standardized and constant environmental conditions. For this purpose, the declared thermal conductivities of the materials are multiplied by the CCF value for each location, which is representative of the characteristic environmental conditions of the respective site. Available mean annual climatic data were used to determine the CCF values. As a result, a map that shows the correction factors to be applied in 52 province capitals of Spain was created (Figure 23). The proposed correction factors CCF are quite high, ranging from 2.35 to 4.03. Higher correction factors can be observed in coastal areas given the higher mean relative humidity values.

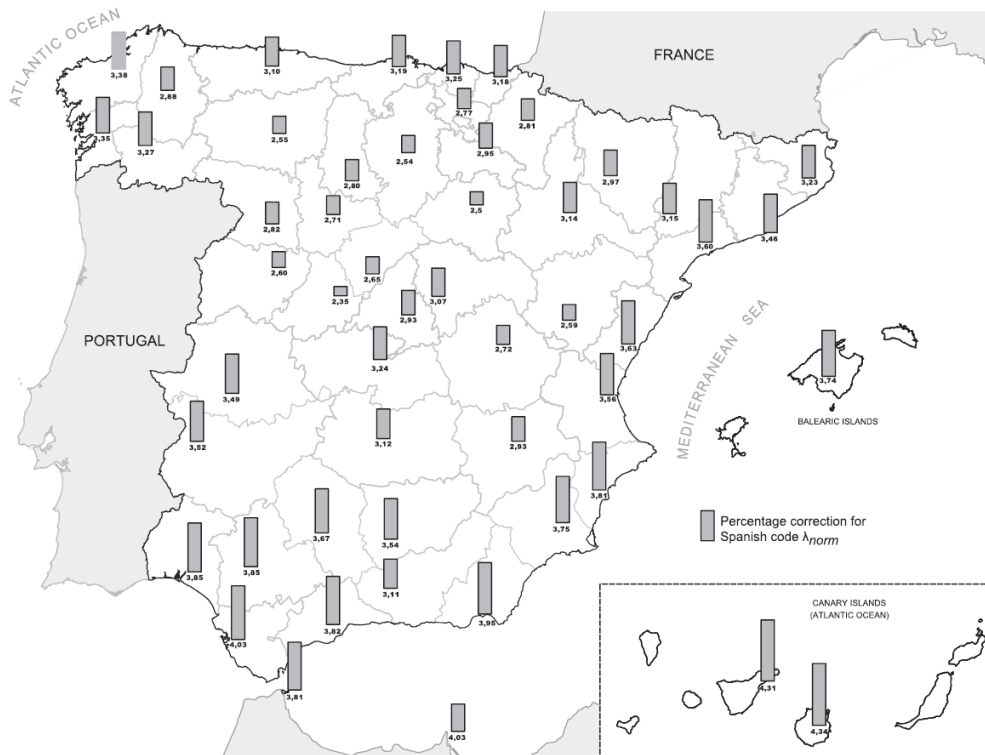


Figure 23. Map that indicates de CCF proposed values in Spain (percentage value) (Pérez-Bella et al. 2015).

Coelho and Henriques (2016) analysed the influence of wind-driven rain on the hygrothermal behaviour of uncoated solid brick walls (with 220, 335 and 450 mm of thickness) with a southwest orientation and located in Lisbon, San Francisco and Montreal, using the Wufi 4.2 Pro software. That study quantified the difference between the steady-state thermal transmittance (obtained with the material’s dry thermal

conductivity  $\lambda_0$ ) and the transient thermal transmittance (obtained with the material's moist thermal conductivity  $\lambda_w$ ) for the same wall. The obtained results are presented in Figure 24. The wetting phase (increase of the water content) occurs between the beginning of October and the end of February, and the drying phase (decrease of the water content) occurs between the beginnings of March and the beginning of October.

Cases	$U_{WUFI}$ [W/m <sup>2</sup> K]	Annual		Wetting phase		Drying phase	
		$U_A$ [W/m <sup>2</sup> K]	Relationship	$U_W$ [W/m <sup>2</sup> K]	Relationship	$U_D$ [W/m <sup>2</sup> K]	Relationship
Standard-case	1.817	2.172	19.5%	2.268	24.8%	2.111	16.2%
340 mm	1.332	1.726	29.5%	1.741	30.7%	1.716	28.8%
450 mm	1.071	1.453	35.7%	1.460	36.3%	1.449	35.3%

(a)

Cases	$U_{WUFI}$ [W/m <sup>2</sup> K]	Annual		Wetting phase		Drying phase	
		$U_A$ [W/m <sup>2</sup> K]	Relationship	$U_W$ [W/m <sup>2</sup> K]	Relationship	$U_D$ [W/m <sup>2</sup> K]	Relationship
Standard-case	1.817	1.995	9.8%	1.922	5.8%	2.011	10.7%
340 mm	1.332	1.491	11.9%	1.443	8.3%	1.502	12.8%
450 mm	1.071	1.214	13.4%	1.184	10.5%	1.222	14.1%

(b)

Cases	$U_{WUFI}$ [W/m <sup>2</sup> K]	Annual		Wetting Phase		Drying Phase	
		$U_A$ [W/m <sup>2</sup> K]	Relationship	$U_W$ [W/m <sup>2</sup> K]	Relationship	$U_D$ [W/m <sup>2</sup> K]	Relationship
Standard-case	1.817	2.251	23.9%	2.266	24.8%	2.231	22.8%
340 mm	1.332	1.754	31.7%	1.770	32.8%	1.733	30.1%
450 mm	1.071	1.461	36.4%	1.471	37.4%	1.447	35.1%

(c)

Figure 24. Thermal transmittance calculated in steady-state conditions ( $U_{WUFI}$ ) and thermal transmittance in transient conditions for a year and for the adopted wetting and drying phases, and the relationship between the steady and transient thermal transmittances for the standard-case, and 340 mm and 450 mm solid brick layer cases in: a) Lisbon; b) San Francisco; and c) Montreal (Coelho and Henriques 2016).

It was verified that the wind-driven rain has a key influence on the hygrothermal behaviour of high capillary water uptake walls, such as solid brick walls, and therefore calculating the thermal transmittance  $U$  in steady-state conditions can have a significant error for this type of walls. It was also verified that the higher the solid brick layer thickness, the higher will be the difference between the steady-state thermal transmittance and transient thermal transmittance. This derives from the fact that for a smaller thickness, moisture will dry faster.

Alonso-Alonso (2017) did a numerical study of hygrothermal behaviour of an open-joint ventilated granite façade in northwest Iberian Peninsula (warm climate with high rainfalls) using Wufi Pro 5.3 software. Figure 25 shows the values of thermal transmittance of the façade obtained. It was verified that the most unfavourable  $U$ -value of the winter months with rainfall was 44% more unfavourable than the  $U$ -value of July,

the most favourable month. It should also be noted that the thermal transmittance for materials subjected to 80% relative humidity (U 80%) increased dry transmittance (U seco) value by 4%.

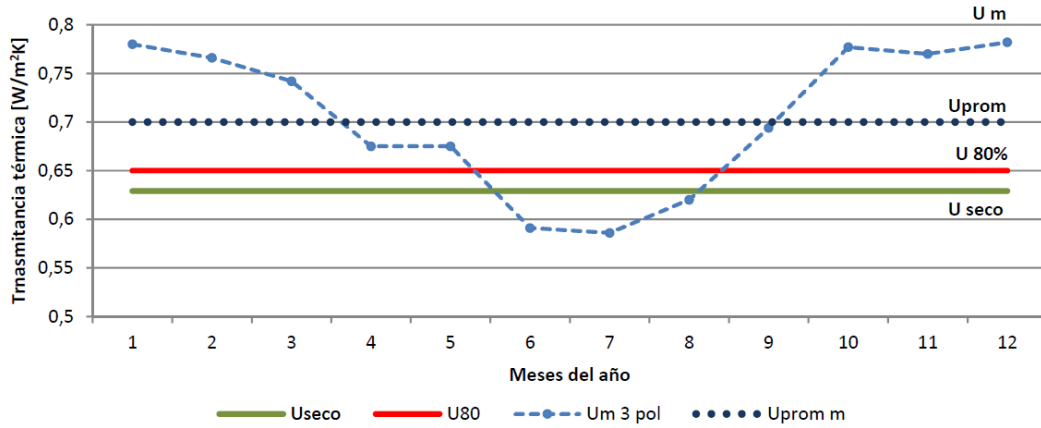


Figure 25. Values of thermal transmittance in steady-state conditions U dry and U 80% relative humidity, and in transient conditions U monthly for the open-joint ventilated façade facing north in A Coruña. Wufi Pro 5.3 results. (m-monthly; prom-average; seco-dry) (Alonso Alonso 2017).

The use of monthly thermal transmittances (U m) supposes to consider an increase of the energy losses of the ventilated façade of granite of 15.6% with respect to the dry thermal transmittance (U seco), that is to say, to pass from 21.2 kWh m<sup>2</sup>/year to 24.5 kWh m<sup>2</sup>/year (Figure 26).

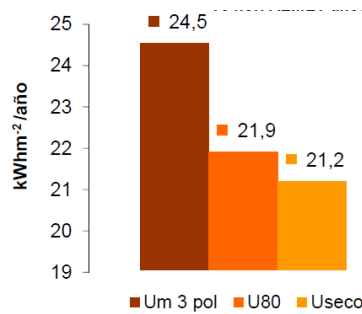


Figure 26. Comparison of energy losses calculated from the different thermal transmittance values previously presented in Figure 25 (Alonso Alonso 2017).

Finally, by submitting the same envelope in the numerical simulation program Wufi Pro 5.3 for different climatic classifications, a difference of 10% lower in thermal transmittance in Madrid than in A Coruña was found as it is shown in Figure 27. The author states that these variations were correlated with greater or lesser amount of rain and/or humidity in the climatic classification.

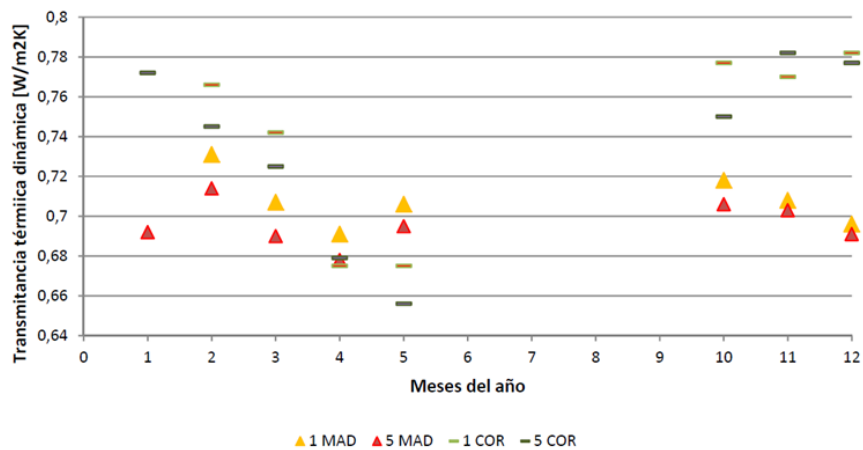


Figure 27. a) Comparison of monthly thermal transmittances of the 1<sup>st</sup> and 5<sup>th</sup> year between Madrid (MAD) and A Coruña (COR); b) Variation in percentage between the values for the 5<sup>th</sup> year (Alonso Alonso 2017).

Fino, Tadeu and Simões (2018) studied experimentally and numerically a wall covered with uncoated medium density expanded cork board (eco-efficient insulation material) during exposure to rain. The specimen was installed inside a hot box. Rainy periods were simulated by setting up a water system in the out chamber to wet the test specimen with a spray flow of 1 L/ (m<sup>2</sup> min). Thermocouples and heat flux sensors were installed to monitor the test prototype. The heat flux sensors were installed on the interior surface and the thermocouples were installed on both surfaces of the test specimen and at different depths, as illustrated in Figure 28.

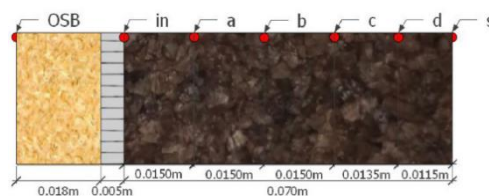


Figure 28. Cross-section of the specimen. Position identification of the thermocouples and heat flux sensors (Fino, Tadeu and Simões 2018).

Figure 29 presents the experimental and analytical temperatures and heat fluxes in winter conditions before, during and after wetting.

The results show that during the rainy period, water penetration in the wall is limited to the surface layers, namely to positions s, d and c. This means that the changes in the hygrothermal material properties, namely the thermal conductivity  $\lambda$ , are almost entirely limited to first layers of the expanded cork board and to the rainy period.

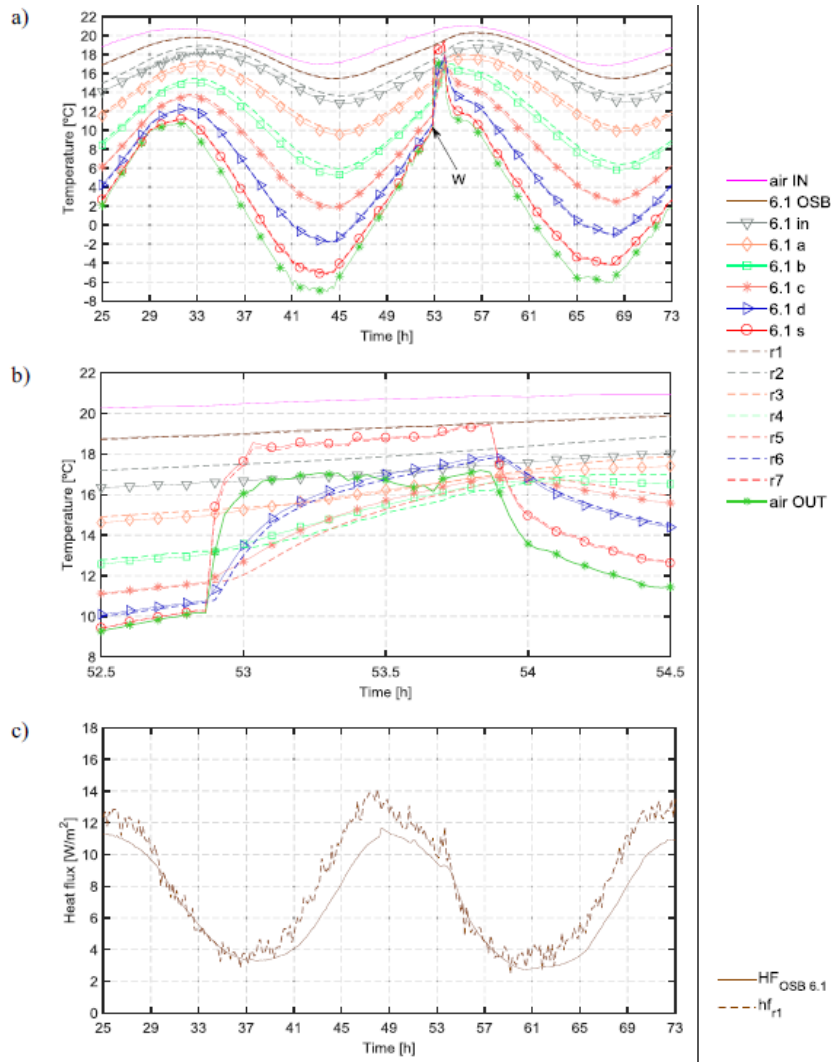


Figure 29. Experimental (solid lines) and analytical (dashed lines) temperatures along the thickness of the wall in winter conditions as boundary conditions: a) before, during and after wetting; b) during wetting; c) heat fluxes. The number 6.1 is the number of the panel on which the group of the thermocouples was placed. The numbering used in the analytical model r1, r2, r3, r4, r5, r6 and r7 relates to the thermocouple positions OSB, in, a, b, c, d and s, respectively. (Fino, Tadeu and Simões 2018).

Maia, Ramos and Veiga (2018) analysed the influence of different European climates (Porto, Nancy and Oslo) on the performance of different thermal render systems with north and south orientations, using WUFI Pro software. The analysed systems were three different thermal renders systems (S1, S2 and S3) and an external thermal insulation composite system (ETICS). Systems S1 and S2 formulated with EPS aggregates and lime or mixed binders were simulated as exterior insulation solutions, whereas system S3 formulated with cork aggregates and gypsum as a binder was simulated as an interior solution. Two solar absorption coefficients were selected, namely 0.27 (white render) and 0.80 (dark render).

The obtained monthly ratio between average and reference U-values, i.e. between transient and steady-state U-values, for the simulated scenarios are presented in Figure 30 and Figure 31.

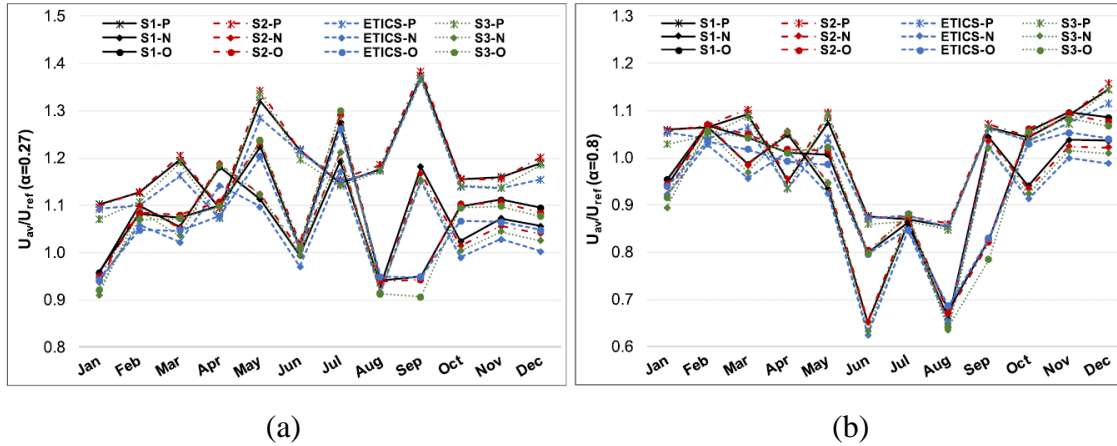


Figure 30. Monthly ratio between average and reference U-values in Porto, Nancy and Oslo, with north orientation, for solar absorption of: a) 0.27 and b) 0.8

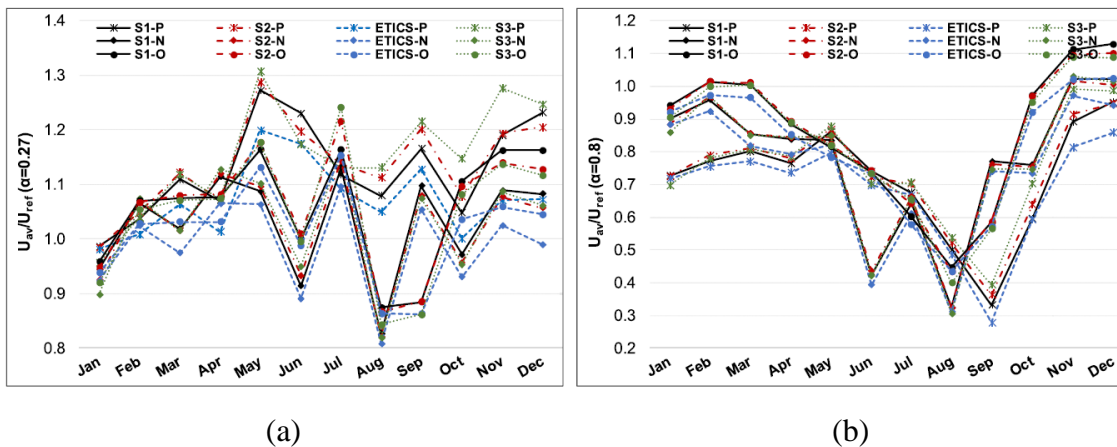


Figure 31. Monthly ratio between average and reference U-values in Porto, Nancy and Oslo, with south orientation, for solar absorption of: a) 0.27 and b) 0.8

It was verified that the lighter coating with solar absorption coefficient equal to 0.27 implies a lower drying process, increasing the water content and consequently the average U-value, compromising the hygrothermal performance of the whole system. Also, the hygrothermal simulation performed demonstrated that the finishing coating have a significant impact on the hygrothermal behaviour of the whole system. The application of finishing coatings with low capillary absorption is decisive for the successful of thermal renders systems in building envelopes as exterior insulation solutions.

## 2.5. SYNTHESIS OF THE AVAILABLE KNOWLEDGE

The studies about the influence of moisture on the energy performance of building materials and wall assemblies were reviewed. That influence can vary as it depends on temperature, wind-driven rain, local exposure conditions, finishing coating’s capillary water absorption and constructive solution.

The influence of moisture on the thermal conductivity of building materials has already been quantified. In fact, in the literature it was found measurements of thermal conductivities  $\lambda$  of building materials as a function of moisture content. Specific attention is paid to materials that compose the retrofitted walls of existing buildings. Table 9 and Figure 32 give an overview of that results. The results demonstrate that the thermal conductivities are considerably affected by moisture content. The greatest increase in thermal conductivity belongs to brick (from 1 to 2 W/(m K)), mineral wool (from 0.04 to 0.12 W/(m K)) and thermal renders (from 0.08 to 0.19 W/(m K)). For gypsum board the thermal conductivity increased from 0.20 to 0.25 W/(m K), whereas for expanded polystyrene (EPS) the thermal conductivity increased from 0.044 to 0.052 W/(m K). Conversely to the other materials, no relevant change was observed in the thermal conductivity of extruded polystyrene (XPS) with increasing moisture content.

Table 9. Overview of the thermal conductivity of building materials as a function of moisture content.

Material	Water content (Kg/Kg)	Thermal conductivity (W/m K)	Variation (%)
Brick	0; 0.02; 0.04; 0.07; 0.12	1; 1.21; 1.42; 1.55; 2	100
Mineral wool (MW)	0; 0.040; 0.047; 0.050	0.04; 0.04; 0.06; 0.12	200
Gypsum board (GB)	0; 0.019; 0.024	0.195; 0.234; 0.245	26
Expanded polystyrene (EPS)	0; 0.06; 0.15	0.044; 0.046; 0.052	18
Extruded polystyrene (XPS)	0; 0.05	0.04; 0.04	0
Thermal render (TR1) EPS aggregates and lime binder	0; 0.14; 0.24	0.05; 0.07; 0.09	84
Thermal render (TR2) EPS aggregates and mixed binders	0; 0.06; 0.30	0.077; 0.095; 0.185	140

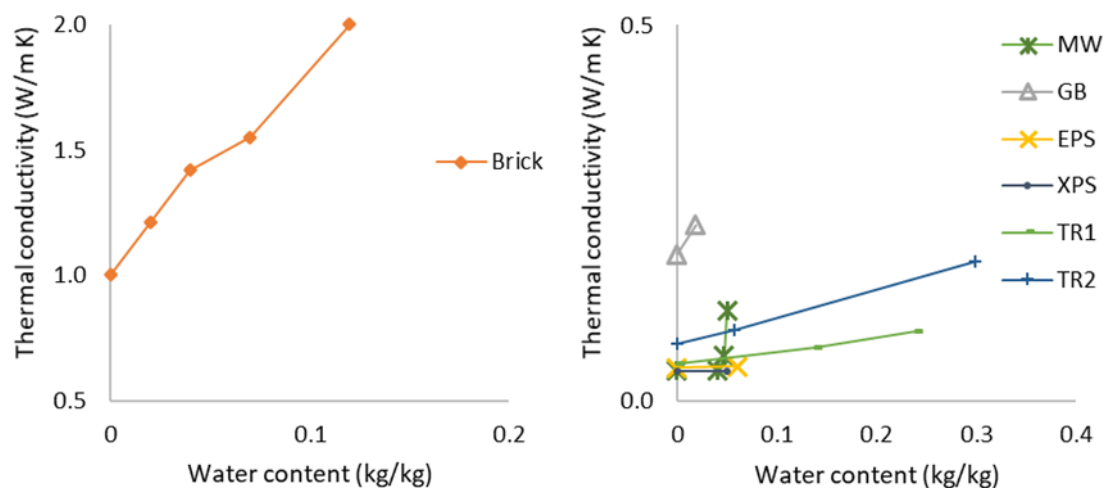


Figure 32. Overview of the thermal conductivity of building materials as a function of moisture content.

Moreover, several studies, experimental and numerical, that investigated the effect of the climate and wind-driven rain on the thermal transmittance  $U$  of different types of exterior walls were analysed. Table 10 gives an overview of the main results. For the applied climatic conditions, the maximum difference between the thermal transmittance of a dry assembly and the thermal transmittance of a moist assembly was, on average, around 30%, depending on the composition of the wall assembly. Therefore, it can be concluded that the humidification of exterior walls can significantly worsen their energy performance.

Another conclusion from the literature review is that wind-driven rain may considerably affect the thermal transmittance of an exterior wall whereas air relative humidity may not influence as much.

Finally, it was found out a lack of experimental studies about the influence of moisture and relative humidity on the heat losses through retrofitted walls of existing buildings which motivates this research work. Furthermore, an investigation of the impact of local climate conditions including wind-driven rain on the dynamic energy performance of retrofitted walls is also lacking.



Table 10. Overview of the results considering the influence of moisture on the energy performance of exterior walls.

Location	Moisture source	Wall assembly composition	U-dry (W/m <sup>2</sup> K)	Orientation	Analysis type	Maximum difference between U-dry and U-wet
-	70 hours of soaking	Uncoated solid brick wall	2.78	-	Simulation TRHUMIDADE	+60%
Riga, Latvia	-	Perforated ceramic blocks (440 mm) with mineral wool outside (type CER)	0.16	-	Measurements	+81%
		Aerated concrete blocks (375 mm) with mineral wool outside (type AER)				+50%
		Modular plywood panels with mineral wool filling (200 mm) and fibrolite (70 mm) inside (type PLY)				+138%
		Perforated ceramic blocks (500 mm) filled with insulating granules (type EXP)				-19%
		Laminated beams (200 mm) with mineral wool and wood paneling inside (type LOG)				+13%
Essen, Germany	WDR	29 cm brick masonry wall-0.4 cm glue mortar-7.5 cm calcium silicate (CaSi)-1 cm plaster	0.64	North-west	Simulation HAMFEM	+16%
		29 cm brick masonry wall-3.88 cm extruded polystyrene (XPS)-1.25 cm uncoated gypsum board				+5%
Lisbon, Portugal San Francisco, USA Montreal, Canada	WDR	Uncoated solid brick wall	220 mm	Southwest	Simulation WUFI Pro	+25%
			335 mm			+33%
			450 mm			+37%
A Coruña, Spain	-	Open-joint ventilated façade 3 cm granite-5 cm air cavity-4 cm polyurethane-25 cm concrete-3 cm granite	0.63	North	Simulation WUFI Pro	+22%
Porto, Portugal Nancy, France Oslo, Norway	-	S1: organic coating- 0.4 cm finishing render-6 cm thermal render (binder: lime; aggregates: EPS)-26 cm aerated concrete-1.5 cm gypsum plaster	0.30	North South	Simulation WUFI Pro	+24%
		S2: painting-0.4 cm finishing render-6 cm thermal render (binder: mixed binder; aggregates: EPS) 32.5 cm aerated concrete-1.5 cm gypsum plaster				+20%
		S3: 0.4 cm finishing render -38 cm aerated concrete-6 cm thermal render (binder: gypsum; aggregates: cork)-0.2 cm finishing render				+28%



# 3

## EXPERIMENTAL ASSESSMENT OF THE IMPACT OF WETTING PERIODS ON THE ENERGY PERFORMANCE OF RETROFITTED WALLS

### 3.1. METHODOLOGY

In order to (1) assess experimentally the impact of wetting periods on the energy performance of retrofitted walls and to (2) collect experimental measurements for validate the selected hygrothermal model, an experimental prototype was developed at the Building Physics Laboratory of the Faculty of Engineering University of Porto. Two wall test specimens (specimen A and specimen B) were built and tested inside a rain chamber composed of two rooms, the control room and the rain room. The rain chamber already existed in the laboratory while the wall test specimens did not. Figure 33 presents that experimental prototype.

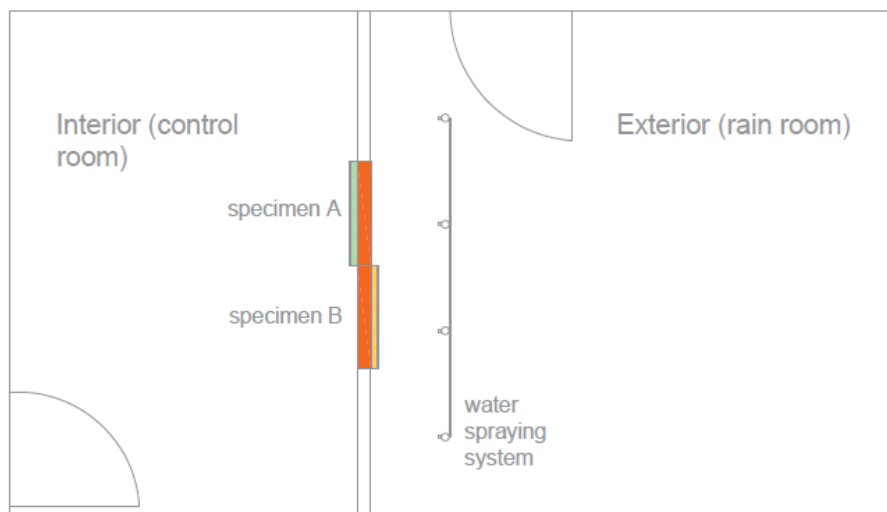


Figure 33. Schematic representation of the experimental prototype.

The tests simulated the exposure of the specimens to a temperature gradient as well as to rainy periods, while a continuous measurement of temperature and relative humidity profiles and heat fluxes through the specimens' surfaces were recorded. Measurements were recorded every 10 minutes. The tests were performed with no wind pressure against the specimens due to restrictions imposed by the COVID-19 pandemic which made the experimental campaign shorter than anticipated.

Over the experimental laboratory work, different precipitation sequences were applied against the specimens. The continuous measurements of surface temperatures, temperature and relative humidity profiles and heat fluxes during the experiments allow a detailed understanding of the specimens' performance.

Below, the investigated wall configurations, the rain chamber, the monitored parameters and the rain sequences and boundary conditions are described. Next, an overview of the results is given. Attention is paid to temperature profiles, relative humidity between masonry and insulation and heat fluxes across the specimens' surfaces. To end, the main conclusions are summarized.

## **3.2. EXPERIMENTAL TEST SETUP**

### **3.2.1. WALL ASSEMBLIES**

The hygrothermal behaviour of single leaf masonry assemblies with different insulation systems were experimentally studied. The investigation was performed on wall test specimens of 0.8 m in length and 2 m in height: specimen A and specimen B. Both consists of a solid brick layer and an insulation system. A traditional interior insulation system was applied to specimen A and an external insulating render system was applied to specimen B.

From the outside to the inside, the specimen A consists of: solid brick, mineral wool and uncoated gypsum board. On its turn, from the outside to the inside, the test specimen B consists of: silicate paint (two coats), finishing render with fibre glass mesh, insulating render and solid brick. These wall assemblies and the thicknesses of each layer are schematically shown in Figure 34. The thickness of the mortar joints in the brick layers is approximately 1 cm.

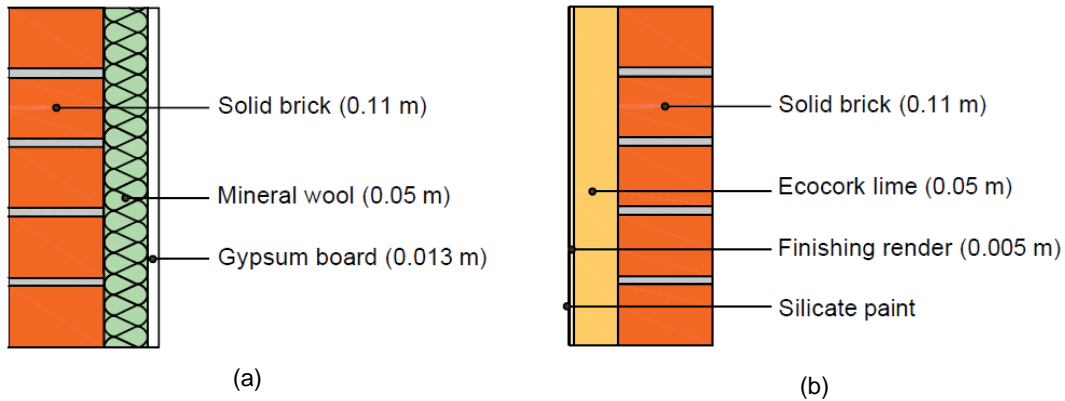


Figure 34. Cross-section of: a) wall test specimen A; b) wall test specimen B.

Dry thermal transmittances  $U_{dry}$  of test specimens A and B calculated from the dry conductivities and dimensions of their components as described in (EN ISO 6946: 2007) are 0.62 and 1.18 W/(m<sup>2</sup> K), respectively. The dry thermal resistance of solid brick masonry and the dry thermal conductivities of mineral wool, gypsum board, insulating render and finishing render considered in the calculations were 0.13 m<sup>2</sup> K/W, and 0.04, 0.20, 0.10 and 0.45 W/(m K), respectively. It should be noted that the insulation thickness applied in both systems is the same, but the thermal resistance of the insulation materials (mineral wool and insulating render) is different.

The wall test specimens were built from February to April 2019 in the Building Physics Laboratory at the Faculty of Engineering University of Porto. Figure 35 shows the construction of the specimens. First, the masonry was built (see Figure 35a) and then the insulating systems were applied. During the construction of the specimens, thermocouples and relative humidity probes were installed between the different material layers.

To construct the masonry, solid bricks with the dimensions of 225x105x70 mm (length x width x height) and consolidation mortar based on natural hydraulic lime (NHL) were used. The insulation of specimen A, namely mineral wool was placed into the cavity between the metal studs (see Figure 35b), making sure that it was correct size and fitted snugly at the sides and ends.

The insulation of specimen B, namely the insulating render, was applied in two layers with identical thicknesses. The second layer was applied after the first has started to set but was still fresh. After that, the render was left to set for five days, before applying the second stage of the system, the finishing render. Finishing render was applied at an overall

thickness of 5 mm in two passes and the fibre glass mesh was conveniently imbedded in this layer. Second coat of finishing render went on soon after the first coat and the fibre glass mesh has been applied. After that, the wall was left to dry for ten days before painting. The paint was applied by a roller. Figure 35c shows the insulating render being applied.

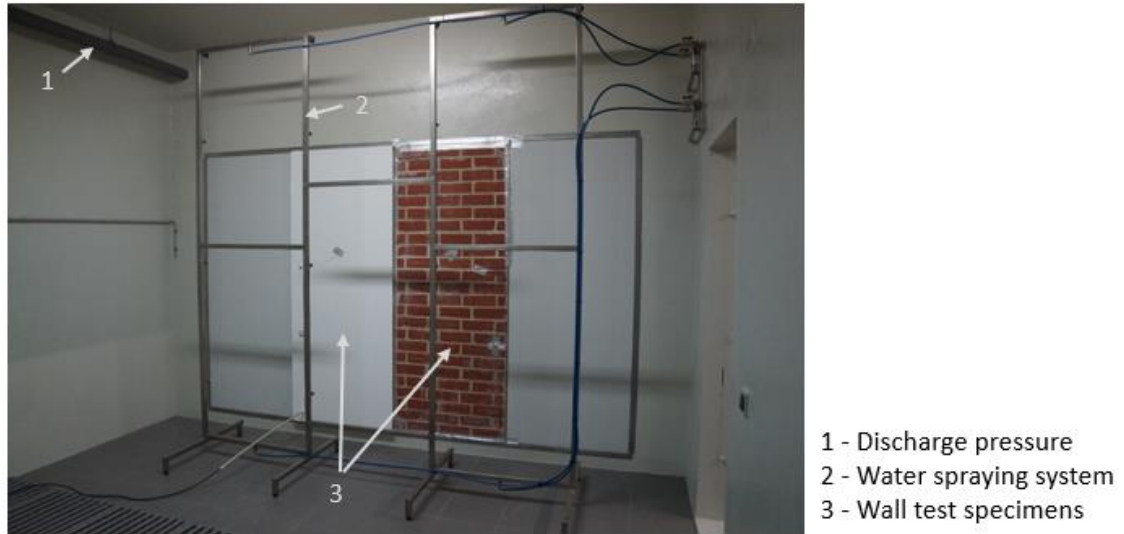


Figure 35. Construction of wall test specimens: a) construction of the solid brick masonry; b) application of the mineral wool on the interior surface of wall A; c) application of the insulating render on the exterior surface of wall B.

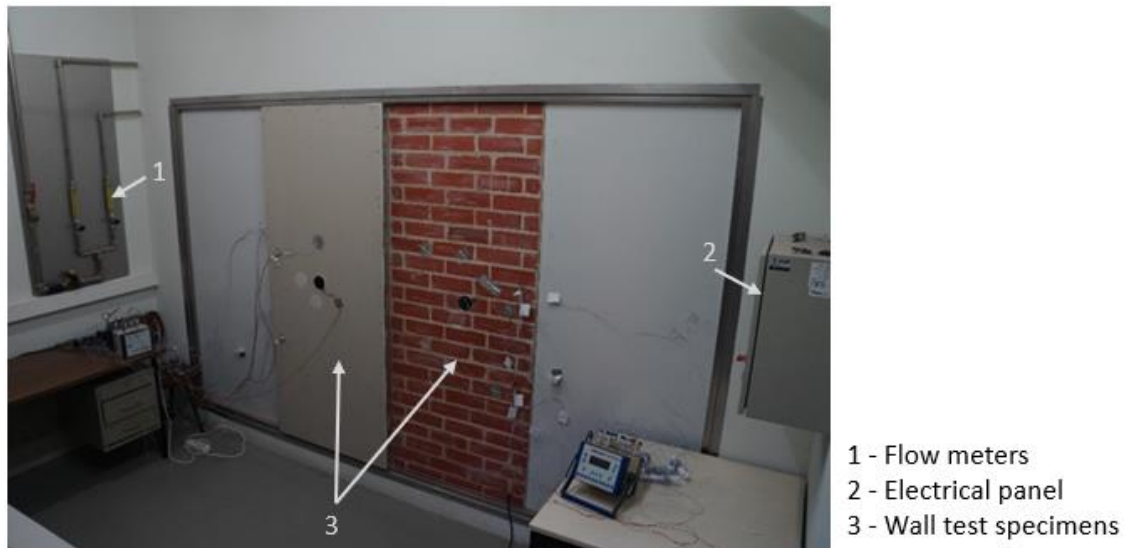
### 3.2.2. RAIN CHAMBER

The wall test specimens were built inside a rain chamber that was already available at Building Physics Laboratory. This rain chamber can simulate the dynamic nature of rain and wind pressure against the walls. The principle of the test is that the test specimens are fitted into the driving rain test apparatus and the external surfaces of the test specimens are sprayed continuously with water at a specific rate while the pulsating air pressure difference is increased in specified steps (EN 12865: 2001).

As previously mentioned, the rain chamber is composed of two parts: a rain room that simulates the outside environment and a control room that simulates the indoor conditions. The test specimens are between those rooms. The rooms of the rain chamber have no ventilation systems. Figure 36 shows photographs of the rain chamber and the test specimens. In Figure 36a, the external surfaces of the test specimens are displayed, whereas in Figure 36b the internal surfaces are displayed.



(a)



(b)

Figure 36. Rain chamber and its components: a) rain room; b) control room.

Like it is shown in the figure above, the rain chamber is composed by a water spraying system, a discharge pressure, an electrical control panel and two flow meters. The water spraying system is composed of 12 sprinklers spaced horizontally and vertically of 82 cm to apply a continuous film of water all over the surface of the test specimens (Barbosa and De Freitas 2015). Figure 37a shows one of the sprinkles/spray nozzles of the water spraying system.

The discharge pressure (see Figure 37b) located on top of the rain room is able to introduce pulsating air pressure difference, simulating wind pressure against the test specimens. It can be applied up to 2500 Pa. It is also possible to perform the test with no pressure. In the rain room there are also the sensors shown in Figure 37c capable of measuring the air temperature and relative humidity (Barbosa and De Freitas 2015).

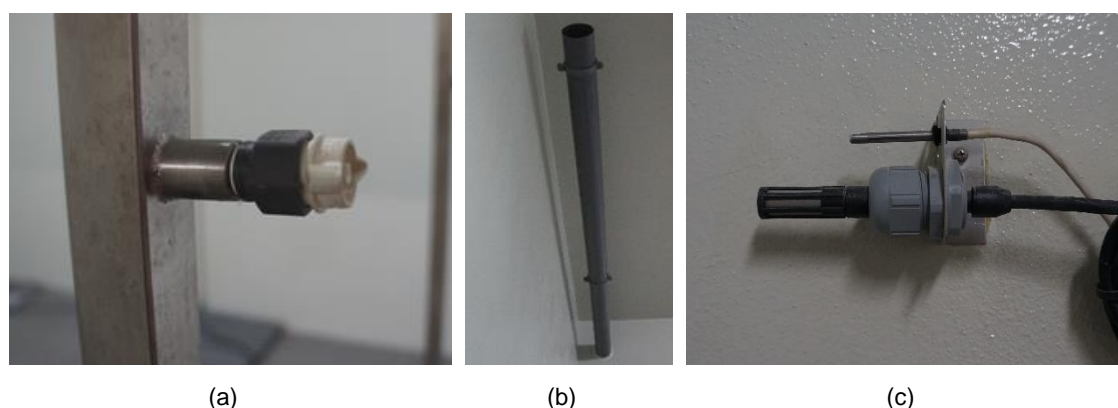


Figure 37. Close-up of rain chamber's components – rain room: a) sprinkler; b) temperature, relative humidity and pressure sensors; c) discharge pressure.

The flow meters (see Figure 38a) allow the user to control the amount of rain to be applied. It can be applied from 0.2 to 22 L/min of driving-rain. Finally, the electrical panel (see Figure 38b) controls the operation of the rain chamber. It runs through the *Climaplus V – version THP 800* with a touch screen. In the electrical panel, it is possible to change the process variables (driving rain and pressure) over time through program execution. Programs can be created or modified in the “PROGRAMS” icon. Each program is composed by segments like the one shown in Figure 38c.

Rain starts when the segment starts and lasts for the time established in the "Rain" line. If the “*L<sub>OFF time</sub>*” is zero, the rain is done only once, but if it is greater than zero, the rain is done at intervals established by the “*L<sub>OFF time</sub>*”. For example, if “Rain” is 00:01:00 and “*L<sub>OFF time</sub>*” is 00:05:00, it will happen 1 minute rain, followed by 5 minutes without rain, and then 1 minute rain again and so on. The “Pressure” Set Point entered is the value that the variable will reach after the “Segment Time”. For example, if segment 0 is 0 Pa and segment 1 is 100 Pa and the “Segment Time” of segment 1 is 1 hour, the chamber will evolve from 0 Pa to 100 Pa over 1 hour. That is, after 15 minutes the chamber should be at 25 Pa, after 30 minutes at 50 Pa and so on. If the “Segment Time” is 0 zero, it means the end of the program (Barbosa and De Freitas 2015).



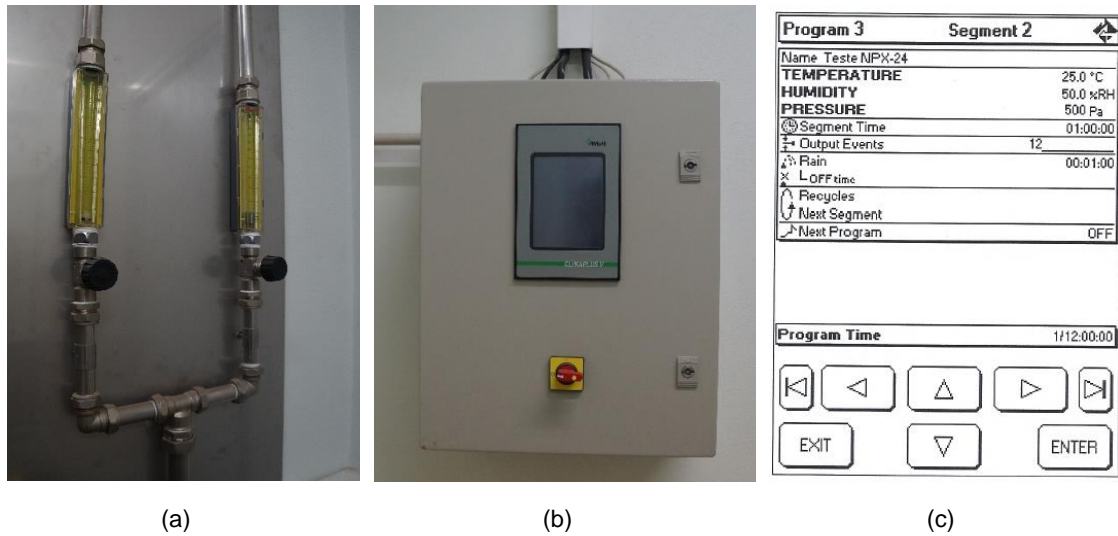


Figure 38. Close-up of rain chamber's components – control room: a) flow meters (hydraulic circuit); b) electrical panel; c) display setting of creating or modifying a program.

### 3.2.3. MONITORED PARAMETERS AND EQUIPMENT

In order to assess the walls hygrothermal behaviour, the following parameters were monitored on both wall test specimens according to the layout presented on Figure 39:

- Temperature profiles (T1 to T6, T7 to T12, T14 to T17 and T21 to T23 - alignments I, II, III and IV, respectively);
- Relative humidity profiles of wall test specimen A (H1 to H2 and H3 to H4 - alignments I and III, respectively);
- Heat fluxes across the walls' surfaces (F83 and F90 - alignment F of specimen A; F86 and F91 - alignment F of specimen B);
- Air temperature and relative humidity between the surroundings of both surfaces of the specimens i.e., air temperature and relative humidity of the rain room and of the control room.

The equipment that was used for temperature, relative humidity and heat flux measurements is described in Table 11, according to following sensors:

- Thermocouples (T1 to T23);
- Relative humidity probes (H1 to H4);
- Heat flux sensors (F1 to F7);
- Air temperature and relative humidity sensors (HOB01 to HOB04).

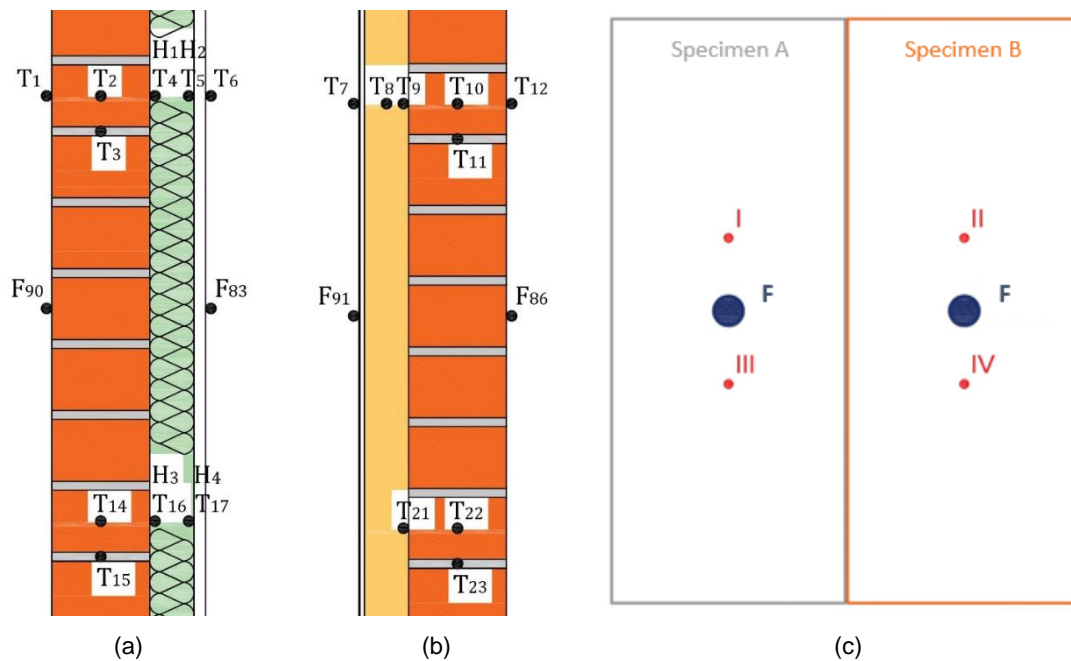
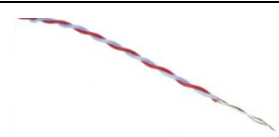





Figure 39. Position identification of the thermocouples – T, relative humidity probes – H and heat flux sensors – F along the constructive solutions: a) cross section of specimen A; b) cross section of specimen B; c) elevation plan of both specimens.

Table 11. Accuracy and range of the installed sensors.

Reference	Type	Accuracy	Range	Photo
T1 to T23	Thermocouple T	$\pm 0.5^{\circ}\text{C}$	$-200^{\circ}\text{C}$ to $350^{\circ}\text{C}$	
H1 to H4	Rotronic Hydroclip SC05 e S3	RH: $\pm 0.8\%$ Temp: $\pm 0.3\text{ K}$	0% to 100% $-100$ to $200^{\circ}\text{C}$	
F1 to F7	Heat flux sensors PU 3.2	$60 \times 10^{-6}$ $\text{V}/(\text{W}/\text{m}^2)$	$-2000$ to $2000\text{ W}/\text{m}^2$	
HOBO1 to HOBO4	Hobo U12 Temp/RH Data Logger (Onset)	Temp: $\pm 0.35^{\circ}\text{C}$ RH: $\pm 3.5\%$	$-20^{\circ}\text{C}$ to $70^{\circ}\text{C}$ 5% to 95%	

The data logger Mikromec multisens of TECHNETICS shown in Figure 40 was used for data acquisition. These devices can register and save the current measurements from multiple channels and they can be operated through a PC with the software *MMgrafix*. The devices are able to store 512 000 readings per recording.



Figure 40. Mikromec Data loggers.

During the construction of the wall test specimens, thermocouples were installed within the wall test specimens to obtain the temperature profiles of both walls in two measurement points, alignments I and II, both at 1.25 m height. Each measurement point consists of six thermocouples at different depths as illustrated in Figure 39: on both surfaces of the wall specimens, in the middle of the substrate (both in brick and mortar), in the interface between the substrate and the insulation, and, in the case of specimen A, in the interface between the insulation and the gypsum board and, in the case of specimen B, in the middle of the insulating render.

Relative humidity probes were installed within the test specimen A to obtain relative humidity profiles in alignment I. The measurement points are illustrated in Figure 39: in the interface between the brick and the mineral wool, and in the interface between the mineral wool and the gypsum board. No relative humidity probes were installed within the test specimen B between the material layers because the relative humidity probes could not be installed there.

In addition, the thermocouples and the relative humidity probes indicated on the bottom of Figure 39 have also been installed in alignments III and IV at 0.75 m height, in order to record in duplicate some of the results and thus avoiding data losses in case of eventual sensors failure.

Four heat flux sensors were installed in the specimens at 1 m height: one on the inner surface and one on the outer surface of each specimen (alignments F). Subsequently, three

more heat flux sensors were placed next to the others. One more on the inner surface of each specimen and one more on the outer surface of specimen A.

The HOBO sensors were placed in the centre of the control room and in the centre of the rain room, at the height of 1.25 m, to monitor the rooms air temperature and relative humidity.

The thermocouples and the relative humidity probes were installed in the wall with aluminium tape, whereas the heat flux sensors were installed with silicone or mortar. All the referred sensors are connected to data loggers, except for the HOBO sensors that have their own battery and data acquisition system.

Before being installed in the experimental prototype, the thermocouples (T), relative humidity probes (H) and air temperature and relative humidity sensors (HOBO) were verified in the Laboratory of Building Physics facilities. The equipment was placed inside the climatic chamber (see Figure 41), which was programmed for a 24 hours cycle, ranging the temperature from 35 °C to 10 °C and relative humidity changing between 50% and 80% as shown in Figure 42. The accuracy of the climatic chamber used is  $\pm 0.30^{\circ}\text{C}$  for temperature and  $\pm 3.0\%$  for relative humidity. The acquired results were analysed only when the climatic chamber had stabilized the imposed conditions, i.e., in the periods of time in which the temperature and relative humidity were constant. The obtained results in terms of the average value for the specific time interval that was analysed are presented in Appendix B.

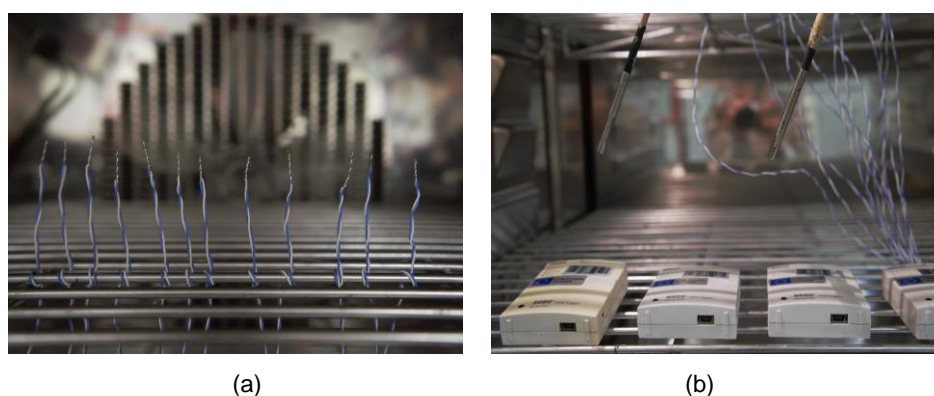


Figure 41. Different sensors inside the climatic chamber: a) thermocouples; b) relative humidity probes and air temperature and relative humidity sensors.

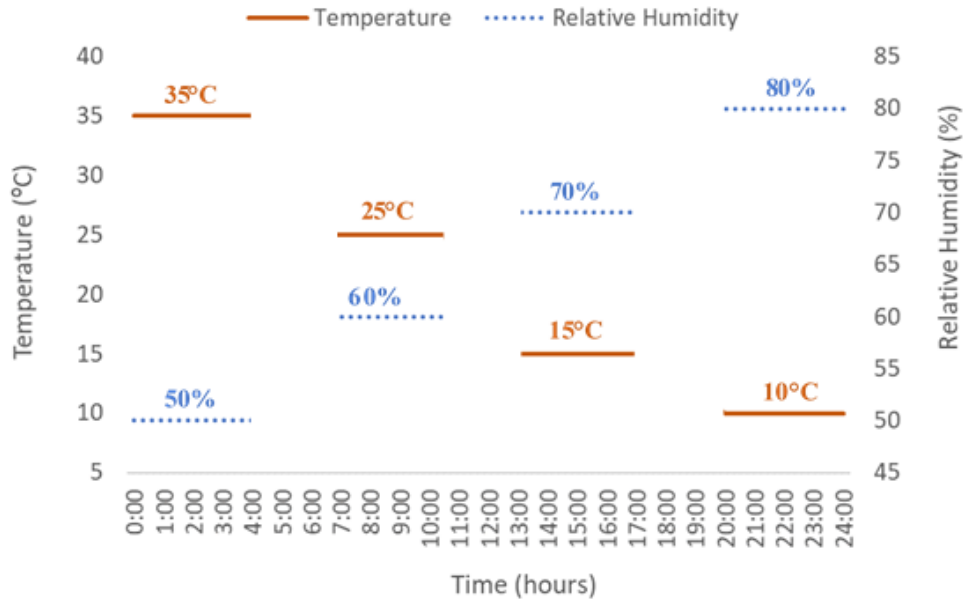


Figure 42. Cycle programmed in the climatic chamber.

The maximum difference between the temperature measured by the thermocouples and the climatic chamber programmed temperature was 0.5 °C. The maximum difference between the relative humidity measured by the relative humidity probes and the climatic chamber programmed relative humidity was 6%. Concerning the air temperature and relative humidity sensors, the maximum differences between the temperature and relative humidity measured by the sensors and the climatic chamber programmed temperature and relative humidity were 0.2 °C and 7%, respectively. Note that the differences obtained in both temperature and relative humidity are low and acceptable values since they are affected not only by the accuracy of the sensor itself but also of the climatic chamber. Therefore, the results showed that the sensors were operating accurately, and the sensors were installed in the experimental prototype inclusively inside the wall test specimens.

### 3.3. RAIN SEQUENCES AND BOUNDARY CONDITIONS

This section shows the precipitation sequences applied against the wall test specimens and the air temperature and relative humidity of the rain room and the control room during the tests. A series of tests were carried out on the experimental prototype developed. Each test consists of subjecting the wall test specimens to driving rain while in the presence of a temperature gradient.

Over five tests, the wall test specimens were exposed to the precipitation sequences indicated in Table 12 and Figure 43. No further tests were carried out due to restrictions imposed by the COVID-19 pandemic. In the preliminary test, the specimens were not subjected to rain at all. In the first test, the specimens were subjected to two rainy periods of 1 hour each, the second rainy period began two days after the first one. In the second test, the specimens were subjected to two rainy periods of 1 hour followed by one rainy period of 4 hours. In the third test, the specimens were subjected to a single rainy period of 4 hours. Finally, in the fourth test, the specimens were subjected to two rainy periods of 4 hours and after the rainy periods a dehumidifier was used in the rain room to accelerate the drying of the specimens.

Table 12. Rain sequence used in each test.

TEST	preliminary	1st	2nd	3rd	4th
RAIN SEQ	-	I	II	III	IV +d

+d test with the dehumidifier.

Figure 43 presents in more detail the rain sequences that were applied against the external surface of the specimens during the tests. As can be seen in Figure 43, sequence I is characterized by 1 hour rain, followed by 47 hours without rain and the cycle is repeated two times. Sequence II is characterized by 1 hour rain, followed by 71 hours without rain (approximately 3 days). The cycle is repeated two times and then is followed by 4 hours rain. Sequence III is characterized by 4 hours rain. Finally, sequence IV is characterized by 4 hours rain, followed by 44 hours without rain and the cycle is repeated two times.

The rainy periods include applying a spray flow of 1.5 L/(m<sup>2</sup> min) evenly distributed over the external surface of the specimens, following the recommendation given in standard EN 12865:2001 – *Hygrothermal performance of building components and building elements. Determination of the resistance of external wall systems to driving rain under pulsating air pressure* (EN 12865: 2001). The temperature of the spraying water was around 23 °C.

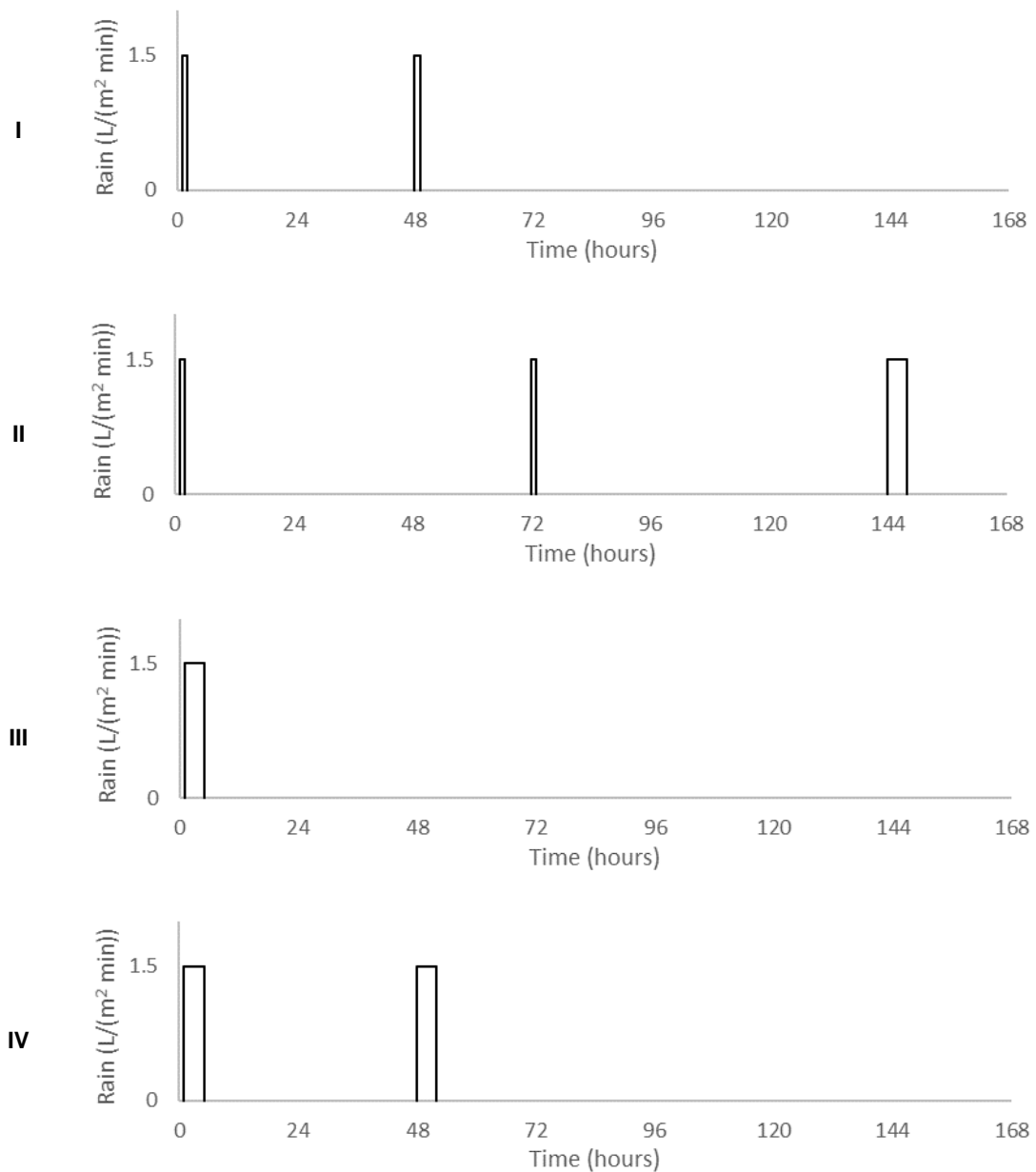
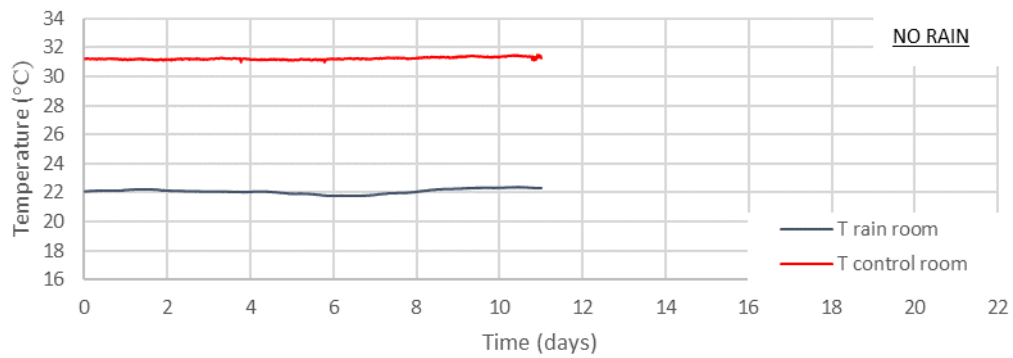


Figure 43. Precipitation sequences applied against the specimens.

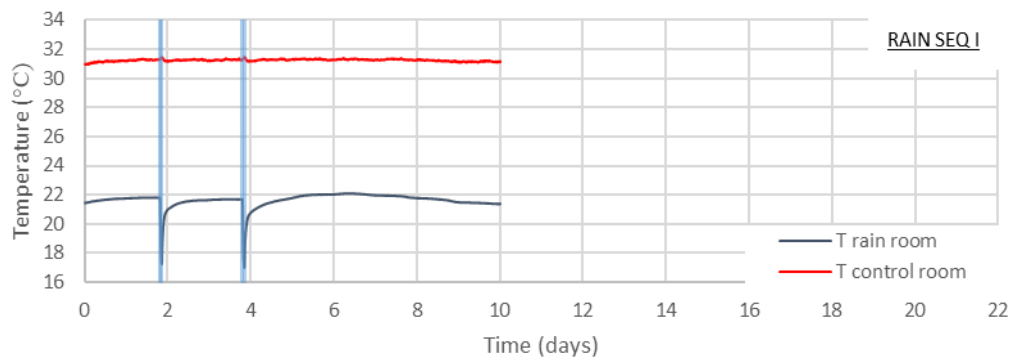
The precipitation sequences were chosen in order to apply different amounts of precipitation and rainy periods against the specimens. Initially, shorter rainy periods of 1 hour were applied and, later, longer rainy periods of 4 hours were applied. In the first, second, third and fourth tests, a total of 2, 6, 4 and 8 hours of driving rain were applied, respectively.

The next test started only after the previous test had ended two months ago and the humidity inside the specimen A had decreased below 80%.

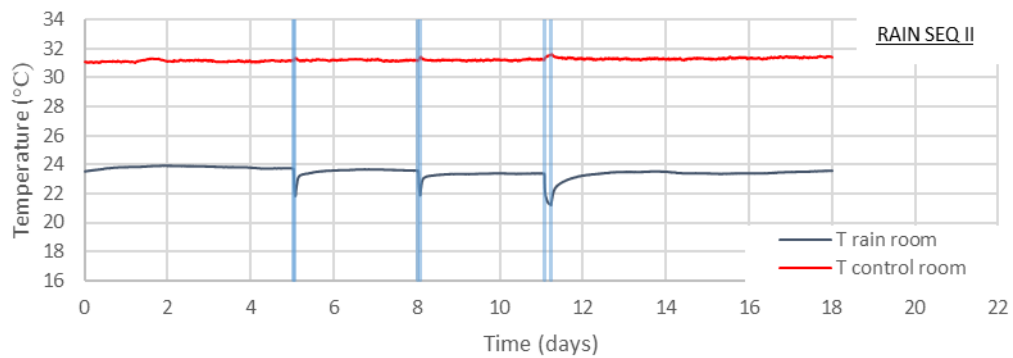
The temperature of the rain room and control room during the tests is shown in Figure 44. The rain room simulates the exterior environment, and the control room simulates the interior environment. The rainy periods are delimited by vertical light blue lines and the period in which the dehumidifier was operating is delimited by dashed vertical grey lines.



(a)

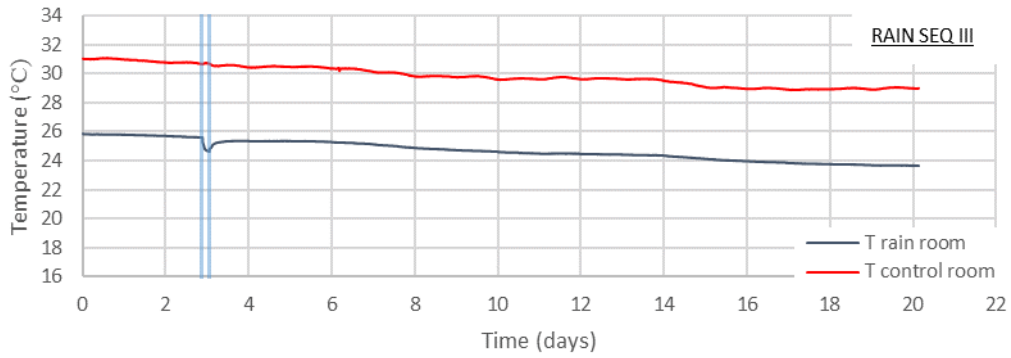


(b)

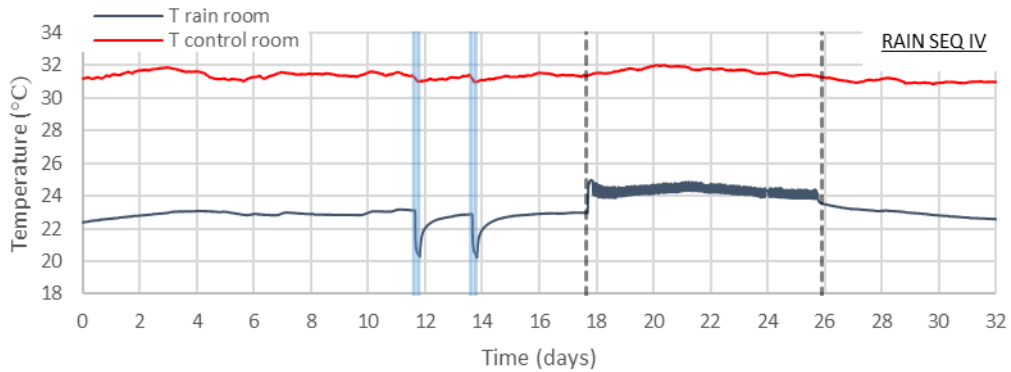


(c)





(d)



(e)

Figure 44. Temperature in the rain room and in the control room during: a) the preliminary test; b) the first test; c) the second test; d) the third test; e) the fourth test.

In the control room a heater was used to obtain a temperature of approximately 30 °C. In the rain room the free-running temperature conditions were implemented as it was not possible to cool the ambient temperature. In the rain room the temperature varied between 20 and 25 °C. Obviously, these conditions do not confirm with realistic boundary conditions, but they were selected to obtain a clear temperature difference between the interior and exterior surfaces of the wall test specimens.

The temperature gradient reached between the rain room and the control room was quasi steady throughout the tests, except during the rainy periods when it was slightly higher because when the precipitation was introduced, the temperature of the rain room decreased by 1 to 4 °C. Moreover, in the fourth test the dehumidifier raised the rain room temperature by around 1 °C.

In the third test, although the temperatures in the rain room and in the control room did not completely stabilize, the temperature gradient between the rooms of 5 °C was constant throughout the test.

Figure 45 shows the temperature gradients between the rain room and the control room during the tests. The maximum temperature gradient was approximately 9.5 °C in the first test in which the rain sequence I was applied, and the minimum temperature gradient was 5 °C in the third test, in which the rain sequence III was applied. The maximum peaks of the temperature gradients correspond to the rainy periods. During the rainy periods, the driving rain was responsible for cooling the rain room increasing the temperature gradient between the rooms. Moreover, in the fourth test in which the rain sequence IV was applied, the dehumidifier was responsible for decreasing the temperature gradient by around 1 °C.

In the second test, in which the rain sequence II was applied, the temperature gradient increased slightly (approximately 1°C) during the test because the temperature in the rain room decreased slightly after the rainy periods.

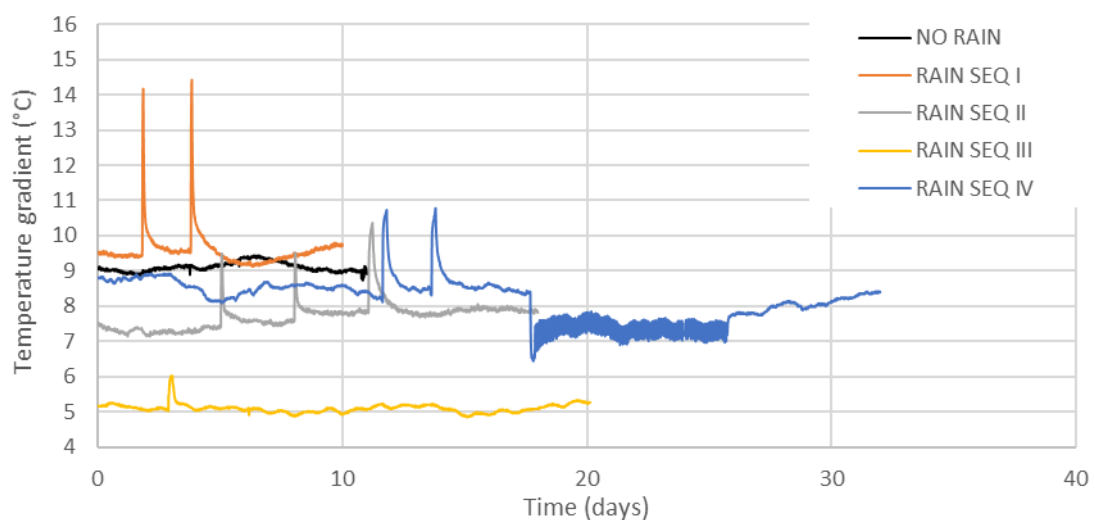
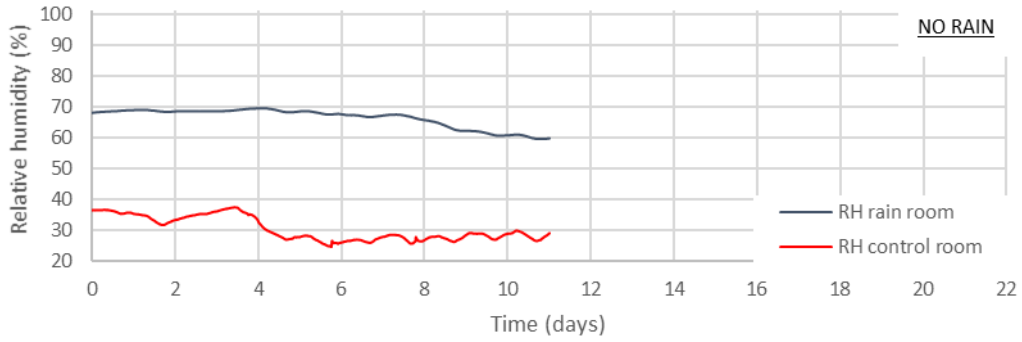


Figure 45. Temperature gradient between the rain room and the control room during the tests.

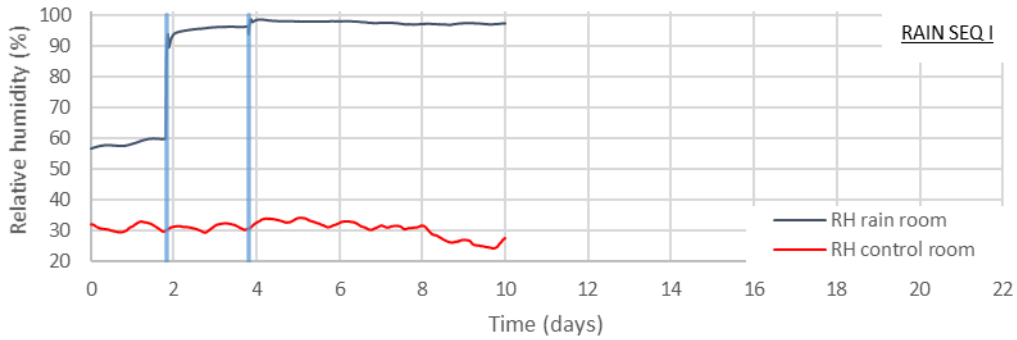
The relative humidity of the rain room and the control room during the tests is shown in Figure 46. Throughout the tests, the relative humidity of the rain room was above 60%, while the relative humidity of the control room was below 50%. That is to say that the presence of water vapour in the rain room was significantly higher than the presence of water vapour in the control room.

The precipitation significantly increased the concentration of water vapour in the rain room. In fact, due to the precipitation the relative humidity in the rain room increased to the maximum relative humidity of 100% reaching saturation. After the precipitation, the

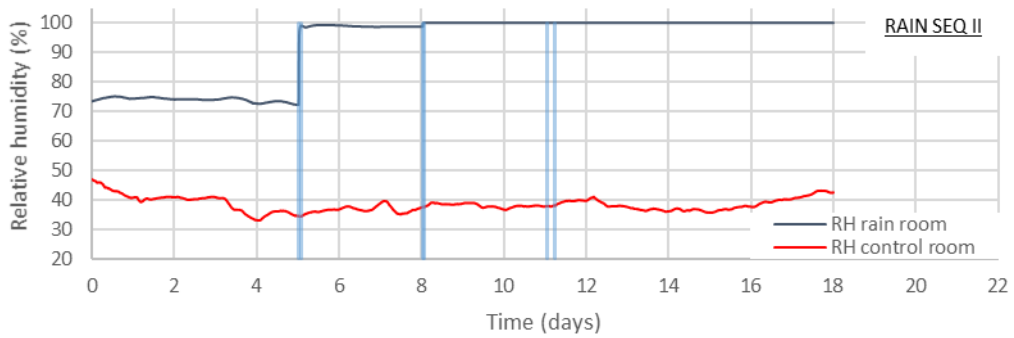
decrease in relative humidity in the rain room occurs extremely slowly due to the low ventilation rate of the rain room. In fact, for several days after the precipitation the relative humidity in the rain room remained 100%.



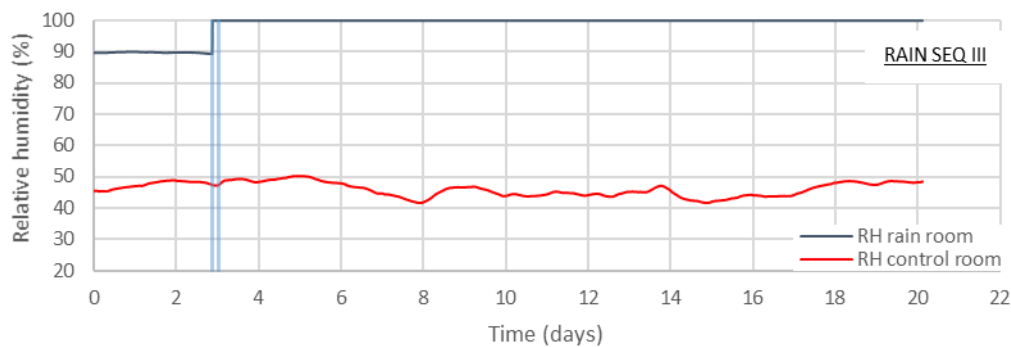
(a)



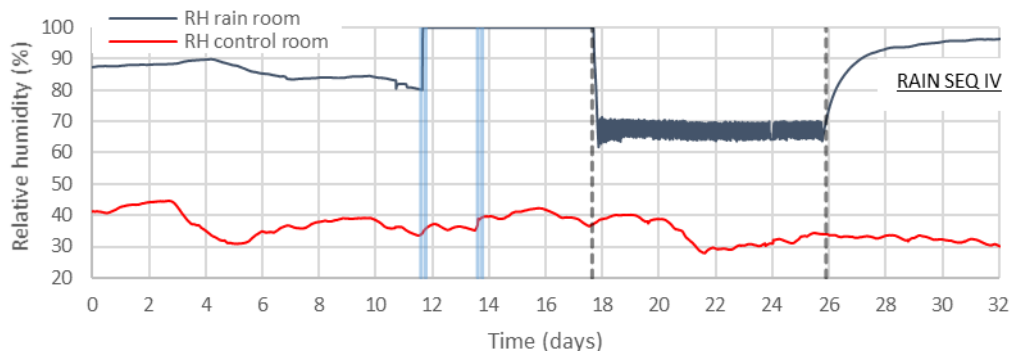
(b)



(c)



(d)



(e)

Figure 46. Relative humidity in the rain room and in the control room during: a) the preliminary test; b) the first test; c) the second test; d) the third test; e) the fourth test.

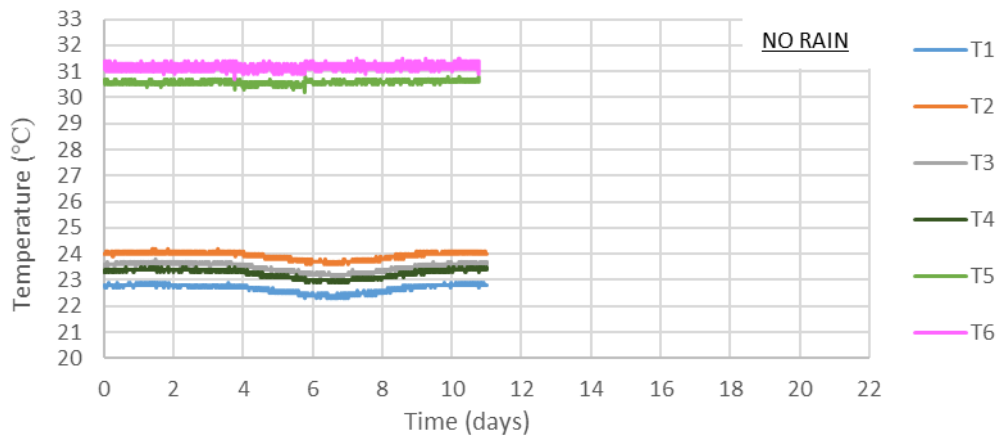
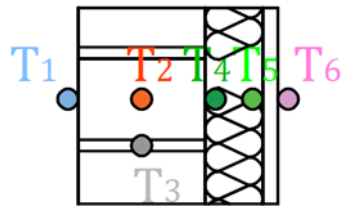
In the fourth test, the dehumidifier was introduced into the rain room to decrease the relative humidity in the room after the rainy periods and to accelerate the drying of the specimens. The dehumidifier reduced the relative humidity in the rain room by 30 percent. Before the dehumidifier was introduced, the relative humidity in the rain room was 100% and changed to circa 70%. However, when the dehumidifier was turned off, the relative humidity in the rain room increased again to close to 100%.

The relative humidity in the control room throughout the tests was above 20% and below 50%. In the control room, the relative humidity remained approximately constant during each test. In fact, it was observed that the driving rain applied against the wall test specimens did not affect the relative humidity in the control room.

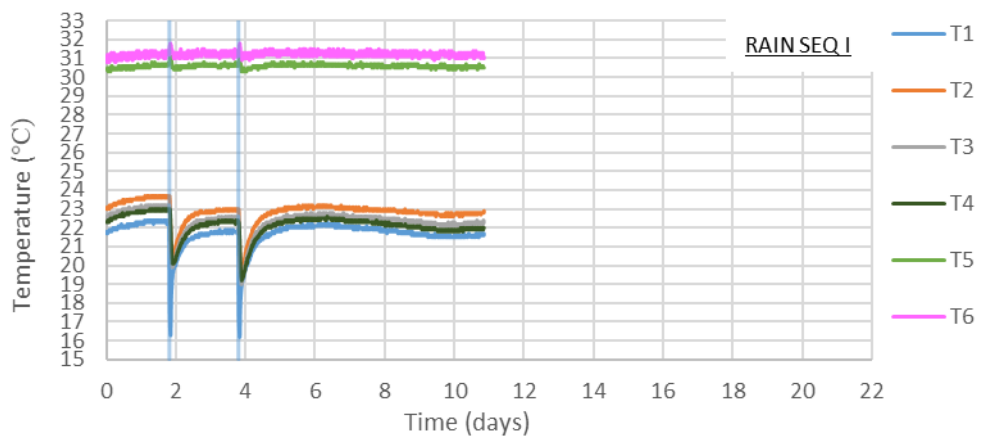
### 3.4. EXPERIMENTAL RESULTS

#### 3.4.1. TEMPERATURE PROFILES

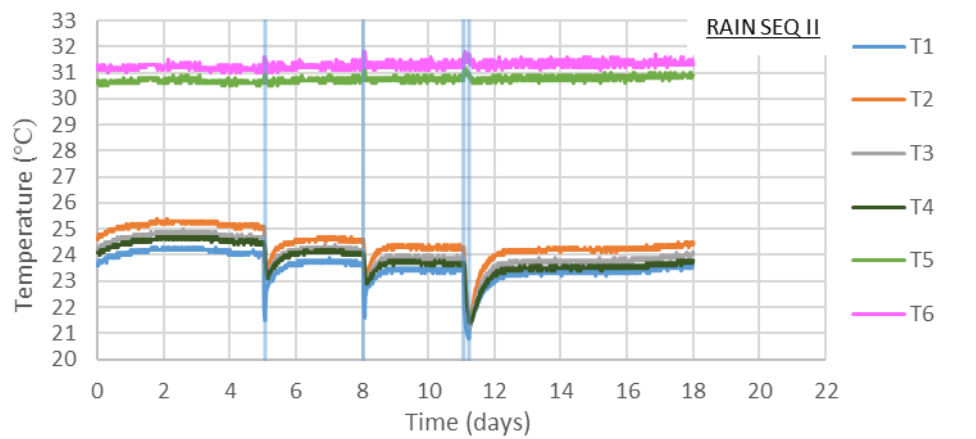
The temperatures on both surfaces and within the wall test specimens were measured by thermocouples. Figure 47 and Figure 48 show the temperatures on the surfaces and inside specimen A and specimen B, respectively, throughout the tests. The rainy periods are delimited by vertical light blue lines and the period in which the dehumidifier was operating is delimited by dashed vertical grey lines.



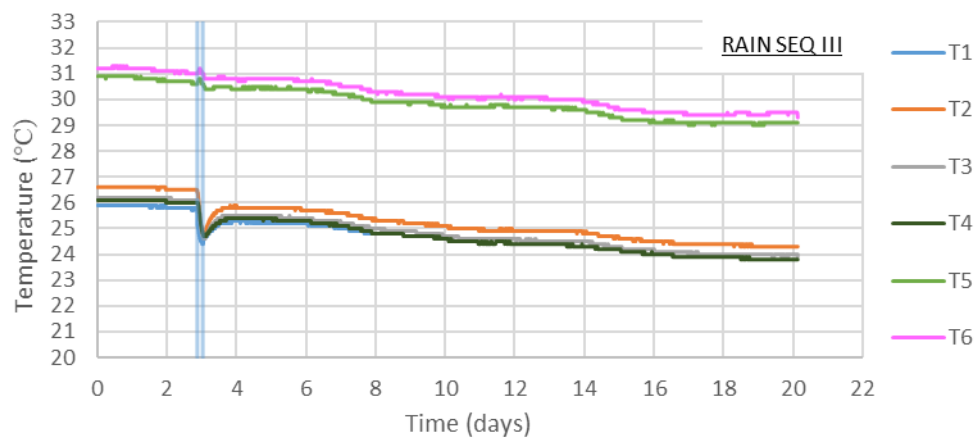
(a)



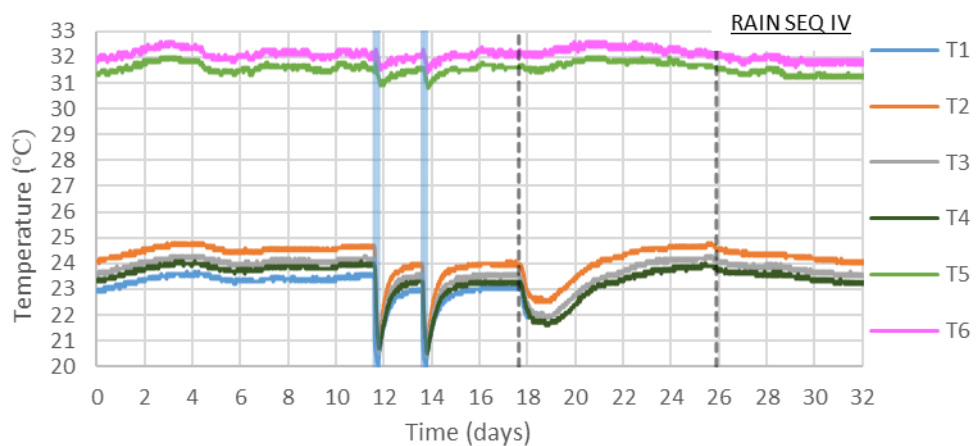
(b)



(c)



(d)



(e)

Figure 47. Temperatures at the surfaces and inside the specimen A during: a) the preliminary test; b) the first test; c) the second test; d) the third test; e) the fourth test.

Throughout the tests, the temperature of the interior surface of specimen A was around 30-31 °C, and temperature of the exterior surface varied between 22 and 25 °C approximately. As for the temperatures inside specimen A, it was found that the temperature of the brick, the mortar, and the brick-mineral wool interface (T2, T3 and T4) was identical. It was also found that the temperature of the mineral wool-gypsum board interface (T5) was identical to the temperature of the interior surface (T6). As for the temperatures inside specimen B, it was observed that the temperature of the thermal render-brick interface, the brick, the mortar, and the interior surface (T9, T10, T11 and T12) were similar.

The temperature of masonry of specimen A is lower than the temperature of masonry of specimen B due to the position of the thermal insulation on the specimens. The average temperature of the masonry of specimen A during the tests is 24°C while the average temperature of the masonry of specimen B is 28°C. This means that there is a higher risk of occurring interstitial condensation in specimen A than in specimen B.

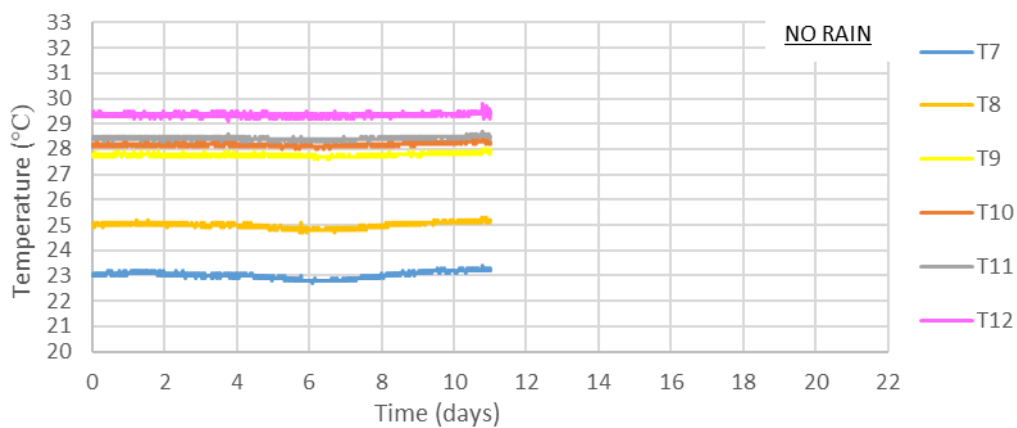
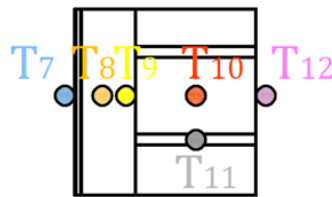
It should also be noted that some of these temperatures varied due to precipitation, in particular the temperatures measured by the thermocouples located closest to the rain room (namely temperatures T1, T2, T3 and T4 for specimen A, and temperatures T7 and T8 for specimen B). In fact, during the rainy periods, the temperature of the masonry of specimen A decreased by around 3 °C, the temperature of the insulating render of specimen B decreased also by around 3°C, and the temperature of the masonry of specimen B decreased only by approximately 0.5 °C.

In the fourth test, the dehumidifier reduced the air humidity in the rain room and, consequently, accelerated the drying process of the specimens. For specimen A, as soon as the dehumidifier was turned on, the temperatures of the brick masonry (temperatures T1, T2, T3 and T4) decreased mainly due to the absorption of latent heat necessary to evaporate the rainwater absorbed in the specimen. For specimen B, the temperatures just slightly increased due to the dehumidifier, as did the temperature of the rain room.

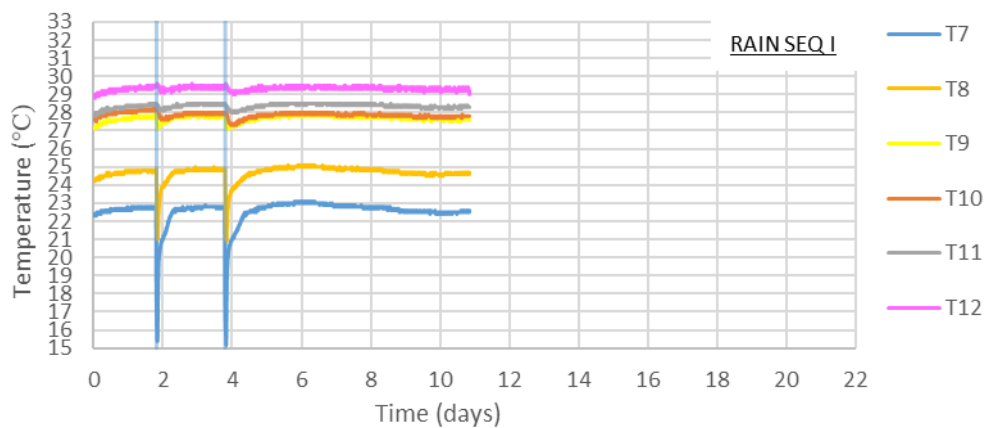
During the tests, the interior surface temperature of specimen B was slightly lower than the interior surface temperature of specimen A, and both were slightly lower than the control room temperature. The temperature of the exterior surface of specimen A that corresponds to the temperature of the gypsum board was around 31 °C, while the

temperature of the exterior surface of specimen B that corresponds to the temperature of the brick masonry was around 29 °C. As for the exterior surface temperatures, in both specimens the exterior surface temperature was similar to the rain room temperature.

Thus, it can be concluded that the driving rain was responsible for cooling the outer side layers of the wall test specimens, especially the brick masonry of specimen A and the insulating render of specimen B. The brick masonry of specimen A also decreased in temperature due to the dehumidifier.

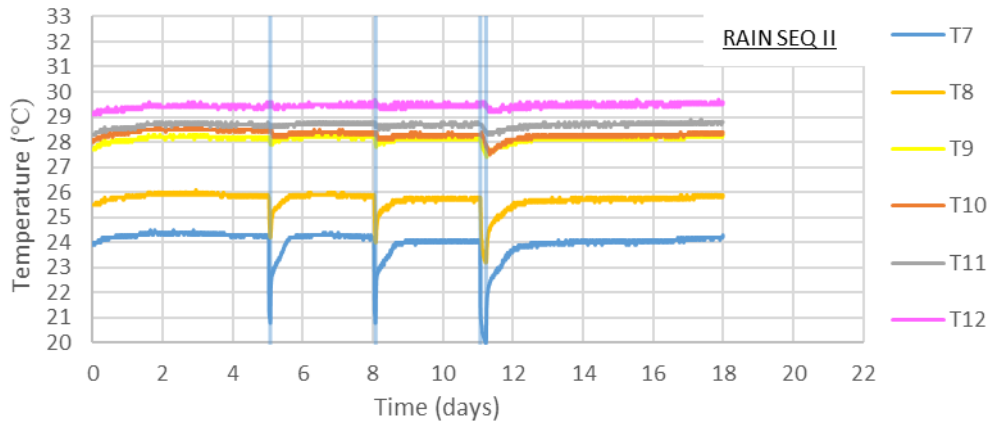


(a)

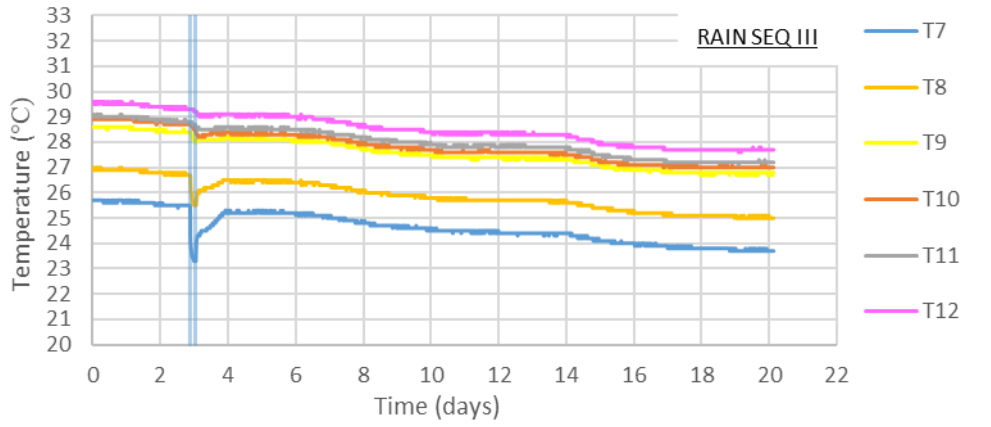


(b)

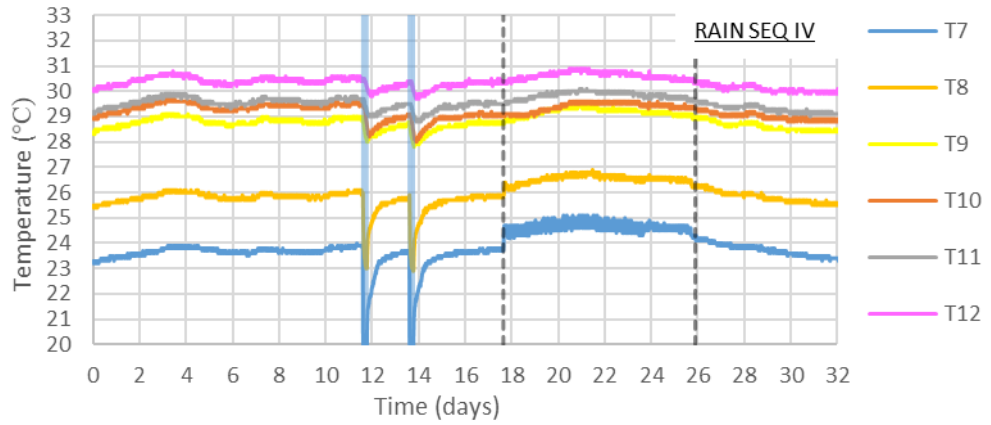




(c)



(d)



(e)

Figure 48. Temperatures at the surfaces and inside the specimen B during: a) the preliminary test; b) the first test; c) the second test; d) the third test; e) the fourth test.

Figure 49 and Figure 50 show the temperature profiles of specimen A and specimen B, respectively. For each test, temperature profiles at certain times are shown, namely before and after the rainy periods. It can be observed that when the specimens were exposed to driving rain, the temperature of specimen A slightly decreased, while the temperature of specimen B almost did not change.

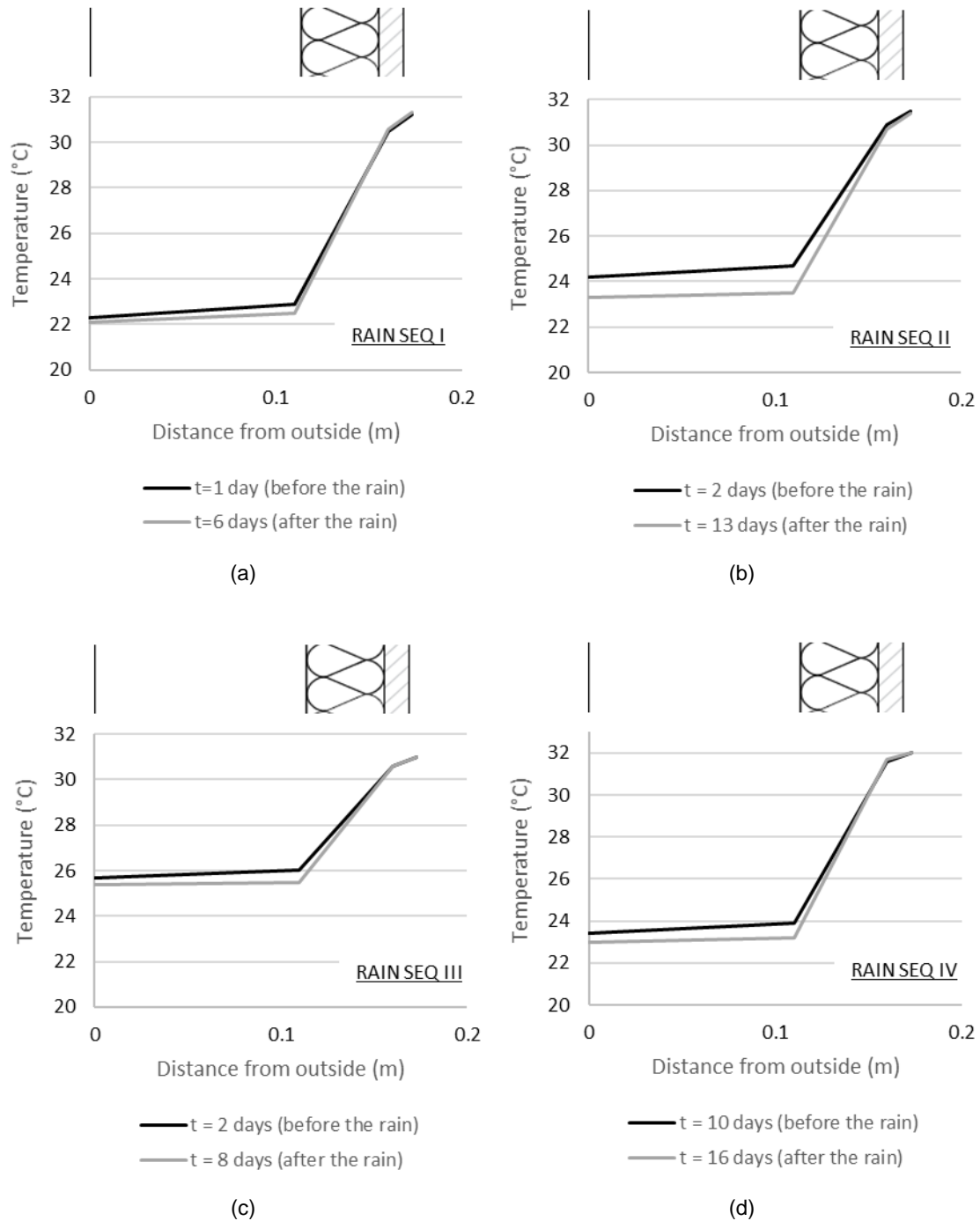


Figure 49. Temperature profiles of specimen A before and after each rain sequence for: a) the first test; b) the second test; c) the third test; d) the fourth test.

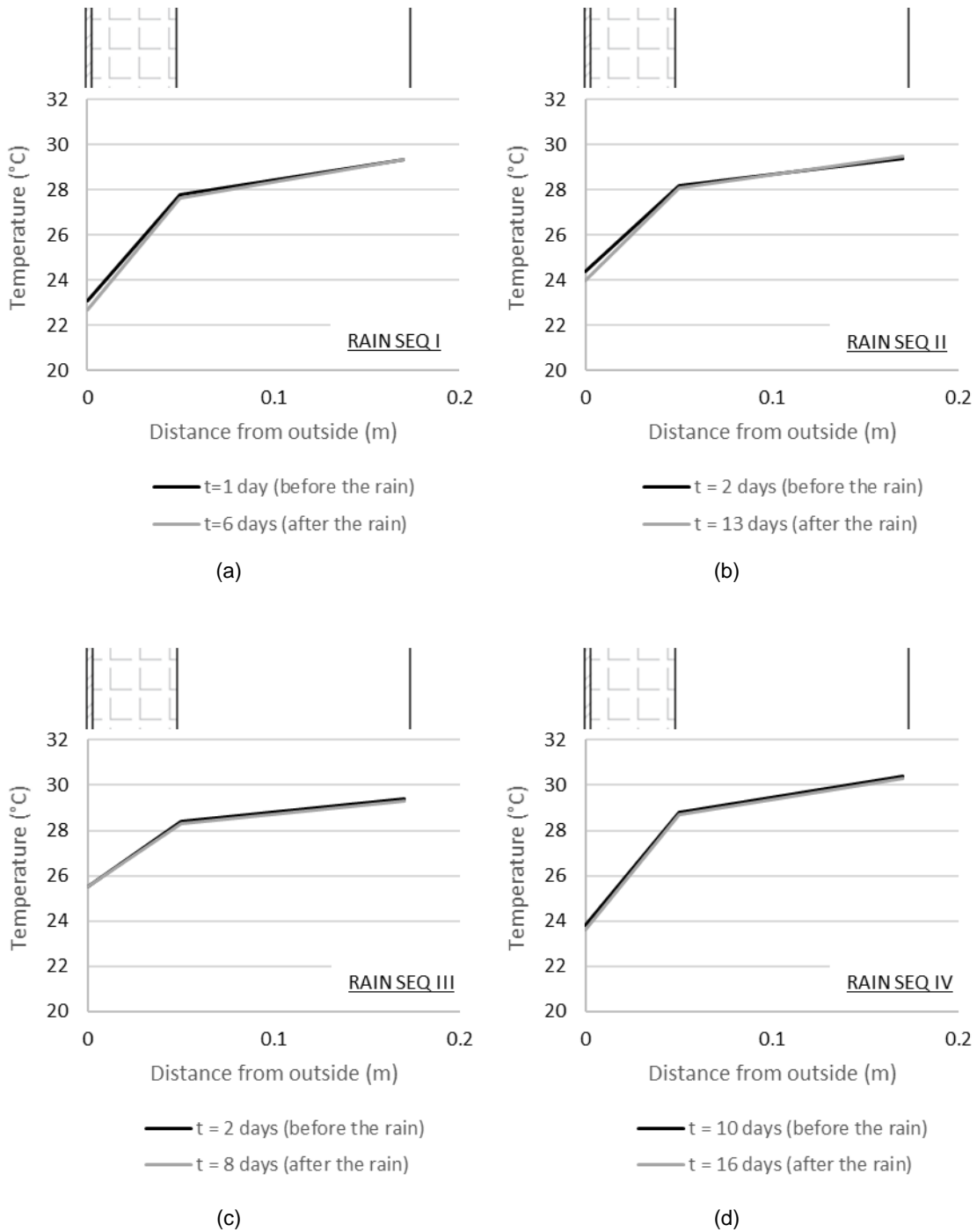


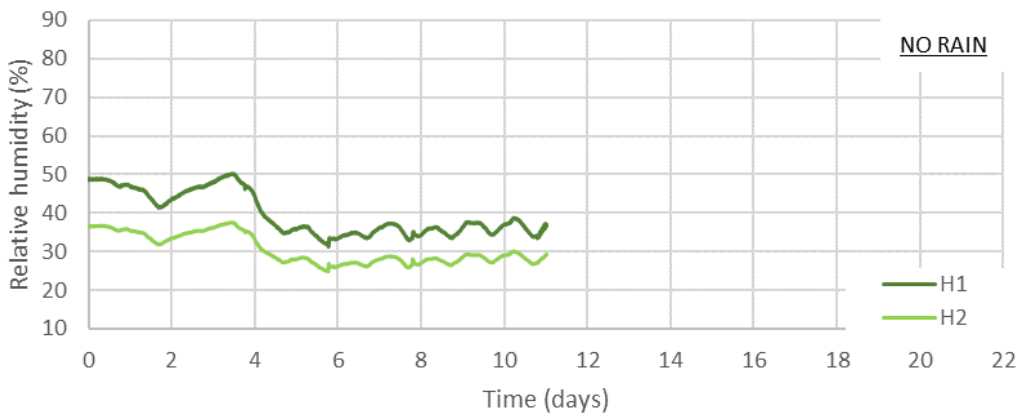
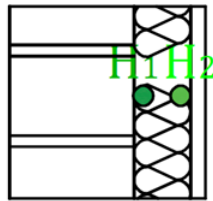
Figure 50. Temperature profiles of specimen B before and after each rain sequence for: a) the first test; b) the second test; c) the third test; d) the fourth test.

Note that the decrease in temperature in the brick masonry of specimen A indicates the presence of moisture. In the tests with more intense precipitation sequences (namely precipitation sequences II and IV), the difference between the temperature profiles of specimen A before and after the rain is slightly more pronounced.

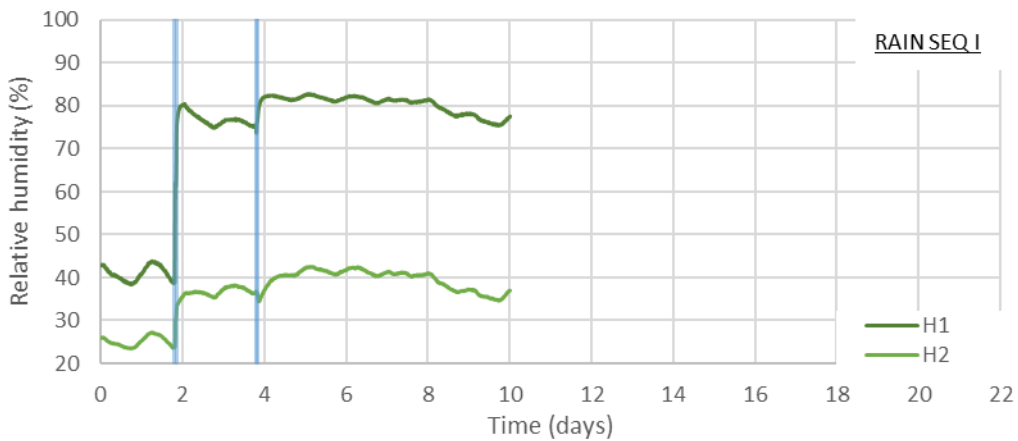
3.4.2. RELATIVE HUMIDITY BETWEEN MASONRY AND INSULATION

Relative humidity probes were installed within the wall test specimen A to monitor the relative humidity between masonry and insulation. As for specimen B, it was not possible to install the relative humidity probes inside the specimen between masonry and insulating render so in specimen B the relative humidity between masonry and insulation was not monitored.

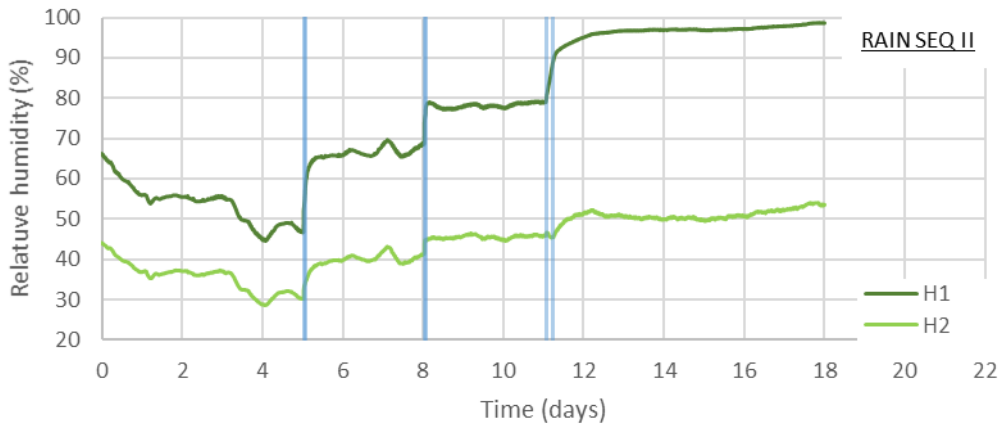
Figure 51 shows the relative humidity inside specimen A throughout the tests, namely the relative humidity between masonry and insulation, and also the relative humidity between insulation and gypsum board.



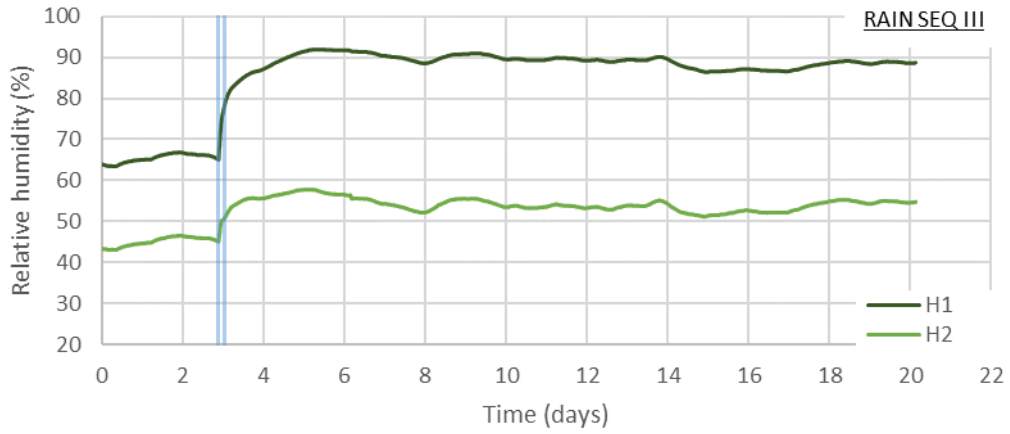
(a)



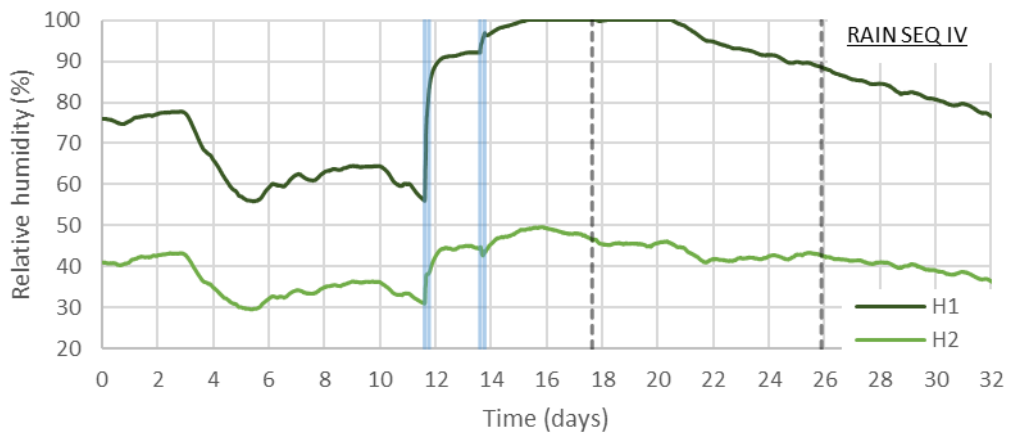
(b)



(c)



(d)



(e)

Figure 51. Relative humidity inside the wall test specimen A during: a) the preliminary test; b) the first test; c) the second test; d) the third test; e) the fourth test.

A significant increase in relative humidity inside the specimen is found due to the rainy periods indicating that the driving rain has significantly increased the moisture content in specimen A. The relative humidity between the brick masonry and insulation increased by 40% and the relative humidity between the insulation and gypsum board increased by 20%. That is to say a larger increase in relative humidity was found between masonry and insulation rather than between insulation and gypsum board.

In the tests with more than one rainy period (precipitation sequences I, II and IV) it was found that each one of the rainy periods increased the relative humidity inside the specimen. However, the first rainy period of the sequences was responsible for the greatest increase.

After the rainy periods, the relative humidity between masonry and insulation was very high in all the tests. However, only in the second and fourth tests, in which the most intense precipitation sequences were applied, did the relative humidity inside the specimen reach the maximum value of 100%.

After the precipitation (wetting phase), the water content of the specimen A begins to decrease (drying phase). However, in the tests the drying occurs very slowly due to the very high air humidity in the rain room and the low ventilation rate of the rain chamber. In fact, at the end of the first, second and third tests (precipitation sequences I, II and III) the relative humidity inside the specimen remains very high. This means that, at the end of those tests, the specimen remains wet.

In the fourth test, the dehumidifier reduced the relative humidity inside the specimen A approximately three days after it started to work. The relative humidity between the masonry and the insulation decreased from 100% to around 80%, demonstrating the drying of the specimen.

During the tests, the relative humidity in the rain room was higher than inside the specimen, and the relative humidity inside the specimen was higher than inside the control room. Before the rainy periods, the relative humidity between masonry and insulation was approximately 20% lower than the relative humidity in the rain room, and the relative humidity between insulation and gypsum board was similar to the relative humidity in the control room.

The relative humidity profiles of specimen A before and after the rain for the several tests are shown in Figure 52. For the test with the dehumidifier (in which the precipitation IV was applied) also the relative humidity profile long after rain is shown.

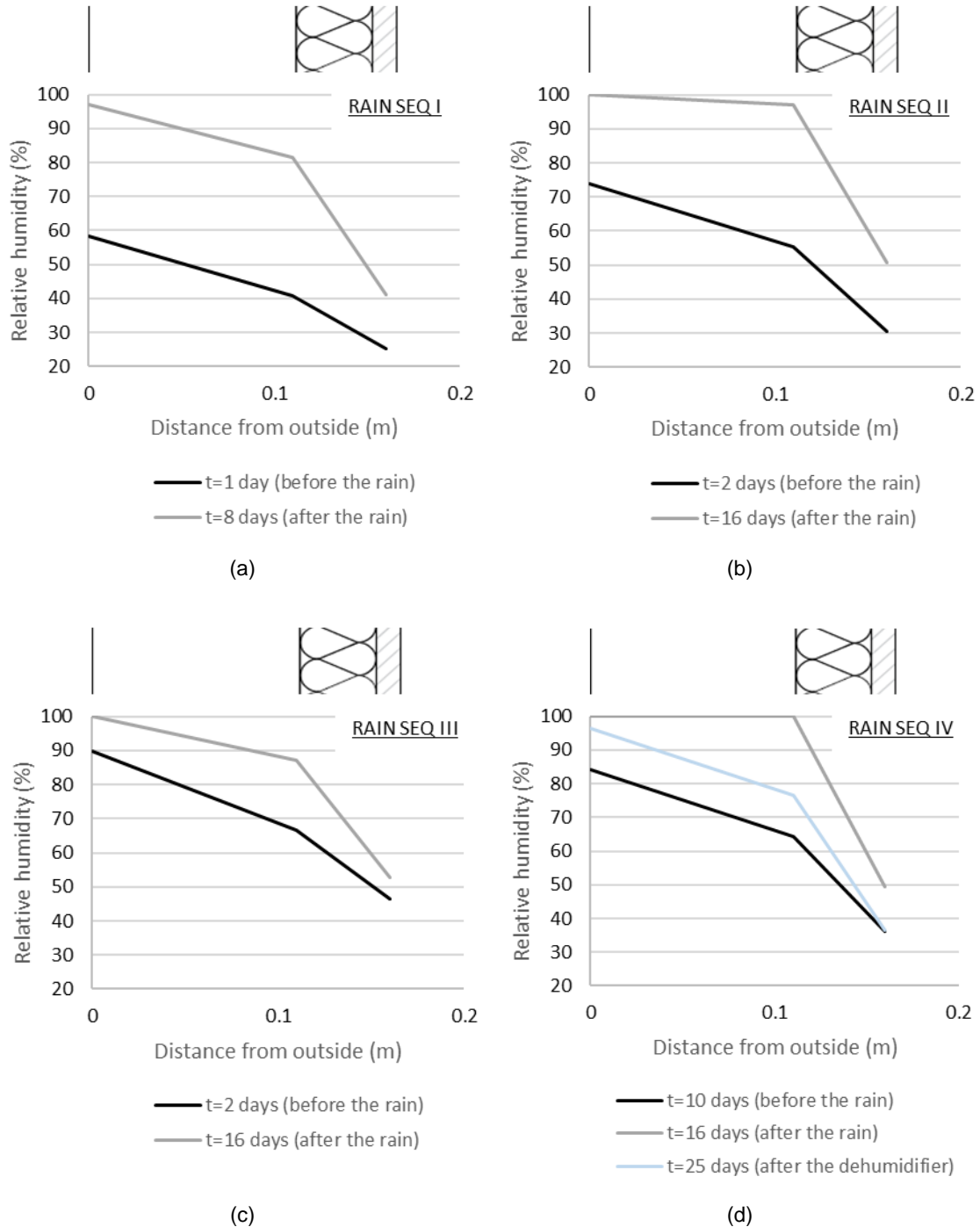


Figure 52. Relative humidity profiles of specimen A before and after each rain sequence for: a) the first test; b) the second test; c) the third test; d) the fourth test.

Once again it can be observed that driving rain has significantly influenced the relative humidity within the specimen. Mainly at the cold side of the specimen, a large increase in relative humidity was found, around 40%. The largest increase in relative humidity was found between masonry and insulation. In fact, the relative humidity profiles after the rain reveal that the moisture content of the specimen increased, especially of the brick masonry. After the dehumidifier was used, the relative humidity inside specimen A significantly decreased indicating that the specimen has dried out.

During the wetting period, the relative humidity in the rain room and inside the specimen increased, while the relative humidity in the control room hardly changed.

In the fourth test, in which precipitation sequence IV was applied, after the rainy periods the relative humidity between the masonry and the insulation reached 100%. To investigate the occurrence of interstitial condensation between masonry and the insulation, the partial water vapor pressure and the vapor saturation pressure were calculated from relative humidity measurements according to equation (5) and equation (6).

$$P = \frac{RH \cdot P_s}{100} \quad (5)$$

where:

P	[P]	partial water vapor pressure
RH	[%]	relative humidity
P <sub>s</sub>	[Pa]	saturation pressure of water vapor

$$P_s = 611 \cdot e^{\left(\frac{a \cdot t}{t' + t}\right)} \quad (6)$$

where:

P <sub>s</sub>	[Pa]	saturation pressure of water vapor
t	[°C]	temperature

$$a=17,08; t'=234.18 \text{ °C} \quad \text{for } t \geq 0 \text{ °C}$$

Figure 53 shows the vapour saturation pressures P<sub>s</sub> and the partial water vapour pressure P between the brick masonry and the insulation (measuring point H1) during the fourth test.



Due to the rainy periods the concentration of water vapour between masonry and insulation increased from approximately 1800 Pa to 2800 Pa. Note that the partial water vapour pressure has reached the vapour saturation pressure during the second rainy period, indicating that interstitial condensation has occurred in that moment.

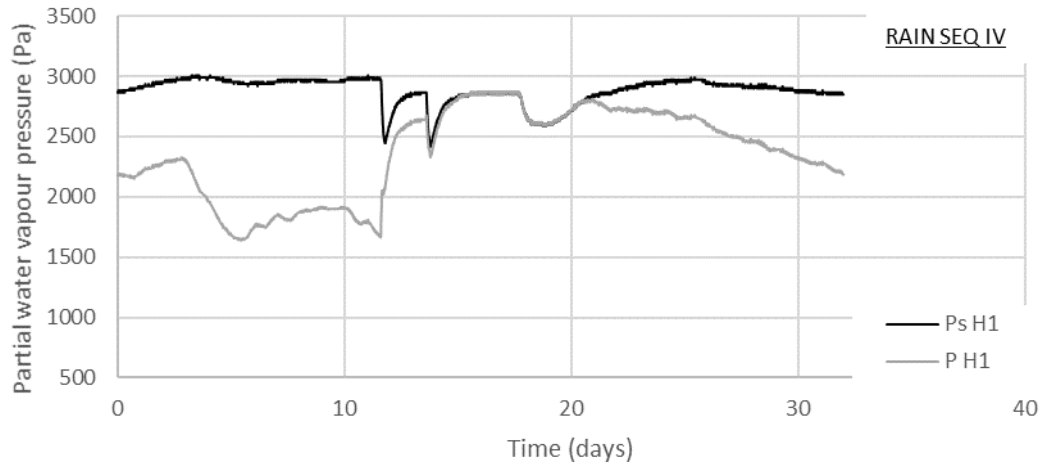


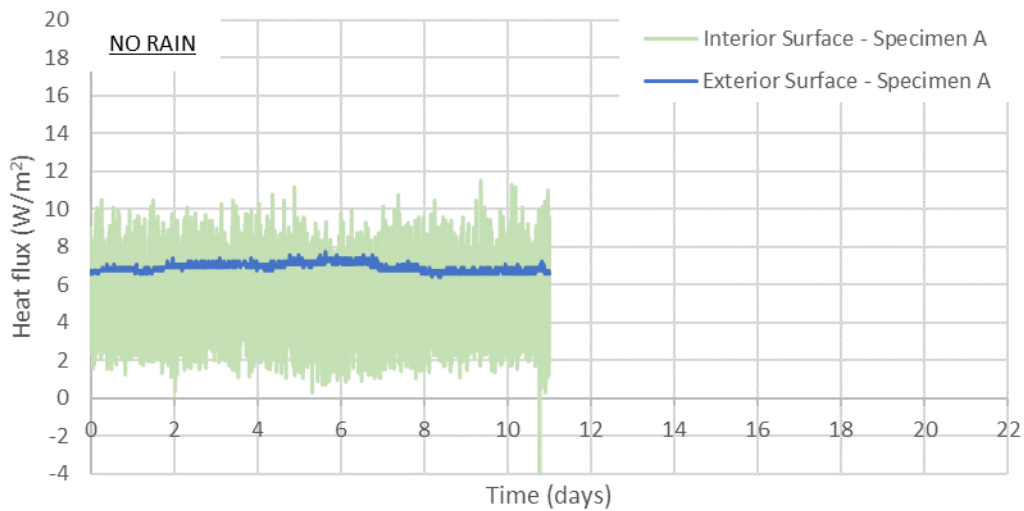
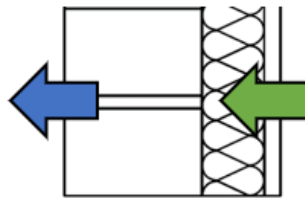
Figure 53. Vapor saturation pressure and partial water vapour pressure between the masonry and the insulation of specimen A throughout the fourth test.

Despite it was not possible to monitor the relative humidity inside the specimen B, it is known that the moisture behaviour found for specimen B is totally different from the moisture behaviour observed for specimen A. This is because the humidification of the specimens due to driving rain depends mainly on the finish capillary water absorption coefficients and the specimens have totally different finish capillary water absorption coefficients. In fact, specimen A is highly capillary active, whereas specimen B is hardly capillary active. Therefore, after the rainy periods the increased water content in specimen A is significantly higher than in specimen B. And the increased water content in specimen B is so negligible that can hence be neglected.

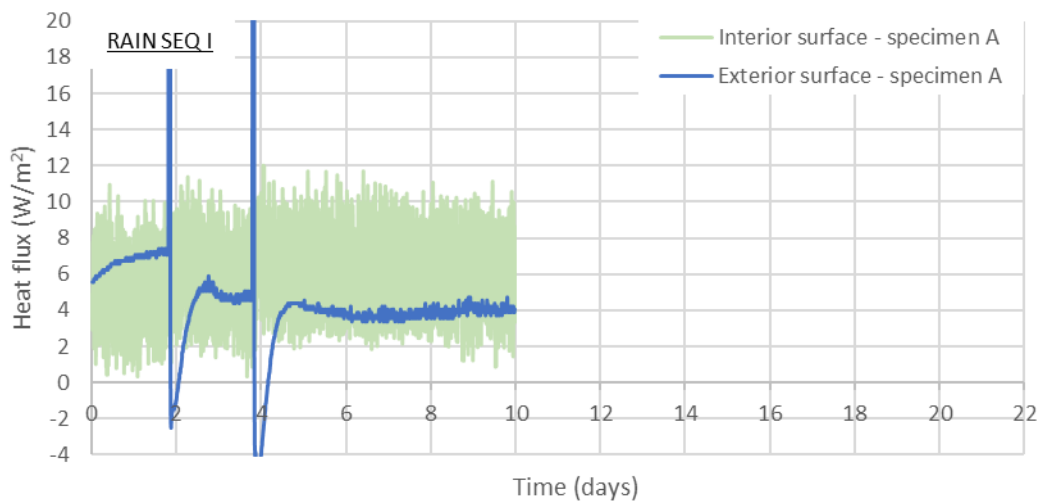
### 3.4.3. HEAT FLUXES

During the experiments, the heat fluxes through both surfaces of the wall test specimens were measured by heat flux sensors. Figure 54 and Figure 55 show the heat fluxes across the interior and exterior surfaces of specimen A and specimen B, respectively, throughout the tests. In the second test in which precipitation sequence II was applied, it was not possible to measure the heat flux through the interior surface of specimen A and in the fourth test the heat fluxes through the interior surfaces of both specimens were measured

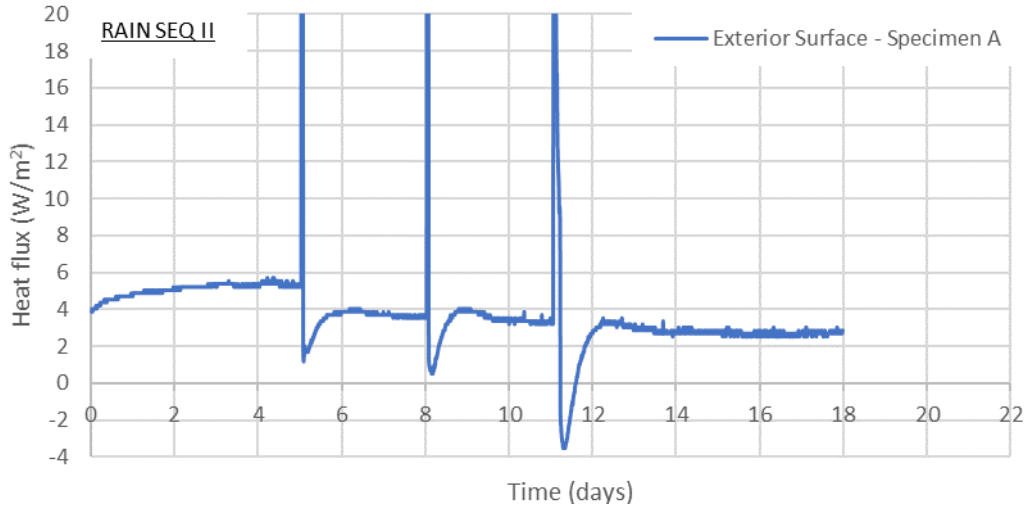
in duplicate. The measurements of the heat flux sensors installed on the interior surface of the specimens showed some instability due to the fact that the heater in the control room was continuously switching on and off during the experiment. In the third test, that instability was significantly reduced by replacing the fan coil heater by an oil heater. The precipitation falling directly on the heat flux sensors installed on the exterior surface of the specimens also cause some disturbance in the measurements of the heat fluxes, however once the precipitation ends the measurements stabilize.



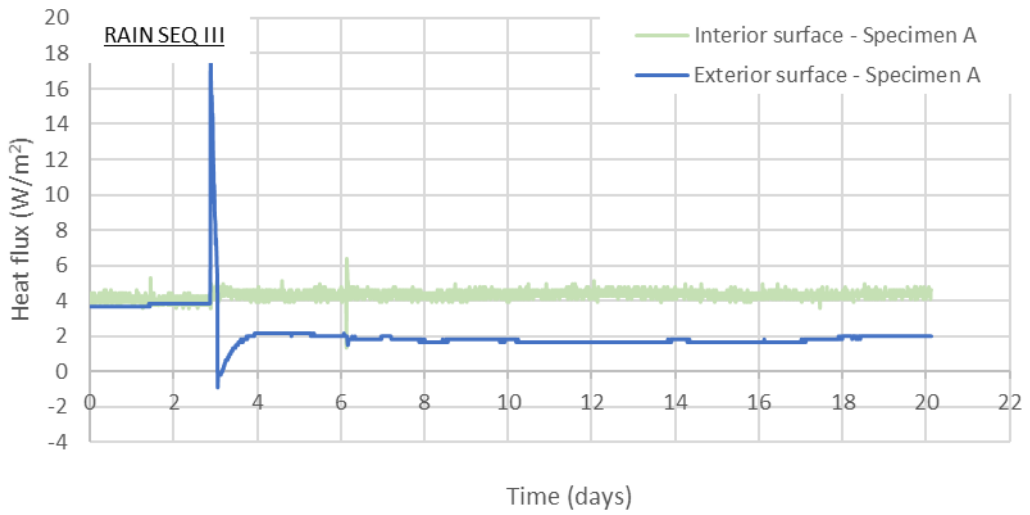
(a)



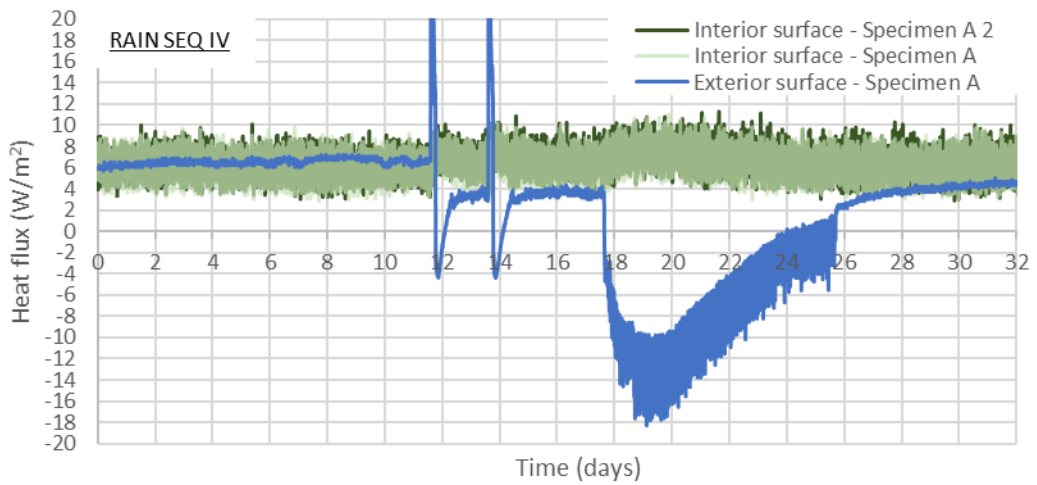
(b)



(c)



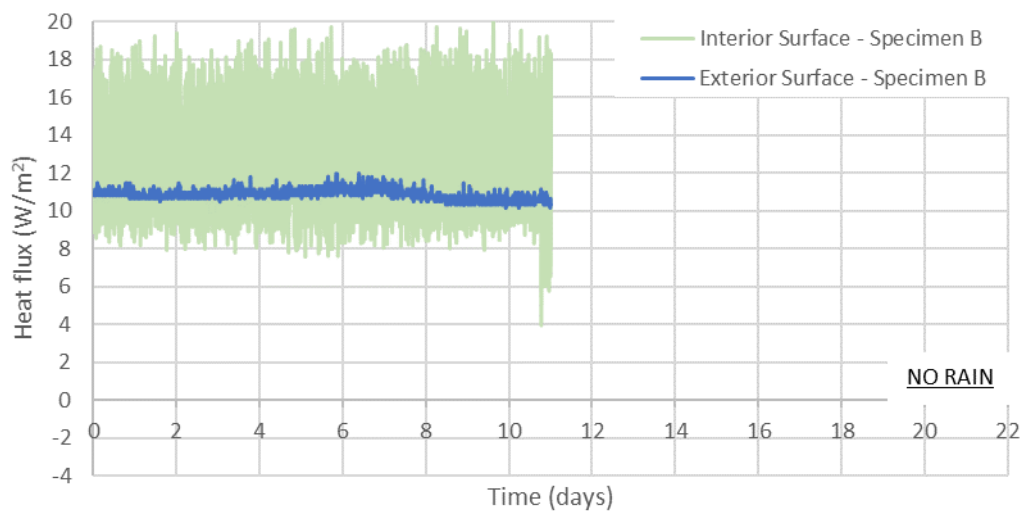
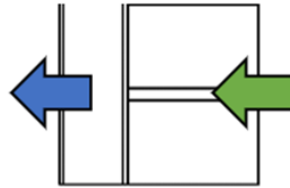
(d)



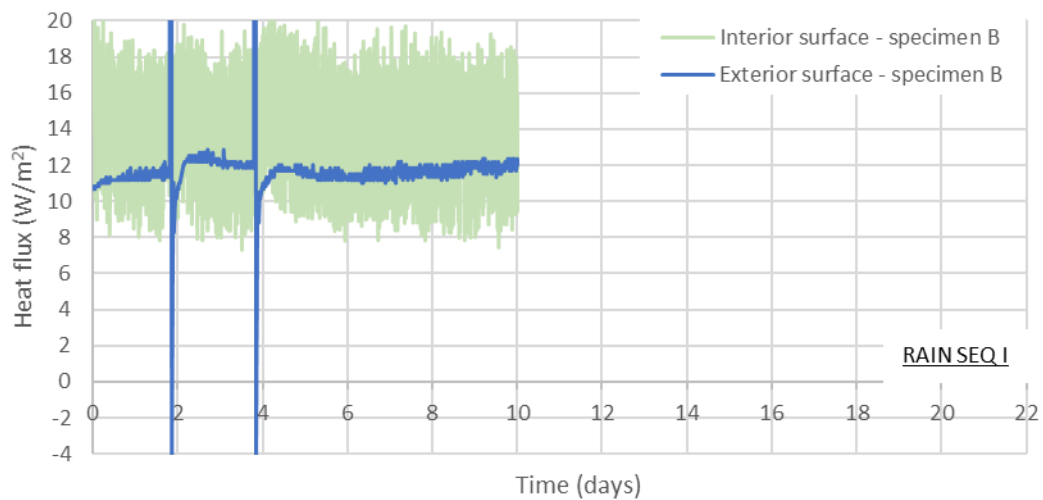
(e)

Figure 54. Heat fluxes across the specimen A during: a) the preliminary test; b) the first test; c) the second test; d) the third test; e) the fourth test.

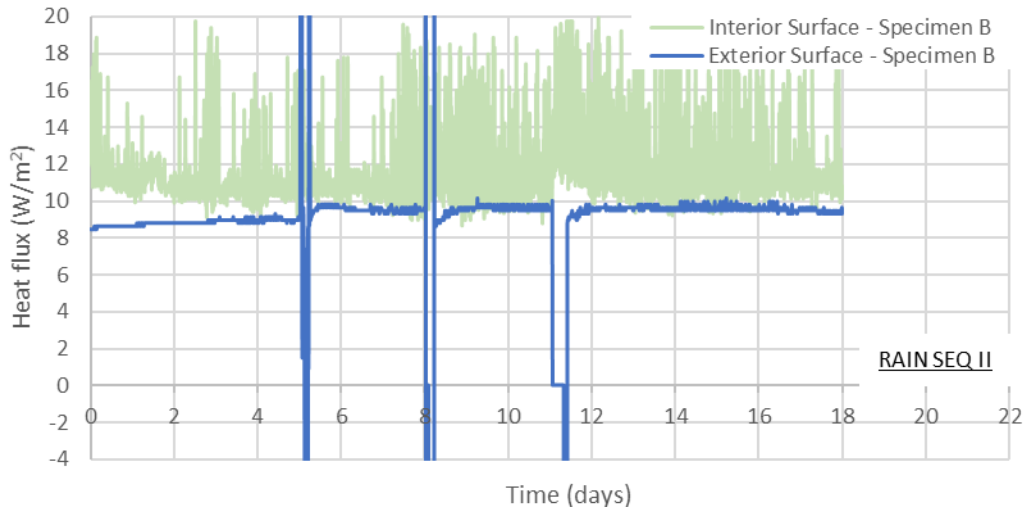
In the fourth test in which precipitation sequence IV was applied, it can be observed that the dehumidifier placed in the rain room also caused some instability in the measurements of the heat flux sensors installed on the exterior surfaces of the specimens. Additionally, it can be observed that both heat flux sensors installed on the interior surface of specimen A measured identical heat fluxes. The same happened with the two heat flux sensors installed on the interior surface of specimen B.



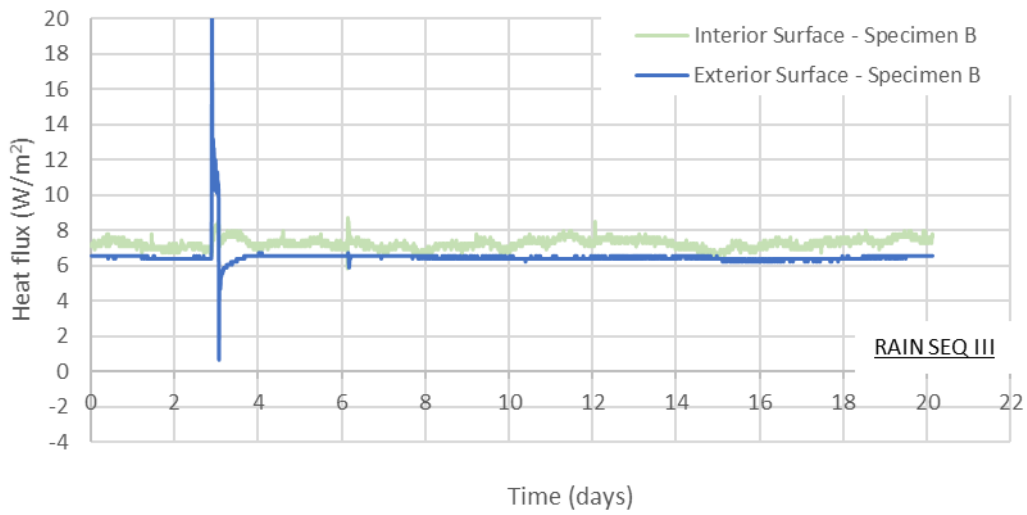
(a)



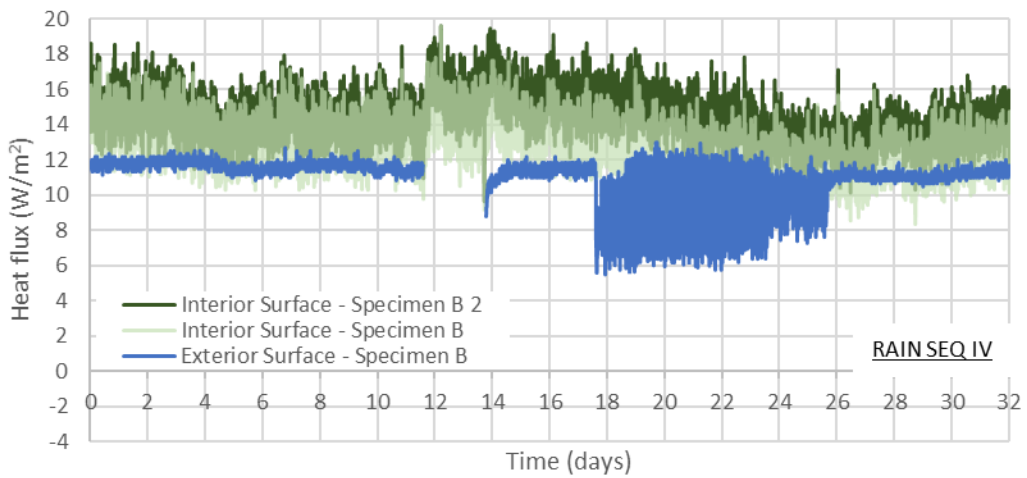
(b)



(c)



(d)



(e)

Figure 55. Heat fluxes across the specimen B during: a) the preliminary test; b) the first test; c) the second test; d) the third test; e) the fourth test.

In the tests, the heat fluxes pass through the specimens from the control room to the rain room i.e., from inside to outside. As expected, lower heat fluxes are found for specimen A when compared to specimen B since the thermal conductivity of mineral wool is lower than the thermal conductivity of the insulating render. For instance, in the preliminary test where no rainy periods were applied and the temperature gradient between the rain room and the control room was 9 °C, the heat flux through specimen A was approximately 7 W/m<sup>2</sup>, whereas through specimen B was approximately 11 W/m<sup>2</sup>.

For specimen A, applying driving rain results in an increase of the heat flux through the interior surface. In the third test, before precipitation the heat flux through the interior surface of specimen A is approximately 4 W/m<sup>2</sup> and after precipitation the heat flux increased to 4.4 W/m<sup>2</sup>. In the fourth test, before precipitation the heat flux is approximately 6 W/m<sup>2</sup> and after precipitation the heat flux increased to 6.7 W/m<sup>2</sup>. The reason for this is the moisture stored in the brick masonry induced by precipitation that increased the bricks thermal conductivity. Thus, the accumulated moisture content in the wall assembly due to the driving rain resulted in an increase of heat losses of 10%.

Since the driving rain hits the specimens at a temperature below the specimens' temperature, the moisture introduced by the precipitation decreases the temperature in the brick masonry of specimen A. Therefore, applying driving rain also results in a decrease of the heat flux through the outer surface of specimen A. In the first test, the heat flux across the outer surface of specimen A decreased from approximately 7 W/m<sup>2</sup> to 4 W/m<sup>2</sup>. In the second test the heat flux diminished from about 5 W/m<sup>2</sup> to 2.5 W/m<sup>2</sup>. In the third test the heat flux lowered from circa 4 W/m<sup>2</sup> to 2 W/m<sup>2</sup>. And finally, in the fourth test the heat flux decreased from approximately 6.4 W/m<sup>2</sup> to 3.4 W/m<sup>2</sup>.

After the wetting period, the drying process begins, absorbing a certain quantity of energy to evaporate the absorbed rainwater and acting as a heat sink. However, as the specimen is tending very slowly to the initial dry state, also the heat fluxes are tending very slowly to the initial values.

For specimen B, it can be observed that the precipitation does not influence the heat fluxes through the specimen. The reason for this is that the rainwater does not enter the wall.

### **3.5. FINAL CONSIDERATIONS**

This chapter examined experimentally the impact of wetting periods on the energy performance of wall test specimens with different insulation systems. Wall test specimen A consists of a masonry wall with a traditional interior insulation system whereas wall test specimen B consists of a masonry wall with an innovative external insulating render system. Four different precipitation sequences were applied against the specimens, while their hygrothermal behaviour was monitored. The obtained measurements of temperatures, relative humidity and heat fluxes are used further ahead to validate a hygrothermal model. Based on the experimental work performed, it can be concluded the following:

- The driving rain was responsible for slightly cooling the rain room and the outer side layers of the wall test specimens.
- There was some instability in the measurements of the heat fluxes due to the use of heater and dehumidifier equipment. Several adjustments were made which enabled the reduction of this effect and carrying out the study.
- In specimen A, the measurement of the relative humidity between the masonry and the insulation clearly showed that the moisture content of the wall increased considerably due to precipitation. In some cases (namely in the fourth test in which the most intense precipitation sequence was applied) saturation was reached (HR=100%) inside the specimen.
- In specimen B, no moisture was found inside the specimen during the tests. Both the temperature profile and the heat fluxes did not vary throughout the tests in spite of the wetting periods.
- After the driving rain, the drying of specimen A occurred very slowly due to the high air humidity of the rain room. Except for the fourth test using the dehumidifier, at the end of all other tests specimen A remained wet, with high moisture content.
- After the rainy periods, the heat flux across the exterior surface of specimen A decreased mainly due to the rainwater absorbed in the wall.

- Driving rain influenced the energy performance of specimen A. Due to the humidification of the wall, the heat flux across the interior surface of specimen A increased by about 10%.
- Driving rain did not significantly influence the energy performance of specimen B as it did not enter the wall since the absorption coefficient of its finishing coating is very low (and classified as nearly waterproof).



# 4

## **VALIDATION OF AN HYGROTHERMAL MODEL WITH EXPERIMENTAL MEASUREMENTS**

### **4.1. METHODOLOGY**

The experimental validation of the one-dimensional WUFI hygrothermal simulation model is performed by comparing the measured and simulated hygrothermal performance of masonry walls with different insulation systems exposed to driving rain. The coupled heat and moisture transfer in the walls is simulated with WUFI Pro. The model accuracy was assessed by comparing the simulated and measured temperature and relative humidity profiles and heat fluxes across the components surfaces. The validation of the hygrothermal model is based on the experimental measurements performed in the experimental prototype developed and described in Chapter 4. Additionally, the determination of the most relevant hygrothermal properties for this study, namely capillary water absorption coefficient, water vapour diffusion resistance factor, and moisture-dependent thermal conductivity of solid brick and insulating render system is carried out to use in the numerical simulation and validate the hygrothermal model.

The accuracy of the validation process is assessed by comparing the measured and simulated temperatures, relative humidity and heat fluxes using the statistical parameters coefficient of determination, goodness-of-fit, normalized mean bias error and coefficient of variation of the root mean square error.

In the first section of this chapter, a description of the selected hygrothermal model and computer program (one-dimensional WUFI advanced hygrothermal simulation model and WUFI Pro) is provided. Next, the comparison between the experimental and numerical results is given. Here, the wall configurations, boundary conditions and

material properties used in the numerical simulations are described. To end, the validation is attested by the statistical parameters and the main conclusions are summarized.

## **4.2. HYGROTHERMAL MODEL**

From the available numerical simulation tools, it was selected the one-dimensional WUFI advanced hygrothermal simulation model to calculate the dynamic hygrothermal behaviour of walls under real climatic conditions. The model allows calculation of the transient coupled one-dimensional heat and moisture transport in walls exposed to natural weather. The WUFI model was selected because it is a well-known model with great potentialities for predict the influence of moisture on the energy performance of walls (Künzel, Schmidt and Holm 2002, Capener et al. 2014).

WUFI is the acronym for "Wärme- und Feuchtetransport instationär" ("Transient Heat and Moisture Transport"). WUFI Pro is the computer program for calculating the simultaneous heat and moisture transport in one-dimensional multi-layer building components with the WUFI hygrothermal model. It has been developed at Fraunhofer IBP and it has repeatedly been validated by comparison with experimental results (Krus 1998, Künzel, Schmidt and Holm 2002, Antretter et al. 2011, Capener et al. 2014).

WUFI Pro takes into account for the heat transport: thermal conduction, enthalpy flows with phase change, short-wave solar radiation and night-time long-wave radiation cooling. The vapour transport mechanisms included in WUFI is vapour diffusion. In turn, the liquid transport mechanisms taken into account are capillary conduction and surface diffusion (Wufi-wiki 2019a). The boundary conditions for each time step are expressed in terms of meteorological data (temperature, relative humidity, driving rain, radiation), since in building physics these are the relevant parameters specifying the conditions at surfaces exposed to natural weather. However, conditions for laboratory experiments can also be expressed as 'meteorological' data.

For the coupled heat and mass transfer for vapor diffusion, liquid flow and thermal transport in the envelope parts the model solves the equations detailed in (Künzel 1995). The driving potentials are temperature and relative humidity. On the left-hand side of equations are the storage terms. The fluxes on the right-hand side in both equations depend on local temperature and humidity conditions (Holm et al. 2004).

Moreover, the following hygric extensions corresponds to refinements of the simulation model. These extensions refer to moisture storage function, liquid transport coefficient and moisture dependent thermal conductivity. The latter extension is essential for this study since it allows taking account of the influence of water content on heat transport across the building component.

- Moisture storage function – can be introduced as a table or approximated using sorption moisture at 80% relative humidity ( $w_{80}$ ) and free water saturation ( $w_f$ ) according to the following equation (Wufi-wiki 2019f):

$$w(\varphi) = w_f \cdot \frac{(b - 1) \cdot \varphi}{b - \varphi} \quad (7)$$

Where:

$w(\varphi)$	[kg/m <sup>3</sup> ]	Moisture content at relative humidity $\varphi$
$w_f$	[kg/m <sup>3</sup> ]	Moisture content at free saturation
$\varphi$	[-]	Relative humidity
$b$	[-]	Approximation factor

- Liquid transport coefficient for suction  $D_w$ s – the predominant moisture transport mechanism in capillary porous materials is the capillary liquid transport which is basically a diffusion phenomenon in the context of building physics (Wufi-wiki 2019b).

$$g_w = -D_w(w) \cdot \text{grad } w \quad (8)$$

Where:

$g_w$	[kg/(m <sup>2</sup> s)]	Liquid transport flux density
$w$	[kg/m <sup>3</sup> ]	Moisture content
$D_w$	[m <sup>2</sup> /s]	Liquid transport coefficient

The liquid transport coefficient for suction  $D_w$ s describes the capillary uptake of water when the imbibing surface is fully wetted. In the context of building physics this corresponds to rain on a façade or an imbibition experiment. This coefficient can be introduced or generated by WUFI from the following approximate relation between  $D_w$ s and the water absorption coefficient  $A$ :

$$D_w = 3.8 \cdot \left(\frac{A}{w_f}\right)^2 \cdot 1000 \left(\frac{w}{w_f}\right)^{-1} \quad (9)$$

Where:

A	[kg/m <sup>2</sup> s <sup>1/2</sup> ]	Water absorption coefficient
w <sub>f</sub>	[kg/m <sup>3</sup> ]	Free water saturation
w	[kg/m <sup>3</sup> ]	Moisture content

- Thermal conductivity, moisture dependent  $\lambda_w$  – the dependence of the heat conductivity on the moisture content can be taken into account by filling in a table with the relevant data. WUFI interpolates linearly between table entries (Wufi-wiki 2019g).

If a simple linear dependence of the heat conductivity on the moisture content is sufficient, a table may be generated by entering the moisture-induced heat conductivity supplement b. The linear interpolation in this table is equivalent to evaluating the formula:

$$\lambda_w(w) = \lambda_0 \cdot \left(1 + b \cdot \frac{w}{\rho_s}\right) \quad (10)$$

Where:

$\lambda_w$	[W/(m K)]	Heat conductivity of moist material
$\lambda_0$	[W/(m K)]	Heat conductivity of dry material
$\rho_s$	[kg/m <sup>3</sup> ]	Bulk density of dry material
b	[%/m-%]	Moisture-induced heat conductivity supplement

The supplement b gives the fractional increase in % of the heat conductivity per mass-% moisture. Its value depends on the material.

Note that, in this context, heat conductivity of moist materials means exclusively the influence of stationary water on heat transport. Water vapor diffusion with phase change (evaporation and condensation of water) also contributes to heat transport, but this is allowed for by separate terms in the transport equations. In fact, water vapor diffusion with phase change is regarded as a heat source/heat sink through condensation/evaporation (Künzel 1994).



---

**Short-Wave (Solar) Radiation Absorptivity**

It determines the fraction of total incident solar radiation that is absorbed by the component -

---

**Long-Wave Radiation Emissivity**

It describes the efficiency of long-wave emission (heat loss by thermal radiation). If it is possible to do without **nighttime cooling**, it is recommended to set the long-wave emissivity to zero. Otherwise, enter the emissivity of the component's surface, but then make sure that you are using appropriate weather data on the **long-wave radiation exchange**. -

---

**Ground Short-Wave Reflectivity**

It gives the fraction of short-wave global radiation reflected by the terrestrial surroundings. Needed for the radiation conversion for inclined surfaces. -

---

**Adhering Fraction of Rain**

It takes into account that some of the rainwater hitting the wall surface splashes off on impact and is not available for capillary absorption. For ordinary walls, WUFI uses a value of 0.7, which is adequate for most cases. You may select "No absorption", however, if the façade is protected from rain and no rain absorption shall take place at all. -

---

Interior Surface	<b>Heat Resistance/ Heat Transfer Coefficient (Rsi)</b>	m <sup>2</sup> K/W
	<b>Sd-Value</b>	m

---

To define the climate boundary conditions, WUFI needs the climate data presented in Table 14 for each time step. The climatic conditions must be defined on each side of the component by selecting a file with weather data or by specifying schematic sine curves for the climate data. The program has weather files for several locations worldwide but other weather files can also be read in \*.WET or \*.TRY or \*.DAT or \*.IWC or \*.WAC or \*.WBC format (Wufi-wiki 2019h). It is possible to use outdoor climates or laboratory climates. In fact, indoor or outdoor conditions can be assigned to both sides of the component.

Table 14. WUFI Pro inputs: climate conditions

Outdoor climate	Temperature	°C
	Relative humidity	%
	Solar global radiation	W/m <sup>2</sup>
	Solar diffuse radiation	W/m <sup>2</sup>
	Rain load vertically incident	L/(m <sup>2</sup> h)
	Wind direction	°
	Wind speed	m/s
	Barometric pressure	hPa
	Long-wave atmospheric radiation, if radiation cooling is to be accounted for during the night	W/m <sup>2</sup>
	Cloud index	-
Indoor climate	Temperature	°C
	Relative humidity	%

WUFI offers two different methods to estimate the wind-driven rain load on the building component. The first method estimates the driving rain load on a surface of arbitrary orientation from data on normal rain, wind velocity and direction using the following relation (Wufi-wiki 2019i):

$$R_{WDR} = R_h \cdot (R_1 + R_2 \cdot V_{10} \cdot \cos \theta) \quad (11)$$

Where:

$R_{WDR}$ [l/(m <sup>2</sup> h)]	Wind-driven rain load or wind-driven rain intensity
$R_1, R_2$ [s/m]	Driving rain coefficients
$R_h$ [mm/h]	Normal rain on a horizontal surface in open field
$V_{10}$ [m/s]	Mean wind velocity measured at a height of 10 m in open area
$\theta$ [°]	Angle between the wind direction and the orthogonal to the wall

Wind velocity is that component of the mean wind velocity (measured at a height of 10 m, in open area), which is orthogonal to the building surface. This component is determined from the mean wind velocity and the mean wind direction. The data on normal rain, wind velocity and wind direction are read from the selected weather file.

$R_1$  and  $R_2$  are strongly dependent on the specific location on the building façade. For vertical surfaces,  $R_1$  is zero. For other inclinations than vertical, WUFI defaults to the rain coefficient  $R_1=1$  and  $R_2=0$  (i.e. wind-driven rain load = normal rain). About the driving rain coefficient  $R_2$ , WUFI have predefined values, one for a low building and three for different heights on a tall building (see Table 15).

Table 15.  $R_2$  values.

Short Building, height up to 10 m	$R_2 = 0.07$
Tall Building, lower part, up to 10 m	$R_2 = 0.05$
Tall Building, middle part, up to 10-20 m	$R_2 = 0.1$
Tall Building, upper part, more than 20 m	$R_2 = 0.2$

Alternatively, the wind-driven rain load on a vertical wall can be estimated with the method of ASHRAE Standard 160P “Design criteria for moisture control in buildings”. This was the method chosen in this study. This method uses the following relation:

$$R_{WDR} = R_h \cdot F_E \cdot F_D \cdot 0.2 \cdot V_{10} \cdot \cos \theta \quad (12)$$

where:

$R_{WDR}$ [l/(m <sup>2</sup> h)]	Wind-driven rain load or wind-driven rain intensity
$R_h$ [mm/h]	Normal rain on a horizontal surface in open field
$F_E$ [s/m]	Rain exposure factor
$F_D$ [s/m]	Rain deposition factor
0.2 [s/m]	Empirical constant
$V_{10}$ [m/s] area	Mean wind velocity measured at a height of 10 m in open area
$\theta$ [°] the wall	Angle between the wind direction and the orthogonal to the wall



The rain exposure factor  $F_E$  depends on the surrounding terrain and the height of the building. ASHRAE Standard 160P recommends the values presented in Table 16 that range from 0.7 to 1.5. Open exposure includes hilltops and coastal areas, whereas sheltered exposure includes shelter from trees, nearby buildings or a valley. The higher the height of the building and its exposure to rain, the higher the rain exposure factor.

Table 16.  $F_E$  values

	Terrain		
	Open	Medium	Sheltered
Height < 10 m	1.3	1.0	0.7
10 – 15 m	1.3	1.1	0.8
15 – 20 m	1.4	1.2	0.9
20 – 30 m	1.5	1.3	1.1
30 – 40 m	1.5	1.4	1.2
40 – 50 m	1.5	1.5	1.3
> 50 m	1.5	1.5	1.5

The rain deposition factor  $F_D$  describes the influences of the building itself. ASHRAE Standard 160P prescribes the estimated values presented in Table 17.

Table 17.  $F_D$  values

Walls on a pitched roof building	$F_D = 0.5$
Walls on a flat roof building	$F_D = 1.0$
Walls subject to rain runoff	$F_D = 2.0$

WUFI Pro offers the results presented in Table 18 as graphs (Zirkelbach et al. 2007). In this study the heat flux is of particular importance, namely the heat flux across the component interior surface which characterizes the heat losses across the component and its energy performance. In fact, WUFI gives the transient heat losses across the component taking into account the moisture content in the component which results from its exposure to real climatic conditions including wind driven rain.

Table 18. Wufi Pro results

Quick Graph	<b>Total water content</b>	kg/m <sup>3</sup>	It shows whether moisture has accumulated or dried during the investigated period.	
	<b>Water content in individual layers</b>	kg/m <sup>3</sup>	Show the water content of each layer.	
	<b>Temperature and dew point at the monitoring positions</b>	°C	Allows examining whether the temperature falls below the dew point at any time during the investigated period at predefined points.	
Result graphs	<b>Heat Flux</b>	W/m <sup>2</sup>	Show the fluxes of heat across the layer interfaces and the component surfaces.	
	<b>Moisture Flux</b>	kg/s m <sup>2</sup>	Show the fluxes of moisture across the layer interfaces and the component surfaces.	
	<b>Temperature, RH</b>	°C, %	Show the courses of temperature and relative humidity for each monitoring position.	
	Profiles	<b>Temperature</b>	°C	The progress in time of the temperature profiles, showing the initial and the last profiles.
		<b>Relative Humidity</b>	%	The progress in time of the RH profiles, showing the initial and the last profiles.
<b>Water Content</b>		kg/m <sup>3</sup>	The progress in time of the water content profiles, showing the initial and the last profiles.	

In addition, WUFI has a postprocessor that gives the transient thermal transmission. The post processor analyses the hourly temperatures and heat flows resulting from the full transient WUFI simulation, taking into account the real hygrothermic conditions in the construction which results from its exposure to weather and from the occupants' behaviour. This includes the following effects (Zirkelbach et al. 2007):

- Variable moisture content on the thermal conductivity.
- Additional thermal transport processes (such as latent heat transport by vapor flows).
- Additional heat sources (such as solar radiation).

- Parameters depending on environmental conditions (such as wind-dependent surface transfer coefficients).

Thus, the postprocessor computes a monthly transient thermal transmittance  $U$  calculated from transient heat flux through the interior surface of the component and temperature difference between indoor and outdoor air temperature, using the following formula:

$$U = \frac{-Q}{\Delta T_a} \quad (13)$$

Where:

$Q$	[W/m <sup>2</sup> ]	Monthly mean value of heat flux through the interior surface
$\Delta T_a$	[K]	Monthly mean value of temperature difference between indoor and outdoor air temperature

In this study it was chosen to analyse the heat flux across the wall interior surface instead of the monthly transient thermal transmittance. This was due to the fact that the monthly transient thermal transmittance is influenced by the monthly temperature difference between indoor and outdoor temperature.

The complex hygrothermal processes in a building component need to be simplified to make their simulation accessible. Therefore, several limitations of the WUFI mathematical model had to be accepted. In particular for external walls, the following aspects should be taken into account. First, WUFI Pro only deals with one-dimensional processes. Also, several transport phenomena have been neglected such as convective heat or vapor transport by air flows. In the calculation the interface between two capillary-active materials is treated as ideally conducting, whereas in reality there often is a transfer resistance which may reduce the moisture transport considerably (Wufi-wiki 2019j).

In addition, if a material has a pronounced hysteresis in its moisture storage function, it may not be sufficient to use an averaged moisture storage function for the calculation. The enthalpy flows resulting from the transport of liquid water across a temperature differential are ignored. The heat transfer coefficients at the surface are treated as constant or exhibiting a simple predefined dependence on wind speed, which is also a simplification (Wufi-wiki 2019j).

### **4.3. COMPARISON BETWEEN EXPERIMENTAL AND NUMERICAL RESULTS**

#### **4.3.1. GEOMETRY, MATERIAL PROPERTIES AND BOUNDARY CONDITIONS**

The hygrothermal behaviour of the two wall test specimens described in section 3.2.1. was studied. They consist of single leaf masonry assemblies with different insulation systems. The insulation systems are a traditional interior insulation system and an innovative external insulating render system. From the outside to the inside, the wall assemblies consist of:

- *Configuration A (masonry wall with traditional interior insulation system):*  
11 cm *solid* brick – 5 cm mineral wool – 1.3 cm gypsum board
- *Configuration B (masonry wall with innovative external insulating render system):*  
silicate paint – 0.5 cm finishing render – 5 cm insulating render – 11 cm solid brick

The dry thermal transmittances U-values of configurations A and B calculated from the dry conductivities and dimensions of their components as described in EN ISO 6946:2017 *Building components and building elements – Thermal resistance and thermal transmittance – Calculation method* (EN ISO 6946: 2007) are 0.62 and 1.18 W/(m<sup>2</sup> K), respectively. Moreover, the insulating render is a lightweight render formulated with natural cork aggregates, sands and natural hydraulic lime. It is around eight times more thermal insulating than traditional renders.

The properties of brick, mineral wool, gypsum board and insulating render system used to simulate the hygrothermal performance of the wall assemblies are given in Table 19 and Table 20. Table 19 presents the values of bulk density, porosity, specific heat capacity, water vapour resistance factor and capillary water absorption coefficient, whereas Table 20 presents the thermal conductivities as a function of moisture content. The thermal conductivities, water vapor diffusion resistance factors and capillary water absorption coefficients of brick and insulating render system were experimentally determined as thoroughly reported in the following section 4.3.1.1. All the other material properties were found in the literature. Note that in Table 19 it was considered that the insulating render system composed of three layers, insulating render, finishing render and paint, works as one.

Table 19. Material properties.

<b>Material</b>	<b>Bulk density</b>	<b>Porosity</b>	<b>Specific heat capacity</b>	<b>Water vapour resistance factor</b>	<b>Capillary water absorption coefficient</b>
	$\rho$	$\epsilon$	$c$	$\mu$	$A$
	kg/m <sup>3</sup>	m <sup>3</sup> /m <sup>3</sup>	J/ (kg K)	-	kg/(m <sup>2</sup> s <sup>1/2</sup> )
Brick	1925	0.28	920	17*	0.06*
Mineral wool	60	0.95	850	1.3	1.3
Gypsum board	850	0.65	850	8.3	16
Insulating render system	650	0.40	900	6*	0.003*

(\*) material properties experimentally determined in following section 4.3.1.1.

Table 20. Thermal conductivities as a function of moisture content.

<b>Material</b>	<b>Water content (kg/kg)</b>	<b>Thermal conductivity (W/m K)</b>
Brick	0; 0.02; 0.07 *	0.75; 1.03; 1.28 *
Mineral wool	0; 0.040; 0.047; 0.050	0.04; 0.04; 0.06; 0.12
Gypsum board	0; 0.019; 0.024	0.195; 0.234; 0.245
Insulating render	0; 0.06; 0.21 *	0.15; 0.17; 0.24 *

(\*) material properties experimentally determined in following section 4.3.1.1.

In the numerical simulations, the climate conditions acting on the walls are exterior and interior laboratory climates, namely the measured air temperature and relative humidity of the surroundings of the walls. Also, the driving rain applied against the external side of the walls is simulated. The walls were not exposed to solar radiation neither in the experiment nor in the simulation.

The temperature and relative humidity in the rain room and in the control room shown in Figure 56 and Figure 57 are assumed as boundary conditions in the numerical simulation. It corresponds to the temperature and relative humidity in the rain room and in the control room during the third experiment that is mentioned in Chapter 3. The third experiment was simulated because it has the least instability in the measurements of heat fluxes.

The wall assemblies are subjected to a temperature gradient of 5 °C between the surroundings of both surfaces, as well as to a rainy period of 4 hours spraying a water flow of 1.5 L/ (m<sup>2</sup> min) evenly distributed over the external surfaces of the walls. The rainy period is delimited by the vertical lines.

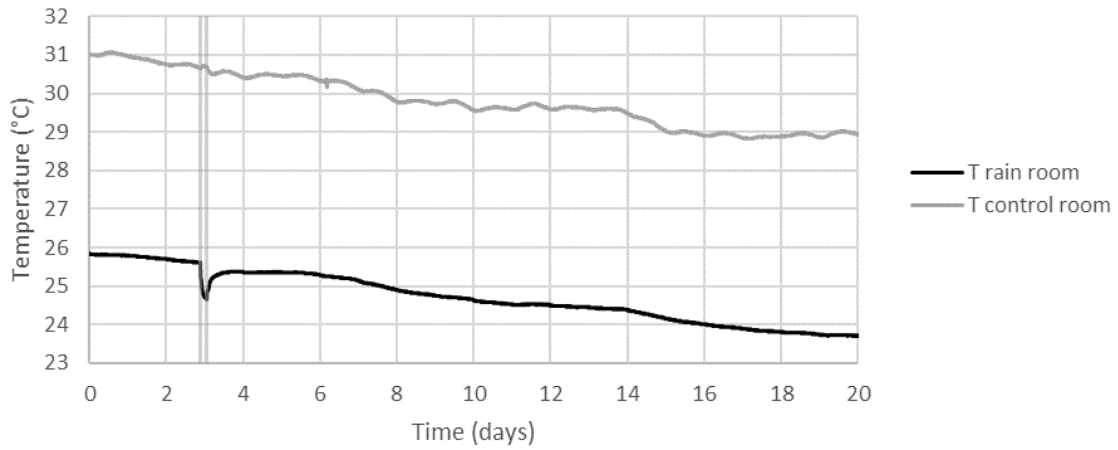


Figure 56. Temperature in the rain room and in the control room during the third experiment

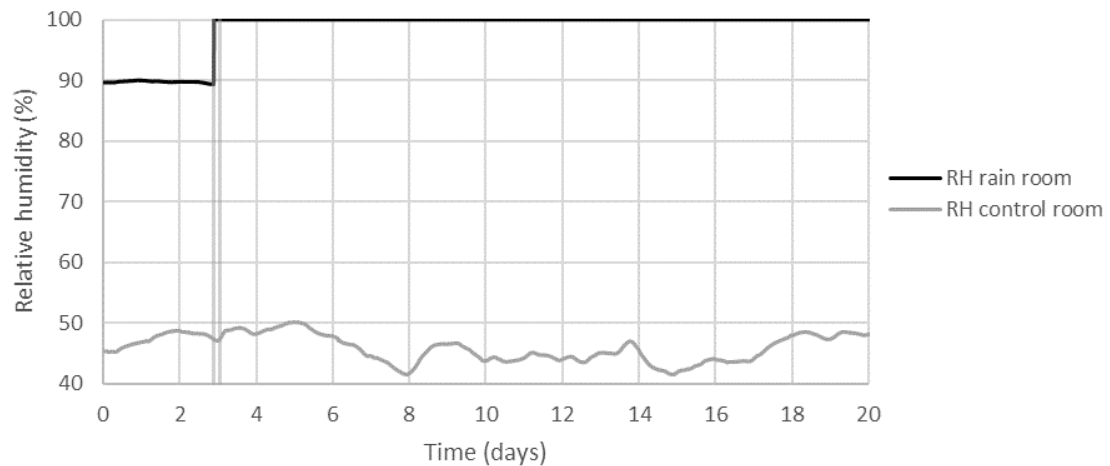


Figure 57. Relative humidity in the rain room and in the control room during the third experiment.

In the control room a heater was used to obtain a temperature of approximately 30 °C. In the rain room the free-running temperature conditions were implemented. The temperature in the rain room was approximately 25 °C and it was observed a slight decrease of around 1 °C due to the driving rain. Obviously, these conditions do not confirm with realistic boundary conditions, but were selected to obtain a temperature gradient between the interior and exterior surfaces of the walls.

The precipitation significantly increased the relative humidity in the rain room, from approximately 90% to 100%, reaching the maximum possible water vapour content in air i.e., the vapour saturation pressure. After the precipitation, the relative humidity remained 100% until the end of the experiment. The relative humidity in the control room varied between 40 and 50% throughout the experiment.

The former temperatures and relative humidity were entered into the WUFI Pro software as outdoor and indoor climate boundary conditions for the calculation, as well as the rainy period. To simulate the rainy period at the software, the ASHRAE Standard 160P method previously mentioned was adapted in order to apply 90 L/(m<sup>2</sup> h) on the walls, which corresponds to 1.5 L/(m<sup>2</sup> min), for 4 hours. The rain exposure factor ( $F_E$ ) was 1.3 because the height of the wall test specimens is below 10 m and the rain exposure of the specimens is open exposure, without any shelter. The rain deposition factor ( $F_D$ ) was 2.0 since the specimens were subjected to rain runoff.

With respect to the surface transfer coefficients, the conventional value of 0.125 m<sup>2</sup> K/W is used for both the internal and external surface heat resistance. No fraction of solar radiation is absorbed by the walls and the long-wave radiation emissivity is also set to 0. The sd-value of the surface coating of configuration A is 0 m because the wall is uncoated. For configuration B, the sd-value of the surface coating (paint coat) is 0.12. The rainwater absorption factor is 0.7.

#### 4.3.1.1. Experimental characterization of brick and insulating render system

One of the important steps of the present work was the determination of the hygrothermal properties to characterize the hygrothermal behaviour of the investigated materials. In that sense, a laboratory test campaign was carried at the Building Physics Laboratory of Faculty of Engineering University of Porto. The main goal of the experimental campaign

is to determine accurate results of the most relevant hygrothermal properties for this study, namely capillary water absorption coefficient, water vapour diffusion resistance factor, and moisture-dependent thermal conductivity of solid brick and an insulating render system. The insulating render system consists of an insulating render, a finishing render, and a paint. The obtained results of material properties presented in this section were used as input to numerical simulation. The relevance of those properties lies in the attainment of reliable simulation results and strong validation of the hygrothermal model.

The selected materials for this study were solid brick and insulating render system. The brick was chosen because the brick masonry is the dominating wall type of existing building stock in European countries (Blumberga et al. 2015) and it was applied in the experimental prototype. The insulating render system was chosen because it became more currently applied in the rehabilitation of exterior walls of existing buildings and there is not enough information that accurately characterizes its hygrothermal properties required for the simulation.

The insulating render system consists of an insulating render, a finishing render, and a paint. The insulating render is a lightweight render, formulated with natural cork aggregates, sands and natural hydraulic lime (NHL). It is a sustainable and ecological building product thanks to the introduction of cork and natural hydraulic lime in the formula. It has the advantage of being around 7 or 8 times more thermal insulating than traditional renders and represents a reduction of almost 50% in weight compared to traditional renders because of the low density of the aggregate.

#### Water absorption coefficient

The capillary water absorption test based on the European standard EN ISO 15148:2002 *Hygrothermal performance of building materials and products — Determination of water absorption coefficient by partial immersion* (EN ISO 15148: 2002) was carried out to determine the water absorption coefficient of the solid brick and the insulating render system applied to the exterior surface of the test specimens. Two specimens of each material were prepared, and the side faces longitudinal sealed at the Building Physics Laboratory. No more specimens were used because none were available. The solid brick specimens' dimensions are 225x105x70 mm and the insulating render system specimens'



dimensions are 210x210x20 mm. The insulating render system specimens consists of insulating render, finishing render and paint.

The test consists in measuring the change in mass of the test specimen which has the bottom surface in contact with water over a period of 24 h. The water adhering to the surface and not absorbed by the test specimen is completely removed by blotting with a sponge before the specimen is weighed. It is intended to assess the rate of absorption of water by capillary action specifically from driving rain.

Each specimen is placed in the tank so that its base is resting on point supports instead of the bottom of the tank, so that there can be a greater surface area of contact with the water. The water level is kept constant during the test at 5 mm above the base of the specimen. The timer starts when the specimen is immersed in the water. After 5 min the specimen is removed from the water and weighed. The procedure of immersion, removal, surface drying and weighing is repeated at times as 20 min, 1 h, 2 h, 4 h, 8 h and 24 h after immersion to give a series of masses  $m_t$  at times  $t$ .

Afterwards the difference between the mass at each weighing and the starting mass per area  $\Delta m_t$  is plotted against the square root of the weighing times  $\sqrt{t}$ . These resulting curves of solid brick and insulating render system are shown in Figure 58. As shown in the figure, for both materials a straight line can be drawn through the values of  $\Delta m_t$  against  $\sqrt{t}$ . The water absorption coefficient  $A_w$  is calculated from equation (14).

$$A_w = \frac{\Delta m'_{tf} - \Delta m'_0}{\sqrt{t_f}} \quad (14)$$

where:

$\Delta m'_{tf}$	[Kg/m <sup>2</sup> ]	value of $\Delta m$ on the straight line at time $t_f$
$\Delta m'_0$	[Kg/m <sup>2</sup> ]	value of $\Delta m$ at the beginning of the test
$t_f$	[s]	duration of the test, generally 1 day

In the brick case the straight line has a sudden decrease in slope on the last data point as shown at the top of Figure 58a, which indicates that liquid water has appeared on the top surface of the solid brick specimens. Therefore, the water absorption coefficient of the brick was calculated with the exclusion of the last value.

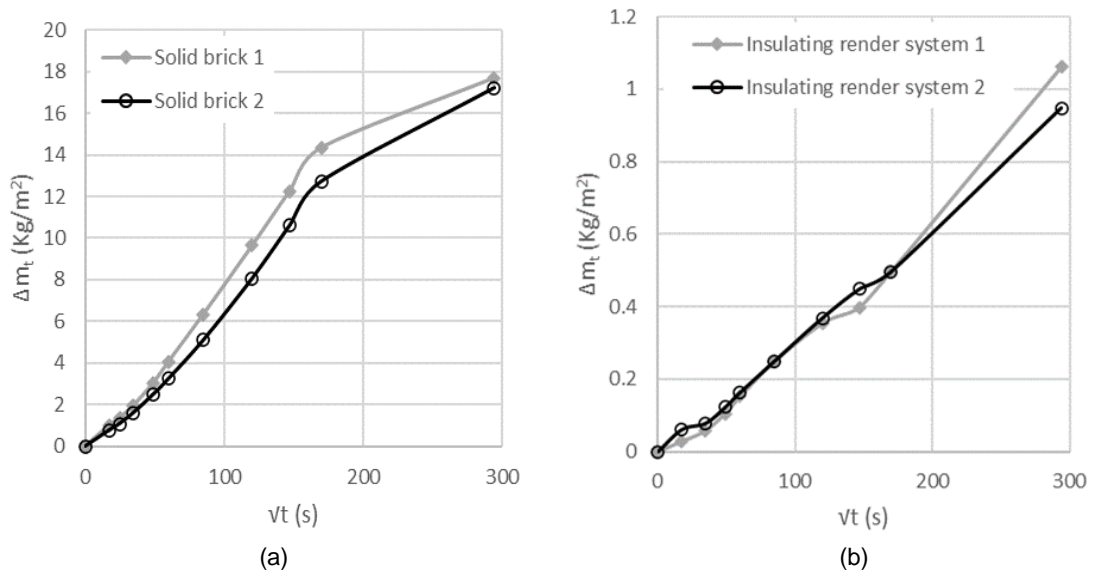


Figure 58. Capillary absorption as a function of the square root of time for: a) solid brick; b) insulating render system.

The capillary water absorption results of the analysed materials are presented in Table 21. The obtained mean capillary water absorption coefficient for the brick was 0.060 Kg/(m<sup>2</sup> s<sup>1/2</sup>), and for the insulating render system was only 0.003 Kg/(m<sup>2</sup> s<sup>1/2</sup>). The different capillary water absorption coefficients and behaviour of the analysed materials stands out. In fact, a large amount of water entered the solid brick specimens while only a very small amount of water entered the insulating render system specimens. This was due to the external paint that kept out moisture from the insulating render system specimens protecting the insulating render.

Table 21. Capillary water absorption coefficient results.

Material	A Kg/ (m <sup>2</sup> s <sup>1/2</sup> )	Classification
Solid brick 1	0.0602	Quick suction
Solid brick 2	0.0586	
Insulating render system 1	0.0036	Nearly waterproof
Insulating render system 2	0.0032	

Therefore, the results of capillary water absorption coefficients show that solid brick is highly capillary active, whereas insulating render system is hardly capillary active. This means that, according to German standard DIN 52 617 (DIN 1987), the brick can be

classified as quick suction while the insulating render system can be classified as nearly waterproof.

De Freitas (1992) and Sousa (1996) also determined the capillary water absorption coefficient of the solid brick, having obtained a value of  $0.05 \text{ Kg}/(\text{m}^2 \text{ s}^{1/2})$ . This value is very close and in agreement with the value obtained in this work.

Regarding the capillary water absorption coefficient of the insulating render system, no value that allows direct comparison is known. However, it can be compared with the capillary water absorption coefficients of other insulating render systems. Maia (2019) determined the capillary water absorption coefficients of an insulating render system composed of EPS aggregates, lime binder and finished with organic coating and of another composed of EPS aggregates, mixed binders and finished with aqueous painting. The value obtained was  $0.002 \text{ Kg}/(\text{m}^2 \text{ s}^{1/2})$  for both insulating render systems. This value is close to the value of the capillary water absorption coefficient determined in the present work although it is not exactly the same insulating render system.

#### Water vapour permeability

The water vapour permeability was determined according to EN ISO 12572:2001 *Hygrothermal performance of building materials and products – Determination of water vapour transmission properties* (EN ISO 12572: 2001). Two specimens of each material (brick and insulating render system) of 210x210x20 mm were used (see Figure 59).



Figure 59. Specimens of brick and insulating render system for the water vapour permeability test.

The method of preparing the solid brick specimens was slicing and joining the solid bricks to obtain the required dimensions. Regarding the preparation of the thermal render system specimens, they were produced by the manufacturer. Note that the thermal render system specimens consist of insulating render, finishing render and paint.

All the specimens were sealed with paraffin to the open side of stainless test cups containing an aqueous saturated solution, as shown in Figure 60. The aqueous saturated solution used was potassium nitrate  $KNO_3$  which produces a relative humidity of 93% (wet cup). The potassium nitrate  $KNO_3$  was placed with a depth of 15 mm in the bottom of each cup. Wet cup tests are the most appropriate tests for this study since they give guidance about the performance of materials under high humidity conditions.



Figure 60. Scheme of the assembly for the wet-cup measurements (Ramos 2007)

The assemblies were then weighed and placed in a temperature and humidity controlled test chamber at 23 °C and 50% of relative humidity (see Figure 61). The temperature and relative humidity within the test cups during the test were 23 °C and 93%, respectively. Taking into account the different partial vapour pressure between the test cup and the chamber, a vapour flow occurs through the specimens. Periodic weighings of the assembly were made to determine the rate of water vapour transmission in the steady state until the mass variation was constant with a  $\pm 5\%$  tolerance. Time interval between successive weighings was 24 or 72 hours. The weighing results are presented in Appendix A.

For each set of successive weighings, the mass change rate  $\Delta m_{12}$  was calculated using:

$$\Delta m_{21} = \frac{m_2 - m_1}{t_2 - t_1} \quad (15)$$

where

$m_1$	[Kg]	mass of the test assembly at time $t_1$
$m_2$	[Kg]	mass of the test assembly at time $t_2$
$t_1$ and $t_2$	[s]	successive times of weighings

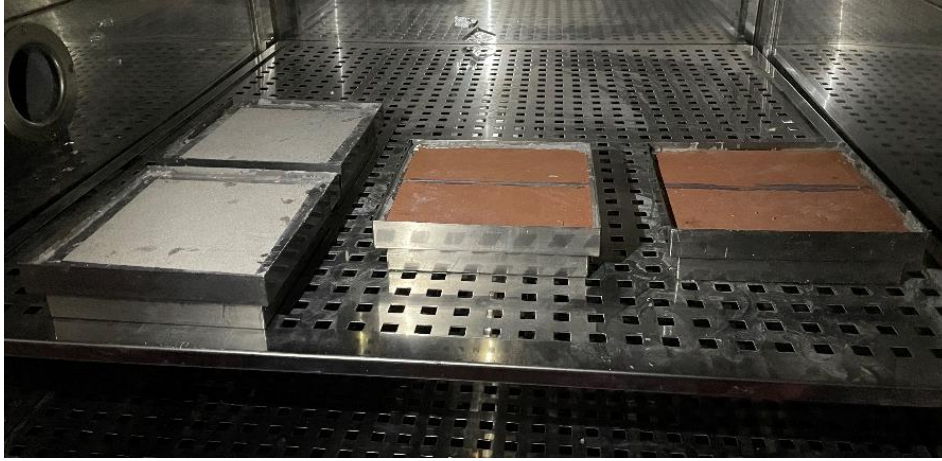


Figure 61. Test cups with the specimens inside the climatic chamber.

The results of water vapour flow  $G$ , water vapour permeance  $W$ , water vapour permeability  $\delta$ , water vapour resistance factor  $\mu$  and water vapour diffusion-equivalent air layer thickness  $s_d$  are shown in Table 22.

Table 22. Results of the water vapour transmission properties of solid brick and insulating render system.

Material	$G$ kg/s	$W$ kg/(m <sup>2</sup> s Pa)	$\delta$ kg/(m s Pa)	$\mu$ -	$S_d$ m
Solid brick 1	2.90E-08	5.85E-10	1.17E-11	17.10	0.34
Solid brick 2	3.06E-08	6.17E-10	1.23E-11	16.21	0.33
Insulating render system 1	7.79E-08	1.57E-09	3.14E-11	6.37	0.13
Insulating render system 2	8.02E-08	1.62E-09	3.23E-11	6.18	0.12

For solid brick, the obtained mean values of water vapour permeability  $\delta$ , water vapor diffusion resistance factor  $\mu$  and water vapour diffusion-equivalent air layer thickness  $s_d$  were  $1.2 \times 10^{-11}$  kg/(m·s·Pa), 17 and 0.34 m, respectively. For insulating render system, the obtained mean values of water vapour permeability  $\delta$ , water vapor diffusion resistance factor  $\mu$  and water vapour diffusion-equivalent air layer thickness  $s_d$  were  $3.2 \times 10^{-11}$  kg/(m·s·Pa), 6 and 0.12 m, respectively.

The reference values of the water vapor diffusion resistance factor of the solid brick differ from each other. In (De Freitas and Pinto 1998) the reference value is 77 while in WUFI database the reference value is 15. Although the value of the water vapor diffusion resistance factor of the solid brick determined in this work is lower than the reference value presented in (De Freitas and Pinto 1998), it is very close and consistent with the reference value presented in the WUFI database.

It should be noted that the water vapour diffusion resistance factor of the insulating render is in accordance with the EN 998-1 *Specification for mortar for masonry – Part 1: Rendering and plastering mortar* requirement of  $\mu \leq 15$  (EN 998-1: 2016) and with the characteristic specified by the manufacturer of  $\mu < 15$ .

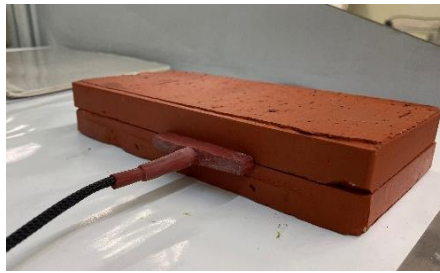
### Thermal conductivity

The thermal conductivity measurements in function of moisture content were performed by the hot-wire method. The hot-wire method (parallel) is a dynamic measuring procedure based on the measurement of the temperature increase at a certain location and at a specific distance from a linear heat source placed between two test specimens. The test was conducted based on ISO 8894-2:2007 *Refractory materials – Determination of thermal conductivity – Part 2: Hot-wire method (parallel)* (ISO 8894-2: 2007) using a CT- Metre equipment and an “anneau” probe. The test assembly of insulating render consist of two identical test pieces of 210x210x20 mm in size. Each test piece of insulating render consists of just the insulating render itself, without finishing render or paint. The test assembly of brick consist of two identical test pieces of 210x105x20 mm. The test has the limitation that the thickness of the available specimens was reduced. Figure 62 presents the CT- Metre equipment and the test assemblies of both materials with the “anneau” probe placed inside.

To wet the test specimens, they were fully immersed in water. The thermal conductivity was measured at different moisture contents progressively from the dry state to the saturated state, calculating in each point its thermal conductivity and moisture content. The moisture content was obtained by dividing the mass of water by the mass of the test specimens in the dry state. Table 23 and Figure 63 show the brick and insulating render behaviour in the presence of moisture.



(a)



(b)

Figure 62. a) CT-Metre equipment measuring the thermal conductivity of insulating render test specimens; b) Brick test specimens with the “anneau” probe placed between them.

Table 23. Thermal conductivity of brick and insulating render as a function of moisture content.

Brick		Insulating render	
Water content kg/kg	Thermal conductivity W/(m K)	Water content kg/kg	Thermal conductivity W/(m K)
0.000	0.733	0.000	0.147
	0.780		0.145
	0.745		0.152
0.018	1.008	0.060	0.176
	1.024		0.171
	1.064		0.172
0.073	1.260	0.215	0.235
	1.283		0.249
	1.232		0.248

From the results it can be observed that moisture considerably influenced the thermal conductivity of both materials, especially that of brick. In fact, thermal conductivity of brick increased from approximately 0.75 to 1.26 W/(m K) which means that it is very sensitive to moisture effects. The direct contact with liquid water over a period of 24 hours of soaking increased its thermal conductivity by almost 70%. The insulating render evidence much lower values of thermal conductivity than brick, however if there is no painting or if the painting does not prevent direct contact with liquid water, its thermal conductivity increases from approximately 0.15 to 0.24 W/(m K).

Figure 63 also compares the thermal conductivities of brick and insulating render as a function of moisture content determined in the present work with results obtained by other authors. Figure 63a shows the behaviour of solid brick in the presence of moisture presented in (De Freitas 1992) and in the WUFI database. Figure 63b compares the behaviour of the insulating render with natural cork aggregates and lime binder with the behaviour of two other insulating renders, one with EPS aggregates and lime binder and the other with EPS aggregates and mixed binders (Maia 2019). In general, it can be concluded that both for the brick and for the insulating render the values of thermal conductivity as a function of moisture content measured in this work do not differ much from the results obtained by the other authors. The differences are mainly due to the analysis of solid bricks produced by different manufacturers and insulating renders with different compositions.

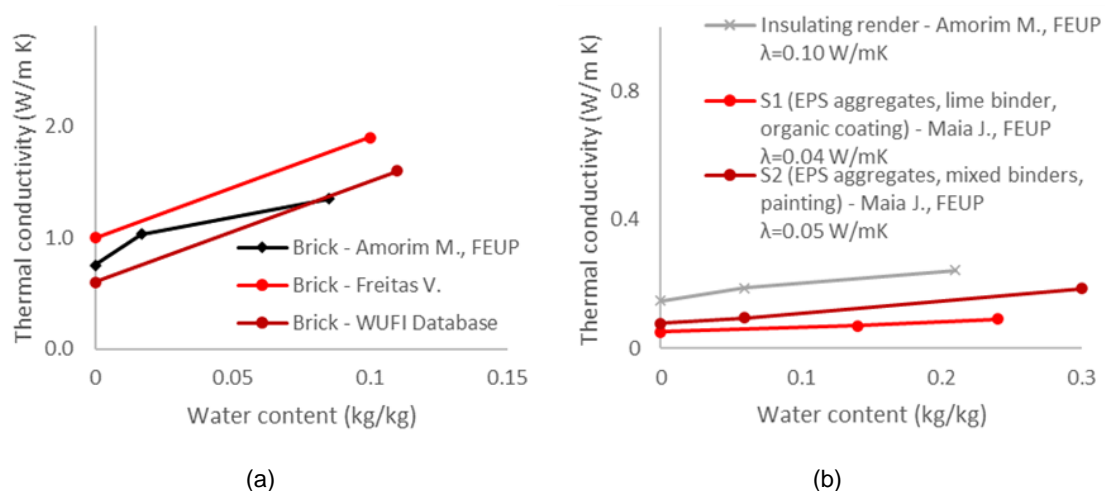


Figure 63. Thermal conductivity of brick and insulating render as a function of moisture content.



Summary of the measured hygrothermal properties

The measurement of the hygrothermal properties capillary water absorption coefficient, water vapour diffusion resistance factor, and moisture-dependent thermal conductivity of brick and insulating render system was carried at the Building Physics Laboratory – Faculty of Engineering University of Porto to use in the numerical simulation and validate the hygrothermal model.

Table 24 and Table 25 summarize the obtained results of material properties. Table 24 presents the capillary water absorption coefficient and the water vapour transmission properties of brick and insulating render system (composed of insulating render, finishing render and paint). Table 25 presents the moisture dependent thermal conductivity of brick and insulating render itself, without finishing render or paint. The obtained results were briefly compared to reference values, and it was concluded that the measurements were consistent with the reference values.

Table 24. Summary of the hygrothermal properties of brick and insulating render system.

<b>Material</b>	<b>Capillary water absorption coefficient</b>	<b>Water vapour permeability</b>	<b>Water vapour resistance factor</b>	<b>Water vapour diffusion-equivalent air layer thickness</b>
	<b>A</b>	<b><math>\delta</math></b>	<b><math>\mu</math></b>	<b>Sd</b>
	<b>kg/(m<sup>2</sup> s<sup>1/2</sup>)</b>	<b>kg/(m·s·Pa)</b>	<b>-</b>	<b>m</b>
Brick	0.06	1.2x10 <sup>-11</sup>	17	0.34
Insulating render system	0.003	3.2x10 <sup>-11</sup>	6	0.12

The results show that the solid brick is highly capillary active ( $A=0.06 \text{ Kg}/(\text{m}^2 \text{ s}^{1/2})$ ), while the insulating render system is hardly capillary active ( $A=0.003 \text{ Kg}/(\text{m}^2 \text{ s}^{1/2})$ ). So, both materials have completely different behaviour when in direct contact with liquid water. The brick can be classified as quick suction while the insulating render system can be classified as nearly waterproof. The measurements of water vapour transmission properties showed that the water vapor diffusion resistance factor of the brick is higher than the water vapor diffusion resistance factor of the insulating render system. For solid

brick and insulating render system, the water vapor diffusion resistance factor  $\mu$  results were 17 and 6, respectively.

Table 25. Thermal conductivity of brick and insulating render as a function of moisture content.

<b>Material</b>	<b>Water content</b>	<b>Thermal conductivity</b>
	<b>w</b> <b>kg/kg</b>	<b><math>\lambda</math></b> <b>W/m K</b>
Brick	0; 0.02; 0.07	0.75; 1.03; 1.28
Insulating render	0; 0.06; 0.21	0.15; 0.17; 0.24

Concerning the thermal conductivity measurements, the insulating render evidence much lower values of thermal conductivity than brick, as expected. However, it was observed that the thermal conductivities of both materials were considerably affected by moisture content, especially that of brick. In fact, the thermal conductivity of brick increased from approximately 0.75 to 1.26 W/(m K), which reveals high sensitivity to moisture effects. For the insulating render itself without finishing render or paint, its thermal conductivity increased from approximately 0.15 to 0.24 W/(m K).

#### 4.3.2. RESULTS

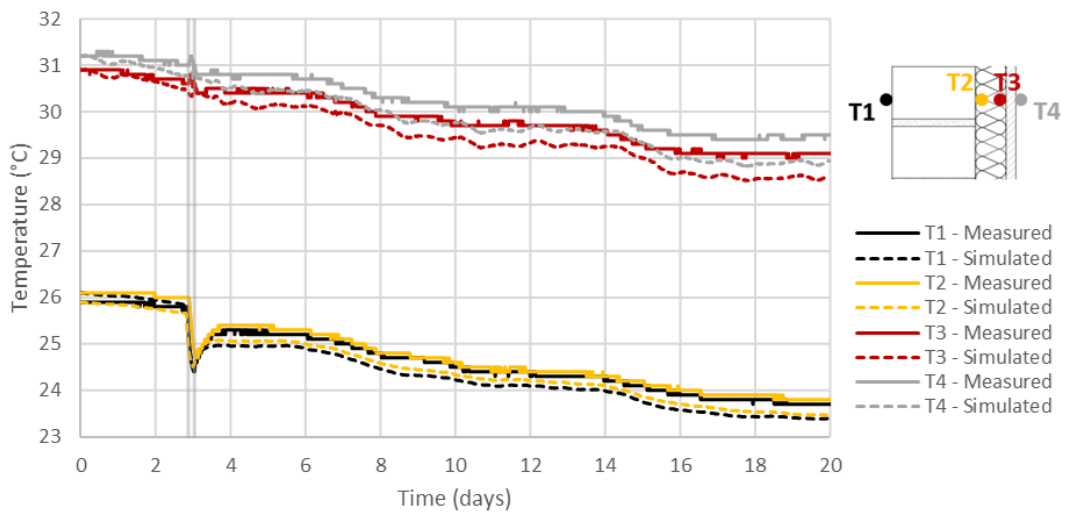
The validation of the WUFI hygrothermal model is performed by comparing the measured and simulated hygrothermal behaviour of the wall test specimens subjected to driving rain. The following three parameters are considered for the validation of the numerical model: temperature, relative humidity, and heat flux. In particular, the temperatures at the surfaces and inside both specimens, the relative humidity inside the specimen A and the heat fluxes through interior and exterior surfaces of the specimens. Ultimately, the validation is quantified using the statistical parameters: coefficient of determination, goodness-of-fit, normalized mean bias error and coefficient of variation of the root mean square error.

The third test, in which the specimens were subjected to a single rainy period of 4 hours, was simulated because it has the least instability in the measurements of heat fluxes.

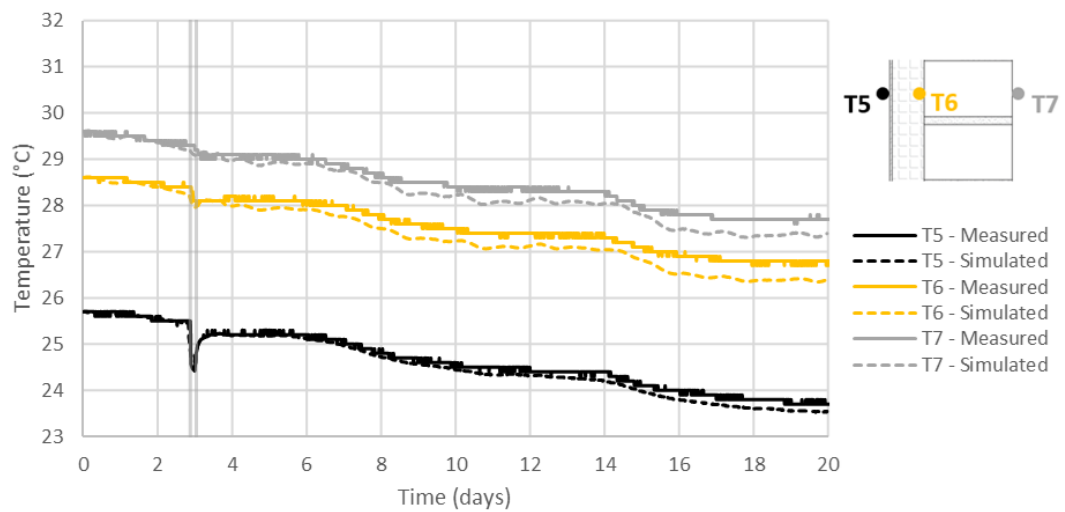
The main objective of the experimental validation is to assess whether the numerical model is capable of accurately determining the influence of moisture on the energy performance of retrofitted walls.

#### 4.3.2.1. Temperature profiles

The measured and simulated temperatures at the surfaces and inside the wall assemblies over time are compared in Figure 64. The walls were exposed to driving rain on the third day of the experiment. The rainy period is delimited by the vertical grey lines.



(a)



(b)

Figure 64. Measured and simulated temperatures at the surfaces and inside the: a) configuration A; b) configuration B.

Both at surface level and inside the wall, the simulated temperatures show good agreement with the correspondent measured temperatures. In fact, the maximum difference between the simulated temperatures and the measured temperatures is below 0.5 °C.

Driving rain is found to influence the temperature at the exterior surfaces of the walls and brick masonry in the case of configuration A. In fact, during the rainy period, a decrease in temperature of approximately 1.5 °C at the exterior surfaces of the walls is found, due to the direct contact between the exterior surfaces and the rainwater. Also, in the case of configuration A, a decrease in temperature of approximately 1.5 °C between masonry and insulation is found. Moreover, due to the position of the insulation on the walls, the temperature of the brick layer was lower in configuration A than in configuration B.

The temperature profiles of the walls before and after the wetting period are shown in Figure 65. The measured and simulated temperature profiles show good agreement. It can be observed in the figure below that when the walls were exposed to driving rain, the temperature at the brick masonry of configuration A slightly decreased, while the temperature of configuration B did not change. The decrease in temperature in the brick masonry of configuration A indicates the presence of moisture.

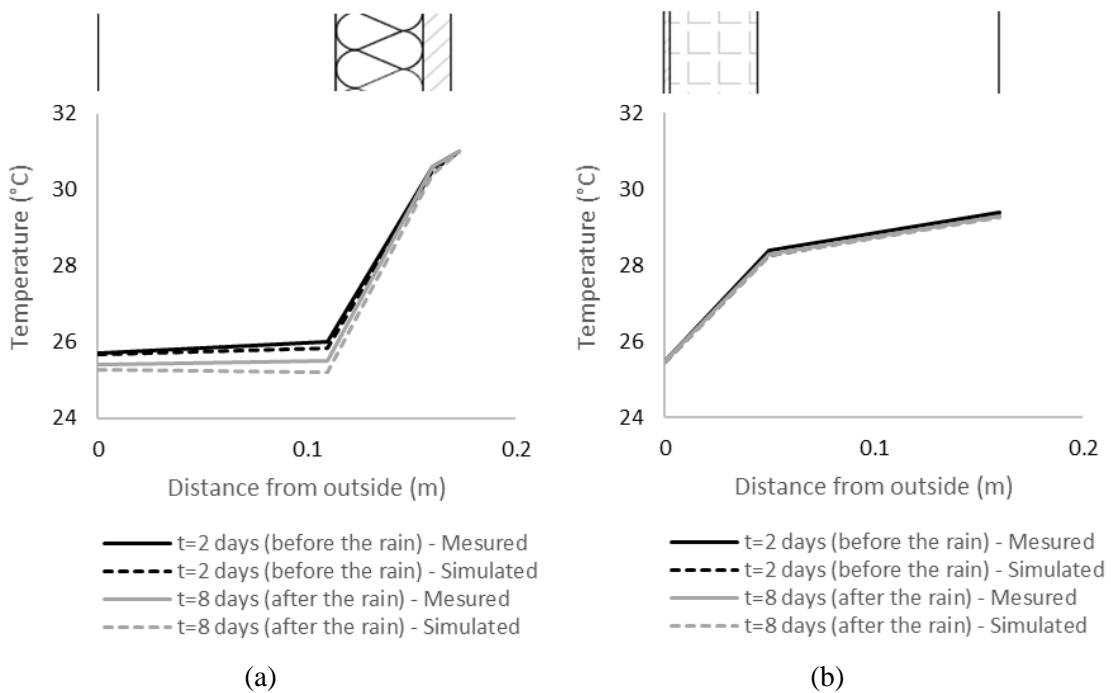


Figure 65. Measured and simulated temperature profiles before and after the rainy period, for: a) configuration A; b) configuration B.

4.3.2.2. Relative humidity between masonry and insulation

The measured and simulated relative humidity inside the configuration A are shown in Figure 66. It can be observed that the calculated relative humidity show acceptable agreement with the measurements. The maximum difference between the simulated relative humidity and the measured relative humidity is below 10%. The discrepancy between measured and simulated data mainly comes from the simplifications and limitations of the WUFI mathematical model, which derive from the enormous complexity of the moisture transfer mechanisms in building components.

Both in experimental test and numerical simulation, driving rain has increased the moisture content in configuration A. A significant increase in relative humidity at the interface between the masonry wall and the insulation is found. The relative humidity between the masonry wall and the insulation increased by 25%. The relative humidity between the insulation and the gypsum board also increased. After the wetting period, the water content of the wall begins to decrease. However, the drying occurs very slowly due to the very high air humidity in the rain room.

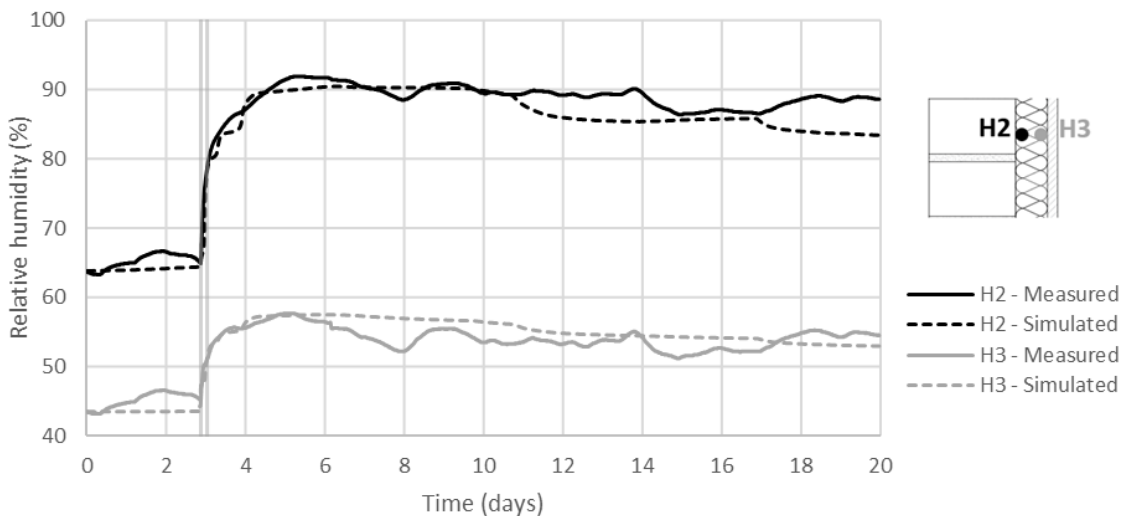


Figure 66. Measured and simulated relative humidity inside the wall configuration A.

The measured and simulated relative humidity profiles of configuration A before and after the rain is shown in Figure 67. The simulated relative humidity profiles show good agreement with the measured ones. Once again it can be observed that driving rain has significantly influenced the relative humidity within the wall. An increased relative

humidity is found, mainly at the cold side of the specimen. The largest increase in relative humidity is found between masonry and insulation.

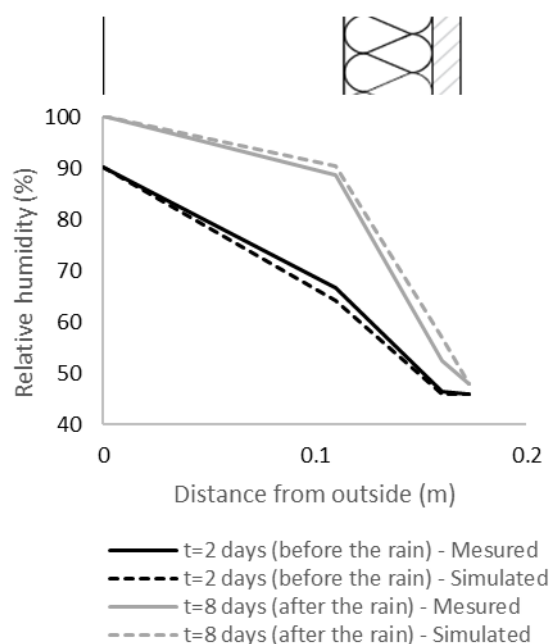


Figure 67. Measured and simulated relative humidity profiles before and after the rainy period for wall configuration A.

#### 4.3.2.3. Heat fluxes

During the experiment, the heat fluxes through both surfaces of the wall test specimens were measured by heat flux sensors. There was some instability in the measurements of those heat fluxes due to the use of heater and precipitation as already mentioned in Section 3.4.3. The measurements of the heat flux sensors installed on the interior surface of the specimens showed some instability due to the fact that the heater in the control room was continuously switching on and off during the experiment. In addition, the precipitation falling directly on the heat flux sensors installed on the exterior surface of the specimens also cause some disturbance in the measurements of the heat fluxes, however once the precipitation ends the measurements stabilize.

Figure 68 shows the comparison between the measured and calculated heat fluxes across the interior and exterior surfaces of the walls. In general, the calculated heat fluxes show acceptable agreement with the measured heat fluxes. The calculated heat fluxes are only

slightly lower than the measured heat fluxes (approximately  $0.6 \text{ W/m}^2$  lower), but it may have to do with the accuracy of the heat flux sensors.

The heat fluxes pass through the walls from inside to outside. Configuration A performs better than configuration B since lower heat losses are found. Before the wetting period, the heat flux through both surfaces of configuration A is approximately  $4 \text{ W/m}^2$ , whereas through both surfaces of configuration B is approximately  $6 \text{ W/m}^2$ .

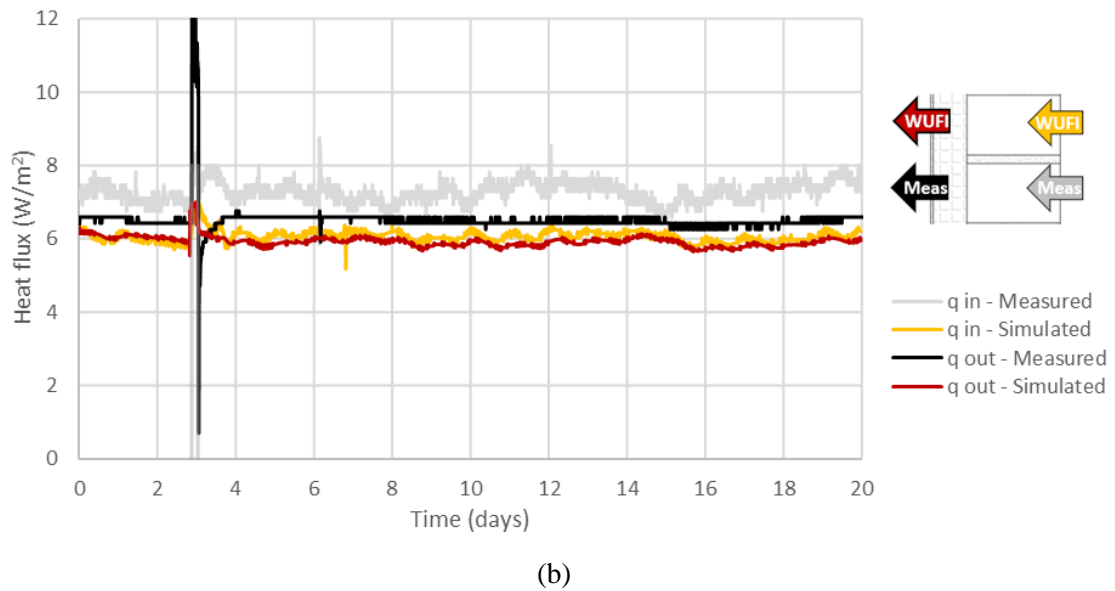
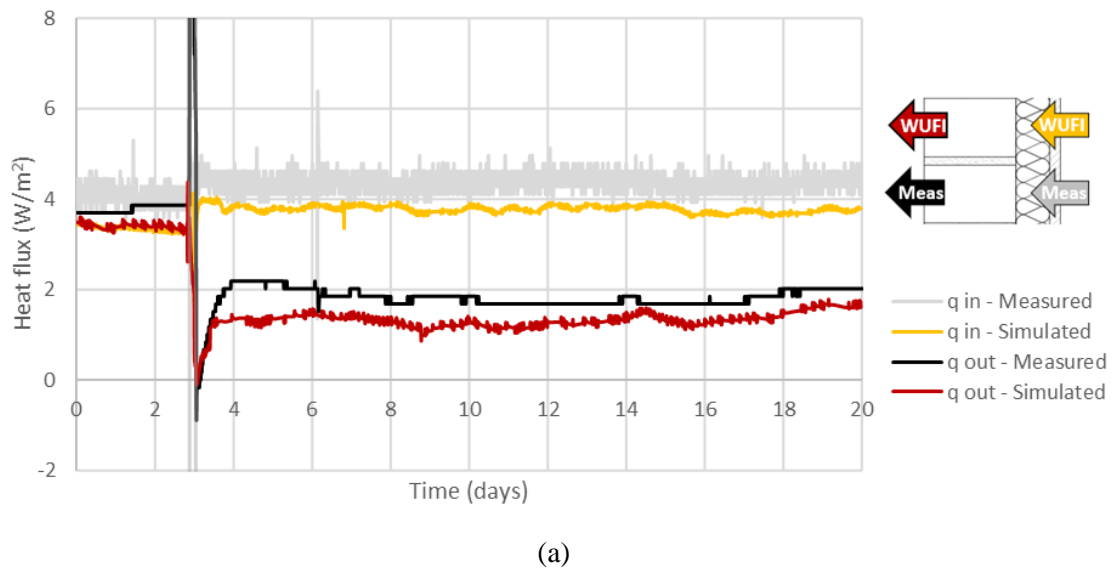


Figure 68. Measured and simulated heat fluxes across: a) configuration A; b) configuration B.

Both in experimental test and numerical simulation, for configuration A applying driving rain results in an increase of the heat flux at the interior surface and a decrease of the heat flux at the exterior surface. The reason for this is the moisture stored in the brick masonry induced by precipitation. The accumulated moisture content in the wall due to the driving rain increased mainly the bricks thermal conductivity resulting in an increase of heat losses of approximately 10%. Moreover, for the conditions of the experiment, the moisture introduced by precipitation decreases the temperature in the brick masonry and consequently the heat flux at the exterior surface decreases. After the wetting period, the drying process of configuration A begins. However, as the wall is tending very slowly to the initial dry state, also the heat fluxes are tending very slowly to the initial values.

For configuration B, it can be observed both in measured and simulated data that the precipitation does not influence the heat fluxes through the wall. The reason for this is that the rainwater does not enter the wall.

#### 4.3.3. STATISTICAL ANALYSIS

The accuracy of the validation is attested by the statistical parameters coefficient of determination  $R^2$ , goodness-of-fit (fit), normalized mean bias error NMBE and coefficient of variation of the root mean square error CV(RMSE), for the hygrothermal variables temperature, relative humidity and heat flux.

The  $R^2$  indicates the correlation between the measured and the simulated values (equation (16)) and it is limited between 0 and 1.  $R^2$  equals 1 if the model equation passes through all the measured data points. At the other extreme,  $R^2$  is 0 if the simulated values have no correlation at all with the measured values (Johnson and Wichern 2002). The fit correlates the two data series and assesses their fluctuation (equation (17)). It is presented in % and the upper values mean that the simulated values fit the measured ones perfectly, whereas the lower ones do not. The NMBE (Normalized Mean Bias Error) describes the general normalized mean error and shows the influence of smaller errors (equation (18)). The CV(RMSE) measures the variability of the errors between measured and simulated values (equation (19)). It overcomes possible compensation mistakes of the NMBE, and it shows the influence of higher errors. The model is more accurate when the NMBE and



the CV(RMSE) are lower (ASHRAE 2002, Ruiz and Bandera 2017, Coelho, Silva and Henriques 2018, Barbosa 2020).

$$R^2 = \left( \frac{\sum_{i=1}^N (X_{i,meas} - \overline{X_{meas}}) \cdot (Y_{i,sim} - \overline{Y_{sim}})}{\sqrt{\sum_{i=1}^N (X_{i,meas} - \overline{X_{meas}})^2 \cdot \sum_{i=1}^N (Y_{i,sim} - \overline{Y_{sim}})^2}} \right)^2 \quad (16)$$

$$fit = \left( 1 - \frac{\sqrt{\sum_{i=1}^N (X_{i,meas} - Y_{i,sim})^2}}{\sqrt{\sum_{i=1}^N (Y_{i,sim} - \overline{X_{meas}})^2}} \right) \cdot 100 \quad (17)$$

$$NMBE = 100 \cdot \frac{\sum_{i=1}^N (X_{i,meas} - Y_{i,sim})}{\overline{X_{meas}} \cdot (N - 1)} \quad (18)$$

$$CV(RMSE) = 100 \cdot \frac{\sqrt{\frac{\sum_{i=1}^N (X_{i,meas} - Y_{i,sim})^2}{(N - 1)}}}{\overline{X_{meas}}} \quad (19)$$

where  $X_{i,meas}$  is the measured value at time  $i$ ,  $Y_{i,sim}$  is the simulated value at time  $i$ ,  $\overline{X_{meas}}$  is the average of the measured values during the complete time  $N$  and  $\overline{Y_{sim}}$  is the average of the simulated values during the complete time  $N$ . The acceptable validation tolerances defined by energy guidelines is the  $R^2$  higher than 0.75, the fit higher than 80% and the NMBE and the CV(RMSE) lower than 10% and 30%, respectively for hourly criteria (ASHRAE 2002, EVO - Efficiency Valuation Organization 2012) These tolerance values are summarized in Table 26.

Table 26 also shows the statistical parameters  $R^2$ , fit, NMBE and CV(RMSE) of the correlation between the measured and simulated data of temperatures (T), relative humidity (RH) and heat fluxes (HF). For temperature, the statistical parameters indicate a very good correlation between measurements and simulation results. The  $R^2$  and fit are quite high, and NMBE and CV(RMSE) are low. In fact, the  $R^2$  is close to 1, the fit is above 90%, whereas the NMBE and CV (RMSE) are close to 0%. For relative humidity, the statistical parameters also indicate a good correlation, with an acceptable  $R^2$  of around 0.80 and a reasonable fit value (75.3%). The NMBE is 9.7%, which is a good result, and

the CV(RMSE) is 16%, also fulfilling the requirement. For heat flux, the statistical parameters indicate that the correlation is slightly worse than the correlation of the previous variables. It is an expected result due to the slight disturbances in the measurements of heat fluxes detected and mentioned before in section 3.4.3. However, there is still a reasonable correlation between measurements and simulation results of heat fluxes with the statistical parameters fulfilling the requirements or not far from fulfilling the requirements.

Table 26. Temperature (T), relative humidity (RH) and heat flux (HF) statistical parameters.

	T		RH		HF		Tolerances
R <sup>2</sup>	0.95	+	0.81	+	0.70	±	>0.75
fit	93.1	+	75.3	±	68.9	±	>80%
NMBE	1.2	+	9.7	+	15.3	±	<±10% (hourly)
CV (RMSE)	5.8	+	16.0	+	27.8	+	<30% (hourly)

(+) requirement fulfilled; (±) not far from the requirement; (-) requirement not fulfilled

Thus, although there are four values that do not meet the requirement, but which are not far from it, a relative humidity value and three heat flux values, the approximation between the measured and the simulated data was considered reasonable.

#### **4.4. FINAL CONSIDERATIONS**

In this chapter the WUFI hygrothermal model was validated against experimental measurements. Specific attention is paid to the influence of moisture on the energy performance of walls. The validation was assessed by comparing the measured and simulated hygrothermal behaviour of masonry walls with different insulation systems exposed to driving rain. The experimental validation performed has the limitation of not taking into account solar radiation.

The results show that the hygrothermal behaviour of the walls throughout the experiment was well reproduced by the model, including rainwater absorption influence. In general, the simulated temperatures, relative humidity and heat fluxes showed acceptable agreement with the measured temperatures, relative humidity and heat fluxes. The maximum differences between the simulated and measured temperatures and relative humidity were below 0.5 °C and 10%, respectively. The simulated heat fluxes were

slightly lower than the measured heat fluxes, the maximum discrepancy was approximately  $0.6 \text{ W/m}^2$ . These slight discrepancies between the measured and simulated data may have to do with the accuracy of the equipment used together with the limitations of the WUFI hygrothermal model which derives from the high complexity of the hygrothermal processes in building components and the fact that the mortar joints of the brick masonry were neglected in the simulation.

It was observed that the hygrothermal model was capable of simulating both moisture and energy performance of walls and the effect of driving rain (and subsequent increase in moisture content) on heat losses through the walls. Both in experimental test and numerical simulation, driving rain has increased the moisture content in wall configuration A and influenced the heat fluxes through both surfaces of the wall. The heat flux through the interior surface of the wall increased by 10 percent while the heat flux through the exterior surface decreased. For wall configuration B, both in measured and simulated data driving rain did not significantly influence the energy performance of the wall. The reason for this is that the rainwater did not enter the wall configuration B since the capillary water absorption coefficient of its finishing coating is very low.

Thus, the hygrothermal model was validated for temperature, relative humidity and heat flux and the statistical analysis proved its strength. The experimental validation of the hygrothermal model showed that WUFI Pro is a good tool to quantify the influence of moisture on the energy performance of retrofitted walls.



# 5

## **SENSITIVITY ANALYSIS AND PERFORMANCE EVALUATION OF RETROFITTED WALLS UNDER IN- SERVICE CONDITIONS**

### **5.1. METHODOLOGY**

To evaluate the impact that wind-driven rain has on the energy performance of retrofitted walls under in-service conditions and quantify the energy losses through the walls taking into account the moisture content in the walls, a numerical sensitivity study was performed with WUFI Pro software. The key factors that most affect the influence of moisture on the energy performance of retrofitted walls were investigated. Moreover, the influence of initial moisture in the masonry when the walls were rehabilitated on the energy performance of the walls over the years was also assessed.

The hygrothermal performance of different retrofitted walls configurations exposed to real climatic conditions was numerically studied. The study was performed for massive masonry walls without insulation or with different insulation systems, namely a traditional interior insulation system and an innovative external insulating render system. The sensitivity analysis was performed concerning several cities located in Europe, different thicknesses of thermal insulation and of masonry wall, different types of masonry wall substrate material and various finishing coatings. The analysis was performed for walls exposed to wind-driven rain as well as for walls not exposed to wind-driven rain.

To evaluate the influence of outdoor climate, a comparison was made between the hygrothermal behaviour of a brick masonry wall with a traditional interior insulation

system located in Porto, Kraków and Brussels. To assess the influence of insulation thickness, the hygrothermal behaviour of a brick massive masonry wall without insulation and with 5 cm and 10 cm of a traditional interior insulation system was investigated. In its turn, to assess the influence of masonry wall thickness, the hygrothermal behaviour of brick masonry walls with a traditional interior insulation system and with 0.22, 0.34 and 0.45 m masonry thicknesses was investigated. To evaluate the influence of wall finishing coatings, a comparison was made between the hygrothermal behaviour of an uncoated brick masonry wall, a brick masonry wall coated with a traditional render, a brick masonry wall coated with an innovative insulating render system and an uncoated granite masonry wall.

Also, to investigate the influence of initial moisture in masonry when the wall is rehabilitated, a comparison was made between the hygrothermal behaviour of a brick masonry wall with a traditional interior insulation system and of a brick masonry wall coated with an innovative external insulating render system over the years, starting with high initial moisture in masonry.

Below, the wall configurations, boundary conditions and material properties used in the numerical simulations are described. Next, an overview of the results is given. Attention is paid to accumulated moisture content in the wall assemblies and energy losses across the walls. To end the main conclusions are summarized.

#### 5.1.1. WALL CONFIGURATIONS

In the current section, reference wall assemblies are investigated. Each of the reference walls consist of a masonry wall without insulation or with an insulation system. In case of existing buildings, brick masonry walls are always very thick for structural stability reasons so wall thicknesses of 0.22, 0.34 and 0.45 m (1, 1 ½ and 2 brick thick, respectively) are considered. The masonry wall is simplified in a single isotropic brick layer, neglecting the mortar joints. This simplification is validated for massive masonry walls exposed to climate conditions as shown in (Vereecken and Roels 2013).

The insulation systems applied to the reference walls consists of a traditional interior insulation system composed by mineral wool and gypsum board, and an innovative external insulating render system composed by silicate paint, finishing render and

insulating render. The insulating render is a lightweight render formulated with natural cork aggregates, sands and natural hydraulic lime that is eight times more thermal insulating than traditional renders. The mineral wool thicknesses applied are 5 cm and 10 cm and the insulating render thickness applied is 5 cm.

Moreover, a masonry wall coated with a traditional lime plaster and a stone masonry wall are also investigated. Masonry walls are often externally protected by a plaster and lime plaster is the most common type of plaster used in masonry walls of existing buildings (Appleton 2003, Blumberga et al. 2015). A 30 cm thick granite masonry wall is also studied since stone masonry walls are also a common wall type of existing buildings (Pinho 2000).

Therefore, from the outside to the inside, the reference walls consist of:

- *Configuration 1 (thinner masonry wall):*  
22 cm solid brick – 5 cm mineral wool – 1.3 cm gypsum board
- *Configuration 2 (masonry wall without insulation system):*  
34 cm solid brick
- *Configuration 3 (masonry wall with traditional interior insulation system):*  
34 cm solid brick – 5 cm mineral wool – 1.3 cm gypsum board
- *Configuration 4 (masonry wall with thicker traditional interior insulation system):*  
34 cm solid brick – 10 cm mineral wool – 1.3 cm gypsum board
- *Configuration 5 (thicker masonry wall):*  
45 cm solid brick – 5 cm mineral wool – 1.3 cm gypsum board
- *Configuration 6 (masonry wall coated with traditional render):*  
2 cm lime plaster – 34 cm solid brick – 5 cm mineral wool – 1.3 cm gypsum board
- *Configuration 7 (masonry wall with innovative external insulating render system):*  
silicate paint – 0.5 cm finishing render – 5 cm insulating render – 34 cm solid brick
- *Configuration 8 (stone wall with traditional interior insulation system):*  
30 cm granite – 5 cm mineral wool – 1.3 cm gypsum board

The dry thermal transmittances  $U_{dry}$  are different for the reference walls. The dry thermal transmittances of wall configuration 1 to wall configuration 8 calculated from dry thermal conductivities and dimensions of their components as described in EN ISO 6946:2017

*Building components and building elements – Thermal resistance and thermal transmittance – Calculation method* (EN ISO 6946: 2007) are 0.55, 1.36, 0.49, 0.31, 0.45, 0.49, 0.81 and 0.62 W/(m<sup>2</sup> K), respectively. The significantly higher value of the thermal transmittance corresponds to the masonry wall without thermal insulation. Masonry walls with the traditional thermal insulation system (composed of mineral wool and gypsum board) have lower thermal transmittance values than the wall with the innovative insulating render system because they have the same insulation thickness, but the thermal conductivity of mineral wool is lower than that of insulating render.

#### 5.1.2. BOUNDARY CONDITIONS

The analysis is performed for west orientated walls located in Porto (Portugal), Kraków (Poland) and Brussels (Belgium). The west orientation was chosen because it is an orientation with high exposure to wind-driven rain. The locations were selected to apply different hygrothermal loads, namely different outdoor temperatures combined with wind-driven rain and solar radiation. In fact, under the Köppen-Geiger climate classification the climates of the three locations belong to different groups, with each group being divided based on seasonal precipitation and temperature patterns. Porto climate is classified as mediterranean climate or dry summer climate (Csb) while Krakow climate is classified as humid continental climate (Dfb) and Brussels is classified as oceanic climate also known as maritime climate (Cfb) (Peixoto 1987).

The temperature and relative humidity in Porto, Krakow and Brussels throughout the year are shown in Appendix C. The extreme and annual mean values of temperature and relative humidity and the sum of the solar radiation and precipitation acting on the west orientated facades located in Porto, Krakow and Brussels per year are shown in Table 27.

Porto experiences the highest outdoor temperature. The annual average temperature in Porto is around 15 °C, while the annual average temperature in Krakow is only around 8 °C and in Brussels is only around 10 °C. The annual average relative humidity at the three locations is approximately equal, around 80%.

Winters in Krakow are the coldest. In fact, in winter season in Porto the minimum temperature is above 0 °C and the location is marked by mild winters. In the case of Krakow, in the coldest months the minimum temperature is above -20 °C and the winters



are cold and severe. Finally, in the case of Brussels, in the coldest months the minimum temperature is above -10 °C and the winters are not so cold as Krakow, but they are also cold. In the three locations precipitation occurs in the coldest months.

Table 27. Temperature, relative humidity, solar radiation, and rain load on the west orientated facades located in Porto, Krakow and Brussels

		<b>Porto</b>	<b>Krakow</b>	<b>Brussels</b>
Temperature (°C)	Mean	15.6	8.3	10.3
	Min.	1.2	-20.1	-9.1
	Max.	37.0	31.0	34.9
Relative humidity (%)	Mean	75	78	81
	Min.	25	22	26
	Max.	100	100	100
Solar radiation (kWh/m <sup>2</sup> year)		997	582	537
Driving rain load (mm/year)		400	300	750

Brussels has the highest wind driven rain load and the lower solar radiation load. It has the wettest climate. The wind-driven rain acting on a west orientated façade located in Brussels is around 750 mm/year (approximately twice the wind-driven rain acting on west orientated façades located in Porto or in Brussels). It should also be noted that the west orientated façades located in Porto are exposed to high solar radiation, circa 1000 kWh/m<sup>2</sup> year, while the façades located in Krakow and in Brussels are exposed to only about half of that solar radiation.

Wind-driven rain on the walls is calculated by wind direction, wind speed and rain according to the method of ASHRAE Standard 160P “Design criteria for moisture control in buildings”. The rain exposure factor (FE) was considered 1.0 since in most cases the height of existing buildings is less than 10 m and the walls are often only moderately exposed to rain due to shelter by nearby buildings. The rain deposition factor (FD) was considered 0.5 due to the common pitched roofs of existing buildings (Teixeira 2014).

The indoor temperature and relative humidity used in the numerical simulations are given in Figure 69. Those indoor conditions were attained through EN 15026, with indoor temperature and relative humidity calculated on the basis of outdoor air temperature, similarly to other studies (Gradeci et al. 2018, Gradeci and Berardi 2019).

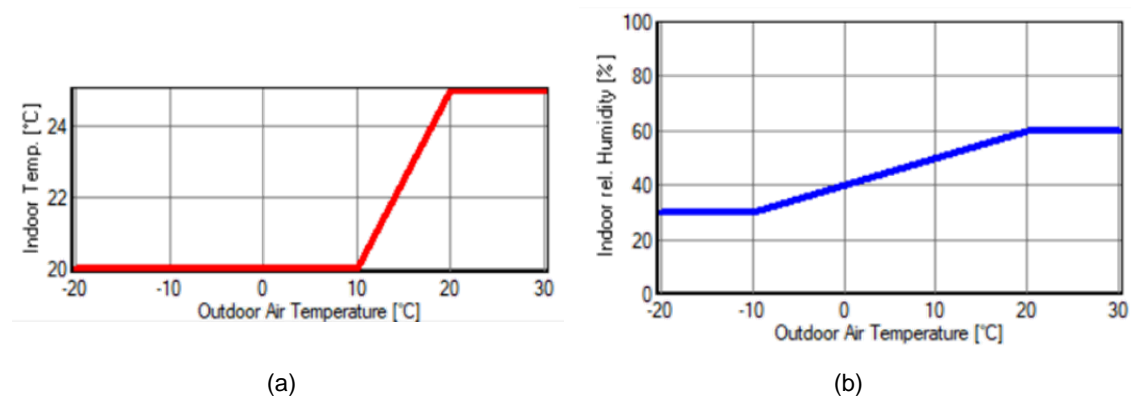


Figure 69. Indoor conditions: a) indoor temperature; b) indoor relative humidity.

The indoor temperature is kept constant at 20°C, except when the outdoor temperature exceeds 10°C. When the outdoor temperature exceeds 10°C, the indoor temperature varies between 20°C and 25°C. The indoor relative humidity varies between 30% and 60%. Hourly climate data are used in the simulation.

### 5.1.3. MATERIAL PROPERTIES

The properties of brick, granite, lime plaster, mineral wool, gypsum board and insulating render system used to simulate the hygrothermal performance of the wall assemblies are given in Table 28 and Figure 70. Table 28 presents the values of bulk density, porosity, specific heat capacity, dry thermal conductivity, water vapour resistance factor and capillary water absorption coefficient, whereas Table 25 presents the thermal conductivities as a function of moisture content.

The thermal conductivities, water vapor diffusion resistance factors and capillary water absorption coefficients of solid brick and insulating render system were determined experimentally as thoroughly reported in section 4.3.1.1. All the other material properties were found in the literature (Kumaran 1996, EN 12524: 2000, Delgado et al. 2012). It should be noted that the insulating render system composed of three layers, insulating render, finishing render and paint was considered that works as one.

Regarding the surface transfer coefficients, the conventional values of 0.125 m<sup>2</sup> K/W and 0.06 m<sup>2</sup> K/W are used for the internal and the external surface heat resistance, respectively. The rainwater absorption factor is either 0.7 or 0, depending on whether the wall is exposed or not to wind-driven rain, respectively.

Table 28. Material properties.

Material	Bulk density	Porosity	Specific heat capacity	Dry thermal conductivity	Water vapour resistance factor	Capillary water absorption coefficient
	$\rho$ kg/m <sup>3</sup>	$\epsilon$ m <sup>3</sup> /m <sup>3</sup>	$c$ J/ (kg K)	$\lambda_0$ W/ (m K)	$\mu$ -	$A$ kg/(m <sup>2</sup> s <sup>1/2</sup> )
Brick	1925	0.28	920	0.75*	17*	0.06*
Granite	2453	0.10	700	1.66	54	0.009
Lime plaster	1600	0.30	850	0.70	7	0.05
Mineral wool	60	0.95	850	0.04	1.3	1.3
Gypsum board	850	0.65	850	0.20	8.3	16
Insulating render system	650	0.40	900	0.15*	6*	0.003*

(\*) material properties experimentally determined in section 4.3.1.1

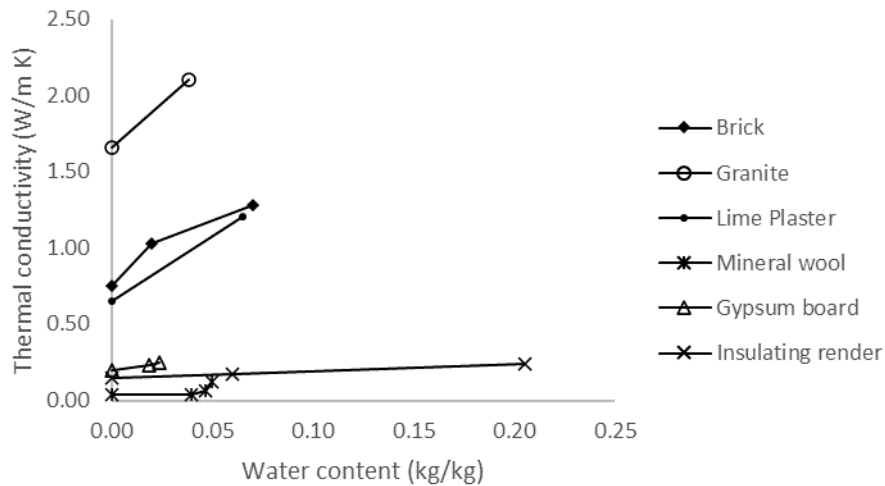


Figure 70. Thermal conductivities as a function of moisture content.

The short-wave radiation absorptivity is 0.4 if the brick masonry wall is coated with exterior plaster or the insulating render system, 0.68 if the brick masonry wall is externally uncoated and 0.5 for the uncoated granite masonry wall. The long-wave radiation emissivity is 0.9. The adopted initial conditions are constant across the wall section with 80% for relative humidity and 20°C for temperature.

## 5.2. INFLUENCE OF CLIMATE

In this section, the hygrothermal behaviour of a brick massive masonry wall with a traditional interior insulation system (Configuration 3 described in section 5.1.1) exposed to different climates is investigated. The wall configuration 3 is investigated since the energy performance of that wall is affected by the outdoor climate. The analysis is performed for a west orientated wall located in Porto (Portugal), Kraków (Poland) and Brussels (Belgium). The locations were selected to apply different hygrothermal loads on the wall, namely different temperature, solar radiation and wind-driven rain loads. Porto, Krakow and Brussels climates are described in subsection 5.1.2.

The hygrothermal behaviour of walls exposed to wind-driven rain as well as walls not exposed to wind-driven rain is studied. To exclude effects due to the starting conditions, in what follows the results starting from January 1<sup>st</sup> in the fifth year are given.

To investigate the accumulated moisture content in the wall assemblies, a subdivision is made between the accumulated moisture content in the brick masonry and the accumulated moisture in the insulation system. The results are shown in Figure 71. If no wind-driven rain is included (not shown), the accumulated moisture content in the brick layer is negligible.

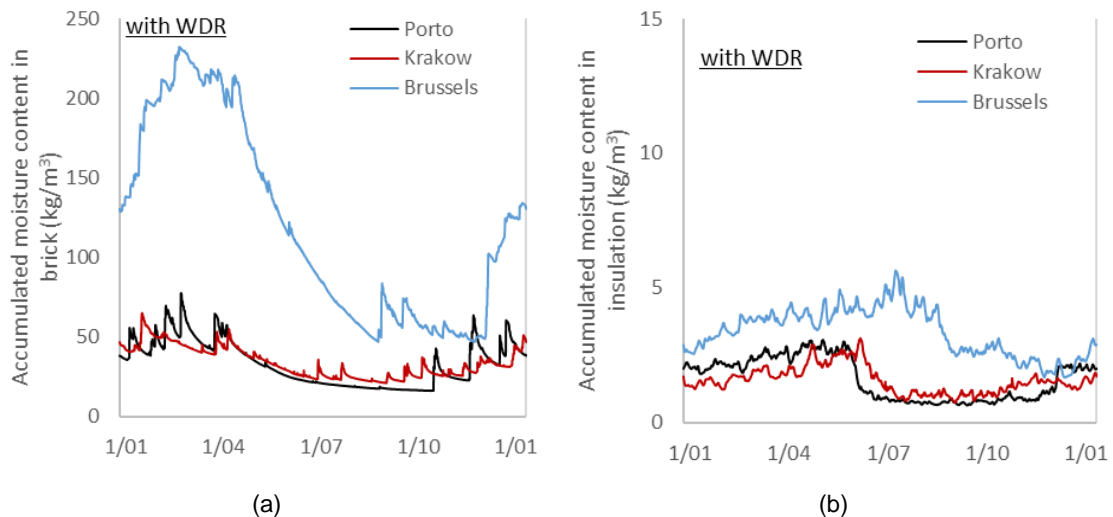


Figure 71. Accumulated moisture content: a) in the masonry and b) in the insulation (if the walls are exposed to WDR loads).

When the walls are exposed to wind-driven rain loads, during the heating season, in the brick layer an increased moisture content is found. The peaks in moisture content in the brick layer are induced by the wind driven rain loads. If the wall is located in Brussels, the accumulated moisture content in the brick layer is significantly higher compared to the accumulated moisture content if the wall is located in Porto or in Krakow. The reason for this is that Brussels has a higher wind-driven rain load. In fact, the maximum values of moisture content in brick masonry are approximately 80 kg/m<sup>3</sup>, 65 kg/m<sup>3</sup> and 230 kg/m<sup>3</sup> for the walls located in Porto, Krakow and Brussels, respectively.

A little moisture is accumulated in the insulation layer. Figure 72 shows for the different locations the annual maximum moisture content in the wall assembly and the annual average moisture content for the walls exposed to wind-driven rain as well as for the walls not exposed to wind-driven rain.

The moisture content in the wall assembly varies significantly depending on the location of the wall. The annual maximum moisture content in the wall assembly in Brussels is 79 Kg/m<sup>2</sup>, while in Porto and in Krakow is only 26 Kg/m<sup>2</sup> and 22 Kg/m<sup>2</sup>, respectively. Moreover, the annual average water content in the wall assembly in Brussels is around four times higher than in Porto or in Krakow. Both maximum and average water contents are significantly higher in Brussels than in Porto and Krakow due to the higher wind driven rain load and the lower solar radiation load.

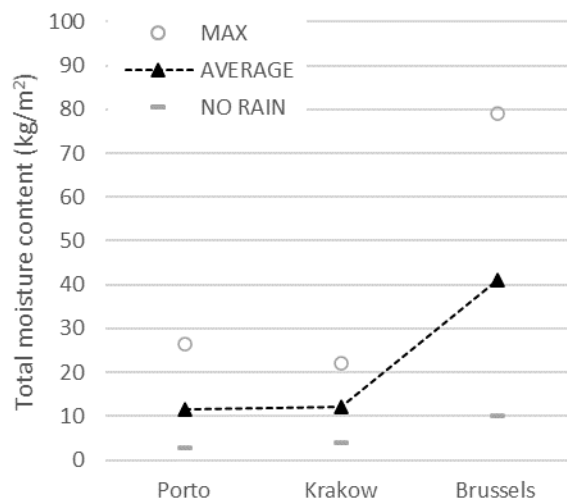


Figure 72. Annual maximum and average moisture content for the walls exposed to WDR loads and annual average moisture content for the walls not exposed to WDR loads.

When the wall is not exposed to wind-driven rain, moisture content values are only 3 Kg/m<sup>2</sup>, 4 Kg/m<sup>2</sup> and 10 Kg/m<sup>2</sup> for Porto, Krakow and Brussels, respectively.

Figure 73a shows the heat fluxes across the interior surface for the walls located in Porto, Krakow and Brussels and exposed to wind-driven rain throughout the year. In Porto, the heat flux through the wall is lower than in Krakow and Brussels mainly due to the higher outside temperature. In fact, as previously mentioned Porto experiences annual average temperature around 15 °C, while the annual average temperature in Krakow is only around 8 °C and in Brussels is only around 10 °C.

During the heating season, since in Porto the minimum temperature is above 0 °C and the location is marked by mild winters, the maximum heat flux across the wall is only approximately 8 W/m<sup>2</sup> and the average heat flux is only approximately 5 W/m<sup>2</sup>. In the case of Krakow, in the coldest months the minimum temperature is above -20 °C and the winters are cold and severe. In Krakow during the heating season the maximum heat flux across the wall is approximately 15 W/m<sup>2</sup> and the average heat flux is 10 W/m<sup>2</sup>. Finally, in the case of Brussels, in the coldest months the minimum temperature is above -10 °C and the winters are not so cold as Krakow, but they are also cold. The heat fluxes across the wall in Brussels and in Krakow during the heating season are similar.

Figure 73b shows the heat fluxes across the interior surface of the walls exposed and not exposed to wind-driven rain for Porto, Krakow and Brussels climates during a winter month. For each location, when wind-driven rain is excluded, lower heat fluxes are found.

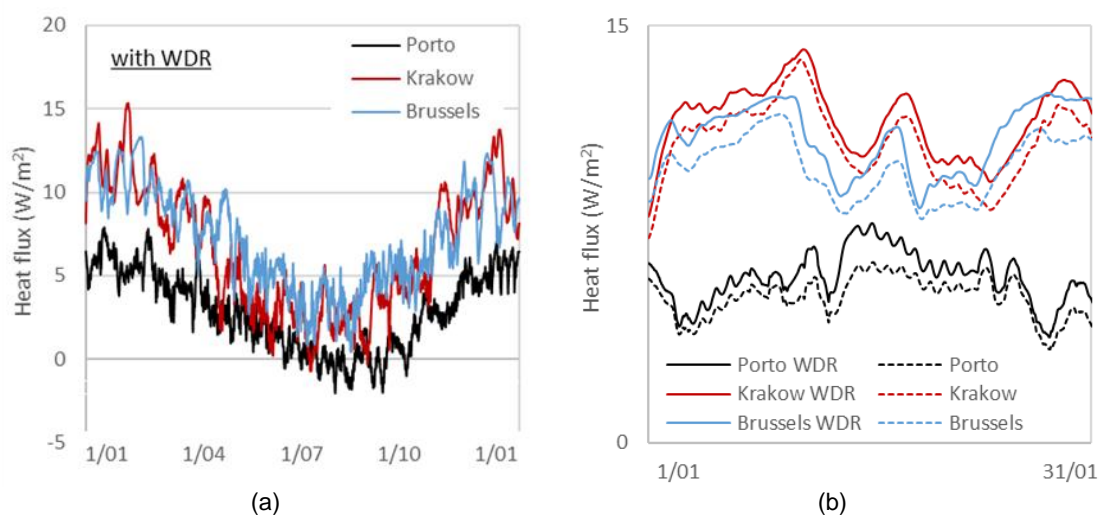


Figure 73. Heat fluxes across the interior surface of the walls: a) throughout the year; b) comparison between the heat fluxes through the walls exposed to WDR loads (solid lines) and through the walls not exposed to WDR loads (dashed lines) during January.

Table 29 presents the energy losses through the wall for Porto, Krakow and Brussels climates when exposed and not exposed to wind driven rain. It also shows the variation between energy losses through the walls exposed and not exposed to wind-driven rain.

The energy losses through the wall located in Krakow and Brussels (and exposed to wind-driven rain) were more than double than in Porto because Krakow and Brussels have colder winters. In Krakow and Brussels the energy losses through the wall were approximately 60 kWh/m<sup>2</sup> year, while in Porto the energy losses were only 25 kWh/m<sup>2</sup> year.

Although winter in Krakow is colder than in Brussels, there are more energy losses through the wall in Brussels. The reason for this is the higher moisture content of the wall in Brussels which increases energy losses.

Table 29. Energy losses for the walls exposed to WDR loads as well as for the walls not exposed to WDR loads.

Wall config.	Exterior Climate	Exposure to rain	Energy losses (kWh/m <sup>2</sup> year)	Variation
3	Porto	WDR	25	↑ 20%
		-	21	
	Krakow	WDR	58	↑ 10%
		-	53	
	Brussels	WDR	63	↑ 15%
		-	55	

It was also found that wind-driven rain had a significant impact on the energy losses through the wall for the different locations. The accumulated moisture content in the wall assembly due to the wind driven rain resulted in an increase in energy losses of 10 to 20%.

It should be noted that although the relative change in the impact of wind-driven rain on energy losses is greater for the wall located in Porto (variation of 20%), the absolute change in the impact is still greater for the wall located in Brussels (variation of 8 kWh/m<sup>2</sup> year).

### 5.3. INFLUENCE OF INSULATION THICKNESS

In the current section, the hygrothermal behaviour of a brick massive masonry wall without insulation or with a traditional interior insulation system is investigated (Configurations 2, 3 and 4 described in section 5.1.1). The interior insulation system studied is mineral wool with gypsum board. The insulation thicknesses applied are 5 cm and 10 cm. The analysis is performed for west orientated walls located in Porto, Portugal. The hygrothermal behaviour of walls exposed to wind-driven rain as well as walls not exposed to wind-driven rain is studied. To exclude effects due to the starting conditions, in what follows the results starting from January 1st in the fifth year are given.

Figure 74 shows the accumulated moisture content in the wall assemblies, namely the accumulated moisture content in the brick masonry and the accumulated moisture in the insulation system. When applying interior insulation, due to the reduced drying potential, more moisture is accumulated in the brick masonry. For the walls with interior insulation the maximum accumulated moisture content in brick masonry is approximately  $80 \text{ Kg/m}^3$ , while for the wall without insulation the maximum accumulated moisture content in brick masonry is approximately  $65 \text{ Kg/m}^3$ . The higher the interior insulation thickness, the higher the accumulated moisture content in the brick masonry.

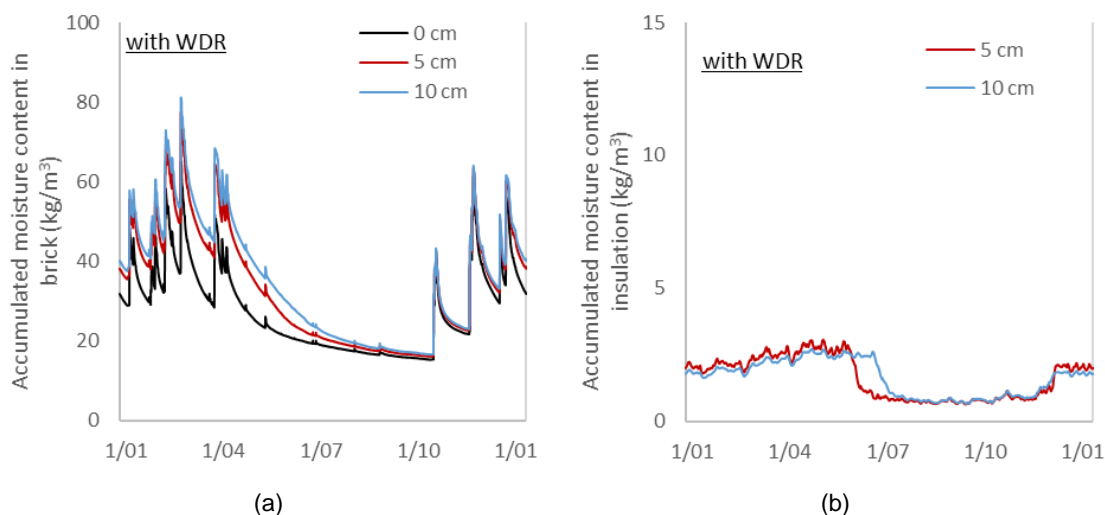


Figure 74. Accumulated moisture content: a) in the masonry and b) in the insulation (if the walls are exposed to WDR loads).

The accumulated moisture content in insulation was low throughout the year, lower than  $3 \text{ Kg/m}^3$ . The interior insulation thickness did not significantly influence the accumulated moisture content in the insulation.



Figure 75 shows the annual maximum total moisture content for the walls exposed to wind-driven rain and the annual average total moisture content for the walls exposed to wind-driven rain as well as for the walls not exposed to wind-driven rain.

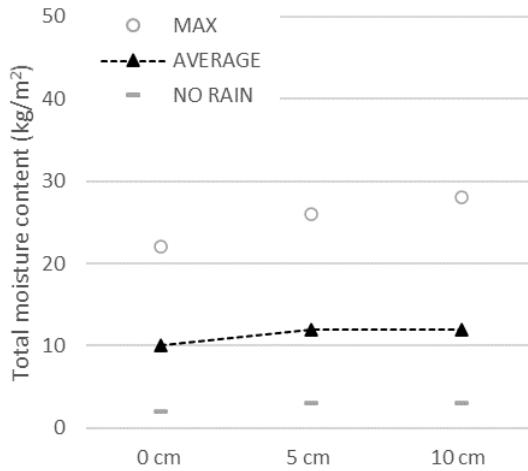


Figure 75. Maximum and average moisture content for the walls exposed to WDR loads and average moisture content for the walls not exposed to WDR loads.

The total moisture contents in the wall assemblies with interior insulation were slightly higher than found in the wall assembly without insulation. The interior insulation system hampers an inward drying out the wall. Hence, the moisture content in the wall increases.

The annual average moisture content in the wall without insulation is 10 Kg/m<sup>2</sup>. For the walls with interior insulation, the annual average moisture content is 12 Kg/m<sup>2</sup>. When wind-driven rain is excluded, the average moisture contents are significantly lower, around 2-3 Kg/m<sup>2</sup>.

Figure 76 shows the heat fluxes across the interior surface of the masonry wall without insulation, the masonry wall with 5 cm of interior insulation and the masonry wall with 10 cm of interior insulation. Figure 76a shows the heat fluxes throughout the year when the walls are exposed to wind driven rain while Figure 76b shows the heat fluxes during a winter month for when the walls are exposed to wind driven rain as well as for when the walls are not exposed to wind-driven rain.

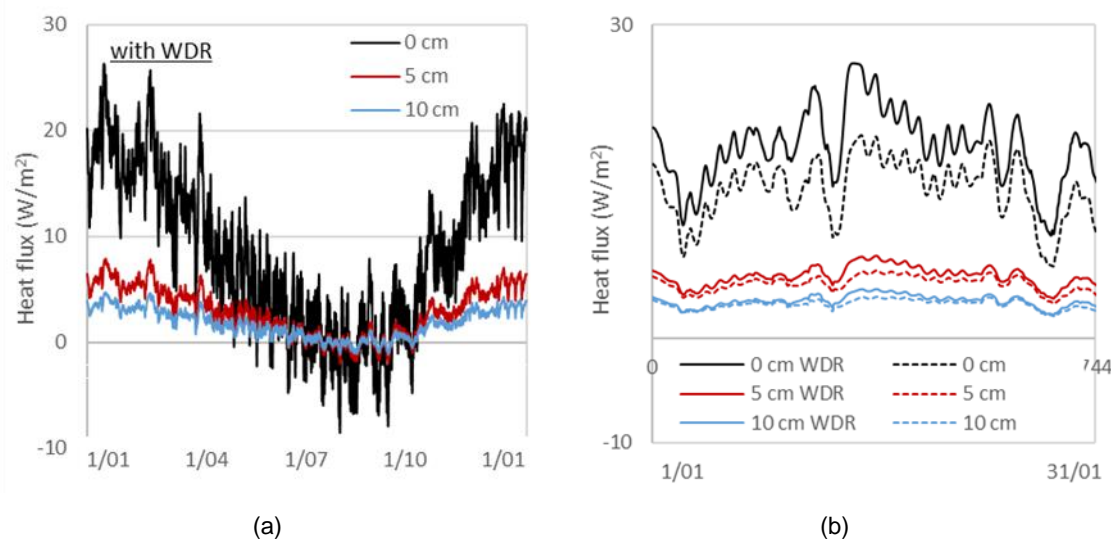


Figure 76. Heat fluxes across the interior surface of the walls: a) throughout the year; b) comparison between the heat fluxes through the walls exposed to WDR loads (solid lines) and through the walls not exposed to WDR loads (dashed lines) during January.

As expected, the presence of interior insulation significantly reduces the heat fluxes and energy losses through the wall. During the heating season, the mean heat flux through the wall without insulation is approximately  $15 \text{ W/m}^2$ , while the mean heat fluxes through the walls with 5 cm and 10 cm insulation are only approximately  $5 \text{ W/m}^2$  and  $3 \text{ W/m}^2$ , respectively. If no wind-driven rain is included, the heat fluxes through the walls decreased, especially the heat flux through the wall without insulation.

When applying thermal insulation, due to the increased thermal resistance of the total assembly, the importance of the thermal resistance of the brickwork decreases and the impact of wind driven rain on the heat fluxes is reduced.

The energy losses through the walls without insulation and with 5 cm and 10 cm of interior insulation and exposed to wind driven rain as well as not exposed to wind-driven rain are shown in Table 30. The variation between the energy losses through the walls exposed and not exposed to wind-driven rain is also shown in the table.

The energy losses through the masonry wall without insulation are approximately  $75 \text{ kWh/m}^2$  year. Applying 5 cm of interior insulation results in energy losses of approximately  $25 \text{ kWh/m}^2$  year (three times lower). Applying 10 cm of interior insulation results in energy losses of approximately  $15 \text{ kWh/m}^2$  year (five times lower).

Table 30. Energy losses for the walls exposed to WDR loads as well as for the walls not exposed to WDR loads.

Wall config.	Insulation thickness	Exposure to rain	Energy losses (kWh/m <sup>2</sup> year)	Variation
2	0 cm	WDR	76	↑ 35%
		-	56	
3	5 cm	WDR	25	↑ 20%
		-	21	
4	10 cm	WDR	15	↑ 15%
		-	13	

If no wind-driven rain is included, the energy losses through the walls decreased significantly. The impact of wind-driven rain on energy losses through the wall without insulation was very high, around 35%. For the walls with interior insulation the impact of wind-driven rain on energy losses was lower. The higher the insulation thickness of the wall, the lower the influence of wind-driven rain on the energy losses.

Thus, it can be concluded that adding insulation to the masonry wall not only improved its energy performance but also reduced the influence of moisture on the energy losses through the wall.

It is also worth mentioning that the absolute change in the impact of wind-driven rain on the energy losses of the wall without insulation of 35% is very significant, equating to an increase in energy losses of 20 kWh/(m<sup>2</sup> year). Meanwhile the absolute change in the impact for the wall with 10 cm of insulation of 15% is less significant, corresponding to an increase in energy losses of just 2 kWh/(m<sup>2</sup> year).

#### **5.4. INFLUENCE OF WALL THICKNESS**

In the current section, the hygrothermal behaviour of brick massive masonry walls with a traditional interior insulation system and with different masonry thicknesses are investigated. Solid brick layers with 0.22, 0.34 and 0.45 m thickness (1, 1 ½ and 2 brick thick, respectively) are considered (Configurations 1, 3 and 5 described in section 5.1.1). All the configurations have the same insulation system and the same insulation thickness. The analysis is performed for west orientated walls located in Porto, Portugal. The

hygrothermal behaviour for walls exposed to wind-driven rain as well as walls not exposed to wind-driven rain is studied. To exclude effects due to the starting conditions, in what follows the results starting from January 1st in the fifth year are given.

The accumulated moisture content in the brick masonry is shown in Figure 77a. The peaks in accumulated moisture content are induced by the wind-driven rain load. After the larger wind driven rain peaks in winter, the drying out is slightly faster for the 22 cm masonry wall due to the larger drying potential.

During the heating season, the higher moisture content in the thinner wall is visible. For the thinner wall, the maximum accumulated moisture content in brick masonry is approximately 100 Kg/m<sup>3</sup>. For the 34 cm masonry wall the maximum accumulated moisture content in brick masonry is approximately 80 Kg/m<sup>3</sup>. At last, for the thicker wall the maximum accumulated moisture content in brick masonry is approximately 65 Kg/m<sup>3</sup>.

Figure 77b shows the accumulated moisture content in the insulation system. In the insulation system only a limited amount of moisture is stored. The influence of the wall thickness on the moisture content in the insulation system was not relevant.

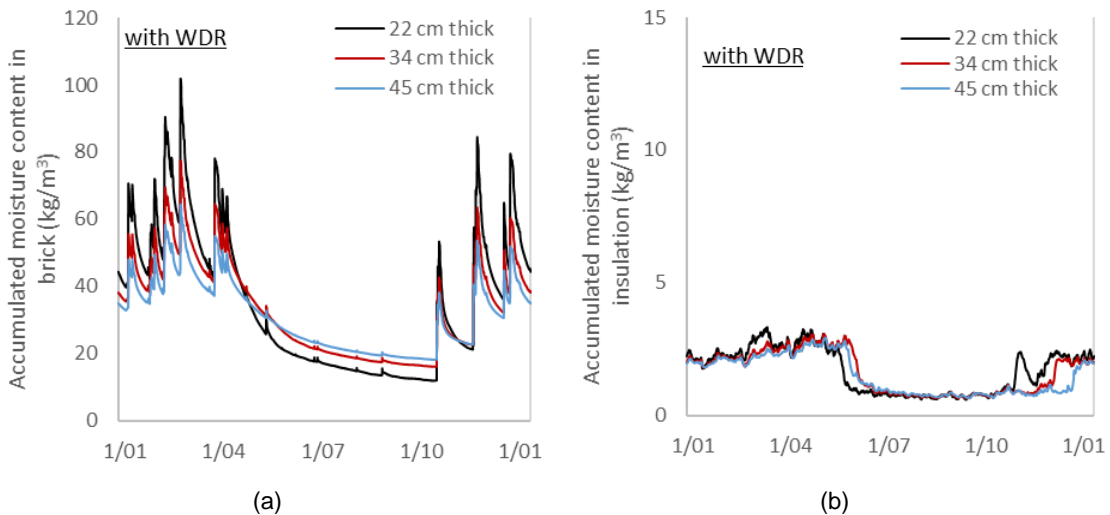


Figure 77. Accumulated moisture content: a) in the masonry and b) in the insulation (if the walls are exposed to WDR loads).

Figure 78 shows the annual maximum total moisture content for the walls exposed to wind-driven rain and the annual average total moisture content for the walls exposed to wind-driven rain as well as for the walls not exposed to wind-driven rain.

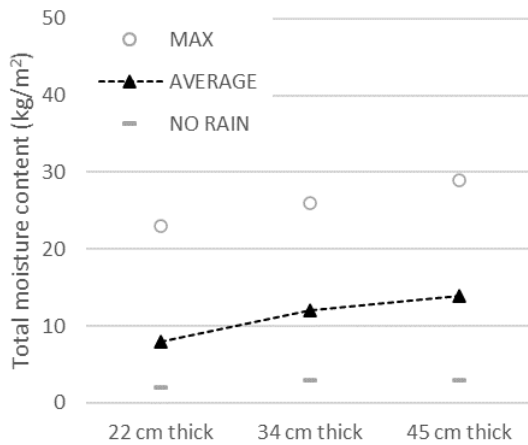


Figure 78. Maximum and average moisture content for the walls exposed to WDR loads and average moisture content for the walls not exposed to WDR loads.

The thicker masonry wall results in higher total moisture contents since more moisture can be captured. The opposite is found for the thinner masonry wall. For the thinner wall the annual average moisture content is 8 Kg/m<sup>2</sup> while for the 34 cm masonry wall the annual average moisture content is 12 Kg/m<sup>2</sup> and for the thicker wall the annual average moisture content is 14 Kg/m<sup>2</sup>. When wind-driven rain is excluded, the annual average moisture contents are significantly lower, around 3 Kg/m<sup>2</sup>.

The heat fluxes across the interior surface of the walls 22 cm, 34 cm, and 45 cm thick and exposed to wind driven rain are shown in Figure 79a. The masonry thickness has only a small impact on the heat fluxes across the walls. During the heating season, the mean heat flux through the walls is around 5 W/m<sup>2</sup>.

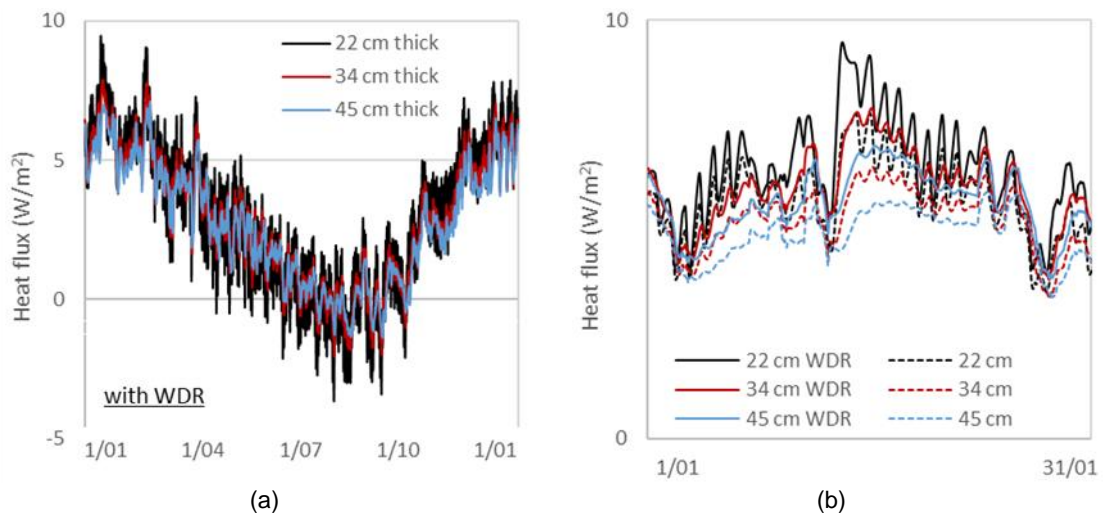


Figure 79. Heat fluxes across the interior surface of the walls: a) throughout the year; b) comparison between the heat fluxes through the walls exposed to WDR loads (solid lines) and through the walls not exposed to WDR loads (dashed lines) during January.

Figure 79b shows the heat fluxes across the interior surface of the walls 22 cm, 34 cm, and 45 cm thick exposed and not exposed to wind-driven rain during a winter month. When wind-driven rain is excluded, lower heat fluxes are found.

The energy losses through the masonry walls with 22 cm, 34 cm and 45 cm thickness exposed to wind driven rain as well as not exposed to wind-driven rain are shown in Table 31. The variation between the energy losses through the walls exposed and not exposed to wind-driven rain is also shown.

Table 31. Energy losses for the walls exposed to WDR as well as for the walls not exposed to WDR.

Wall config.	Masonry thickness	Exposure to rain	Energy losses (kWh/m <sup>2</sup> year)	Variation
1	22 cm	WDR	27	↑ 19%
		-	23	
3	34 cm	WDR	25	↑ 20%
		-	21	
5	45 cm	WDR	24	↑ 26%
		-	19	

For brick massive masonry walls with a traditional interior insulation system, the masonry thickness has only a small impact on the influence of moisture on the energy performance of the walls. For the 22 cm masonry wall the energy losses are approximately 27 kWh/m<sup>2</sup> year. When the masonry wall thickness increases to 45 cm (twice the thickness), the energy losses only reduce to 24 kWh/m<sup>2</sup> year.

If no wind-driven rain is included, the energy losses through the walls decreased. The accumulated moisture content in the wall assemblies due to wind driven rain resulted in an increase in energy losses of 19 to 26%. The higher the masonry wall thickness, the higher the influence of moisture on the energy performance of the wall.

## **5.5. INFLUENCE OF FINISHING COATING**

In the current section, the hygrothermal behaviour of brick massive masonry walls with different external finishing coatings and a stone massive masonry wall are investigated. A brick masonry wall without finishing coating, a brick masonry wall coated with a

traditional lime plaster, a brick masonry wall coated with an innovative external insulating render system and a granite masonry wall without finishing coating are considered (Configurations 3, 6, 7 and 8 described in section 5.1.1). The innovative insulating render is a lightweight insulating render formulated with natural cork aggregates, sands and natural hydraulic lime. The analysis is performed for west orientated walls located in Porto, Portugal. The hygrothermal behaviour of walls exposed to wind-driven rain as well as walls not exposed to wind-driven rain is studied. To exclude effects due to the starting conditions, in what follows the results starting from January 1st in the fifth year are given.

To investigate the accumulated moisture content in the wall assemblies, a subdivision is made between the accumulated moisture content in the masonry wall and the accumulated moisture in the insulation system, namely in the traditional interior insulation system or in the innovative external insulating render system. The results are shown in Figure 80.

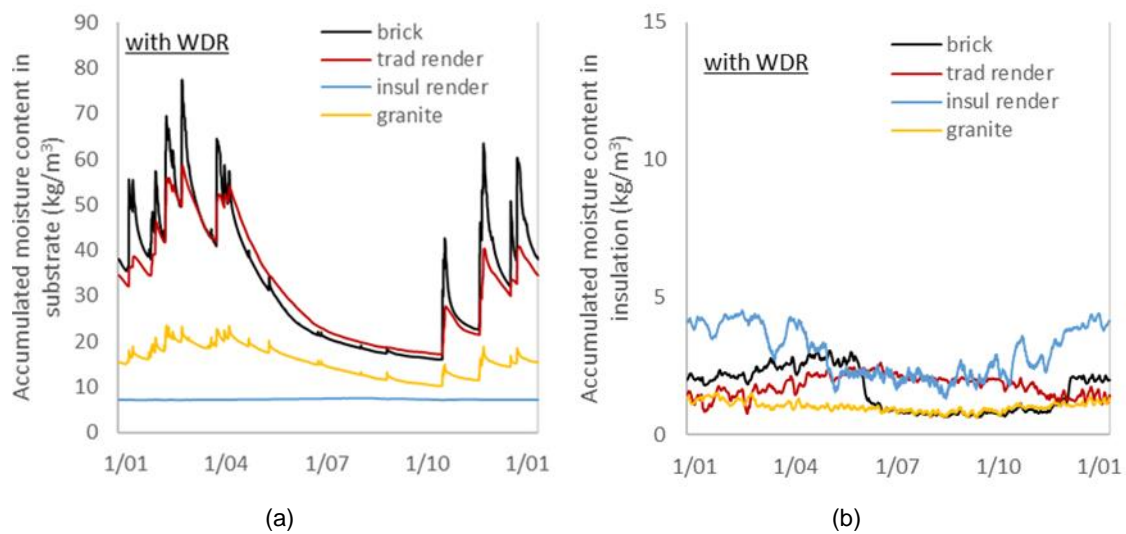


Figure 80. Accumulated moisture content: a) in the brick or stone masonry and b) in the insulation (if the walls are exposed to WDR loads).

When the walls are exposed to wind driven rain loads, during the heating season, the largest accumulated moisture content in the brick layer is found for the uncoated brick masonry wall. For the brick masonry wall coated with a traditional render, during the heating season a slightly lower moisture content in the brick layer is found. For the brick masonry wall externally coated with the insulating render system, a significantly lower moisture content in the brick layer is found since the insulating render system is hardly capillary active and consequently moisture hardly enters the wall. For instance, the

moisture content in brick layer reaches a value of 80 Kg/m<sup>3</sup> and 60 Kg/m<sup>3</sup> when the brick masonry wall is uncoated or coated with the traditional render, respectively, while with the insulating render system only a value of 8 Kg/m<sup>3</sup> is obtained. Note that for the brick masonry wall externally coated with the insulating render system, the variation in the moisture content of the brick masonry throughout the year is not noticed in Figure 80a due to the large scale of the graph.

The moisture content in the uncoated granite masonry wall is significantly lower than the accumulated moisture content in the uncoated brick masonry wall. The moisture content in granite layer only reaches a value of 23 Kg/m<sup>3</sup>. The reason for this is the lower capillary water absorption coefficient of granite compared to the capillary water absorption coefficient of brick. In the insulation layers no relevant moisture is accumulated.

Figure 81 shows the annual maximum total moisture content for the walls exposed to wind-driven rain and the annual average total moisture content for the walls exposed to wind-driven rain as well as for the walls not exposed to wind-driven rain. The uncoated brick masonry wall and the brick masonry wall coated with traditional render results in significantly higher total moisture contents than the brick masonry wall coated with insulating render system and the uncoated granite masonry wall. In fact, for the uncoated brick masonry wall and the brick masonry wall coated with traditional render the annual average total moisture content is 12 Kg/m<sup>2</sup> while for the brick masonry wall coated with insulating render system the annual average total moisture content is only 4 Kg/m<sup>2</sup> and for the uncoated granite masonry wall is only 5 Kg/m<sup>2</sup>.

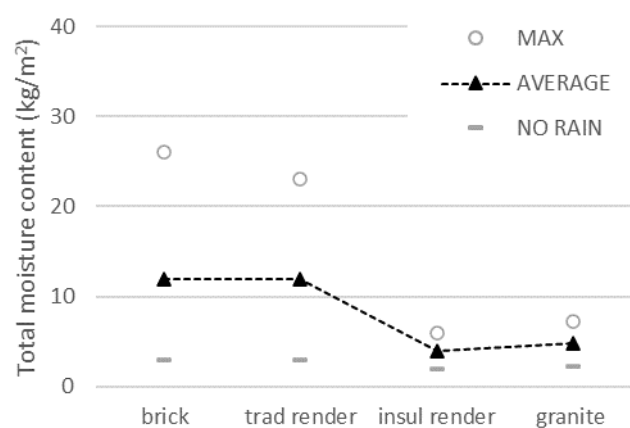


Figure 81. Maximum and average moisture content for the walls exposed to WDR loads and average moisture content for the walls not exposed to WDR loads.



When wind-driven rain is excluded, for the uncoated brick masonry wall and the brick masonry wall coated with traditional render the annual average total moisture contents are significantly lower while for the brick masonry wall coated with insulating render system and the uncoated granite masonry wall the annual average total moisture content is very similar.

The heat fluxes across the interior surfaces of the uncoated brick masonry wall, the brick masonry wall coated with traditional lime render, the brick masonry wall coated with insulating render system and the uncoated granite masonry wall are shown in Figure 82a. The heat flux through the uncoated brick masonry wall and the heat flux through the brick masonry wall coated with traditional render are very similar. The traditional render has a negligible impact on the heat flux across the wall. The heat flux through the uncoated granite masonry wall is slightly higher than the heat flux through the uncoated brick masonry wall since the thermal conductivity of the stone is higher than that of brick.

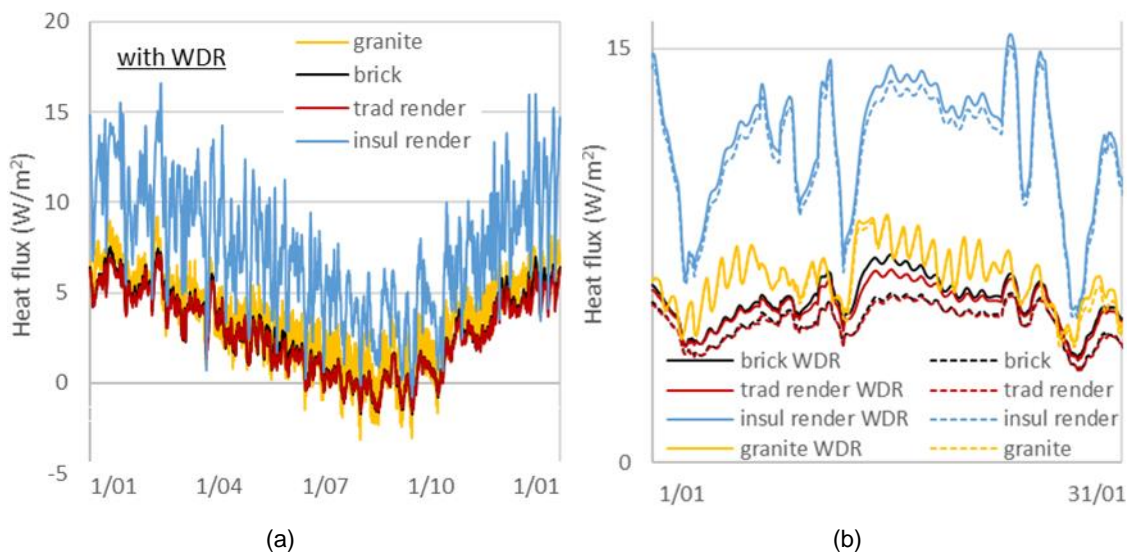


Figure 82. Heat fluxes across the interior surface of the walls: a) throughout the year; b) comparison between the heat fluxes through the walls exposed to WDR loads (solid lines) and through the walls not exposed to WDR loads (dashed lines) during January.

During the heating season the highest heat losses are found for the brick masonry wall coated with insulating render system due to the higher thermal conductivity of the insulation material. The mean heat flux through the uncoated brick masonry wall or the brick masonry wall coated with traditional render during the heating season is approximately 5 W/m<sup>2</sup>, while the mean heat flux through the brick masonry wall coated with insulating render system is approximately 10 W/m<sup>2</sup>.

Figure 82b shows the heat fluxes across the interior surface of the walls exposed and not exposed to wind-driven rain during a winter month. When wind-driven rain is excluded, lower heat fluxes are found for the uncoated brick masonry wall and the brick masonry wall coated with traditional render while for the brick masonry wall coated with insulating render system and for the uncoated granite masonry wall similar heat fluxes are obtained. The energy losses through the uncoated brick masonry wall, the brick masonry wall coated with traditional lime render, the brick masonry wall coated with insulating render system and the uncoated granite masonry wall exposed to wind driven rain as well as not exposed to wind-driven rain are shown in Table 32. The variation between the energy losses through the wall exposed and not exposed to wind-driven rain is also shown.

Table 32. Energy losses for the walls exposed to WDR as well as for the walls not exposed to WDR.

Wall config.	Finishing coating	Exposure to rain	Energy losses (kWh/m <sup>2</sup> year)	Variation
3	brick	WDR	25	↑ 20%
		-	21	
6	trad render	WDR	24	↑ 20%
		-	20	
7	insul render	WDR	62	↑ 4%
		-	59	
8	granite	WDR	32	↑ 3%
		-	31	

For the uncoated brick masonry wall the energy losses are 25 kWh/m<sup>2</sup> year. For the brick masonry wall coated with traditional render the energy losses are only slightly lower. For both walls the accumulated moisture content in the wall assemblies due to wind driven rain resulted in an increase in energy losses of 20%. Although the higher energy losses through the brick masonry wall externally coated with insulating render system (around 60 kWh/m<sup>2</sup> year), the impact of wind driven rain on the energy performance of the wall is significantly lower, only 4%. For the uncoated granite masonry wall the energy losses are 32 kWh/m<sup>2</sup> year and the impact of wind driven rain on the energy performance of the wall is also low of only 3%.

## 5.6. INFLUENCE OF INITIAL MOISTURE IN MASONRY

This section compares the hygrothermal behaviour of a brick massive masonry wall with a traditional interior insulation system (Configuration 3) to this of a brick massive masonry wall coated with an innovative external insulating render system (Configurations 3 and 7 described in section 5.1.1). The innovative insulating render is a lightweight insulating render formulated with natural cork aggregates, sands and natural hydraulic lime. The analysis is performed for west orientated walls located in Brussels, Belgium. Brussels climate is simulated because it has a high wind-driven rain load. The hygrothermal behaviour of walls exposed to wind-driven rain is studied. In the analysis, the initial condition of both walls is high initial moisture in the masonry, assuming the scenario that the masonry was wet when the walls were rehabilitated, i.e., when the thermal insulation systems were applied to the walls. The objective is to assess the influence of this initial moisture in the masonry on the energy performance of the walls over the years.

The accumulated moisture content in the brick masonry of the masonry wall with interior insulation system and of the masonry wall with external insulating render system is shown in Figure 83. The initial moisture in brick is  $246 \text{ kg/m}^3$  for both walls.

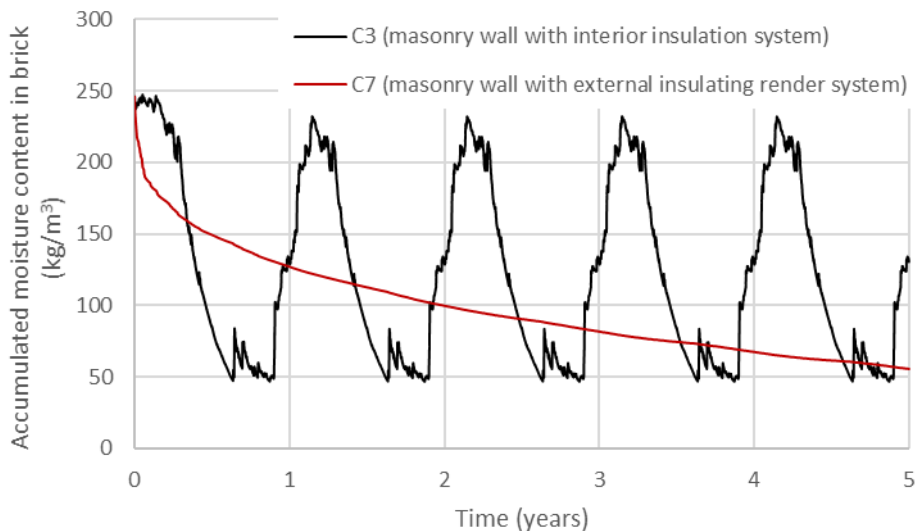


Figure 83. Accumulated moisture content in brick masonry of wall configuration 3 (C3) and wall configuration 7 (C7) over time.

The two walls started from the same initial conditions (high humidity in the brick masonry) but showed completely different behaviours. The initial moisture in the masonry wall with interior insulation system dried out within the first year, while the

initial moisture in the masonry wall with external insulating render system dried much more slowly over the five years.

For the masonry wall with interior insulation system, the impact of the initial moisture in masonry is only visible in the first year. From the first year onwards, the moisture content in the masonry resumes its usual annual cycle, with the moisture content varying between approximately 50 and 230 kg/m<sup>3</sup>.

For the masonry wall with external insulating render, the moisture in the brick masonry decreases continuously over the several years, with the greatest decrease occurring in the first year. After five years, the accumulated moisture content in the brick masonry is around 50 kg/m<sup>3</sup> and the trend is to continue to decline. In fact, applying insulation systems to masonry walls reduces their drying potential, especially if the insulation system is applied from the outside. Indeed, the initial moisture in the masonry wall after applying the external insulating render takes a long time to dry, several years.

The annual maximum and average moisture content in the wall assemblies per year is shown in Figure 84. Both walls started from the same initial humidity conditions, however, the average moisture content in the first year of the wall with interior thermal insulation is much lower than that of the wall with external insulating render, revealing that the initial humidity of the wall with interior thermal insulation dries significantly faster than the initial humidity of the wall with external insulating render.

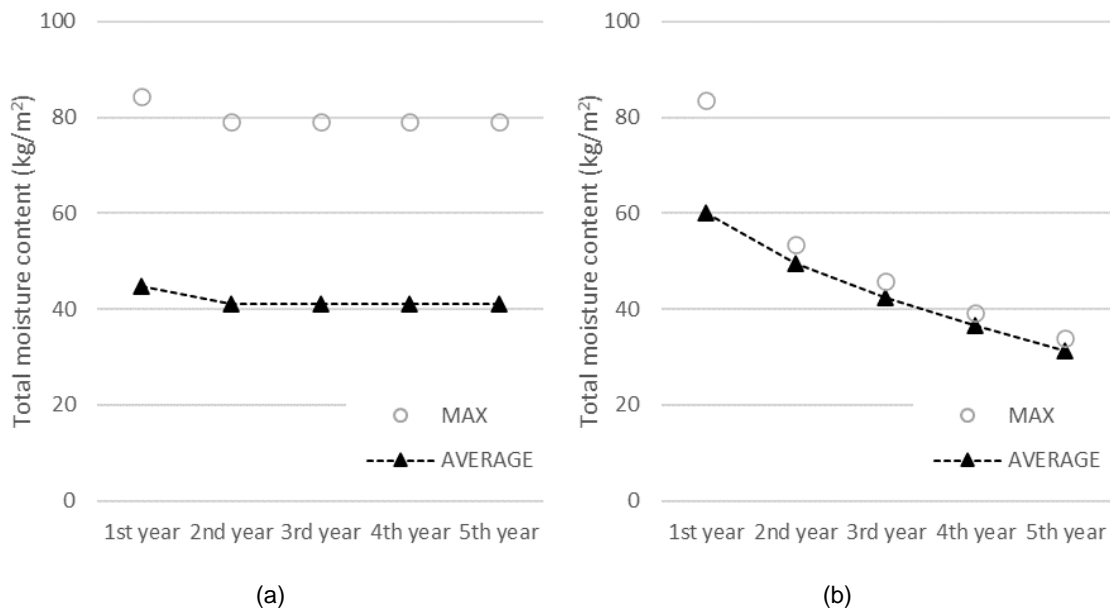


Figure 84. Annual maximum and average moisture content in the walls: a) configuration 3 (masonry wall with interior insulation system); b) configuration 7 (masonry wall with external insulating render system)

For the masonry wall with interior insulation system, the average annual moisture content in the wall is higher in the first year than in subsequent years. In the first year the average wall moisture content is  $45 \text{ kg/m}^2$  while in subsequent years it is  $41 \text{ kg/m}^2$ . The maximum annual moisture content in this wall is significantly higher than the average annual moisture content. In the first year the maximum moisture content in the wall is  $84 \text{ kg/m}^2$  while in the following years it is  $79 \text{ kg/m}^2$ .

For masonry walls with external insulating render, the annual average and maximum moisture content decreases every year. In the initial year the average moisture content in the wall was  $60 \text{ kg/m}^2$  and after five years it decreased to half that value. Except for the first year, for this wall the maximum annual moisture content is close to the average annual moisture content.

Figure 85 shows the heat fluxes across the interior surface of the brick masonry wall with interior insulation system and of the brick masonry wall coated with the external insulating render system throughout the years. The highest heat losses are found for the masonry wall coated with the external insulating render due to the higher thermal conductivity of the insulation material. In fact, during the heating season in the fifth year the mean heat flux through the masonry wall with the external insulating render is approximately  $22 \text{ W/m}^2$ , while the mean heat flux through the masonry wall with interior insulation is only around  $9 \text{ W/m}^2$ .

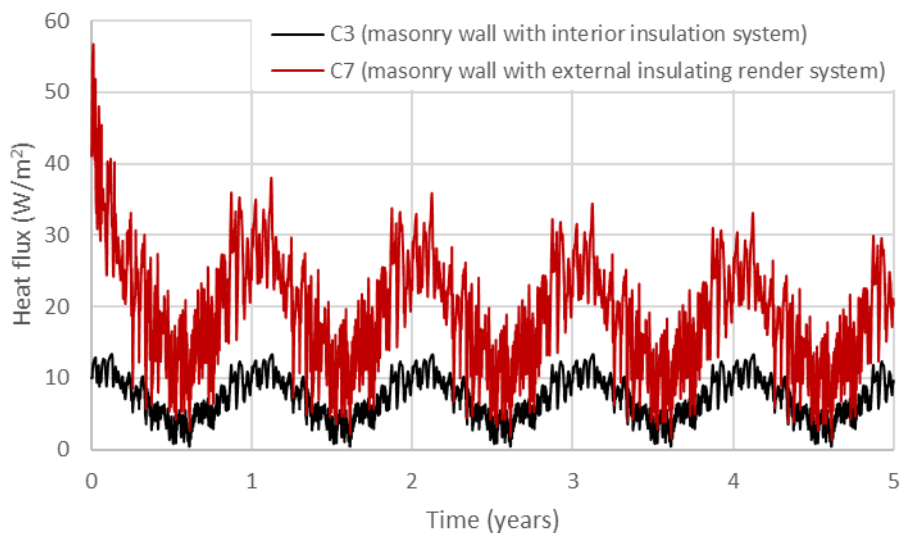


Figure 85. Heat fluxes across the interior surface of the walls over time.

In the figure it can be clearly seen that the heat flux through the wall coated with the external insulating render is higher in the first year than in the others, due to the initial moisture in the masonry. For the wall with interior thermal insulation, no change is clearly detected in the heat flux through the wall due to the initial moisture in the masonry.

The energy losses through the masonry wall with interior insulation system and through the masonry wall with external insulating render system exposed to wind driven rain per year is shown in Table 33. The table also shows the variation between energy losses throughout the year relative to the previous year.

Table 33. Energy losses through the walls per year.

Wall config.	Exterior Climate	Year	Energy losses (kWh/m <sup>2</sup> year)	Variation
3	Brussels	1 <sup>st</sup> year	63	
		2 <sup>nd</sup> year	63	↑ 0.1%
		3 <sup>rd</sup> year	63	↑ 0%
		4 <sup>th</sup> year	63	↑ 0%
		5 <sup>th</sup> year	63	↑ 0%
7	Brussels	1 <sup>st</sup> year	193	
		2 <sup>nd</sup> year	172	↑ 11%
		3 <sup>rd</sup> year	164	↑ 5%
		4 <sup>th</sup> year	157	↑ 4%
		5 <sup>th</sup> year	151	↑ 4%

It can be concluded that the initial moisture in the masonry did not influence the energy performance of the wall where the interior insulation system was applied, but it did

influence the energy performance of the wall where the exterior insulating render was applied.

For the masonry wall with interior insulation system the energy losses are approximately 60 kWh/m<sup>2</sup> year in every year. For the masonry wall with external insulating render, the energy losses in the first year due to the initial moisture in the masonry are around 190 kWh/m<sup>2</sup> year. Over time the wall dries out and consequently the energy losses through the wall decrease. In the second year the energy losses through the wall are about 10% less than in the first year and in the fifth year it is about 20% less.

## **5.7. FINAL CONSIDERATIONS**

In this chapter the hygrothermal performance of retrofitted walls exposed to realistic environmental conditions with inclusion of wind-driven rain is numerically studied. A comparison is made between the hygrothermal behaviour of a brick masonry wall with a traditional interior insulation system located in Porto, Kraków and Brussels. The hygrothermal behaviour of walls with different insulation thickness and different brick masonry thickness is investigated. Moreover, a comparison between an uncoated brick masonry wall, a brick masonry wall coated with a traditional render, a brick masonry wall coated with an innovative insulating render system and an uncoated granite masonry wall is obtained.

The impact of wind driven rain on the energy losses through the walls is quantified. Table 34 gives the summary of those results. A colour scale was assigned to the variation between energy losses through the walls exposed and not exposed to wind-driven rain. The green colour was attributed to variations below 10% (situations in which moisture has little influence on the energy performance of the wall), the yellow colour was attributed to variations between 10 and 30% (situations in which moisture significantly influences the energy performance of the wall) and the colour red for variations greater than 30% (situations where moisture greatly influences the energy performance of the wall).

The influence of initial moisture on the energy performance, over the years, of a rehabilitated masonry wall with interior thermal insulation and a rehabilitated masonry wall with external insulating render is also assessed.

Table 34. Overview of results of energy losses through the walls exposed and not exposed to wind-driven rain (WDR).

Wall config.	Climate	Insulation thickness	Masonry thickness	Finishing coating	Exposure to rain	Energy losses (kWh/m <sup>2</sup> year)	Var
1 thinner wall	Porto	5 cm	22 cm	Uncoated brick	WDR	27	↑ 19%
					-	23	
2 without insulation	Porto	0 cm	34 cm	Uncoated brick	WDR	76	↑ 35%
					-	56	
3 Interior insulation	Porto	5 cm	34 cm	Uncoated brick	WDR	25	↑ 20%
					-	21	
	Krakow				WDR	58	↑ 10%
					-	53	
	Brussels				WDR	63	↑ 15%
					-	55	
4 thicker interior insulation	Porto	10 cm	34 cm	Uncoated brick	WDR	15	↑ 15%
					-	13	
5 Thicker wall	Porto	5 cm	45 cm	Uncoated brick	WDR	24	↑ 26%
					-	19	
6 trad render coating	Porto	5 cm	34 cm	Traditional render	WDR	24	↑ 20%
					-	20	
7 external insulating render	Porto	5 cm	34 cm	Insulating render system	WDR	62	↑ 4%
					-	59	
8 stone wall	Porto	5 cm	30 cm	Uncoated granite	WDR	32	↑ 3%
					-	31	



The main findings obtained in the current chapter are as follows:

- Outdoor climate was found to be determinant for the energy performance of a brick masonry wall with a traditional interior insulation system. Although the outdoor climate in Krakow is colder than in Brussels, there were more energy losses through the wall in Brussels due to the higher humidity and consequent higher moisture content of the wall.
- Wind-driven rain had a significant impact on the energy losses through a brick masonry wall with a traditional interior insulation system located both in Porto, Krakow and Brussels. The accumulated moisture content in the wall due to wind driven rain resulted in an increase in energy losses of 10 to 20%.
- The impact of wind-driven rain on energy losses through a brick masonry wall without insulation was very high, around 35%. Adding interior insulation to the wall not only improved its energy performance but also significantly reduced the influence of moisture on the energy losses through the wall. However, adding interior insulation also results in a higher moisture content in the masonry wall and may induce moisture related damage patterns.
- The higher the insulation thickness, the lower the influence of moisture on the energy performance of a masonry wall.
- For a brick masonry wall with a traditional interior insulation system, the brick masonry thickness had only a small impact on the influence of moisture on the energy performance of the wall. Also, the thicker masonry wall results in higher moisture content and higher influence of moisture on the energy performance.
- Mainly the finishing coating determines the influence of moisture on the energy performance of a wall assembly. For a brick masonry wall externally coated with an insulating render system hardly capillary active, the impact of wind driven rain on the energy losses through the wall was only 4% as moisture barely enters the wall.
- Wind-driven rain did not significantly impact the energy losses through an uncoated granite masonry wall since the capillary water absorption coefficient of granite is low.
- Initial moisture in the masonry did not influence the energy performance of the wall where the interior thermal insulation system was applied, but it did influence

the energy performance of the wall where the external insulating render was applied. Over time the wall coated with external insulating render dries out and the energy losses through the wall decrease. In the second year the energy losses through that wall are about 10% less than in the first year and in the following years energy losses reduce by about 5% per year.

# 6

## CONCLUSION

### 6.1. FINAL CONCLUSIONS

The main objective of the current thesis was to expand the knowledge on the influence of moisture on the energy performance of retrofitted walls. This is an important subject these days due to the need to improve the energy efficiency of existing building façades and to reduce the buildings energy needs for heating. In the current chapter, an overview of the main results and conclusions can be found. Additionally, an onset for further research is suggested.

The moisture content in walls under in-service conditions may considerably affect their energy performance. The heat losses through walls can be higher if they are wet. Thus, it is crucial to consider the influence of moisture on the energy performance of walls during their renovation, in order to reduce the energy losses and the energy consumption for heating. This work assessed how moisture influences the energy performance of retrofitted walls and what the consequences for the energy consumption are. The main objective was to contribute to identifying how energy efficiency of exterior walls of existing buildings can be improved, taking into account the influence of moisture on the energy performance of the walls.

The moisture effects on heat transport across a wall assembly are mainly the moisture-dependent thermal conductivity of building materials and phase changes such as drying processes. In the literature review, a compilation of measurements of thermal conductivities of building materials as a function of moisture content was found. Also, several experimental and numerical studies that investigated the influence of moisture on

the energy performance of wall assemblies were analysed. The following conclusions were reached:

- The influence of moisture on the energy performance of wall assemblies can vary as it depends on temperature, wind-driven rain, local exposure conditions, finishing coating's capillary water absorption and wall constructive solution.
- Wind-driven rain may considerably affect the energy performance of a wall while relative humidity may not influence it as much. Nevertheless, relative humidity influences the drying time of a wall.
- The thermal conductivities of certain building materials were considerably affected by moisture content. The greatest increase in thermal conductivity belongs to brick, mineral wool and thermal renders. For gypsum board and expanded polystyrene (EPS) there was also an increase in thermal conductivity, albeit smaller. Conversely to the other materials, no relevant change was observed in the thermal conductivity of extruded polystyrene (XPS) with increasing moisture content.
- The humidification of exterior walls can significantly worsen their energy performance. On average, the maximum difference found between the thermal transmittance of a dry wall assembly and of a moist wall assembly was around 30%, depending on the composition of the wall assembly (De Freitas 1992, Jakovics et al. 2014, Vereecken and Roles 2015, Coelho and Henriques 2016, Alonso-Alonso 2017, Maia, Ramos and Veiga 2018).
- It was found a lack of experimental studies about the influence of moisture on the heat flux across retrofitted walls as well as a lack of research on the impact of local climate conditions including wind-driven rain on the dynamic energy performance of retrofitted walls.

An experimental prototype was developed at the Building Physics Laboratory – Faculty of Engineering University of Porto to assess the impact of wetting periods on the energy performance of brick masonry walls with different insulation systems. The tests simulated the exposure of wall test specimens to a quasi-steady temperature gradient as well as rainy periods, with a continuous record of the heat fluxes across the specimens' surfaces. Different precipitation sequences were applied against the specimens. Specimen A consisted of a masonry wall with a traditional interior insulation system, whereas

Specimen B consisted of a masonry wall with an innovative external insulating render system formulated with natural cork aggregates, sands and natural hydraulic lime. There was some instability in the measurements of the heat fluxes due to the use of heating and dehumidifying equipment. However, several adjustments were made to the experimental prototype which enabled the reduction of this effect and permitted carrying out the study. The following conclusions were drawn:

- In specimen A, the measurement of the relative humidity between the masonry and the insulation clearly showed that the moisture content of the wall increased considerably due to precipitation. In the test in which the most intense precipitation sequence was applied, saturation was reached inside the specimen.
- In specimen B, no moisture was found inside the specimen during the tests. Both the temperature profile and the heat fluxes did not vary throughout the tests in spite of the wetting periods.
- After the precipitation sequences, the drying of specimen A occurred very slowly due to the high air humidity of the rain room.
- After the rainy periods, the heat flux across the exterior surface of specimen A decreased due to the rainwater absorbed in the wall, that slightly cooled the brick masonry of the specimen.
- Driving rain influenced the energy performance of specimen A. Due to the humidification of the wall, the heat flux across the interior surface of specimen A increased by about 10%.
- Driving rain did not significantly influence the energy performance of specimen B as it did not enter the wall, since the absorption coefficient of its finishing coating is very low (and classified as nearly waterproof).

Afterwards, an experimental validation of the one-dimensional WUFI advanced hygrothermal simulation model was performed by comparing the measured and simulated hygrothermal performance of the wall test specimens, i.e., the masonry walls with different insulation systems, exposed to driving rain. The validation of the hygrothermal model was based on the measurements performed in the experimental prototype developed and the hygrothermal properties experimentally determined and following described. (The validation has the limitation of not taking into account solar radiation).

The experimental characterization of materials was performed to generate the inputs required for the correct numerical simulations. The experimental determination of the most relevant hygrothermal properties, namely capillary water absorption coefficient, water vapour diffusion resistance factor, and moisture-dependent thermal conductivity of solid brick and insulating render system (composed by insulating render, finishing render and paint, and formulated with natural cork aggregates, sands and natural hydraulic lime) led to the following results:

- Brick and insulating render system showed very different behaviour when in direct contact with liquid water. Brick was highly capillary active ( $A=0.06 \text{ Kg}/(\text{m}^2 \text{ s}^{1/2})$ ) and can be classified as quick suction, while insulating render system was hardly capillary active ( $A=0.003 \text{ Kg}/(\text{m}^2 \text{ s}^{1/2})$ ) and can be classified as nearly waterproof.
- Water vapour permeability of brick was lower than the water vapour permeability of insulating render system. The obtained value of water vapor diffusion resistance factor  $\mu$  of brick was 17, while the obtained value of water vapor diffusion resistance factor  $\mu$  of insulating render system was 6.
- Note that in the case of moisture-dependent thermal conductivity, only the insulating render was measured and not the complete insulating render system. Both the thermal conductivities of brick and insulating render were considerably affected by moisture content, especially that of brick. Thermal conductivity of brick increased from approximately 0.75 to 1.26 W/(m K), which reveals high sensitivity to moisture effects. For insulating render (if the insulating render is not protected by the paint and is in direct contact with liquid water), its thermal conductivity increased from approximately 0.15 to 0.24 W/(m K).

The validation results showed that the hygrothermal behaviour of the walls throughout the experiment was well reproduced by the model. The simulated temperatures, relative humidity and heat fluxes showed discrepancies below 0.5 °C, 10% and 0.6 W/m<sup>2</sup> when compared with the measured ones. The slight discrepancies between the measured and simulated data may have to do with the accuracy of the equipment used in the experiment, together with the simplifications and limitations of the WUFI hygrothermal model, which derives from the enormous complexity of the hygrothermal processes in building

components and the fact that the mortar joints of the brick masonry were neglected in the simulation.

It was observed that the hygrothermal model was capable of simulating both moisture and energy performance of walls and the effect of driving rain (and subsequent increase in moisture content) on heat losses. Both in experimental test and numerical simulation, driving rain increased the moisture content in wall configuration A and influenced the heat fluxes through both surfaces of the wall. For wall configuration B, both in experimental test and numerical simulation, driving rain did not influence the heat fluxes since the rainwater did not enter the wall. Thus, the hygrothermal model was validated for temperature, relative humidity and heat flux and the statistical analysis proved its strength. The experimental validation of the hygrothermal model showed that WUFI Pro is a good tool to quantify the influence of moisture on the energy performance of retrofitted walls.

Thereafter, the hygrothermal performance of retrofitted walls exposed to realistic environmental conditions was numerically studied using the WUFI Pro software (with the WUFI hygrothermal model previously validated). The impact of wind driven rain and initial moisture in the masonry on the energy losses through retrofitted walls was quantified. Moreover, the key factors (climate conditions, insulation thickness, wall thickness and finishing coating) that most affect the influence of moisture on the energy performance of retrofitted walls were investigated through a sensitivity analysis.

In the sensitivity analysis a comparison was made between the hygrothermal performance of a brick masonry wall with a traditional interior insulation system located in Porto, Kraków and Brussels. The hygrothermal performance of brick masonry walls with different insulation thicknesses and different brick masonry thicknesses was investigated. Moreover, a comparison between the hygrothermal performance of an uncoated brick masonry wall, a brick masonry wall coated with a traditional render, a brick masonry wall coated with an innovative insulating render system and an uncoated granite masonry wall was obtained. Table 34 summarises the results of the impact of wind-driven rain on the energy performance of the investigated walls. The influence of initial moisture on the energy performance, over the years, of a rehabilitated masonry wall with interior thermal

insulation and a rehabilitated masonry wall with external insulating render was also assessed. The main findings are as follows:

- The outdoor climate was found to be determinant for the energy performance of a brick masonry wall with a traditional interior insulation system. Although the climate in Krakow is colder than in Brussels, there were more energy losses through the wall in Brussels due to the higher wind-driven rain load and consequent higher moisture content of the wall.
- Wind-driven rain had a significant impact on the energy losses through a brick masonry wall with a traditional interior insulation system (Configuration 3) located both in Porto, Krakow and Brussels. The accumulated moisture content in the wall due to wind driven rain increased the thermal conductivity of brick and resulted in a rise of energy losses between 10 to 20%.
- The impact of wind-driven rain on energy losses through a brick masonry wall without insulation (Configuration 2) was very high, around 35%. Adding interior insulation to the wall not only improved its energy performance but also significantly reduced the influence of moisture on the energy losses through the wall. However, adding interior insulation also results in a higher moisture content in the brick masonry wall so it increases the risk of moisture related damage patterns.
- The higher the insulation thickness, the lower the influence of moisture on the energy performance of a masonry wall.
- For a brick masonry wall with a traditional interior insulation system, the brick masonry thickness had only a small impact on the influence of moisture on the energy performance of the wall. Also, the thicker brick masonry wall results in higher moisture content and higher influence of moisture on the energy performance.
- Mainly the finishing coating determines the influence of moisture on the energy performance of a wall assembly. For a brick masonry wall externally coated with an insulating render system hardly capillary active (Configuration 7) the impact of wind driven rain on the energy losses through the wall was only 4% as moisture barely enters the wall.



- Wind-driven rain did not significantly impact the energy losses through an uncoated granite masonry wall (Configuration 8) since the capillary water absorption coefficient of granite is low.
- Initial moisture in the masonry when the wall is rehabilitated did not influence the energy performance of the wall where the interior thermal insulation system was applied (Configuration 3), but it did influence the energy performance of the wall where the external insulating render was applied (Configuration 7). Over time, the masonry of wall coated with external insulating render dries out and the energy losses through the wall decrease. In the second year, the energy losses through the wall were about 10% less than in the first year and in the following years energy losses reduced by about 5% per year.

To sum up, it should be noted that this work demonstrated that wind driven rain significantly influences the energy performance of brick masonry walls uncoated or coated with traditional lime plaster. It was also observed that adding interior thermal insulation to those walls did not only significantly improve their energy performance, but also reduced the influence of moisture on the energy losses through the walls. However, adding interior thermal insulation may not be sufficient, with moisture continuing to worsen the energy performance of these walls by around 10 to 20%. In fact, the most effective measure to limit the influence of moisture on the energy performance of a brick masonry wall is to externally protect it from rain by applying coatings with low capillary absorption coefficients. This study also showed that wind driven rain has little influence (less than 5%) on the energy performance of masonry walls coated with external insulating render system (composed by insulating render, finishing render and paint) and uncoated granite masonry walls. However, if the masonry is wet when the external insulating render system is applied, that initial moisture in the masonry impacts the energy losses through the wall over the years.

This thesis answered the research questions based on numerical analysis as well as experimental study. It was observed that moisture content in the retrofitted walls under in-service conditions increased the thermal conductivity of the materials, influencing the energy performance of the walls. The consequences were the increase in heat losses and energy consumption of around 3 to 35%, depending mainly on the configuration of the wall. The heat losses through the investigated retrofitted walls taking into account the

moisture content in the walls under in-service conditions were quantified in Chapter 5. In addition, the study of the hygrothermal behaviour of the walls exposed and not exposed to wind-driven rain allowed to quantify the impact of wind-driven rain on their energy performance. Although the climate in Krakow is colder than in Brussels, there were more heat losses through the wall in Brussels due to the higher humidity. The finishing coating (with low capillary absorption coefficient) was found to be the key factor that most prevented the harmful moisture effects on the energy performance of retrofitted walls. Finally, the need to rehabilitate the existing building walls taking into account the influence of moisture on their energy performance is reinforced in order to contribute to reducing energy needs for heating.

## **6.2. FUTURE DEVELOPMENTS**

As future or complementary developments, an additional experiment with this prototype can be suggested in order to assess the influence of moisture on the energy performance of the wall test specimens, but in which not only rain is acting on the specimens but also wind pressure. In fact, the rain chamber can introduce pulsating air pressure differences simulating the wind pressure against the wall test specimens from 0 to 2500 Pa. The development of guidelines for the renovation of exterior walls of existing buildings considering the influence of moisture on their energy performance is also suggested. Finally, the study of the influence of moisture on the energy performance of retrofitted walls can be expanded for different stone masonry walls, other insulation materials and walls of newer buildings.

## REFERENCES

- Alonso Alonso, Patricia. 2017. An experimental and numerical study of hygrothermal behaviour of an open-joint ventilated façade in Northwest Iberian Peninsula. Tese de Doutoramento Universidad da Coruña.
- Antretter, Florian, Fabian Sauer, Teresa Schöpfer and Andreas Holm. 2011. Validation of a hygrothermal whole building simulation software. Proceedings of Building Simulation 2011: 12th Conference of International Building Performance Simulation Association, Sydney, Australia.
- Appleton, João. 2003. Reabilitação de edifícios antigos: patologias e tecnologias de intervenção.
- ASHRAE. 2002. ASHRAE Guideline 14: Measurement of Energy and Demand Savings. American Society of Heating, Refrigerating and Air-Conditioning Engineers 35: 41-63.
- ASHRAE. 2017. Handbook fundamentals. Atlanta, American Society of Heating and Air-Conditioning Engineers (ASHRAE).
- Barbosa, Francisca Cavaleiro. 2020. School Building Rehabilitation in Southern European Climate Combining Comfort and Low Energy Consumption. Ph.D. Thesis. Faculty of Engineering University of Porto.
- Barbosa, Francisca Cavaleiro and Vasco Peixoto De Freitas. 2015. A câmara de chuva do LFC, FEUP.
- Blumberga, Andra, Dagnija Blumberga, Edite Kamendere, Agris Kamenders, Kristaps Kass, Reinis Purvins and Gatis Zogla. 2015. Report on historical building types and combinations of structural solutions, RIBuild - Robust Internal Thermal Insulation of Historic Buildings.
- Blumberga, Andra, Kristaps Kašs, Edīte Kamendere, Gatis Žogla, Agris Kamenders, Dagnija Blumberga, Armands Grāvelsiņš, Reinis Purviņš, Marika Rošā, Lelde Timma, Hans Janssen, Peggy Freudenberg, Fredrik Stahl, Ruut Peuhkuri, Pierryves Padey, Sebastien Lasvaux, Elisa di Giuseppe and Ernst Jan de Place Hansen. 2015. State of the art on historic building insulation materials and retrofit strategies RIBuild - Robust Internal Thermal Insulation of Historic Buildings.
- Capener, C, Stephen Burke, Simon Le Roux and Stephan Ott. 2014. Hygrothermal Performance of TES Energy Façade at two European residential building demonstrations—Comparison between Field Measurements and Simulations. NSB 2014 10th Nordic Symposium on Building Physics.
- Coelho, Guilherme BA and Fernando MA Henriques. 2016. Influence of driving rain on the hygrothermal behaviour of solid brick walls. Journal of Building Engineering 7: 121-132.
- Coelho, Guilherme BA, Hugo Entradas Silva and Fernando MA Henriques. 2018. Calibrated hygrothermal simulation models for historical buildings. Building and Environment 142: 439-450.
- De Freitas, Sara. 2011. Avaliação do comportamento higrótérmico de revestimentos exteriores de fachadas devido à acção da chuva incidente. Master's thesis Faculty of Engineering (FEUP), University of Porto

De Freitas, Sara, Eva Barreira and Vasco Peixoto De Freitas. 2013. Quantification of wind-driven rain and evaluation of façade humidification. Proceedings of the 2nd Central European Symposium on Building Physics (CESBP 2013).

De Freitas, Vasco Peixoto. 1992. Transferência de humidade em paredes de edifícios análise do fenómeno de interface. Ph.D. Thesis. Faculty of Engineering University of Porto.

De Freitas, Vasco Peixoto and Paulo Pinto. 1998. Nota de Informação Técnica–NIT• 002–LFC 1998,. Permeabilidade ao Vapor de Materiais de Construção–Condensações Internas, LFC–FEUP.

Delgado, João , Eva Barreira, Nuno Ramos and Vasco Peixoto de Freitas. 2012. Hygrothermal numerical simulation tools applied to building physics, Springer Science & Business Media.

Despacho (extrato) n.º 15793-F/2013

DIN 187 DIN 52 617 Determination of the water absorption coefficient of construction materials.

Directive 2010/31/EU of the European Parliament and of the Council of 19 May 2010 on the energy performance of buildings.

Dos Santos, Pina and Luis Matias. 2006. ITE 50 – Coeficientes de transmissão Térmica de elementos da envolvente dos Edifícios. Lisboa, Laboratório Nacional de Engenharia Civil.

EN 998-1: 2016 Specification for mortar for masonry - Part 1: Rendering and plastering mortar.

EN 1991-1-4: 2005 Eurocode 1: Actions on structures - Part 1-4: General actions - Wind actions.

EN 12524: 2000 Building materials and products - Hygrothermal properties - Tabulated design values.

EN 12865: 2001 Hygrothermal performance of building components and building elements. Determination of the resistance of external wall systems to driving rain under pulsating air pressure.

EN ISO 6946: 2007 Building components and building elements - Thermal resistance and thermal transmittance - Calculation method.

EN ISO 10456: 2007 Building materials and products - Hygrothermal properties -Tabulated design values and procedures for determining declared and design thermal values.

EN ISO 12572: 2001 Hygrothermal performance of building materials and products – Determination of water vapour transmission properties

EN ISO 15148: 2002 Hygrothermal performance of building materials and products - Determination of water absorption coefficient by partial immersion.

Eurostat. (2019a). Retrieved 02/01/2019, from [https://ec.europa.eu/eurostat/statistics-explained/index.php/Energy\\_consumption\\_in\\_households#Energy\\_consumption\\_in\\_households\\_by\\_type\\_of\\_end-use](https://ec.europa.eu/eurostat/statistics-explained/index.php/Energy_consumption_in_households#Energy_consumption_in_households_by_type_of_end-use).

- Eurostat. (2019b). Retrieved 02/01/2019, from [https://ec.europa.eu/eurostat/statistics-explained/index.php?title=File:Share\\_of\\_final\\_energy\\_consumption\\_in\\_the\\_residential\\_sector\\_by\\_type\\_of\\_end-use,\\_2017\\_\(%25\).png](https://ec.europa.eu/eurostat/statistics-explained/index.php?title=File:Share_of_final_energy_consumption_in_the_residential_sector_by_type_of_end-use,_2017_(%25).png).
- EVO - Efficiency Valuation Organization. 2012. International Performance Measurement and Verification Protocol: Concepts and Options for Determining Energy and Water Savings.
- Fino, Rosário, António Tadeu and Nuno Simões. 2018. Influence of a period of wet weather on the heat transfer across a wall covered with uncoated medium density expanded cork. *Energy and Buildings* 165: 118-131.
- Gomes, M Glória, I Flores-Colen, LM Manga, A Soares and J de Brito. 2017. The influence of moisture content on the thermal conductivity of external thermal mortars. *Construction and Building Materials* 135: 279-286.
- Gradeci, Klodian and Umberto Berardi. 2019. Application of probabilistic approaches to the performance evaluation of building envelopes to withstand mould growth. *Journal of Building Physics* 43(3): 187-207.
- Gradeci, Klodian, Umberto Berardi, Berit Time and Jochen Köhler. 2018. Evaluating highly insulated walls to withstand biodeterioration: A probabilistic-based methodology. *Energy and Buildings* 177: 112-124.
- Henriques, Fernando. 1994. *Humidade em paredes*, LNEC.
- Hens, Hugo. 2017. *Building physics heat, air and moisture*. Berlin, Germany, Wilhelm Ernst & Sohn.
- Holm, Andreas, Jan Radon, Hartwig Künzler and Klaus Sedlbauer. 2004. Description of the IBP holistic hygrothermal model. IEA Annex 41 1st working meeting, Zurich, Switzerland, May.
- IPMA. (2019). Instituto Português do Mar e da Atmosfera from [https://www.ipma.pt/pt/educativa/faq/meteorologia/previsao/faqdetail.html?f=/pt/educativa/faq/meteorologia/previsao/faq\\_0033.html](https://www.ipma.pt/pt/educativa/faq/meteorologia/previsao/faqdetail.html?f=/pt/educativa/faq/meteorologia/previsao/faq_0033.html).
- ISO 8301 1991 Thermal insulation - Determination of steady-state thermal resistance and related properties - Heat flow meter apparatus.
- ISO 8302 1991 Thermal insulation - Determination of steady-state thermal resistance and related properties - Guarded hot plate apparatus
- ISO 8894-2: 2007 Refractory materials – Determination of thermal conductivity – Part 2: Hot-wire method (parallel).
- ISO 8990 1994 Thermal insulation - Determination of steady-state thermal transmission properties - Calibrated and guarded hot box.
- Jakovics, Andris, Stanislavs Gendelis, Ansis Ozolins and Saule Sakipova. 2014. Energy efficiency and sustainability of low energy houses in latvian climate conditions. *Int. Conf.” Energy, Environment, Development and Economics*.
- Jerman, Miloš and Robert Černý. 2012. Effect of moisture content on heat and moisture transport and storage properties of thermal insulation materials. *Energy and Buildings* 53: 39-46.

Johnson, Richard Arnold and Dean W. Wichern. 2002. Applied multivariate statistical analysis. Upper Saddle River, NJ, Prentice Hall.

Kočí, Václav, Eva Vejmelková, Monika Čáchová, Dana Koňáková, Martin Keppert, Jiří Maděra and Robert Černý. 2017. Effect of moisture content on thermal properties of porous building materials. *International Journal of Thermophysics* 38(2): 28.

Krus, M. 1998. Hygrothermal Calculations applied to water-repellent surfaces-Validation and Application. Proceedings Second International Conference on Surface Technology with Water Repellent Agents, ETH Zürich S.

Kumaran, M. K. . 1996. Heat, Air and Moisture Transfer in Insulated Envelope Parts Task 3: Material properties.

Künzel, H. M. 1994. Simultaneous heat and moisture transport in building components. One- and two-dimensional calculation using simple parameters. Ph. D. Thesis, University of Stuttgart.

Künzel, Hartwig M. 1995. Simultaneous heat and moisture transport in building components. One- and two-dimensional calculation using simple parameters. Fraunhofer IRB Verlag Stuttgart.

Künzel, HM, Th Schmidt and A Holm. 2002. Exterior surface temperature of different wall constructions comparison of numerical simulation and experiment. Proceedings of 11th Symposium of Building Physics, Technische Universität Dresden, Dresden, Germany.

Lakatos, Ákos. 2016. Moisture induced changes in the building physics parameters of insulation materials. *Science and Technology for the Built Environment* 22(3): 252-260.

Lakatos, Ákos and Ferenc Kalmár. 2014. Examination of the change of the overall heat transfer coefficients of building structures in function of water content. *Building Services Engineering Research and Technology* 35(5): 507-515.

Maia, Joana. 2019. Durability of thermal rendering and plastering systems. Ph.D. Thesis. Faculty of Engineering University of Porto.

Maia, Joana, Nuno Ramos and Rosário Veiga. 2018. Evaluation of the hygrothermal properties of thermal rendering systems. *Building and Environment* 144: 437-449.

Peixoto, José Pinto. 1987. O sistema climático e as bases físicas do clima, Ministério do Plano e da Administração do Território. Gabinete de Estudos e Planeamento da Administração do Território.

Pérez-Bella, José M, Javier Dominguez-Hernandez, Enrique Cano-Suñén, Juan J del Coz-Diaz and Felipe P Álvarez Rabanal. 2015. A correction factor to approximate the design thermal conductivity of building materials. Application to Spanish façades. *Energy and Buildings* 88: 153-164.

Pinho, Fernando FS. 2000. Paredes de edifícios antigos em Portugal. Laboratório Nacional de Engenharia Civil, Lisboa.

Portaria n.º 297/2019 de 9 de setembro.

Portaria n.º 379-A/2015 de 22 de outubro.

- Ramos, Nuno. 2007. A importância da inércia higroscópica no comportamento higrótérmico dos edifícios. Tese de Doutoramento. FEUP.
- Ruiz, Germán Ramos and Carlos Fernández Bandera. 2017. Validation of calibrated energy models: Common errors. *Energies* 10(10): 1587.
- Sousa, José Manuel Martins Soares de. 1996. Caracterização da capilaridade de revestimentos de fachada. Master's thesis. Faculty of Engineering of University of Porto.
- Svärd, Jesper and John Holstein. 2015. Moistureproof energy efficiency of culture historic building-A case study of the E-building at LTH School of engineering. LTH School of Engineering at Campus Helsingborg, Department of Building and Environmental Technology / Building Physics, Sweden.
- Szodrai, Ferenc and Ákos Lakatos. 2014. Measurements of the thermal conductivities of some commonly used insulating materials after wetting. *Environmental Engineering and Management Journal* 13(11): 2881-2886.
- Teixeira, Joaquim. 2014. Salvaguarda e valorização do edificado habitacional da cidade histórica. Metodologia de intervenção no sistema construtivo da casa burguesa do Porto.
- Tejeda-Vázquez, R., Macias-Melo, E. V., Hernández-Pérez, I., Aguilar-Castro, K. M., and Serrano-Arellano, J. 2021. Empirical model of hygrothermal behavior of masonry wall under different climatic conditions using a hot box. *Energy and Buildings*, 249, 111209.
- Tipler, Paul A and Gene Mosca. 2007. *Physics for scientists and engineers*, Macmillan.
- Valovirta, Ilkka and Juha Vinha. 2004. Water vapor permeability and thermal conductivity as a function of temperature and relative humidity. Performance of exterior envelopes of whole buildings IX.
- Vereecken, Evy and Staf Roels. 2013. Hygric performance of a massive masonry wall: How do the mortar joints influence the moisture flux? *Construction and Building Materials* 41: 697-707.
- Vereecken, Evy and Staf Roels. 2015. Capillary active interior insulation: do the advantages really offset potential disadvantages? *Materials and Structures* 48(9): 3009-3021.
- Vereecken, Evy, Liesje Van Gelder, Hans Janssen and Staf Roels. 2015. Interior insulation for wall retrofitting—A probabilistic analysis of energy savings and hygrothermal risks. *Energy and Buildings* 89: 231-244.
- Verma, S. K., Anand, Y., Gupta, N., Jindal, B. B., Tyagi, V. V., and Anand, S. 2022. Hygrothermal dynamics for developing energy-efficient buildings: Building materials and ventilation system considerations. *Energy and Buildings*, 111932.
- Wufi-wiki. (2019a). [https://www.wufi-wiki.com/mediawiki/index.php/1D:Wufi\\_1D\\_What\\_is](https://www.wufi-wiki.com/mediawiki/index.php/1D:Wufi_1D_What_is). Retrieved 12/03/2019.
- Wufi-wiki. (2019b). <https://www.wufi-wiki.com/mediawiki/index.php/Details:LiquidTransportCoefficients>. Retrieved 12/03/2019.
- Wufi-wiki. (2019d). <https://www.wufi-wiki.com/mediawiki/index.php/Details:SurfaceCoatings>. Retrieved 12/03/2019.

Wufi-wiki. (2019e). [https://www.wufi-wiki.com/mediawiki/index.php/1D:Dialog\\_SurfaceTransferCoefficients](https://www.wufi-wiki.com/mediawiki/index.php/1D:Dialog_SurfaceTransferCoefficients). Retrieved 12/03/2019.

Wufi-wiki. (2019f). <https://www.wufi-wiki.com/mediawiki/index.php/Details:MoistureStorageFunction>. Retrieved 12/03/2019.

Wufi-wiki. (2019g). <https://www.wufi-wiki.com/mediawiki/index.php/Details:HeatConductivityMoistureDependent>. Retrieved 12/03/2019.

Wufi-wiki. (2019h). <https://www.wufi-wiki.com/mediawiki/index.php/Details:Climate>. Retrieved 12/03/2019.

Wufi-wiki. (2019i). [https://www.wufi-wiki.com/mediawiki/index.php/1D:Dialog\\_Orientation](https://www.wufi-wiki.com/mediawiki/index.php/1D:Dialog_Orientation). Retrieved 12/03/2019.

Wufi-wiki. (2019j). [https://www.wufi-wiki.com/mediawiki/index.php/Discussion:WUFI-Pro\\_PerformanceandLimitations](https://www.wufi-wiki.com/mediawiki/index.php/Discussion:WUFI-Pro_PerformanceandLimitations). Retrieved 25/03/2019.

Zirkelbach, D, Th Schmidt, M Kehrer and HM Künzel. 2007. Wufi® Pro–Manual. Fraunhofer Institute.



## **APPENDICES**

## **A. DETERMINATION OF WATER VAPOUR PERMEABILITY**

### **A.1. SOLID BRICK**

<b>Test identification</b>
Determination of water vapour transmission properties of solid brick

<b>Standard</b>
EN ISO 12572 – Hygrothermal performance of building materials and products – Determination of water vapour transmission properties

<b>Product identification</b>
Name: Solid brick test specimens
Method of preparation of the specimens: Slicing the solid brick
Dimensions of test specimens: 210x210x20 mm <sup>3</sup>

<b>Equipment</b>
Climatic chamber: <ul style="list-style-type: none"><li>- Brand/model: Vötsch VC 4034</li><li>- Temperature control: - 40 °C ≤ T ≤ 180 °C – fluctuation in time &lt; ± 0.3 °C</li><li>- Humidity control: 10 % ≤ T ≤ 98 % – fluctuation in time &lt; ± 3 %</li></ul>
Balance: <ul style="list-style-type: none"><li>- Brand/model: Precisa 5000D-12000G</li><li>- Accuracy: 0.1 g</li></ul>
Cups – Material: stainless

<b>Test procedure</b>
<p><b>Initial conditioning:</b>                  Temperature: <math>(23 \pm 0.5) ^\circ\text{C}</math>                  Relative humidity: <math>(50 \pm 3) \%</math>                  Stopping criterion: Five successive determinations of change in mass per weighing interval for each test specimen constant within <math>\pm 5 \%</math> of the mean value</p>
<p><b>Preparation of specimen and test assembly:</b>                  The aqueous saturated solution potassium nitrate <math>\text{KNO}_3</math> was placed with a depth of 15 mm in the bottom of each cup.                  The test specimens were sealed into the cups with paraffin.                  The test assemblies were weighed and then placed in the climatic chamber.</p>
<p><b>Test conditions:</b>                  Temperature within the cups: <math>(23 \pm 0.5) ^\circ\text{C}</math>                  Relative humidity within the cups: <math>(93 \pm 3) \%</math>                  Temperature within the climatic chamber: <math>(23 \pm 0.5) ^\circ\text{C}</math>                  Relative humidity within the climatic chamber: <math>(50 \pm 3) \%</math>                  Time interval between successive weighings: (24 – 72) hours</p>

<b>Results</b>				
Weighings				
			m (kg)	
			solid brick test assembly 1	solid brick test assembly 2
0	15:50	0	3.424	3.399
1st	15:30	86400	3.423	3.397
2nd	16:00	172800	3.421	3.394
5th	15:40	432000	3.413	3.386
6th	16:00	518400	3.409	3.383
7th	18:05	604800	3.406	3.380
8th	15:30	691200	3.405	3.379
9th	15:45	777600	3.403	3.377
12th	18:10	1036800	3.395	3.367
13th	18:00	1123200	3.392	3.365
14th	17:25	1209600	3.390	3.362
15th	17:10	1296000	3.387	3.360
16th	18:00	1382400	3.385	3.357
19th	18:00	1641600	3.378	3.349

<b>Water vapour transmission properties</b>	<b>solid brick test assembly 1</b>	<b>solid brick test assembly 2</b>	<b>Average</b>	<b>Standard deviation</b>
Water vapour flow G [kg/s]	2.90E-08	3.06E-08	2.98E-08	8.0E-10
Density of water vapour flow rate g [kg/(m <sup>2</sup> s)] $g = \frac{G}{A}$	7.25E-07	7.65E-07	7.45E-07	2.0E-08
Water vapour permeance W [kg/(m <sup>2</sup> s Pa)] $W = \frac{G}{A \cdot \Delta p_v}$	5.85E-10	6.17E-10	6.01E-10	1.6E-11
Water vapour permeability $\delta$ [kg/(m s Pa)] $\delta = W \cdot d$	1.17E-11	1.23E-11	1.20E-11	3.0E-13
Water vapour resistance factor $\mu$ [-] $\mu = \frac{\delta_a}{\delta}$	17.10	16.21	16.7	0.45
Water vapour diffusion-equivalent air layer thickness $s_d$ [m] $s_d = \mu \cdot d$	0.34	0.33	0.34	0.01

**Additional symbology:**

A	m <sup>2</sup>	Exposed area of test specimen
d	m	Thickness of the specimen
$\Delta p_v$	Pa	Water vapour pressure difference across specimen
$\delta_a$	Kg/(m s Pa)	Water vapour permeability of air

A.2. INSULATING RENDER SYSTEM

<b>Test identification</b>
----------------------------

Determination of water vapour transmission properties of insulating render system
---

<b>Standard</b>
-----------------

EN ISO 12572 – Hygrothermal performance of building materials and products – Determination of water vapour transmission properties
--

<b>Product identification</b>
-------------------------------

Name: Insulating render system test specimens
---

Method of preparation of the specimens: Manufactured by molding
---

Dimensions of test specimens: 210x210x20 mm <sup>3</sup>
--

<b>Equipment</b>
------------------

Climatic chamber:
-------------------

- |  |
|--|
| <ul style="list-style-type: none"><li>- Brand/model: Vötsch VC 4034</li><li>- Temperature control: <math>-40\text{ °C} \leq T \leq 180\text{ °C}</math> – fluctuation in time <math>&lt; \pm 0.3\text{ °C}</math></li><li>- Humidity control: <math>10\% \leq T \leq 98\%</math> – fluctuation in time <math>&lt; \pm 3\%</math></li></ul> |
|--|

Balance:
----------

- |   |
|---|
| <ul style="list-style-type: none"><li>- Brand/model: Precisa 5000D-12000G</li><li>- Accuracy: 0.1 g</li></ul> |
|---|

Cups – Material: stainless
----------------------------

<b>Test procedure</b>
<p><b>Initial conditioning:</b>                  Temperature: <math>(23 \pm 0.5) ^\circ\text{C}</math>                  Relative humidity: <math>(50 \pm 3) \%</math>                  Stopping criterion: Five successive determinations of change in mass per weighing interval for each test specimen constant within <math>\pm 5 \%</math> of the mean value</p>
<p><b>Preparation of specimen and test assembly:</b>                  The aqueous saturated solution potassium nitrate <math>\text{KNO}_3</math> was placed with a depth of 15 mm in the bottom of each cup.                  The test specimens were sealed into the cups with paraffin.                  The test assemblies were weighed and then placed in the climatic chamber.</p>
<p><b>Test conditions:</b>                  Temperature within the cups: <math>(23 \pm 0.5) ^\circ\text{C}</math>                  Relative humidity within the cups: <math>(93 \pm 3) \%</math>                  Temperature within the climatic chamber: <math>(23 \pm 0.5) ^\circ\text{C}</math>                  Relative humidity within the climatic chamber: <math>(50 \pm 3) \%</math>                  Time interval between successive weighings: (24 – 72) hours</p>

<b>Results</b>				
Weighings				
Day	Time	t (s)	m (kg)	
			insulating render system test assembly 1	Insulating render system test assembly 2
0	15:50	0	2.246	2.304
1st	15:30	86400	2.240	2.299
2nd	16:00	172800	2.234	2.291
5th	15:40	432000	2.214	2.269
6th	16:00	518400	2.206	2.263
7th	18:05	604800	2.198	2.256
8th	15:30	691200	2.193	2.251
9th	15:45	777600	2.186	2.246
12th	18:10	1036800	2.164	2.223
13th	18:00	1123200	2.157	2.216
14th	17:25	1209600	2.150	2.210
15th	17:10	1296000	2.144	2.203
16th	18:00	1382400	2.137	2.197
19th	18:00	1641600	2.117	2.177

<b>Water vapour transmission properties</b>	<b>Insulating render system test assembly 1</b>	<b>Insulating render system test assembly 2</b>	<b>Average</b>	<b>Standard deviation</b>
Water vapour flow G [kg/s]	7.79E-08	8.02E-08	7.91E-08	1.15E-09
Density of water vapour flow rate g [kg/(m <sup>2</sup> s)] $g = \frac{G}{A}$	1.95E-06	2.01E-06	1.98E-06	2.87E-08
Water vapour permeance W [kg/(m <sup>2</sup> s Pa)] $W = \frac{G}{A \cdot \Delta p_v}$	1.57E-09	1.62E-09	1.60E-09	2.50E-11
Water vapour permeability $\delta$ [kg/(m s Pa)] $\delta = W \cdot d$	3.14E-11	3.23E-11	3.19E-11	4.50E-13
Water vapour resistance factor $\mu$ [-] $\mu = \frac{\delta_a}{\delta}$	6.37	6.18	6.28	0.10
Water vapour diffusion-equivalent air layer thickness $s_d$ [m] $s_d = \mu \cdot d$	0.13	0.12	0.12	0.01

**Additional symbology:**

A	m <sup>2</sup>	Exposed area of test specimen
d	m	Thickness of the specimen
$\Delta p_v$	Pa	Water vapour pressure difference across specimen
$\delta_a$	Kg/(m s Pa)	Water vapour permeability of air

## B. EQUIPMENT VERIFICATION

Table B-1. Results of the equipment verification (difference between measured values by the sensors and the climatic chamber programed temperature (T) or relative humidity (RH))

Temperature	Climatic chamber			
	35°C	25°C	15°C	10°C
Relative Humidity	50%	60%	70%	80%
T1	-0.2	-0.1	-0.1	-0.1
T2	0.0	0.0	-0.1	-0.1
T3	-0.4	-0.4	-0.4	-0.3
T4	-0.3	-0.4	-0.3	-0.2
T5	-0.3	-0.4	-0.3	-0.3
T6	-0.3	-0.4	-0.3	-0.3
T7	0.1	-0.1	-0.2	-0.3
T8	-0.1	-0.2	-0.3	-0.3
T9	-0.3	-0.3	-0.2	-0.2
T10	-0.2	-0.3	-0.2	-0.1
T11	-0.3	-0.4	-0.3	-0.3
T12	-0.5	-0.5	-0.4	-0.4
T13	-0.4	-0.4	-0.3	-0.3
T14	-0.3	-0.3	-0.2	-0.2
T15	-0.4	-0.4	-0.3	-0.3
T16	-0.3	-0.4	-0.3	-0.3
T17	-0.3	-0.3	-0.2	-0.2
T18	-0.3	-0.3	-0.3	-0.2
T19	-0.3	-0.2	-0.1	-0.1
T20	-0.3	-0.3	-0.2	-0.2
T21	-0.5	-0.5	-0.4	-0.4
H1	3.5	3.6	4.3	4.4
H2	3.5	4.2	5.6	6.3
H3	3.1	3.8	5.1	5.7
H4	2.7	3.2	4.5	5.4
HOB01_T	-0.1	-0.1	-0.1	-0.1
HOB02_T	0.0	0.0	0.0	0.0
HOB03_T	-0.1	-0.1	-0.1	-0.1
HOB04_T	-0.2	-0.1	-0.1	-0.1
HOB01_RH	-0.8	0.0	1.7	3.1
HOB02_RH	-0.8	0.3	2.8	7.0
HOB03_RH	-1.6	-0.3	1.8	3.6
HOB04_RH	-1.7	-1.1	0.3	1.6

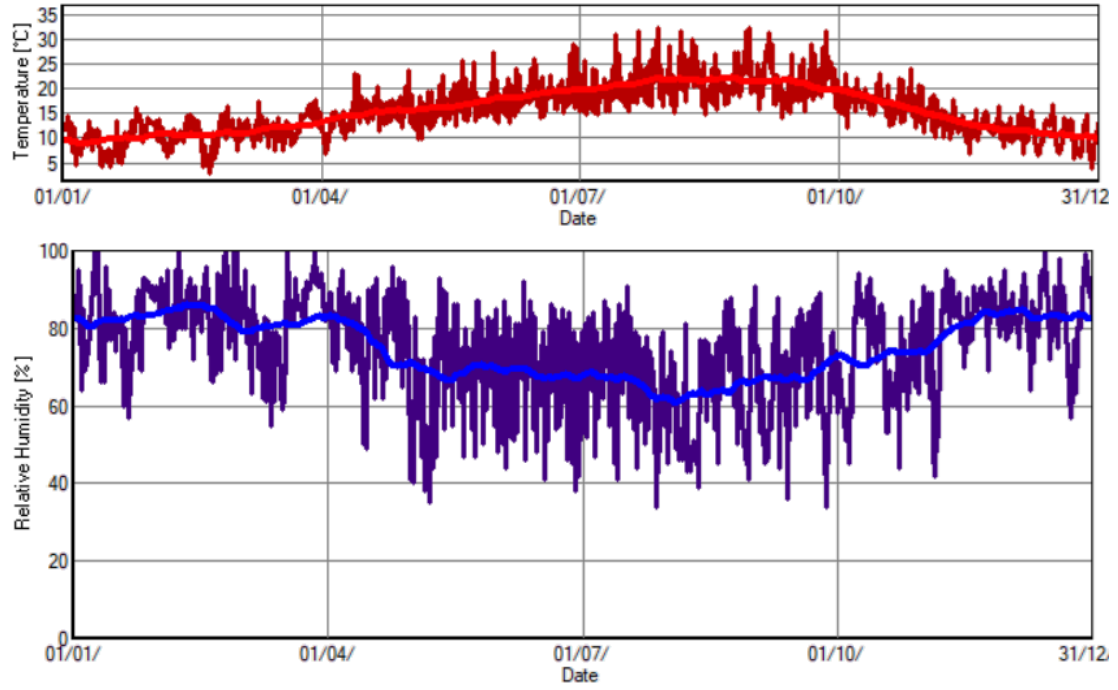
(T1 to T21) Thermocouples

(H1 to H4) Relative humidity probes

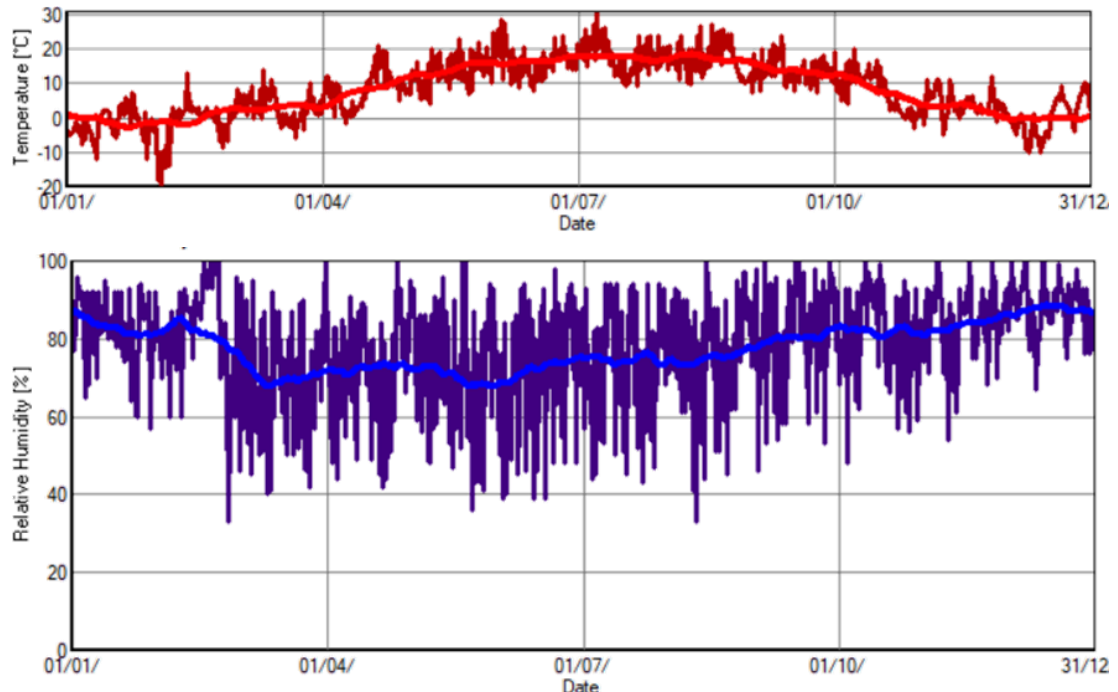
(HOB01 to HOB04) Air temperature and relative humidity sensors



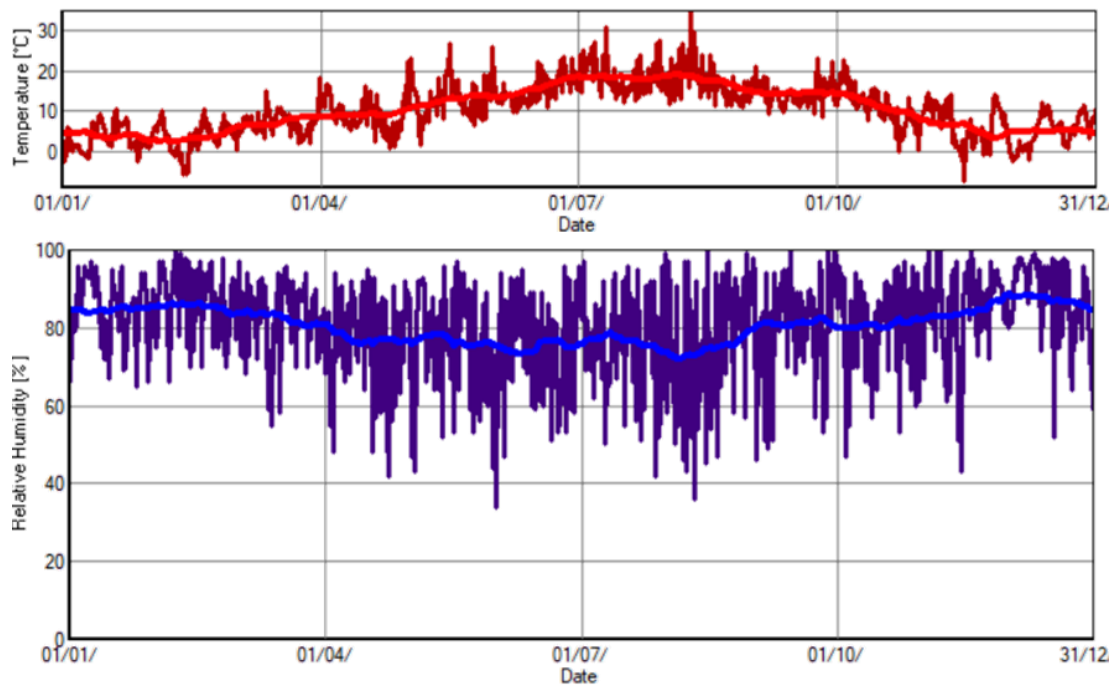
### C. TEMPERATURE AND RELATIVE HUMIDITY IN PORTO, KRAKOW AND BRUSSEL



(a)



(b)



(c)

Figure C-1. Temperature and relative humidity throughout the year in: a) Porto; b) Krakow; c) Brussels